Non-Stationary Responses of Hoisting Cables with Slowly Varying Length

Stefan Kaczmarczyk

A thesis submitted in fulfillment of the academic requirements

for the degree of

Doctor of Philosophy

in the School of Mechanical Engineering

University of Natal

Durban 1999

It turns out to be very difficult to devise a theory to describe the universe all in one go. Instead, we break the problem up into bits and invent a number of partial theories. Each of these partial theories describes and predicts a certain limited class of observations, neglecting the effects of other quantities, or representing them by simple sets of numbers. It may be that this approach is completely wrong. If everything in the universe depends on everything else in a fundamental way, it might be impossible to get close to a full solution by investigating parts of the problem in isolation. Nevertheless, it is certainly the way we have made progress in the past.

Stephen Hawking

Abstract

Cables in hoisting installations, due to their flexibility, are susceptible to vibrations. A common arrangement in industrial hoisting systems comprises a driving winder drum, a steel wire cable, a sheave mounted in headgear, a vertical shaft and a conveyance. This system can be treated as an assemblage of two connected interactive, continuous substructures, namely of the catenary and of the vertical rope, with the sheave acting as a coupling member, and with the winder drum regarded as an ideal energy source. The length of the vertical rope is varying during the wind so that the mean catenary tension is continuously varying. Therefore, the natural frequencies of both subsystems are time-dependent and the entire structure represents a non-stationary dynamic system.

The main dynamic response, namely lateral vibrations of the catenary and longitudinal vibrations of the vertical rope, are caused by various sources of excitation present in the system. The most significant sources are loads due to the winding cycle acceleration/deceleration profile and a mechanism applied on the winder drum surface in order to achieve a uniform coiling pattern. The classical moving frame approach is used to derive a mathematical model describing the non-stationary response of the system. First the longitudinal response and passage through primary resonance is examined. The response is analyzed using a combined perturbation and numerical technique. The method of multiple scales is used to formulate a uniformly valid perturbation expansion for the response near the resonance, and a system of first order ordinary differential equations for the slowly varying amplitude and phase of the response results. This system is integrated numerically on a slow time scale. A model example is discussed, and the behaviour of the essential dynamic properties of the system during the transition through resonance is examined.

Interactions between various types of vibration within the system exist. The sheave inertial coupling between the catenary and the vertical rope subsystems fa-

cilitates extensive interactions between the catenary and the vertical rope motions. The nature of these interactions is strongly non-linear. The lateral vibration of the catenary induces the longitudinal oscillations in the vertical system and vice-versa. In order to analyze dynamic phenomena arising due these interactions the non-linear partial-differential equations of motion are discretised by writing the deflections in terms of the linear, free-vibration modes of the system, which result in a non-linear set of coupled, second order ordinary differential equations with slowly varying coefficients. Using this formulation, the dynamic response of an existing hoisting installation, where problematic dynamic behaviour was observed, is simulated numerically. The simulation predicts strong modal interactions during passage through external, parametric and internal resonances, confirming the autoparametric and non-stationary nature of the system recorded during its operation.

The results of this research demonstrate the non-stationary and non-linear behaviour of hoisting cables with slowly varying length. It is shown that during passage through resonance a large response may lead to high oscillations in the cables' tensions, which in turn contribute directly to fatigue damage effects. The results obtained show also that the non-linear coupling in the system promotes significant modal interactions during the passage through the instability regions. The analysis techniques presented in the study form a useful tool that can be employed in determining the design parameters of hoisting systems, as well as in developing a careful winding strategy, to ensure that the regions of excessive dynamic response are avoided during the normal operating regimes.

Acknowledgments

The author is grateful to his supervisor Professor S Adali who has provided stimulus, support and encouragement over the period in which these studies have been carried out.

Thanks are also due to Professor R R Mankowski and to Dr C P Constancon who have helped with technical advice and discussion of a number of problems.

The author gratefully acknowledges the financial support received from the University of Natal Research Fund.

Mention must also be made of colleagues at the University of Natal. Thanks are due to Professor G D J Smith who gave valuable support in lightening the author's teaching and administrative load during the crucial stage of this research. Special thanks to Professor V E Verijenko for his kind advice and encouragement. The author is also grateful to Professor L W Roberts for his valuable help provided at the beginning of this project.

The author would also like to acknowledge Professor B Skalmierski, formerly of the Silesian University of Technology, Poland, for his guidance through the avenues of Applied Mechanics.

Finally, the author wishes to thank his wife May for her patience, understanding and faithful support throughout the entire period of this work.

Contents

List of Figures

List of Tables

List of Symbols

A	cable effective cross-sectional area
c	longitudinal wave speed
$\bar{c}$	lateral wave speed
I	mass moment of inertia of the sheave
M	conveyance mass
m	linear cable mass
l	slowly varying length parameter
L_c	catenary length
L_v	vertical rope length
N_{lat}	number of lateral modes
N_{long}	number of longitudinal modes
p_n	n^{th} lateral in-plane modal co-ordinate
P_k	lateral in-plane load
q_n	n^{th} lateral out–of-plane modal co-ordinate
Q_k	lateral out-of-plane load
R	sheave radius
s	Lagrangian co-ordinate
t	time
T	fast time scale
T_c^i	catenary mean tension
T_v^i	vertical rope mean tension
u_v	longitudinal displacement of the vertical rope
u_l	longitudinal boundary excitation
v	catenary in-plane lateral displacement
v_l	lateral in-plane boundary excitation
w	catenary out-of-plane lateral displacement
w_l	lateral out-of-plane boundary excitation
z_n	n^{th} longitudinal modal co-ordinate
Z_r	longitudinal load
Φ_n	n^{th} lateral mode shape
Y_n	n^{th} longitudinal mode shape
γ_n	longitudinal eigenvalue
ε	small parameter
λ_i	lateral damping coefficient
μ_i	longitudinal damping coefficient
Φ_n	n^{th} lateral mode shape
ω_n	n^{th} longitudinal natural frequency
$\bar{\omega}_n$	n^{th} lateral natural frequency
Ω_n	n^{th} harmonic of excitation
$\bar{\varsigma}_n$	lateral damping ratio of the n^{th} mode
τ	slow time scale

Preface

This whole thesis is the author's own work, and has not been submitted in part, or in whole to any other university. The research work was carried out in the School of Mechanical Engineering of the University of Natal under supervision of Professor S Adali.

The research results reported on in this dissertation form a culmination of the author's interest in the dynamics of non-stationary systems, and in the dynamic behaviour of hoisting cables in particular. The importance of the subject cannot be overestimated, especially in the context of the mining industry, where the safety of personnel and profitability rely on stable designs.

It is hoped that the results of this study would shine more light on the dynamic phenomena occurring in hoisting installations, and would provide stimulation for further research in the field.

Chapter 1
Introduction

Structural elements such as ropes and cables are among the oldest tools used by humanity in its quest for technological advancement. For example, a copper wire rope was found in the ruins of Nemeveh near Babylon which originate from about 700 B.C. [Costello, 1990], and in Pompeii bronze ropes estimated to be 2400 years old were excavated [Glushko, 1966]. Thus, it is not surprising that the behaviour and mechanical properties of cable elements have been studied extensively for many hundreds of years, and these studies have resulted in the introduction of a number of well-known theories and techniques. For example, Stevin in 1586 instituted the triangle of forces by experimenting with loaded strings, Beeckman in about 1615 solved the suspension bridge problem, and James and John Bernoulli between 1690 and 1691 established the foundations of the catenary theory [1] [Irvine, 1981].

Cable elements are known to be of low bending and torsional stiffness, and to have the ability to resist relatively large axial loads. Therefore, they have been widely used in towing operations, to support structures, to conduct signals, and to carry payloads. In this latter application cables have played indispensable role in cranes, in building elevators and in industrial hoisting installations. In this research the dynamics of cables in hoisting systems is investigated.

1.1 Typical Hoisting Systems

A schematic configuration of a common arrangement in industrial hoisting systems, referred to as a single-drum system, is shown in Figure 1. It comprises a driving winding drum, a steel wire cable, a sheave mounted in headgear, and a conveyance. The cable passes from the drum over the sheave, forming a horizontal or inclined catenary, to the

[1] The word *catenary* comes from the Latin for chain, and means the shape of a chain suspended between two supports.

conveyance constrained to move in a vertical shaft, and forms the vertical rope hanging below the headsheave. A cable storage mechanism on the winder drum is applied in order to facilitate a uniform coiling pattern. This system can be treated principally as an assemblage of two connected interactive, continuous substructures, namely of the catenary and of the vertical rope, with the sheave acting as a coupling member, and with the winder drum regarded as an ideal energy source.

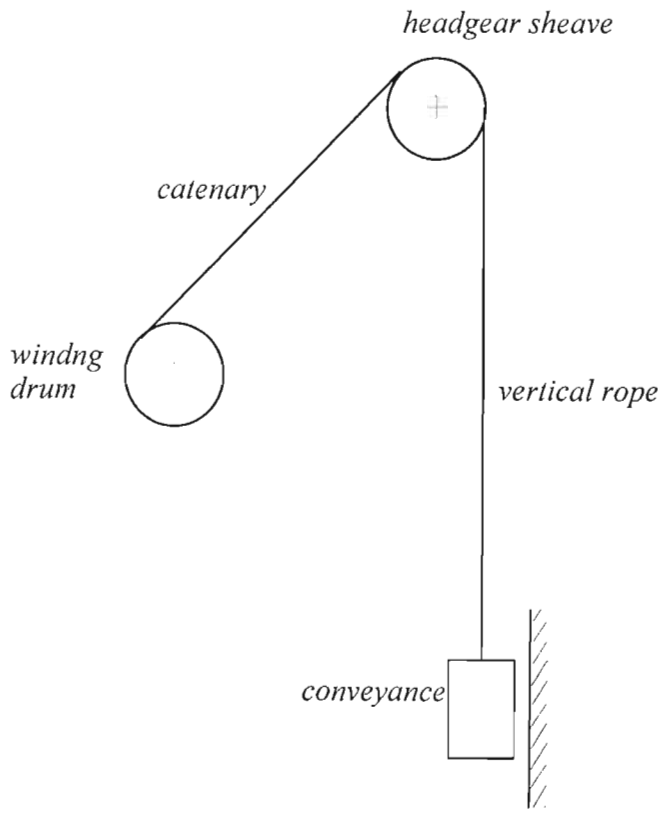

Figure 1. Configuration of a typical industrial hoisting installation.

The dynamic behaviour of this typical installation, further referred to as the catenary-vertical rope system, is addressed in this study. Other different configurations of the hoisting

system are used in various industries, however they usually can be modelled as a simple single-drum installation. For example in the mining industry, double-drum systems operate at higher depths. These systems are formed essentially by two mechanically coupled single-drum systems, with one system acting as the overlay and the other as the underlay installation. This system is driven by two electric motors, as shown schematically in Figure 2. Another common configuration is the Blair Multi-Rope system (BMR). The configuration of this system is similar to a typical double-drum winder with two conveyances, however each conveyance is supported by two ropes, and the drums are twin rope compartment drums. A compensating sheave fitted on the conveyance ensures that loads are distributed equally between the ropes.

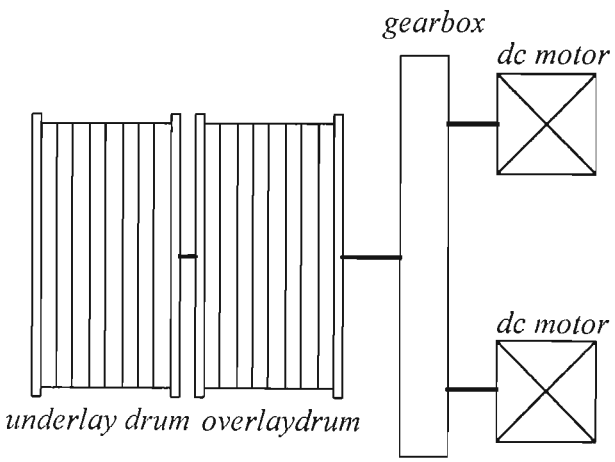

Figure 2. Double-drum winder layout.

In some installations the Koepe system is employed. This winding system is schematically depicted in Figure 3. It has two conveyances, each supported by the head rope passing over the friction wheel driven by an electric motor. The tail rope attached to the conveyances improves the balance of the system. The dynamic behaviour of each conveyance together

with the respective section of the head rope, with the tail rope mass incorporated into the conveyance mass, can be modelled as a single drum system without a catenary cable. As there is no rope storage facility in the Koepe system, the effects resulting from the coiling mechanism on the winder drum should be then neglected.

An important feature of hoisting systems is that the hoisting cables are of time-varying length.. However, the rate of change is small and the length is said to vary slowly. Consequently, the dynamic characteristics of the system vary slowly during the wind, rendering the system non-stationary.

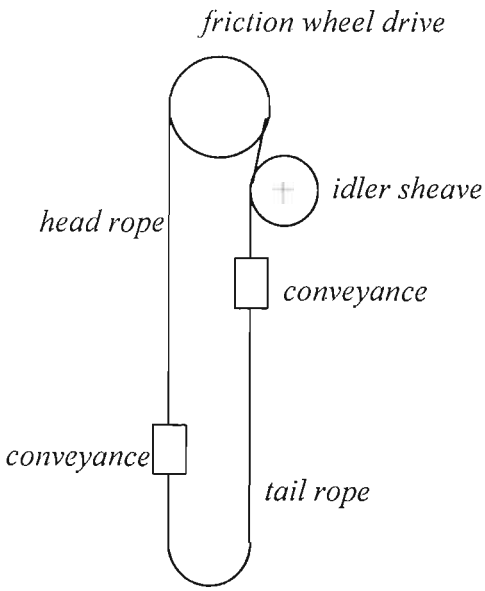

Figure 3. Configuration of the Koepe system.

1.2 Summary of Previous Work

Numerous aspects of the dynamic behaviour of cable elements with slowly varying length, in particular in elevators and in mine hoists, have been studied in the past. A concern for the safety factors was the main cause for embarking on these investigations.

1.2.1 Stationary Parameter Studies

In early research attempts the scope of the studies was limited to the longitudinal dynamic behaviour of a vertical rope of fixed length with end mass. This model was used to investigate the dynamic stresses under emergency braking. Vaughan (1904) investigated the effect of kinetic shocks on loaded winding ropes of various lengths when they were moving with constant velocity and suddenly stopped. He concluded that the portion of the rope near the end load suffered the most and was expected to deteriorate more rapidly than other portions. Perry (1906) considered oscillations of a vertical rope with an end weight, moving downwards with a constant velocity, when its upper end was stopped and held fixed. He formulated a mathematical model in terms of the wave equation and corresponding boundary conditions, and obtained a closed-form solution to the problem. Perry & Smith (1932) analyzed mechanical breaking procedures and their influence on winding equipment, and established a criterion to determine whether or not slip of a rope on headgear sheave occurs during acceleration and deceleration phase. Pollock and Alexander [1950] extended the preceding investigations on deceleration control, concluding that no advantage was gained by building up a rate of deceleration gradually. They stated that a definite maximum rate of deceleration is preferable. Harvey & Laubscher [1965] accounted for inertial effects of the winder drum and head sheave in the longitudinal behaviour of mine hoists, and proposed that a new braking control system be implemented on deep-level winders. Dimitriou & Whillier [1973] discussed the problematic transverse-longitudinal dynamic behaviour of hoisting ca-

bles occurring in some mine hoist installations. They concluded that whirling motions of catenary cable, referred to as *rope whip*, was the result of non-linear couplings in the system, and a method of reducing rope whip was proposed.

Czaja (1977) proposed a distributed-parameter longitudinal model of head and tail ropes in the Koepe winding system with the overwind arresting of conveyances. A closed-form solution was formulated and the rope forces were calculated for a set of model parameters. Wojnarowski & Tejszerska (1977) developed a stationary distributed-parameter model of longitudinal - torsional vibrations of ropes in the Koepe system. The Laplace transform combined with a numerical technique was used to determine the natural frequencies, elastic rope forces and torques in order to verify the safety criteria in the system. A lumped-mass longitudinal model of a multi-rope Koepe system was presented by Wojnarowski & Meder (1977). The model was used to numerically determine the response and the rope tensions resulting from a step torque applied at the wheel drive. Klich (1981) presented a computer method to determine the head and tail dynamic loads taking into account the interactions between a conveyance and shaft steelwork.

More recently Greenway [1990a] and Hamilton & Greenway [1991] used the finite element method to analyze the influence of longitudinal-torsional coupling on the response of vertical rope. They found that the natural frequencies and mode shapes were strongly affected, however the tensile forces due to typical dynamic loads were not influenced by the coupling. It was concluded that the use of longitudinal models could be usually justified. Greenway [1990b] studied peak rope loads that develop during conveyance loading. An analytical closed-form solution to the problem was found, and forces due to the loading of payload material, and due to the sudden release of kepping clamps were determined.

1.2.2 Non-Stationary Parameter Studies

The true nature of hoisting systems is non-stationary, due to the time-varying length of the hoisting cables. This nature complicates substantially the dynamic analysis. Goroshko & Savin [1962; 1971] studied the dynamics of hoisting cables with slowly varying length applying integro-differential equations with time-varying intervals and kernels. Following the fundamental concepts for non-linear oscillating systems with slowly varying parameters, established by Bogolubov & Mitropolskii [1961], they developed an innovative and efficient approach to model one-dimensional systems with time-varying length. This approach was used to investigate longitudinal and transverse oscillations of a vertical rope due to the acceleration and deceleration inertial loads. Visco-elastic characteristics of the rope and slip phenomena occurring on the winder drum were accommodated in the analysis.

Klich [1977] considered the non-stationary dynamics of winding ropes together with the driving electrical system. The problem of optimal control of the driving system was analyzed and modelling techniques were discussed. Kotera [1978] treated free and forced vibrations of a vertical rope with end mass and proposed an analytical method based on the method of separation of variables. Marczyk & Niziol [1979] analyzed the influence of longitudinal oscillations on the lateral behaviour of vertical hoisting ropes. The methodology developed by Goroshko & Savin [1962] was applied to construct an asymptotic solution to the problem. Model examples of calculations were presented showing the resonant behaviour of the system.

Mankowski [1982] carried out a computer simulation of the dynamic behaviour of a typical hoisting cable system. A lumped-mass model of the system was developed to describe the lateral motions of the catenary cable and the longitudinal dynamics of the vertical rope due to a kinematic excitation arising at the winder drum. Parameters of the Kloof Gold Mine winder was used to implement the numerical simulation of non-linear equations of

motion. Numerical instability was reported to occur during the simulation at a depth of approximately 800 m during the ascending cycle. This instability was attributed to the neglect of rope slip at the sheave in the simulation model and to the autoparametric resonance taking place in this depth region.

Constancon [1993] re-addressed the problem as stated by Mankowski [1982] and proposed a distributed-parameter model describing the lateral-longitudinal dynamics of the system applying the theory of travelling cables formulated by Perkins & Mote Jr. [1987]. In this study first a stationary model was used to investigate the stability of linear steady-state motion in the context of the non-linear equations of motion of the system by applying a harmonic balance method. The stability analysis established that regions of secondary resonance might occur at sum and difference combinations of the linear lateral and longitudinal natural frequencies due to autoparametric excitation. These regions were confirmed by a laboratory experiment. It was appreciated by the author that the system was non-stationary, and the stationary analysis could only serve as broad guidelines of how to avoid regions of instability in the hoisting system. A numerical simulation of equations of motion conducted in the final stage of the study, in which Kloof parameters were used, and the non-stationary nature of the system was accounted for, confirmed these reservations. It was noted that in the numerical simulation of the nominal ascending cycle, the cable tension across the sheave exceeded the limits for no slip at a depth of approximately 300 m, which violated the model assumptions and rendered the results above this depth unrealistic. In conclusion, the necessity to account for the non-stationary aspects of the winding cycle in order to achieve realistic interpretation of the observed dynamic phenomena was affirmed.

More recently Kumaniecka & Niziol [1994] presented interesting results on parametric resonance in a longitudinal-transverse model of a vertical rope with dry friction, material non-linearity and slowly varying length. They extended the research done by Marczyk and Niziol [1979] and applied the method of harmonic balance to identify parametric com-

bination resonance regions. It was found that as a result of non-linear coupling between the longitudinal and transverse modes, parametric resonance was possible, but only at high amplitudes of longitudinal motion, which could take place during emergency braking operations. Non-stationary parametric resonance was considered also by Terumichi, Ohtsuka, Yoshizawa, Fukawa, & Tsujioka [1997]. They analyzed passage through resonance in a model of a high-rise building elevator and studied vibrations of a vertical string with time-varying length and a mass-spring system attached at the lower end. The upper end was subject to a harmonic motion. The influence of the axial velocity on the transverse amplitude was examined and was shown that the amplitude decreased when the velocity was increased. The results also revealed that the higher the velocity, the larger the delay of peak amplitudes during the passage.

1.3 Objectives of the Study

A good understanding of the non-stationary nature of the dynamic behaviour of hoisting cables is essential for determining an appropriate design methodology, as well as for establishing a winding strategy, to ensure that the regions of excessive vibrational interactions are avoided during the normal and emergency operating regimes. This is particularly important in the South African mining industry, where it is currently being considered that the depth limits of rope hoisting in single-lift shafts be extended to at least 4000 m [Greenway, 1990c]. The non-stationary aspects have been analyzed in previous research work, however a strong need exists to formulate new efficient models in order to verify results of previous research and to carry out more in-depth analysis of transient resonance phenomena occurring in hoisting systems. The intention of this study is to address these issues. Thus, this thesis has the following objectives:

- The review of fundamental characteristics and methods of analysis of the dynamic response of systems with slowly varying parameters.
- The development of the non-linear mathematical model of the catenary-vertical rope hoisting system with slowly varying parameters.
- The development of a combined perturbation - numerical technique to investigate the passage through longitudinal primary resonances in the system.
- The development and the implementation of the non-linear numerical simulation of the non-linear model of the system in order to analyze the non-linear transient resonance phenomena occurring in the system.
- The formulation of recommendations for the design methodology and for the operation strategy of hoisting systems so that the adverse dynamic response is reduced during the winding cycle.

Chapter 2
Vibrations of One-Dimensional Continua with Slowly Varying Length

Physical systems such as beams, bars, strings and cables are classified in the category of one-dimensional continuous systems. In this case the displacement field depends on time and on a single spatial co-ordinate. Such elements are commonly used as structural members in engineering arrangements. Often lengths of these members vary with time in installations where an axial transport motion occurs. For example, this takes place in cable systems used to carry payloads in various transport installations. Also other axially moving continua, such as conveyor belts, magnetic tapes and band saw blades can be modelled efficiently as systems with time-varying length via an appropriate choice of co-ordinates [Goroshko & Savin, 1971]. A number of studies of vibrations in systems having members with time-varying length were conducted. These include investigations into transverse and longitudinal oscillations of mine hoisting cables [Goroshko & Savin, 1962; Savin & Goroshko, 1965; Savin & Kayuk, 1965; Goroshko & Titova, 1971; Stühler, 1978; Ögüt, 1978; Kumaniecka & Niziol; 1994], vibrations of strings with time-varying length [Vesnitzky & Potapov, 1975; Kotera, 1978; Tagata, 1983; Kevorkian & Li, 1984; Ram & Caldwell, 1996; Terumichi *et al*, 1997], and oscillations of beams of varying length [Zajaczkowski & Lipinski, 1979; Zajaczkowski & Yamada, 1980].

In many practical cases the rate of change of the length is small, and the respective system can be treated as a slowly varying system. In what follows, fundamental characteristics and equations describing the dynamic response of one-dimensional mechanical systems with slowly varying length are formulated and discussed.

2.1 Governing Equations

Consider a mechanical structure regarded as an assemblage of one-dimensional distributed subsystems (referred to as components) and acting together as a single system due to constraints imposed between adjacent subsystems. Assume that the components have time dependent lengths. The entire system is then non-stationary and its response can be described by a system of partial differential equations of the form

$$\rho_s(x)\mathbf{U}^s_{,tt} + \mathbf{L}^s[\mathbf{U}^s] = \mathbf{N}^s[\mathbf{U}] - \mathbf{C}^s[\mathbf{U}^s_{,t}] + \mathbf{F}^s(x,t,\theta_s), \quad x \in D_s(t),\ 0 \leq t < \infty, \tag{2.1}$$

with $s = 1, 2, \ldots$, where x denotes spatial material (Lagrangian) co-ordinate, $\mathbf{U}^s(x,t) = [U^s_1, U^s_2, \ldots U^s_i, \ldots]^T$ is a local (component) dynamic displacement vector representing motion of component s, $\mathbf{U} = [\mathbf{U}^{1^T}, \mathbf{U}^{2^T}, \ldots, \mathbf{U}^{s^T}, \ldots]^T$ represents global dynamic displacement vector of the entire assemblage, $(\,)_{,t}$ designates partial derivatives with respect to time, $\mathbf{L}^s$ is a local linear spatial operator. $\mathbf{N}^s$ is an operator acting upon the global displacement vector, and representing non-linear couplings and inter-component constraints in the system. $\mathbf{C}^s$ denotes a local damping operator, $\mathbf{F}^s$ is a forcing function with harmonic terms of frequency $\dot{\theta}_s = \Omega_s$, where the overdot indicates total differentiation with respect to time, and ρ_s is a local mass distribution function.

D_s is a local spatial domain. The global spatial domain is a sum of all local subdomains, namely $D = D_1 \smile D_2 \smile \cdots \smile D_s \smile \cdots$, with its components defined as

$$D_s(t) = \{x : l_{s1}(t) < x < l_{s2}(t)\}. \tag{2.2}$$

Furthermore, the displacement $\mathbf{U}^s$ is subject to the following homogeneous boundary conditions

$$\mathbf{B}^s_1[\mathbf{U}^s] = 0, \ \ at \ \ x = l_{s1}, \ \ \mathbf{B}^s_2[\mathbf{U}^s] = 0, \ \ at \ \ x = l_{s2}, \ \ s = 1, 2, \ldots \tag{2.3}$$

where $\mathbf{B}^s_1$, $\mathbf{B}^s_2$ are linear spatial differential operators.

The time-varying length of the component s is given as $L_s(t) = l_{s2}(t) - l_{s1}(t)$. When the variation of L_s, and therefore also the variation of the parameters l_{si}, $i = 1, 2$, is small over a time period corresponding to the fundamental frequency of the system considered at fixed values of these parameters, the length is said to vary slowly with time. This requires the introduction of a slow time scale τ_s, to observe the variation of l_{si}. Consider the linear

variation case, when $l_{si}(t) = l_{si}(0) + v_{si}t$, $i = 1, 2$, where $v_{si} = const$ denotes the rate of variation of l_{si}. One can introduce the non-dimensional fast time scale $T = \omega_0 t$, where ω_0 is the initial fundamental frequency of the entire system, and also the non-dimensional length $l^*_{si} = l_{si}/L_{s0}$, where $L_{s0} = l_{s2}(0) - l_{s1}(0)$. It can be shown that the time rate of variation of l^*_{si} with respect to the fast time scale is given as

$$\frac{dl^*_{si}}{dT} = \frac{v_{si}}{\omega_0 L_{s0}}. \tag{2.4}$$

Noting that the non-dimensional length of the component is $L^*_s = l^*_{s2} - l^*_{s1}$, the rate of variation of L^*_s is defined as

$$\frac{dL^*_s}{dT} = \frac{v_s}{\omega_0 L_{s0}}, \tag{2.5}$$

where $v_s = v_{s2} - v_{s1}$.

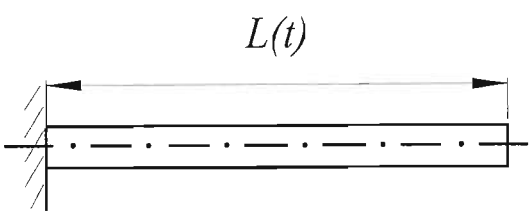

Figure 4. Uniform rod with time-varying length.

Goroshko and Savin [1971] used this non-dimensional quantity as a small parameter to assess the slow variability of length in non-stationary one-dimensional structures. They argued that in a number of cases this parameter has a simple physical interpretation. Consider for instance longitudinal oscillations of the elastic uniform rod shown in Figure 4. If the rod is of mass per unit length m, of Young's modulus E, of cross-sectional area A, and of time-varying length $L(t)$, its initial fundamental natural frequency can be determined as

$$\omega_0 = \frac{\pi}{2L_0} c, \tag{2.6}$$

where $L_0 = L(0)$, and $c = \sqrt{\frac{EA}{m}}$ defines the velocity of propagation of the longitudinal stress wave. Therefore, if the rate of change of L is denoted by v, and the frequency (2.6) is used in equation (2.5) the small parameter is given as

$$\varepsilon = \frac{2}{\pi}\frac{v}{c}, \tag{2.7}$$

and is directly related to the ratio of the rate of variation of the length of the rod and the longitudinal wave velocity.

Upon assuming that $v_{s2} > v_{s1}$ the local small parameter can be defined as

$$\varepsilon_s = \frac{v_s}{\omega_0 L_{s0}}, \tag{2.8}$$

and local slow time scale is established as $\tau_s = \varepsilon_s T$, noting that $0 < \varepsilon_s \ll 1$. It is convenient to establish a global slow time scale for the entire system as $\tau = \varepsilon T$, where ε is the smallest element in $[\varepsilon_1 \varepsilon_2 \ldots \varepsilon_s \ldots]$. Therefore, in this formulation the length of component s is expressed in terms of the slow time τ as

$$L_s(\tau) = L_{s0} + \alpha_s \tau, \tag{2.9}$$

where $\alpha_s = \frac{\varepsilon_s}{\varepsilon} L_{s0}$, so that $D_s = D_s(\tau)$.

In the approach proposed by Goroshko and Savin [1962] differential equations of the type given by the equation (2.1) were integrated over the domain $D_s(\tau)$ and an equivalent formulation in terms of integro-differential equations was formed. Global discretization of these equations was achieved by expansion in terms of eigenfunctions of the corresponding linear system. However, discretization can be applied directly to the differential equation system (2.1). Using the Rayleigh-Ritz method an approximate solution to this system can be represented by

$$U_i^s = \sum_{n=1}^{N_s} \Psi_{in}^s(x, L_s) r_{in}^s(t), \quad i = 1, 2, \ldots \tag{2.10}$$

where r_{in}^s are generalized co-ordinates, and Ψ_{in}^s are slowly varying normal free-oscillation modes of the corresponding linear undamped stationary component s. They are solutions of

$$\begin{array}{c} \mathbf{L}^s[\mathbf{\Psi}^s(x, L_s)] = \lambda^s(L_s)\rho_s\mathbf{\Psi}^s(x, L_s), \quad x \in D, \\ \mathbf{B}_1^s[\mathbf{\Psi}^s(x, L_s)] = 0, \quad at\ x = l_{s1}, \quad \mathbf{B}_2^s[\mathbf{\Psi}^s(x, L_s)] = 0, \quad at\ x = l_{s2}, \end{array} \tag{2.11}$$

where $\mathbf{\Psi}^s = [\Psi_1^s, \Psi_2^s, \ldots, \Psi_i^s, \ldots]^T$, and the parameter L_s is considered to be instantaneously frozen. The eigenvalue problem defined by (2.11) yields a denumerably infinite sequence of eigenvalues λ_{in}^s related to the natural frequencies ω_{in}^s of the sub-system s, and corresponding eigenfunctions Ψ_{in}^s, for each value of L_s. Thus, the local natural frequencies are treated as slowly varying and are considered to be functions of the slow time, namely $\omega_{in}^s = \omega_{in}^s(\tau)$.

By substituting the expansion (2.10) into (2.1), and by multiplying the result by Ψ_{ik}^s, integrating over the domain D_s, using the boundary conditions (2.3), a second-order ordinary differential equation system for the generalized coordinates is obtained. Using the fast non-dimensional time scale T, and the slow time scale τ, this system can in turn be put into the standard first-order matrix form

$$\dot{\mathbf{y}}\,(T) = \mathbf{A}\,(T, \tau; \varepsilon)\,\mathbf{y}\,(T) + \varepsilon\tilde{\mathbf{N}}\,(\tau, \mathbf{y}) + \mathbf{F}\,(T, \tau)\,, \tag{2.12}$$

in which dots designate differentiation with respect to fast time, $\mathbf{y}\,(T) = [\mathbf{r}^T, \dot{\mathbf{r}}^T]^T$ denotes the system state vector, where $\mathbf{r}\,(T) = \left[\mathbf{r}^{1^T}, \mathbf{r}^{2^T}, \ldots, \mathbf{r}^{s^T}, \ldots\right]^T$, and $\mathbf{r}^s\,(T) = [r_{11}^s, r_{12}^s, \ldots, r_{1N_s}^s, r_{21}^s, r_{22}^s, \ldots, r_{2N_s}^s, \ldots, r_{i1}^s, r_{i2}^s, \ldots, r_{iN_s}^s, \ldots]^T$, $\mathbf{A}\,(\tau; \varepsilon)$ is slowly varying linear coefficient matrix, the vector $\tilde{\mathbf{N}}\,(\tau, \mathbf{y})$ represents non-linear coupling terms, and $\mathbf{F}\,(\tau, T)$ is the external excitation vector.

The form (2.12) represents a slowly varying (non-stationary) weakly non-linear dynamic system. In this representation the system is treated as a multi-degree-of freedom system, with the natural slowly varying frequencies $\omega_1, \omega_2, \ldots, \omega_N$, where N denotes the number of degrees of freedom, and the non-linearities are assumed to be primarily quadratic and/or cubic.

2.2 The Dynamic Characteristics and Methods of Analysis

An appreciation and correct interpretation of the dynamic characteristics of a non-linear system is important for its design and control. The non-linearities are responsible for a wide range of pivotal dynamic phenomena in mechanical structures. A number of these phenomena were described and classified by Nayfeh & Mook [1995]. Mitropolskii [1965] developed fundamental concepts and methods in the analysis of non-stationary dynamic systems. A comprehensive survey of perturbation techniques to investigate resonant behaviour of non-linear oscillatory systems with slowly varying parameters was conducted by Kevorkian [1987]. Nayfeh & Balachandran [1989] presented an extensive review of research carried out and concerning possible modal and resonance interactions in dynamical systems with stationary parameters.

Important resonance phenomena and modal interactions arise when certain frequency tuning conditions take place in the system [Nayfeh & Mook, 1979]. The phenomenon of parametric resonance may arise in systems governed by differential equations with time-dependent coefficients. These coefficients form parametric excitations, and the principal parametric resonance arise when the frequency of this excitation Ω is close to twice of one of the natural frequencies of the system ($\Omega \approx 2\omega_n$). Also, combination parametric resonances may occur if, for example, $\Omega \approx \frac{\omega_m \pm \omega_n}{k}$, where k denotes an integer.

If the natural frequencies are commensurable or nearly commensurable internal (autoparametric) resonances may occur. When the non-linearity is quadratic internal resonance may occur if $\omega_n \approx 2\omega_m$ or $\omega_n \approx \omega_m \pm \omega_k$. When the non-linearity is cubic internal resonance can arise if $\omega_n \approx \omega_m$, $\omega_n \approx 3\omega_m$, $\omega_n \approx |\pm 2\omega_m \pm \omega_k|$, or $\omega_n \approx |\pm\omega_m \pm \omega_k \pm \omega_l|$. In a free multi-degree-of freedom system with an internal resonance frequency tuning, energy initially contributed to one of the modes involved in the internal resonance is continuously being exchanged between all the modes involved in that resonance. In this phenomenon

the mode with the initially imparted energy forms essentially a parametric excitation for the non-linearly coupled other modes taking part in the resonance.

In a multi-degree-of freedom system with a harmonic external excitation of frequency Ω primary resonances ($\Omega = \omega_m$), secondary resonances ($p\Omega = q\omega_m$, with p and q being integers) and combination resonances may occur. The type of combination resonance that might arise in a system depends on the order of non-linearity and on the number of modes involved. If quadratic non-linearities are present combination summed and/or difference resonances, that is $\Omega = |\pm\omega_m \pm \omega_k|$, might be excited. For a cubic non-linearity combination resonances may occur if $\Omega = |\pm\omega_m \pm \omega_k \pm \omega_l|$, $\Omega = |\pm 2\omega_m \pm \omega_k|$, or $2\Omega = |\pm\omega_m \pm \omega_k|$. Similar combination resonances might arise in parametrically excited systems. These combination resonances may lead to interactions between high- and low-frequency modes, and a high-frequency excitation may produce large-amplitude responses in the low-frequency modes involved in the combination resonance.

An internal resonance may exist in addition to an external primary resonance, or to a combination resonance. In these cases many interesting phenomena occur. For example, a saturation phenomenon might take place in the forced response of a system with quadratic non-linearities that has an internal resonance. In another case, two or more fractional harmonics might exist in the response of a system involved in a combination resonance. This phenomenon may occur in systems with quadratic or cubic non-linearities. When the internal resonance $\omega_2 \approx 2\omega_1$ and the combination resonance $\Omega \approx \omega_1 + \omega_2$ take place for a quadratic non-linearity, the fractional pair $\left(\frac{1}{3}\Omega, \frac{2}{3}\Omega\right)$ might exist in the response. Similarly, for a cubic non-linearity with the internal resonance $\omega_2 \approx 3\omega_1$ and the combination resonance $\Omega \approx \omega_2 + 2\omega_1$ the fractional pair $\left(\frac{1}{5}\Omega, \frac{3}{5}\Omega\right)$ may result.

Resonance phenomena and modal interactions in mechanical structures have been the subject of extensive research. It was widely recognized that in actual practice the parameters and dynamic characteristics of these structures are not stationary, and vary slowly with

time. However, in many cases an idealization was made that the system components were time independent and stationary models were studied. Multi-degree-of-freedom systems with parametric excitations were considered by Hsu [1963], who applied the method of variation of parameters together with the series expansion of the perturbation method to identify the regions of parametric instabilities when the parametric coupling terms were small. Ostachowicz [1979] proposed the finite element method for the dynamic analysis of mechanical structures with periodic stiffness. Combination parametric resonances in systems having multiple degrees of freedom were discussed and treated by the method of harmonic balance by Kruszewski, Gawronski, Ostachowicz, Tarnowski & Wittbrodt (1984). Nayfeh & Zavodny [1986] used the method of multiple scales to investigate the response of two-degree-of-freedom systems with quadratic non-linearities to a combination parametric resonance in the presence of two-to-one internal resonances.

An important investigation on autoparametric phenomena was conducted by Nayfeh, Mook & Marshall [1973]. They analyzed the non-linear coupling between the pitch and roll modes of ship motions with their frequencies being in the ratio of two to one. The perturbation analysis by the method of multiple scales showed that a saturation phenomenon occurred when the excitation frequency was near the pitch frequency. Namely, it was revealed that when the amplitude of the excitation was small, only the pitch mode was excited. As this amplitude increased and reached a critical value, the pitch mode became saturated and all the extra energy was transferred to the roll mode due to the internal (autoparametric) resonance.

Nayfeh, Mook & Lobitz [1974] established a numerical-perturbation method for treating non-linear structures having complicated geometry. According to this method, the problem is represented as a non-linear temporal problem, and a linear spatial problem describing the boundary conditions. The spatial problem is then solved numerically, and the temporal problem is solved by the method of multiple scales.

Autoparametric coupling effects in a beam system were studied by Roberts & Cartmell [1984]. They examined a two to one internal resonance between two bending modes of vibration in a pair of coupled cantilever beams using the method of multiple scales, and verified the perturbation analysis results by a laboratory experiment. It was shown that small non-linear coupling terms in the system had a significant effect under the condition of internal resonance. A similar two-degree-of freedom model of a beam system was also investigated by Haddow, Barr & Mook [1984], demonstrating a saturation phenomenon. These studies were extended by Cartmell & Roberts [1988]. They illustrated a complex response arising in a four-degree-of-freedom model of a cantilever beam structure with external excitation and two internal resonances, each in the form of a combination resonance, existing in close proximity to each other. The system was treated by the multiple scales method and a laboratory experiment was conducted. It was established that in addition to the saturation phenomenon, the resulting four mode interaction could exhibit non-synchronous large amplitude responses of indirectly excited modes, and that small shifts in internal tunings could noticeably affect the modal responses of the system. Interesting investigations into the theme of absorption of unwanted vibration by means of suitably arranged autoparametric interaction between the vibrating components, and an added-on absorber element were recently carried out by Cartmell & Lawson [1994].

A mechanism of the energy transfer from high- to low frequency modes was studied analytically by Nayfeh & Nayfeh [1993]. In this investigation the response of a perturbation model of a two-degree-of freedom system with cubic non-linearities, and with widely spaced modes to a harmonic excitation near the natural frequency of its high-frequency mode was presented. The system served as a paradigm for the interaction of high- and low-frequency modes, with the high natural frequency normalized to unity and the low frequency to a small positive parameter ε. This analytical study confirmed that an excitation applied to the high-frequency mode could result in large-amplitude responses in the low frequency mode, with

the mechanism of this energy transfer being neither an internal mechanism nor an external or parametric resonance. In an experimental study reported by Nayfeh & Nayfeh [1994] it was confirmed that modal interactions in systems with widely space modes do not necessarily require any special frequency relationships in the system. It was concluded that these interactions could arise whenever there exist modes whose natural frequencies are much lower than the natural frequencies of the modes being directly driven. Also, it was deduced that the interactions could occur whenever the amplitudes and phases of the high-frequency modes undergo slow modulation.

The responses of non-linear systems with non-stationary parameters and excitations are qualitatively different from the responses of stationary systems, especially in the neighbourhood of some critical values of the parameters, when transitions through resonance regions occur. The non-stationary resonance phenomena are often delayed, and frequently accompanied by beat phenomena. Hence, specialized treatment is required in order to analyze the responses of these systems. A number of studies were carried out in this area.

Agrawal & Evan-Iwanowski [1973], Agrawal [1975] and Evan-Iwanowski [1976] extended the asymptotic method developed by Bogolubov & Mitropolskii [1961] and Mitropolskii [1965] for determining resonant responses of non-stationary, non-linear multi-degree-of-freedom systems. The first approximation to the solution was established for the general case of combination resonances, with the concept of virtual work applied to define the resonance conditions. This method was applied to analyze a two-degree-of-freedom model of a gyroscopic rotor system exhibiting combination resonances, subjected to a non-stationary excitation due to unbalance.

Kevorkian [1971] considered passage through resonance in a harmonically excited single-degree-of-freedom system with slowly varying natural frequency. In this study the solution was constructed by matching two asymptotic expansions: the outer expansion away from resonance, and the inner expansion near resonance. It was shown that this approach

could also be applied to non-stationary multi-degree-of freedom systems, and the method was successfully implemented in the analysis of a mathematical model for the problem of roll build up encountered in the high altitude flight vehicles with slight aerodynamic and mass asymmetries [Kevorkian, 1974; Lewin & Kevorkian, 1978].

The theory and methodology to describe the behaviour of a system evolving slowly through internal non-linear resonance was presented by Ablowitz, Funk & Newell [1973] and Kevorkian [1980]. They investigated interactions in a two-degree-of freedom model with quadratic non-linear coupling and two to one internal resonance, and also applied outer and inner perturbation expansions together with a matching procedure. A similar problem was analyzed by Rubenfeld [1977] who adopted a modified version of the derivative-expansion method to investigate the system response.

More recently Kevorkian [1982; 1987], Bosley & Kevorkian [1991; 1992] and Bosley [1996] proposed that in order to generate an approximate solution, the slowly varying oscillatory second-order system of N equation can be transformed into a Hamiltonian standard form of $2N$ first-order differential equations using action and angle variables together with the concept of adiabatic invariance. Later perturbation techniques, namely the method of averaging or the method of multiple scales, can be applied to determine the solution.

Alternatively, the perturbation techniques can be applied directly to the second-order model. For example, using the method of multiple scales a first-order system can be obtained to compute the amplitudes and the phases for the first approximation of the response. Nayfeh & Asfar [1988] and Neal & Nayfeh [1990] used this methodology to study single-degree-of-freedom systems with non-stationary parametric excitations. This technique was also implemented by Tran & Evan-Iwanowski [1990] to study the response of the Van der Pol oscillator with non-stationary external excitation, and by Cveticanin [1991] in the analysis of non-stationary oscillations of a textile machine rotor.

In conclusion, a number of classical approximate analytical methods have been used to analyze both stationary and non-stationary non-linear dynamic systems. Usually they form a combination of a suitable perturbation method with a numerical technique. However, often systems of a more complicated nature are intractable to a perturbation analysis, and the classical approximate analysis is not adequate to predict their adverse dynamic behaviour. In these cases a direct numerical simulation of the equations of motion is the most feasible and convenient approach.

Chapter 3
Mathematical Model of a Hoisting System

A configuration of cables in typical industrial hoisting system has been described in Chapter 1. In this system, treated as an assemblage of two interactive substructures, namely of the catenary and of the vertical rope, the length of the vertical rope is varying during the wind so that the mean catenary tension is also continuously varying. Therefore, the natural frequencies of both subsystems are time-dependent and the entire structure represents a non-stationary dynamic system. Hence, vibrations of cables in the hoisting installation can be described by differential equations of the type given by equation (2.1). These differential equations of motion are formulated in what follows.

3.1 Vibrations in the Hoisting Cable

Cables in hoisting installations, due to their flexibility, are susceptible to vibrations. They are often classified as transverse and longitudinal vibrations [Dimitriou & Whillier, 1973]. Steel wire cables can also respond in torsion to applied axial load, and the torsional response is coupled with the longitudinal response [Greenway, 1990; Goroshko & Savin, 1971]. The torsional vibration may occur in cables of certain construction, for example in the triangular strand winding ropes, which have become the industry norm for some hoisting installations. The wires in the strands in these ropes are bent over a triangular center wire, as shown in Figure 5. Due to the large effective cross-sectional area this type of rope is suitable for multi-layer coiling on drum hoists [Hitchen, 1963]. It was shown by Hamilton & Greenway [1991] that the effect of the torsional coupling on the dynamic response of the triangular strand rope was not significant, and it was concluded that it can be ne-

glected in the dynamic analysis of hoisting cables. Thus, the torsional vibrations are not considered in the present analysis.

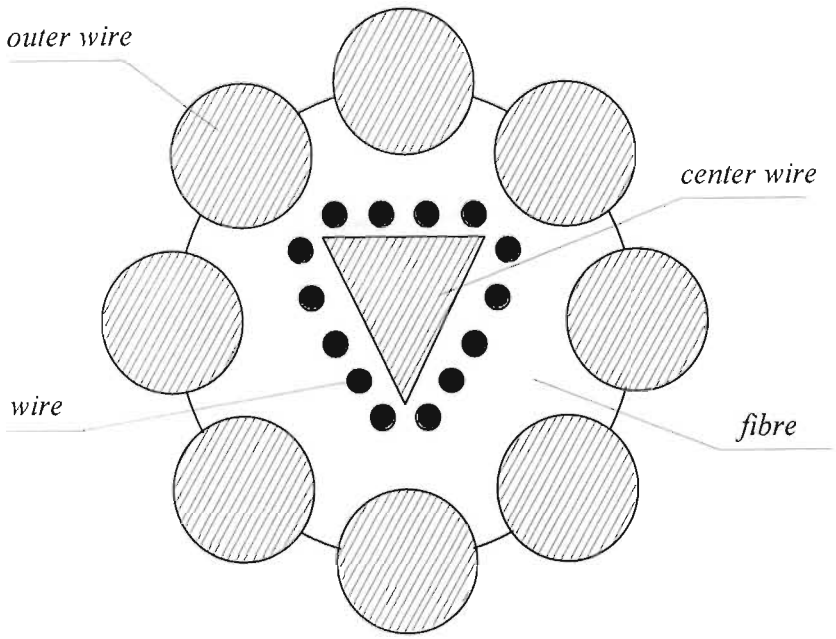

Figure 5. Strand cross-section of the triangular strand rope.

The winding cable vibrations are caused by various sources of excitation present in the system. The most significant sources are load due to the winding cycle acceleration/deceleration profile and a mechanism applied on the winder drum surface in order to achieve a uniform coiling pattern. Other sources may include motions of the headgear, shape imperfections and eccentricity of the winder drum and sheave, misalignment in the shaft steelwork, and aerodynamic effects. Some of these sources may be manifested as *external excitations* in the system, and appear as inhomogeneities in the governing differential equations, and some may lead to *parametric excitations*, which appear as coefficients in the governing differential equations.

In the catenary-vertical rope system the longitudinal vibration is usually associated with the vertical rope. This vibration affects the motion of the conveyance introducing the so called "yo-yo" type oscillation, and may also be observed at the headsheave. The inertial load due to the winding cycle acceleration/deceleration profile is primarily responsible for the longitudinal transient response. Longitudinal pulses arising due to coil cross-over zones, and also due to the cable layer change at the winder drum, cause additional longitudinal response.

The transverse oscillations are usually associated with the catenary. They often lead to the catenary whirling motion referred to as "rope whip", which may cause miscoiling at the winder drum, may lead to the cable jumping out of the sheave groove, and also to damage caused by impact of the cable against the frame of the headgear structure or against the winding house openings [Dimitriou & Whillier, 1973]. The primary sources of these oscillations are the periodic excitation due to the coil cross-over motion and the layer change pulses. The transverse vibrations are also noticeable in the vertical rope, mainly at the upper level of the shaft. Mankowski [1982] noted that they were of small amplitude and of a wide range of frequencies, and may be induced by the misalignment in the shaft steelwork or irregularities at the sheave. Also, the rope transverse vibration may result due to a parametric excitation when the dynamic tension fluctuations in the catenary are transmitted to the vertical section via the headsheve.

Interactions between various types of vibration within each subsystem exist. The sheave inertial coupling between the two subsystems also facilitates extensive interactions between the catenary and the vertical rope motions. The nature of these interactions is strongly non-linear. The lateral vibration of the catenary induces the longitudinal oscillations in the vertical system and vice-versa. Also, significant coupling between the lateral vibration of the vertical system and the lateral motion of the catenary can be observed [Constancon, 1993].

Hence, the hoisting cable system is essentially a non-linear non-stationary oscillatory system with slowly varying natural frequencies and mode shapes. The dynamic behaviour of this system is very complex, and a passage through various resonance conditions may occur during its operation.

3.2 Equations of Motion

In general, two main approaches can be distinguished in mathematical modelling of the dynamics of cable hoisting systems. In the first, a motion of the winder drum is assumed to be prescribed, usually through a known velocity or acceleration profile. In this model the driving system, usually an electric dc or ac motor, is not taken into consideration. In the second approach, in order to define the transportation motion, the dynamic characteristics of an external source of power are included into the studies. This means that additional differential equations describing the driving motor dynamic characteristics must be added to the governing differential equations of the system which result in additional degrees of freedom.

In modern installations advanced control systems are used, which allow accurately prescribed velocity and acceleration profiles of the winder drum to be realized. Therefore, the first approach is often well justified, in which the system power supply is considered to be unlimited. The winder drum is therefore treated as an *ideal source of energy*, and the system is referred to as *an ideal system*.

A model of the hoisting cable system is represented in Figure 6. In this model, the cable is divided into a horizontal catenary[2] of length $OC = L_c$ passing over a sheave of radius R,

[2] Using the justification that the effect of gravity due to a catenary inclination is small in comparison to the total quasi-static tension, this model is valid also in the case of a system with an incline catenary cable. This approximation results in a uniform mean catenary tension, and was also applied by Mankowski [1982] and by Constancon [1993].

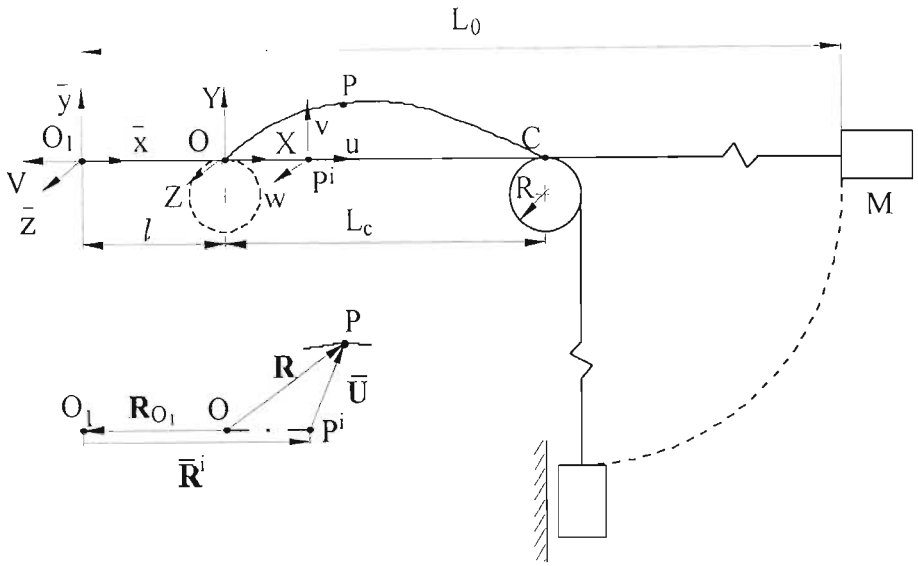

Figure 6. Model of a Catenary-Vertical Rope System.

and of mass moment of inertia I, and into a vertical rope with a mass M, representing the conveyance mass and payload, attached to its bottom end. The end O_1 of the cable is moving with a prescribed winding velocity $V(t)$ due to the cable being coiled onto a rotating cylindrical drum, so that the entire system translates axially, with the mass M being constrained in a lateral direction. The section $l = OO_1$ represents a time-varying length of this part of the cable that is already coiled onto the winder drum. The cable has a constant effective cross-sectional area A, a constant mass per unit length m, and effective Young's modulus E.

In order to describe the oscillations of the cable the classical moving frame approach is applied [de Jalon & Bayo, 1994]. Two frames of reference are established: a coordinate system $O_1\bar{x}\bar{y}\bar{z}$ attached to, and moving with the upper end of the cable, and a stationary inertial system $OXYZ$. The following fundamental assumptions are made:

1. The system is an ideal system.

2. The cable material is uniform.

3. The winder drum, headgear, sheave, conveyance, and shaft steelwork are perfectly rigid.

4. There is no cable slip on the winder drum or across the sheave.

5. The effect of torsional coupling on the dynamic response is not significant and can be neglected.

6. The catenary cable is taut and flat in its initial equilibrium configuration.[3]

7. Only longitudinal motion in the vertical subsystem is admitted.

The dynamic deformed position P of an arbitrary section of the cable during its motion is defined in the inertial frame by the position vector

$$\mathbf{R}(s,t) = \mathbf{R}_{O_1}(t) + \bar{\mathbf{R}}^i(s) + \bar{\mathbf{U}}(s,t), \tag{3.1}$$

where s denotes the Lagrangian (material) coordinate of P^i, representing the dynamically undeformed position of the cable section, and measured from the origin O_1. In this representation the axial transport motion is treated as essentially an overall rigid body translation, and the dynamic elastic deformations are referred to the moving frame associated with this

[3] The catenary profile lies very close to the chord between the drum and the sheave under the normal loading conditions due to the payload and mass of the vertical cable. Thus, the catenary tension is high and it is assumed that the catenary cable forms the limiting configuration of a taut string, with its initial curvature being, by definition, zero. Detailed discussion of this approximation is presented in Appendix D.

motion. The entire cable is prestressed, and all dynamic characteristics of the cable are functions of the independent variables (s,t), with s being referred to the prestressed state and the moving frame. The vector $\mathbf{R}_{O_1}(t) = [-l,\ 0,\ 0]^T$ represents the position of the origin O_1 in the inertial frame, $\bar{\mathbf{R}}^i = [s,\ 0,\ 0]^T$ defines the initial reference position P^i of the cable section, $\bar{\mathbf{U}} = [u(s,t),\ v(s,t),\ w(s,t)]^T$ is the dynamic displacement vector from the reference configuration, with u, v, and w representing the longitudinal, in-plane lateral, and out-of-plane lateral motion, respectively. The upper bar denotes vectors referred to the moving frame. Upon assuming that the modulus E of the cable material is high, the strain of the cable wound around the drum can be neglected [Savin & Goroshko, 1971], and the length l is then given by

$$l(t) = l(0) \pm \int_0^t V(\xi)d\xi, \tag{3.2}$$

where signs "+" and "-" correspond to ascending and descending respectively, and $l(0)$ is the initial length[4].

Taking into consideration the assumption that there is no lateral motion in the vertical rope, and denoting the longitudinal dynamic deflection in the catenary and in the vertical rope as $u_c(s,t)$ and $u_v(s,t)$, respectively, the deformed position vector is defined as

$$\mathbf{R} = \left\{ \begin{array}{l} [s + u_c(s,t) - l, v(s,t), w(s,t)]^T,\ l \le s \le L_1, \\ [s + u_v(s,t) - l, 0, 0)]^T,\ L_1 \le s \le L_0, \end{array} \right\} \tag{3.3}$$

---

[4] The exact geometric relationship should read

$$l(t) + u(l,t) = \pm \int_0^t V(\xi)\, d\xi,$$

where $u(l,t)$ denotes a longitudinal deformation of the cable wound around the drum. This expression can be differentiated with respect to t, so that

$$\dot{l}(t) = \frac{V(t)}{1 + \frac{\partial u(l,t)}{\partial s}},$$

or

$$l(t) = l(0) \pm \int_0^t \frac{V(\xi)}{1 + \frac{\partial u(l,\xi)}{\partial s}} d\xi.$$

For cables of high Young's modulus, for example for steel wire cables, the longitudinal strain is small, namely $\frac{\partial u(l,t)}{\partial s} \ll 1$, so that the approximation (3.2) can be applied.

where $L_1 = l + L_c$, and L_0 denotes the total length of the cable in the reference configuration. The continuity of deflection across the sheave requires $u_c(L_1, t) = u_v(L_1, t) = u_1$, and the dynamic elastic deflection at the vertical cable bottom end is $u_2 = u_v(L_0, t)$. The velocity vector of a cable particle P is then determined as

$$\dot{\mathbf{R}} = \left\{ \begin{array}{l} \mathbf{V}_c = [u_{c,t}(s,t) - \dot{l},\ v_{,t}(s,t),\ w_{,t}(s,t)]^T,\ \ l \le s \le L_1 \\ \mathbf{V}_v = [u_{v,t}(s,t) - \dot{l},\ 0,\ 0]^T,\ \ L_1 \le s \le L_0 \end{array} \right\} \tag{3.4}$$

where the overdot indicates total differentiation with respect to time, and $(\ )_{,t}$ denotes partial derivatives with respect to time.

3.2.1 Free Undamped Motion

The equations governing the free undamped response of the system can be derived by applying the variational approach of analytical mechanics. In this approach Hamilton's principle can be used which requires that *the measure of action, namely the time-integral* of *the difference between the kinetic and potential energies, shall be stationary* [Lanczos, 1962]. Thus, Hamilton's procedure asserts that *the actual motion realized in nature is that particular motion for which action assumes its smallest value.* Hence, the Hamilton formulation applied to the hoisting cable system yields

$$\int_{t_1}^{t_2} (\delta E - \delta \Pi_e - \delta \Pi_g)\, dt = 0, \tag{3.5}$$

where E, Π_e, and Π_g denote the system kinetic energy, the cable elastic strain energy, and the system gravitational potential energy, respectively. Upon assuming that dynamic deflections of section OO_1 of the cable can be neglected, the kinetic energy of the system is expressed as follows

$$E = \int_{l}^{L_1} \hat{E}_c(u_{c,t}, v_{,t}, w_{,t}) ds + \int_{L_1}^{L_0} \hat{E}_v(u_{v,t}) ds + E_s(\dot{q}_1) + E_M(\dot{q}_2), \tag{3.6}$$

where

$$\hat{E}_c = \frac{1}{2} m \mathbf{V}_c \cdot \mathbf{V}_c, \tag{3.7a}$$

$$\hat{E}_v = \frac{1}{2} m \mathbf{V}_v \cdot \mathbf{V}_v, \tag{3.7b}$$

$$E_s = \frac{1}{2} \frac{I}{R^2} \dot{q}_1^2, \tag{3.7c}$$

$$E_M = \frac{1}{2} M \dot{q}_2^2, \tag{3.7d}$$

where $\dot{q}_1 = u_{v,t}(L_1, t) - \dot{l}$, and $\dot{q}_2 = u_{v,t}(L_0, t) - \dot{l}$, with q_1, q_2 representing the total displacements at the sheave and at the conveyance, respectively.

The elastic strain energy of the cable is

$$\Pi_e = \Pi_e^i + \int_l^{L_1} \hat{\Pi}_c(u_{c,s}, v_{,s}, w_{,s}) ds + \int_{L_1}^{L_0} \hat{\Pi}_v(u_{v,s}) ds \tag{3.8}$$

where Π_e^i is the strain energy in the reference prestressed configuration, and

$$\hat{\Pi}_c = (T_c^i + \frac{1}{2} EA\epsilon_c)\epsilon_c, \tag{3.9a}$$

$$\hat{\Pi}_v = (T_v^i + \frac{1}{2} EA\epsilon_v)\epsilon_v, \tag{3.9b}$$

where ϵ_c and ϵ_v represent the strain measure in the catenary section and the vertical section of the cable respectively, T_c^i, and T_v^i represent the quasi-static tension in the catenary, and in the vertical cable in the reference configuration, respectively. Using the so called *large displacement approach* [Géradin & Rixen, 1994], the catenary strain measure resulting from *Green's symmetric strain tensor* is given by

$$\epsilon_c = u_{c,s} + \frac{1}{2}(v_{,s}^2 + w_{,s}^2), \tag{3.10}$$

where $(\ )_{,s}$ denotes partial differentiation with respect to s. In this non-linear strain measure large displacements generated by the rotations are accounted for, with the assumption that the axial deformations remain small. The strain measure in the vertical rope is given in the classical linear straight bar form [Géradin & Rixen, 1994], where both rotations and

displacements are assumed to be small, namely

$$\epsilon_v = u_{v,s}. \tag{3.11}$$

The gravitational potential energy of the cable expressed in terms of the dynamic deflections is given by

$$\Pi_g = \Pi_g^i - \int_{L_1}^{L_0} mgu_v ds - Mgq_2, \tag{3.12}$$

where Π_g^i is the gravitational potential energy in the undeformed reference configuration.

Hamilton's principle requires also that any virtual displacement, arbitrary between two instants t_1 and t_2, vanishes at the ends of the time interval, so that

$$\delta u_c = \delta v = \delta w = 0,\ l \leq s \leq L_1, \tag{3.13a}$$

$$\delta u_v = 0,\ l \leq s \leq L_1, \tag{3.13b}$$

$$\delta q_1 = \delta q_2 = 0, \tag{3.13c}$$

at $t = t_1$ and t_2. Inserting equations (3.6), (3.8), and (3.12) into equation (3.5) the following result is obtained

$$\int_{t_1}^{t_2} \left\{ \begin{array}{r} \int_l^{L_1} \left(\delta\hat{E}_c - \delta\hat{\Pi}_c\right) ds + \int_{L_1}^{L_0} \left(\delta\hat{E}_v - \delta\hat{\Pi}_v + mg\delta u_v\right) ds + \\ \delta E_s + \delta E_M + Mg\delta q_2 \end{array} \right\} dt = 0, \tag{3.14}$$

where

$$\delta\hat{E}_c = \frac{\partial\hat{E}_c}{\partial u_{c,t}}\delta u_{c,t} + \frac{\partial\hat{E}_c}{\partial v_{,t}}\delta v_{,t} + \frac{\partial\hat{E}_c}{\partial w_{,t}}\delta w_{,t}, \tag{3.15a}$$

$$\delta\hat{\Pi}_c = \frac{\partial\hat{\Pi}_c}{\partial u_{c,s}}\delta u_{c,s} + \frac{\partial\hat{\Pi}_c}{\partial v_{,s}}\delta v_{,s} + \frac{\partial\hat{\Pi}_c}{\partial w_{,s}}\delta w_{,s}, \tag{3.15b}$$

$$\delta\hat{E}_v = \frac{\partial\hat{E}_c}{\partial u_{v,t}}\delta u_{v,t}, \tag{3.15c}$$

$$\delta\hat{\Pi}_v = \frac{\partial\hat{\Pi}_v}{\partial u_{v,s}}\delta u_{v,s}, \tag{3.15d}$$

$$\delta E_s = \frac{\partial E_s}{\partial \dot{q}_1}\delta\dot{q}_1, \tag{3.15e}$$

$$\delta E_M = \frac{\partial E_M}{\partial \dot{q}_2}\delta\dot{q}_2. \tag{3.15f}$$

Upon assuming that the operators δ and $\partial/\partial t$, as well as δ and $\partial/\partial s$, are commutative, and also that integration with respect to t and s are interchangeable, integrating by parts in (3.14) both with respect to s and t, accounting for (3.13a)-(3.13c), and noting that

$$\begin{aligned} &\delta u_c(l,t) = \delta v(l,t) = \delta w(l,t) = 0,\\ &\delta v(L_1,t) = \delta w(L_1,t) = 0,\\ &\delta u_c(L_1,t) = \delta u_v(L_1,t) = \delta q_1,\\ &\delta u_v(L_0,t) = \delta q_2, \end{aligned} \tag{3.16}$$

the following result is obtained

$$\int_{t_1}^{t_2}\left\{\begin{array}{l} \int_l^{L_1}\left\{\begin{array}{l}\left[-\frac{\partial}{\partial t}\left(\frac{\partial \hat{E}_c}{\partial u_{c,t}}\right)+\frac{\partial}{\partial s}\left(\frac{\partial \hat{\Pi}_c}{\partial u_{c,s}}\right)\right]\delta u_c+\\ \left[-\frac{\partial}{\partial t}\left(\frac{\partial \hat{E}_c}{\partial v_{,t}}\right)+\frac{\partial}{\partial s}\left(\frac{\partial \hat{\Pi}_c}{\partial v_{,s}}\right)\right]\delta v+\\ \left[-\frac{\partial}{\partial t}\left(\frac{\partial \hat{E}_c}{\partial w_{,t}}\right)+\frac{\partial}{\partial s}\left(\frac{\partial \hat{\Pi}_c}{\partial w_{,s}}\right)\right]\delta w\end{array}\right\}ds+\\ \int_{L_1}^{L_0}\left[-\frac{\partial}{\partial t}\left(\frac{\partial \hat{E}_v}{\partial u_{v,t}}\right)+\frac{\partial}{\partial s}\left(\frac{\partial \hat{\Pi}_v}{\partial u_{v,s}}\right)+mg\right]\delta u_v ds+\\ \left[\left(\frac{\partial \hat{\Pi}_v}{\partial u_{v,s}}-\frac{\partial \hat{\Pi}_c}{\partial u_{c,s}}\right)_{s=L_1}-\frac{d}{dt}\left(\frac{\partial E_s}{\partial \dot{q}_1}\right)\right]\delta q_1+\\ \left[Mg-\frac{d}{dt}\left(\frac{\partial E_M}{\partial \dot{q}_2}\right)-\left(\frac{\partial \hat{\Pi}_v}{\partial u_{v,s}}\right)_{s=L_0}\right]\delta q_2 \end{array}\right\}dt = 0 \tag{3.17}$$

The virtual displacements δu_c, δv, δw, δu, δu_v, δq_1,and δq_2 are arbitrary, and the equation (3.17) can be satisfied for all values of the virtual displacements if and only if

$$-\frac{\partial}{\partial t}\left(\frac{\partial \hat{E}_c}{\partial u_{c,t}}\right)+\frac{\partial}{\partial s}\left(\frac{\partial \hat{\Pi}_c}{\partial u_{c,s}}\right)=0,\ l<s<L_1, \tag{3.18}$$

$$-\frac{\partial}{\partial t}\left(\frac{\partial \hat{E}_c}{\partial v_{,t}}\right)+\frac{\partial}{\partial s}\left(\frac{\partial \hat{\Pi}_c}{\partial v_{,s}}\right)=0,\ l<s<L_1, \tag{3.19}$$

$$-\frac{\partial}{\partial t}\left(\frac{\partial \hat{E}_c}{\partial w_{,t}}\right)+\frac{\partial}{\partial s}\left(\frac{\partial \hat{\Pi}_c}{\partial w_{,s}}\right)=0,\ l<s<L_1, \tag{3.20}$$

$$-\frac{\partial}{\partial t}\left(\frac{\partial \hat{E}_v}{\partial u_{v,t}}\right)+\frac{\partial}{\partial s}\left(\frac{\partial \hat{\Pi}_v}{\partial u_{v,s}}\right)+mg=0,\ L_1<s<L_0, \tag{3.21}$$

$$-\frac{d}{dt}\left(\frac{\partial E_s}{\partial \dot{q}_1}\right)+\left(\frac{\partial \hat{\Pi}_v}{\partial u_{v,s}}-\frac{\partial \hat{\Pi}_c}{\partial u_{c,s}}\right)_{s=L_1}=0, \tag{3.22}$$

$$-\frac{d}{dt}\left(\frac{\partial E_M}{\partial \dot{q}_2}\right)-\left(\frac{\partial \hat{\Pi}_v}{\partial u_{v,s}}\right)_{s=L_0}+Mg=0. \tag{3.23}$$

Equations (3.18)-(3.21) are the equations of motion for the system, and equations (3.22)-(3.23) represent the longitudinal boundary conditions.

Substituting equations (3.7a)-(3.7d), and (3.9a)-(3.9b) together with (3.10) and (3.11) into the equations (3.18)-(3.23) yields the non-linear equations of motion

$$m(u_{c,tt}-\ddot{l})-EA[u_{c,s}+\frac{1}{2}(v_{,s}^2+w_{,s}^2)]_{,s}-T_{c,s}^i=0,\quad l<s<L_1, \tag{3.24}$$

$$mv_{,tt}-EA\left\{\left[u_{c,s}+\frac{1}{2}(v_{,s}^2+w_{,s}^2)\right]v_{,s}\right\}_{,s}-T_c^i v_{,ss}-T_{c,s}^i v_{,s}=0,\quad l<s<L_1, \tag{3.25}$$

$$mw_{,tt}-EA\left\{\left[u_{c,s}+\frac{1}{2}(v_{,s}^2+w_{,s}^2)\right]w_{,s}\right\}_{,s}-T_c^i w_{,ss}-T_{c,s}^i w_{,s}=0,\quad l<s<L_1, \tag{3.26}$$

$$m(u_{v,tt}-\ddot{l})-EAu_{v,ss}-T_{v,s}^i-mg=0,\quad L_1<s<L_0, \tag{3.27}$$

$$\frac{I}{R^2}\left[(u_{v,tt}+u_{v,st}\dot{l})_{s=L_1}-\ddot{l}\right]+EA(\epsilon_c-\epsilon_v)_{s=L_1}+(T_c^i-T_v^i)_{s=L_1}=0, \tag{3.28}$$

$$M\left[(u_{v,tt})_{s=L_0}-\ddot{l}\right]+EA(u_{v,s})_{s=L_0}+(T_v^i)_{s=L_0}-Mg=0. \tag{3.29}$$

In this non-linear system, the equations (3.24)-(3.27) describe the dynamics of the catenary and the vertical rope, the equation (3.28) represents the balance of forces across the sheave, and the last equation (3.29) defines motion of the end mass.

The equations governing the reference configuration can be extracted from the system (3.24)-(3.29) by setting all time derivatives and the dynamic strain components to zero. The following conditions result

$$T_{c,s}^i = 0, \tag{3.30}$$

$$T_{v,s}^i+mg = 0, \tag{3.31}$$

$$(T_c^i-T_v^i)_{s=L_1} = 0, \tag{3.32}$$

$$(T_v^i)_{s=L_0}-Mg = 0. \tag{3.33}$$

Integrating equation (3.31) yields

$$T_v^i(s) = T_v^i(L_1) - mg(s - L_1). \tag{3.34}$$

Furthermore, it results from (3.30) and from (3.31) that the mean (quasi-static) catenary tension is uniform over its entire length, and that this tension is equal to the vertical rope mean tension at the sheave, that is

$$T_c^i = T_v^i(L_1). \tag{3.35}$$

Thus, using (3.35) in (3.34), and accounting for the condition (3.33) yields the following expression for the catenary tension

$$T_c^i(l) = Mg + mg[L_0 - L_1]. \tag{3.36}$$

Consequently, when the result (3.36) is used in (3.34), the vertical rope tension is given as

$$T_v^i(s) = Mg + mg(L_0 - s), \quad L_1 \leq s \leq L_0. \tag{3.37}$$

It is possible to reduce the differential equations of motion (3.24)-(3.29). The longitudinal inertia term $m(u_{c,tt} - \ddot{l})$ can be neglected in equation (3.24) upon assuming that the catenary cable stretches in a *quasi-static* manner [Perkins, 1992]. This simplification, applied also by Luongo, Rega & Vestroni [1984] and Watzky [1992], is a consequence of the fact that the longitudinal wave speed is large, and greatly exceeds that of the lateral waves. Therefore, taking into account the condition (3.30), equation (3.24) can be integrated once to give

$$u_{c,s} + \frac{1}{2}(v_{,s}^2 + w_{,s}^2) = e(t), \tag{3.38}$$

where $e(t)$ represents the spatially uniform catenary strain. Hence, the following equations describe the lateral dynamics of the catenary

$$mv_{,tt} - EAe(t)v_{,ss} - T_c^i v_{,ss} = 0, \tag{3.39}$$

$$mw_{,tt} - EAe(t)w_{,ss} - T_c^i w_{,ss} = 0, \tag{3.40}$$

which are defined over the spatial interval $l < s < L_1$, with $0 \leq t < \infty$. It is assumed at this stage that lateral motions, both at the drum and the sheave ends, are not allowed. This results in trivial boundary conditions for v and w at $s = l,\ L_1$, respectively.

Treating the sheave and the end mass M as additional inertial loads applied to the system, and using the conditions (3.31)-(3.33), the following dynamic model of the vertical rope subsystem results

$$\rho(s)u_{v,tt} - EAu_{v,ss} = \rho(s)\ddot{l} - M_S u_{v,st}\dot{l}\delta(s - L_1), \tag{3.41}$$

where $L_1^- < s < L_0^+,\ 0 \leq t < \infty$, with the boundary conditions

$$EA\left[e(t) - u_{v,s}(L_1^-, t)\right] = 0, \tag{3.42a}$$

$$EAu_{v,s}(L_0^+, t) = 0, \tag{3.42b}$$

where $M_S = \frac{I}{R^2}$ is the effective mass of the sheave, $e(t)$ is given by ((3.38)), δ is the Dirac delta function, L_1^- denotes the point immediately to the left of M_S, L_0^+ is the point immediately to the right of M, and the mass distribution function $\rho(s)$ is defined as

$$\rho = m + M_S\delta(s - L_1) + M\delta(s - L_0). \tag{3.43}$$

Thus, in this formulation the vertical subsystem is modeled as constrained by the catenary at $s = L_1^-$, free at $s = L_0^+$, and acted upon by an inertial load due to the axial transport motion.

3.2.2 Boundary excitation

The cable cross-over motion at the drum results in additional longitudinal, in-plane lateral, and out-of-plane lateral displacements at $s = l$, relative to the overall rigid body translation. This results in a boundary excitation, which can be accounted for by suitable formulation of boundary conditions at $s = l$. Thus, for the longitudinal motion the boundary condition

should read

$$u_c(l,t) = u_l(t), \tag{3.44}$$

and for the lateral motions the boundary conditions are formulated as

$$\begin{aligned} v(l,t) &= v_l(t), \\ w(l,t) &= w_l(t), \end{aligned} \tag{3.45}$$

where $u_l(t)$, $v_l(t)$, and $w_l(t)$ are periodic functions prescribed by the geometry of the cross-over zones.

The inertial load in the in-plane and out-of-plane lateral direction due to the cross-over geometry can be accommodated via a suitable coordinate transformation, with the cross-over displacements being regarded as additional rigid-body translations in the lateral directions. Since the catenary is constrained in the lateral directions at the sheave end, these translations vary from v_l and w_l respectively at the drum, to zero at the sheave. Thus the absolute displacements v and w can be expressed as

$$v(s,t) = \bar{v}(s,t) + v_l(1 - \frac{s-l}{L_c}) \tag{3.46}$$

$$w(s,t) = \bar{w}(s,t) + w_l(1 - \frac{s-l}{L_c}) \tag{3.47}$$

where $\bar{v}$ and $\bar{w}$ represent displacements relative to the rigid-body motions in the lateral directions. It follows from (3.46) and (3.47) that

$$\begin{aligned} v_{,s} &= \bar{v}_{,s} - \tfrac{v_l}{L_c}, \\ w_{,s} &= \bar{w}_{,s} - \tfrac{w_l}{L_c}, \end{aligned} \tag{3.48}$$

$$\begin{aligned} v_{,ss} &= \bar{v}_{,ss}, \\ w_{,ss} &= \bar{w}_{,ss}, \end{aligned} \tag{3.49}$$

and also that

$$\begin{aligned} v_{,tt} &= \bar{v}_{,tt} + \ddot{v}_l(1 - \tfrac{s-l}{L_c}) + 2\dot{v}_l\tfrac{\dot{l}}{L_c} + v_l\tfrac{\ddot{l}}{L_c}, \\ w_{,tt} &= \bar{w}_{,tt} + \ddot{w}_l(1 - \tfrac{s-l}{L_c}) + 2\dot{w}_l\tfrac{\dot{l}}{L_c} + w_l\tfrac{\ddot{l}}{L_c}. \end{aligned} \tag{3.50}$$

Inserting (3.49) and (3.50) into (3.39) and (3.40) respectively, the catenary dynamics is described by equations

$$m\bar{v}_{,tt} - T_c^i\bar{v}_{,ss} = EAe(t)\bar{v}_{,ss} + F_v(s,t), \tag{3.51a}$$

$$m\bar{w}_{,tt} - T_c^i\bar{w}_{,ss} = EAe(t)\bar{w}_{,ss} + F_w(s,t), \tag{3.51b}$$

defined over the spatial interval $l < s < L_1^-$, with trivial boundary conditions for $\bar{v}$ and $\bar{w}$ at $s = l, L_1$, and where the inertial loads F_v and F_w are defined as

$$\begin{aligned} F_v(s,t) &= -m\left[\ddot{v}_l(1-\tfrac{s-l}{L_c}) + 2\dot{v}_l\tfrac{\dot{l}}{L_c} + v_l\tfrac{\ddot{l}}{L_c},\right], \\ F_w(s,t) &= -m\left[\ddot{w}_l(1-\tfrac{s-l}{L_c}) + 2\dot{w}_l\tfrac{\dot{l}}{L_c} + w_l\tfrac{\ddot{l}}{L_c}\right]. \end{aligned} \tag{3.52}$$

The catenary strain e can be determined from equation (3.38), which can be re-written as

$$u_{c,s} = e(t) - \frac{1}{2}(v_{,s}^2 + w_{,s}^2). \tag{3.53}$$

Integrating (3.53) and using the boundary condition (3.44) gives

$$u_c(s,t) = u_l(t) + (s-l)e(t) - \frac{1}{2}\int_l^s (v_{,s}^2 + w_{,s}^2)ds. \tag{3.54}$$

Consequently, when the continuity of longitudinal deflection across the sheave is accounted for, the following results

$$e(t) = \frac{1}{L_c}\left[u_v(L_1,t) - u_l(t) + \frac{1}{2}\int_l^{L_1}(v_{,s}^2 + w_{,s}^2)ds\right]. \tag{3.55}$$

When the boundary conditions (3.45) are used together with the transformation (3.48) the catenary strain is given as

$$e(t) = \frac{1}{L_c}\left[u_v(L_1,t) - u_l + \frac{1}{2}\int_l^{L_1}(\bar{v}_{,s}^2 + \bar{w}_{,s}^2)ds + \frac{1}{2L_c}(v_l^2 + w_l^2) - \frac{1}{L_c}\int_l^{L_1}(v_l\bar{v}_{,s} + w_l\bar{w}_{,s})ds\right]. \tag{3.56}$$

This result can be accommodated in the boundary condition (3.42a) as follows

$$k_c u_v(L_1^-,t) - EAu_{v,s}(L_1^-,t) = k_c[u_l(t) - f_c(t)], \tag{3.57}$$

where $k_c = \frac{EA}{L_c}$, and

$$f_c(t) = \frac{1}{2}\int_l^{L_1}(\bar{v}_{,s}^2 + \bar{w}_{,s}^2)ds + \frac{1}{2L_c}(v_l^2 + w_l^2) - \frac{1}{L_c}\int_l^{L_1}(v_l\bar{v}_{,s} + w_l\bar{w}_{,s})ds. \tag{3.58}$$

Consequently, the dynamic model of the vertical rope is formulated as

$$\rho(s)u_{v,tt} - EAu_{v,ss} = \rho(s)\ddot{l} + \left\{k_c[u_l(t) - f_c(t)] - M_S u_{v,st}\dot{l}\right\}\delta(s - L_1), \tag{3.59}$$

for $L_1^- < s < L_0^+$, with the homogeneous boundary conditions

$$k_c u_v(L_1^-, t) - EAu_{v,s}(L_1^-, t) = 0, \tag{3.60a}$$

$$EAu_{v,s}(L_0^+, t) = 0, \tag{3.60b}$$

Hence, the undamped response of the hoisting cable system is defined by equations (3.51a) and (3.51b) for the catenary cable ($l < s < L_1^-$), with trivial boundary conditions, and by equation (3.59) for the vertical system ($L_1^- < s < L_0^+$), with boundary conditions (3.60a)-(3.60b). In this formulation the vertical system is modeled as a system constrained at $s = L_1^-$ by a linear spring of constant k_c, representing the longitudinal elastic catenary effects, and free at $s = L_0^+$. This system is acted upon by an inertial load due to the transport motion, and is subjected to the boundary excitation and to an elastic force resulting from the catenary lateral strain.

3.2.3 Damping Model

The correct definition of damping in the system presents a difficult problem, as both lateral and longitudinal damping mechanisms in hoisting steel wire cables are complex phenomena. However, it is a recognized practice to replace resisting forces of a complicated nature by equivalent viscous damping for purposes of analysis [Timoshenko, Young & Weaver 1974; Tse, Morse & Hinkle, 1978]. The equivalent damping coefficients can then be determined from energy considerations and through an experiment. For example, Kumaniecka & Niziol [1994] considered the combination of viscous and dry friction damping in a steel wire rope, and found the equivalent viscous damping coefficient from the equality of the energy dissipated by dry friction forces, and the energy dissipated by the equivalent viscous damping

forces over one period of vibration. A brief discussion regarding the equivalent viscous damping is presented in Appendix E.

The viscous damping distributed force in a continuous structural member can be given in the following form

$$F_c = -\mathcal{C}[U_{,t}], \tag{3.61}$$

where $\mathcal{C}$ is a linear damping operator, and U denotes the displacement. The special case of viscous damping known as proportional damping has the advantage of being particularly convenient to analyze. In this case the operator $\mathcal{C}$ is a linear combination of the stiffness operator $\mathcal{L}$ and of the mass distribution function ρ, and is given as

$$\mathcal{C} = \alpha_1 \mathcal{L} + \alpha_2 \rho, \tag{3.62}$$

where α_1 and α_2 are coefficients of damping. In this model the first term in the operator (3.62) can accommodate internal damping effects, often modeled as proportional to the rate of strain in the structure and referred to as Kelvin-Voigt damping [Inman, 1994]. The second term may account for the external damping, such as air damping for example. When modal analysis is applied the modal damping ratio defined as

$$\varsigma_n = \frac{1}{2}(\alpha_1 \omega_n + \frac{\alpha_2}{\omega_n}) \tag{3.63}$$

where ω_n is the n^{th} natural frequency, represents the damping effect on the n^{th} mode. When $\alpha_2 = 0$ (while $\alpha_1 > 0$) the resulting damping model is referred to as *relative damping*. In this case the damping ratio in each mode is proportional to the corresponding natural frequency, which means that the responses of the higher modes will be more rapidly damped than those of the lower modes. On the other hand, when $\alpha_1 = 0$ (while $\alpha_2 > 0$) the resulting model is often called *absolute damping*. In this model the damping ratio is inversely proportional to the corresponding natural frequency, so that the lower modes will be damped more strongly that the higher modes. Hence, the *relative damping* and the *absolute damping* represent extreme cases which, when combined together into the general proportional model

(3.62), the most representative damping model arises for the dynamic response analysis of structures.

Following this approach, the catenary lateral damping forces are introduced as

$$F_{cv} = -C_l[\bar{v}_{,t}], \tag{3.64a}$$

$$F_{cw} = -C_l[\bar{w}_{,t}], \tag{3.64b}$$

where the lateral damping operator is defined as

$$C_l = -\lambda_1 T_c^i \frac{\partial^2}{\partial s^2} + \lambda_2 m, \tag{3.65}$$

where λ_1 and λ_2 are constant coefficients of lateral damping. Similarly, the vertical rope damping force can be expressed as

$$F_{cu} = -C_u[u_{v,t}], \tag{3.66}$$

where

$$C_u = -\mu_1 EA \frac{\partial^2}{\partial s^2} + \mu_2 \rho, \tag{3.67}$$

where μ_1 and μ_2 are coefficients of longitudinal damping.

Thus, when the damping terms are taken into consideration, the response of the system is governed by the following equations

$$m\bar{v}_{,tt} - \lambda_1 T_c^i \bar{v}_{,sst} + \lambda_2 m\bar{v}_{,t} - T_c^i \bar{v}_{,ss} = EAe(t)\bar{v}_{,ss} + F_v(s,t), \tag{3.68}$$

$$m\bar{w}_{,tt} - \lambda_1 T_c^i \bar{w}_{,sst} + \lambda_2 m\bar{w}_{,t} - T_c^i \bar{w}_{,ss} = EAe(t)\bar{w}_{,ss} + F_w(s,t), \tag{3.69}$$

$$\rho u_{v,tt} - \mu_1 EA u_{v,sst} + \mu_2 \rho u_{v,t} - EA u_{v,ss} = \rho \ddot{l} + \left\{ k_c[u_l(t) - f_c(t)] - M_S u_{v,st} \dot{l} \right\} \delta(s - L_1), \tag{3.70}$$

where the lateral equations of motion (3.68) and (3.69) are defined over $l < s < L_1^-$ with trivial boundary conditions, and the longitudinal equation of motion (3.70) is defined over $L_1^- < s < L_0^+$ with the boundary conditions remaining in the form of equations (3.60a)-(3.60b).

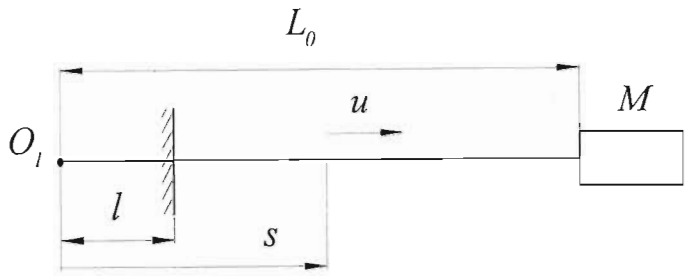

Figure 7. Simplified longitudinal model of a hoisting cable.

Chapter 4
Longitudinal Dynamics

An analysis of the longitudinal dynamics of hoisting cables is essential to understand the main characteristics of the dynamic behaviour of this system and to predict the dynamic loads that occur in winding ropes. These loads arise during normal and emergency operating conditions, and a knowledge of their amplitudes is fundamental to the definition of safety factors during hoisting.

A simplified longitudinal model of a hoisting cable is shown in Figure 7. This model has been used extensively in the analysis of vibration phenomena in hoisting systems. The equation of longitudinal motion of this system can be obtained from equations (3.24), and (3.27)-(3.29), with the catenary lateral motions and the sheave inertia neglected. Noting the conditions (3.30)-(3.33), and combining the catenary motion u_c and the vertical rope motion u_v into a single variable u, the following equation of motion results

$$\bar{\rho}(s)u_{,tt} - EAu_{,ss} = \bar{\rho}(s)\ddot{l}, \quad l < s < L_0^+, \tag{4.1}$$

where $\bar{\rho} = m + M\delta(s - L_0)$ denotes the mass distribution function. Accounting for the longitudinal boundary excitation (3.44), and noting that the end mass M is accommodated in the mass distribution function, the boundary conditions are given as

$$u(l,t) = f_l(t), \tag{4.2}$$

$$EAu_{,s}(L_0^+,t) = 0, \tag{4.3}$$

where $f_l(t)$ denotes boundary excitation function[5]. The mean catenary and vertical cable tensions are then defined by equations (3.36) and (3.37), respectively. Regarding the longitudinal boundary excitation as an additional rigid-body translation the substitution

$$u(s,t) = \bar{u}(s,t) + u_l(t) \tag{4.4}$$

accommodates this excitation as an additional inertial load in the equation of motion. Therefore, when the proportional damping model with the operator (3.67) is used over the domain $l < s < L_0^+$, the variable transformation (5.31) leads to the following equation

$$\bar{\rho}(s)\bar{u}_{,tt} - \mu_1 EA\bar{u}_{,sst} + \mu_2\rho\bar{u}_{,t} - EA\bar{u}_{,ss} = \bar{\rho}(s)\left(\ddot{l} - \ddot{u}_l\right), \quad l < s < L_0^+, \tag{4.5}$$

with the homogeneous boundary conditions

$$\bar{u}(l,t) = 0, \tag{4.6}$$

$$EA\bar{u}_{,s}(L_0^+,t) = 0. \tag{4.7}$$

In order to accommodate the sheave inertia in the longitudinal response of the vertical rope, it is convenient to assume the quasi-static catenary strain model, and to use equation (3.70). If the lateral catenary motion is not accounted for this equation yields

$$\rho u_{v,tt} - \mu_1 EAu_{v,sst} + \mu_2\rho u_{v,t} - EAu_{v,ss} = f(s,t) + \left[k_c u_l(t) - M_S u_{v,st}\dot{l}\right]\delta(s-L_1), \tag{4.8}$$

where $f(s,t) = \rho\ddot{l}$, and the boundary conditions are given by equations (3.60a)-(3.60b).

4.1 Longitudinal Discrete Model

[5] This function can be assumed in the form of a periodic excitation prescribed by the geometry of the drum cross-over zones, as suggested earlier in equation (3.44). However, other boundary phenomena can be also accommodated in this formulation. Goroshko & Savin [1971] considered slip and non-slip conditions at the winder drum for example.

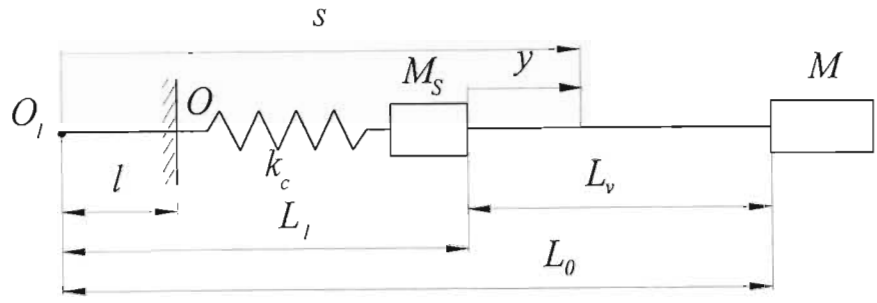

Figure 8. Longitudinal model of a vertical rope.

In order to determine the longitudinal response during the entire winding cycle an approximate solution to the equations of motion can be sought using the Rayleigh-Ritz method.

Hence, for the simplified model (4.5) the motion is assumed in the form

$$\bar{u} = \sum_{n=1}^{N_{long}} \bar{Y}_n(s,l)\bar{z}_n(t), \tag{4.9}$$

where $\bar{z}_n(t)$ are generalized co-ordinates, and $\bar{Y}_n$ can be specified as

$$\bar{Y}_n = \sin\bar{\gamma}_n(s-l), \tag{4.10}$$

and are free-oscillation modes of the system with l being instantaneously frozen, and $\bar{\gamma}_n$ are the eigenvalues of the frozen system calculated from the transcendental equation

$$\bar{\gamma}_n \tan\bar{\gamma}_n(L_0 - l) = \frac{m}{M}. \tag{4.11}$$

This formulation can be used successfully to study transient resonance phenomena in a hoisting cable [Kaczmarczyk, 1997a]. The functions $\bar{Y}_n$ defined by (4.10) are essentially eigenfunctions of the corresponding frozen system. However, it is possible to use another class of functions, namely admissible functions[6] in the series (4.9). It can be shown [Kaczmarczyk,

[6] In the differential eigenvalue problem three classes of functions of special interest can be distinguished [Meirovitch, 1990]: *eigenfunctions*, *comparison functions,* and *admissible functions*. There are two types of boundary conditions, namely *geometric conditions* and *natural conditions*. The first type accounts for a gemet-

1994] that so called *cable functions* defined by the determinant

$$\bar{Y}_n(s,l) = det \begin{bmatrix} s-l & \frac{(s-l)^2}{L_0-l} & \cdots & \frac{(s-l)^n}{(L_0-l)^{n-1}} \\ b_3 & b_4 & \cdots & b_{n+2} \\ \vdots & \vdots & \vdots & \vdots \\ b_{n+1} & b_{n+2} & \cdots & b_{n+n} \end{bmatrix} \tag{4.12}$$

where $b_n = M + \frac{m(L_0-l)}{n}$, $n = 1, 2, ..., N_{long}$ present a convenient set of admissible functions. They form a complete orthogonal set with a weight $\bar{\rho}(s)$

$$\int_l^L \bar{\rho}(s) Y_r(s,l) Y_n(s,l) dx = 0, \; r \neq n, \tag{4.13}$$

and also, over a wide range of values of the ratio $m(L_0 - l)/M$, represent a good approximation to the free-oscillation modes of the frozen system. Therefore, a fast rate of convergence is guaranteed by the series (4.9).

In many industrial hoisting arrangements the sheave inertia is substantial and should not be neglected in the dynamic analysis, as it may considerably affect the response of the entire system. Therefore, the present study of the longitudinal dynamics is focused on the formulation given by equation (4.8), where the catenary cable is modeled as a non-inertial spring element of constant k_c, and the sheave is represented by an effective mass M_S in the mass distribution function ρ, which results in an additional inertial load due to the axial transport motion. Thus, using the Rayleigh-Ritz method the vertical rope motion is approximated by the series

$$u_v = \sum_{n=1}^{N_{long}} Y_n(s,l) z_n(t), \tag{4.14}$$

---

ric condition at the boundary (zero displacement or zero slope, for example), and the second type reflects force or moment balance at the boundary. The eigenfunctions satisfy all the boundary conditions and the differential equation of the eigenvalue equation. The class of comparison functions consists of arbitrary functions which satisfy all the boundary conditions, but not necessarily the differential equation. This class is larger than the class of eigenfunctions corresponding to the eigenvalue problem. Admissible functions are any arbitrary functions satisfying only the geometric boundary conditions, and form a far larger class of functions than the class of comparison functions.

where $z_n(t)$ are generalized co-ordinates, and Y_n are free-oscillation modes of the corresponding system constrained at $s = L_1^-$ by the catenary spring, with the parameter l considered to be instantaneously frozen, as shown in Figure 8. These modes are given by the following equation

$$Y_n(s,l) = \cos\gamma_n y(s,l) + \left(\frac{1}{L_c\gamma_n} - \gamma_n\frac{M_S}{m}\right)\sin\gamma_n y(s,l), \tag{4.15}$$

where $\gamma_n = \frac{\omega_n(l)}{c}$, with $c = \sqrt{\frac{EA}{m}}$, and ω_n represents the longitudinal natural frequency, and $y = s - L_1$. The eigenvalues γ_n are determined from the following frequency equation

$$\left(\frac{1}{L_c} - \frac{M_S}{m}\gamma_n^2\right)\left(\cos\gamma_n L_v - \frac{M}{m}\gamma_n\sin\gamma_n L_v\right) - \gamma_n\left(\frac{M}{m}\gamma_n\cos\gamma_n L_v + \sin\gamma_n L_v\right) = 0, \tag{4.16}$$

where $L_v = L_0 - L_1$. The details of this eigenvalue problem are given in Appendix A.

The representation (4.14) results in the following expressions for partial derivatives of u_v

$$u_{v,t} = \sum_{n=1}^{N_{lat}}\left(\frac{\partial Y_n}{\partial l}\dot{l}z_n + Y_n\dot{z}_n\right), \tag{4.17}$$

$$u_{v,tt} = \sum_{n=1}^{N_{long}}\left[\left(\frac{\partial^2 Y_n}{\partial l^2}\dot{l}^2 + \frac{\partial Y_n}{\partial l}\ddot{l}\right)z_n + 2\frac{\partial Y_n}{\partial l}\dot{l}\dot{z}_n + Y_n\ddot{z}_n\right], \tag{4.18}$$

$$u_{v,ss} = \sum_{n=1}^{N_{long}} Y_n'' z_n, \tag{4.19}$$

$$u_{v,st} = \sum_{n=1}^{N_{long}}\left(\frac{\partial Y_n'}{\partial l}\dot{l}z_n + Y_n'\dot{z}_n\right),\ u_{v,sst} = \sum_{n=1}^{N_{long}}\left(\frac{\partial Y_n''}{\partial l}\dot{l}z_n + Y_n''\dot{z}_n\right). \tag{4.20}$$

It can be also found from equation (4.15) that

$$Y_n' = -\gamma_n\left[\sin\gamma_n y - \left(\frac{1}{L_c\gamma_n} - \frac{M_S}{m}\gamma_n\right)\cos\gamma_n y\right], \tag{4.21a}$$

$$\frac{\partial Y_n'}{\partial l} = -\left(\frac{d\gamma_n}{dl}y - \gamma_n\right)\left[\gamma_n\cos\gamma_n y + \left(\frac{1}{L_c} - \frac{M_S}{m}\gamma_n^2\right)\sin\gamma_n y\right] -$$

$$\frac{d\gamma_n}{dl}\left[\sin\gamma_n + 2\frac{M_S}{m}\gamma_n\cos\gamma_n y\right], \tag{4.21b}$$

so that

$$Y'(L_1,l) = \gamma_n\left(\frac{1}{L_c\gamma_n} - \frac{M_S}{m}\gamma_n\right), \tag{4.22a}$$

$$\frac{\partial Y_n'}{\partial l}(L_1,l) = \gamma_n^2 - 2\frac{M_S}{m}\gamma_n\frac{d\gamma_n}{dl}. \tag{4.22b}$$

By substituting the expressions (4.17)-(4.20) into equation (4.8), multiplying the result by Y_r, by integrating from L_1^- to L_0^+, and by accounting for the boundary conditions (3.60a)-(3.60b), using the orthogonality properties of the eigenfunctions Y_n, and finally by applying the relationships (4.22a)-(4.22b), the following system of equations results

$$\begin{aligned}
&\ddot{z}_r + \mu_2\dot{z}_r + \omega_r^2 z_r = \\
&-\frac{1}{m_r^v}\sum_{n=1}^{N_{long}}\left[2\dot{l}C_{rn}^v - EA\Lambda_{rn} + M_S\dot{l}\left(\frac{1}{L_c} - \frac{M_S}{m}\gamma_n^2\right)\right]\dot{z}_n - \\
&\frac{1}{m_r^v}\sum_{n=1}^{N_{long}}\left(\dot{l}^2 D_{rn}^v + \ddot{l}C_{rn}^v - EA\dot{l}B_{rn}^v + \mu_2\dot{l}C_{rn}^v + M_S\dot{l}^2\Gamma_n\right)z_n + \\
&g_r(t) + Z_r(t),
\end{aligned} \tag{4.23}$$

where $g_r(t) = \frac{1}{m_r^v}k_c u_l(t)$, $r = 1, 2, \ldots, N_{long}$, and

$$m_r^v = \int_{L_1}^{L_0}\rho(s)Y_r^2 ds, \tag{4.24a}$$

$$B_{rn}^v = \int_{L_1}^{L_0}\mu_1 Y_r\frac{\partial Y_n''}{\partial l}ds, \tag{4.24b}$$

$$C_{rn}^v = \int_{L_1}^{L_0}\rho(s)Y_r\frac{\partial Y_n}{\partial l}ds, \tag{4.24c}$$

$$D_{rn}^v = \int_{L_1}^{L_0}\rho(s)Y_r\frac{\partial^2 Y_n}{\partial l^2}ds, \tag{4.24d}$$

$$\Gamma_n = \gamma_n(\gamma_n - 2\frac{M_s}{m}\frac{d\gamma_n}{dl}), \tag{4.24e}$$

$$\Lambda_{rn} = \int_{L_1}^{L_0} \mu_1 Y_r Y_n'' ds, \tag{4.24f}$$

$$Z_r = \frac{1}{m_r^v} \int_{L_1}^{L_0} f(s,t) Y_r ds. \tag{4.24g}$$

The system of equation (4.23) forms a multi-degree-of -freedom model of the linear longitudinal dynamics of the system. It should be noted that the time-varying coefficients in this system depend on the eigenvalues γ_n, that must be determined from the transcendental frequency equation (4.16). The detailed procedure of their determination is given in Appendix B. The system (4.23) can be integrated numerically to determine the overall longitudinal dynamic response of the vertical cable during the winding cycle. This numerical simulation enables one to obtain transient components arising during the cycle acceleration/deceleration phase as well as to monitor the response due the periodic cross-over excitation acted upon the system during the constant velocity winding phase. This latter response is caused by relatively small longitudinal pulses. However, the axial stiffness of the rope is high, and this results in high amplitude oscillations in the rope tension contributing directly to fatigue damage effects [Dimitriou & Whillier, 1973]. In view of this, a passage through main longitudinal resonance would be of particular interest. A suitable computational technique to study this passage in more detail is discussed in what follows.

4.2 Single-Mode Approximation

When a single term is taken in the expansion (4.14) the result is referred to as a single-mode approximation, and the system is reduced to a single-degree-of-freedom model. This simple model has been used extensively and successfully in the analysis of free and forced vibrations of structures [Szemplinska-Stupnicka, 1990]. This approach can be applied to investigate the passage through resonance in the hoisting cable system [Kaczmarczyk, 1997a, b]. Near the

resonance region, the actual resonant mode is dominant, and it is reasonable to conclude that the shape of the vibration is close to this mode during the passage. Hence, the single-mode approximation to the response given by (4.8) can be assumed as

$$u_v = Y_r(s,l)z_r(t), \tag{4.25}$$

where Y_r denotes the resonant mode shape function which can be determined from equation (4.15)[7]. Substituting this form into equation (4.8) and applying the Rayleigh-Ritz procedure yields

$$\begin{aligned}
&\ddot{z}_r + \omega_r^2(l)z_r = \\
&-\frac{1}{m_r^v(l)}\left[2\dot{l}C_{rr}^v(l) - EA\Lambda_{rr}(l) + M_S\dot{l}\left(\frac{1}{L_c} - \frac{M_S}{m}\gamma_r^2(l)\right) + m_r^v(l)\mu_2\right]\dot{z}_r - \\
&\frac{1}{m_r^v(l)}\left(\dot{l}^2 D_{rr}^v(l) + \ddot{l}C_{rr}^v(l) - EA\dot{l}B_{rr}^v(l) + \mu_2\dot{l}C_{rr}^v(l) + M_S\dot{l}^2\Gamma_r(l)\right)z_r + \\
&K_r(l)\cos\Omega t + Z_r(t),
\end{aligned} \tag{4.26}$$

where $K_r = \frac{1}{m_r^v}k_c u_0$. In this formulation, the cable cross-over motion at the drum is represented by a harmonic boundary excitation of the form

$$u_l(t) = u_0\cos\Omega t, \tag{4.27}$$

with the amplitude u_0 defined by the geometry of the cross-over zone, and the frequency $\Omega = n\omega_d$, where n is an integer and ω_d denotes the drum frequency.

Following the approach outlined in Chapter 2, two time scales are defined in order to seek the solution of equation (4.26). The first one, a fast non-dimensional scale, is determined as

$$T = \omega_0 t, \tag{4.28}$$

---

[7] Alternatively the longitudinal system can be modeled by treating the vertical rope as an unconstrained subsystem [Kaczmarczyk, 1997b], and by using $Y_r = \cos\gamma_r y(s,l) - \gamma_r\frac{M_S}{m}\sin\gamma_r y(s,l)$ in equation (4.25). However, the present approach yields more accurate results.

where $\omega_0 = \omega_r(l(0))$. The second scale is a slow scale $\tau = \varepsilon T$, and a variation of l is observed on this scale. For example, during the ascending constant velocity winding phase, following the relationship (3.2), this length is given as

$$l = l(0) + V_c t, \tag{4.29}$$

where V_c denotes the nominal winding velocity. Assuming $l(0) = 0$, and defining the small parameter ε according to the relationship (2.8) as

$$\varepsilon = \frac{V_c}{\omega_0 L_{v0}}, \tag{4.30}$$

where $L_{v0} = L_v\,(l(0))$, yields

$$l = L_{v0}\tau. \tag{4.31}$$

Noting that

$$\dot{z}_r = \omega_0 \frac{dz_r}{dT}, \tag{4.32}$$

$$\ddot{z}_r = \omega_0^2 \frac{d^2 z_r}{dT^2}, \tag{4.33}$$

$$\dot{l} = \omega_0 \varepsilon l', \tag{4.34}$$

$$\ddot{l} = \omega_0^2 \varepsilon^2 l'' \tag{4.35}$$

where the prime denotes the derivative with respect to τ, and assuming that the damping is small, so that one may set

$$\mu_1 = \varepsilon \mu_1^*, \tag{4.36}$$

$$\mu_2 = \varepsilon \mu_2^*, \tag{4.37}$$

the following equation valid for the constant velocity winding phase is obtained

$$\frac{d^2 z_r}{dT^2} + \tilde{\omega}_r^2(\tau) z_r = \varepsilon f_r(\tau, \frac{dz_r}{dT}) + \tilde{K}_r(\tau) \cos \tilde{\Omega} T + O(\varepsilon^2), \tag{4.38}$$

where $\tilde{\omega}_r = \frac{\omega_r}{\omega_0}$, $\tilde{\Omega} = \frac{\Omega}{\omega_0}$, $\tilde{K}_r = \frac{K_r}{\omega_0^2}$, and

$$f_r(\tau, \frac{dz_r}{dT}) = \left\{ \frac{1}{m_r^v(\tau)} \left[EA\frac{L_{v0}}{V_c}\Lambda_{rr}(\tau) - 2l'C_{rr}^v(\tau) - M_S l' \left(\frac{1}{L_c} - \frac{M_S}{m}\gamma_r^2(\tau) \right) \right] - \frac{L_{v0}}{V_c}\mu_2 \right\} \frac{dz_r}{dT}. \tag{4.39}$$

4.3 The Multiple Scales Solution

Equation (4.38) represents a single-degree-of-freedom system having slowly varying natural frequency and coefficients. Studies to predict the response of this system during the transition through primary resonance, when the slowly varying frequency coincides with the frequency of the periodic excitation at some critical time instant, can be carried out by the method of multiple scales [Nayfeh & Mook, 1979]. This method is discussed in detail in Appendix C. Thus, the solution is sought in terms of the fast and slow scales in the form

$$z_r = z_{r0}(\phi_r, \tau) + \varepsilon z_{r1}(\phi_r, \tau) + O(\varepsilon^2), \tag{4.40}$$

where ϕ_r represents the fast scale and is defined by

$$\frac{d\phi_r}{dT} = \tilde{\omega}_r(\tau). \tag{4.41}$$

In the resonant case values $\tilde{\omega}_r(\tau)$ are near $\tilde{\Omega}$. This nearness can be quantified by a slowly varying detuning parameter $\sigma_r(\tau)$ introduced as follows

$$\tilde{\Omega} - \tilde{\omega}_r(\tau) = \varepsilon\sigma_r(\tau). \tag{4.42}$$

Therefore, when the relationship (4.41) is taken into account, one gets from (4.42)

$$\tilde{\Omega}T = \phi_r + \vartheta_r(\tau), \tag{4.43}$$

where

$$\vartheta_r(\tau) = \varepsilon \int_0^T \sigma_r(\varepsilon\xi)d\xi. \tag{4.44}$$

When $\sigma_r = 0$, unbounded oscillations would be predicted for a corresponding undamped system with constant parameters. In the actual system, the oscillations are limited by the damping and influenced by the non-stationary terms on the right hand side of equation (4.38), present as components of the function (4.39). Therefore, the excitation needs to be ordered so that it will appear when the damping and the non-stationary terms appear. Thus, in order to determine the first approximation one sets

$$K_r = 2\varepsilon k_r, \tag{4.45}$$

so that $K_r = O(\varepsilon)$. By substituting (4.40) into (4.38) and by equating the coefficients of ε^0 and ε on both sides of the resulting equation, the following results

$$\tilde{\omega}_r^2\left(\frac{\partial^2 z_{r0}}{\partial \phi_r^2} + z_{r0}\right) = 0, \tag{4.46}$$

$$\tilde{\omega}_r^2\left(\frac{\partial^2 z_{r1}}{\partial \phi_r^2} + z_{r1}\right) = -2\tilde{\omega}_r \frac{\partial^2 z_{r0}}{\partial \phi_r \partial \tau} - \tilde{\omega}_r' \frac{\partial z_{r0}}{\partial \phi_r} + f_r\left(\tau, \tilde{\omega}_r \frac{\partial z_{r0}}{\partial \phi_r}\right) + 2k_r \cos \tilde{\Omega} T. \tag{4.47}$$

The general solution of (4.46) is found to be

$$z_{r0} = A_r(\tau) e^{i\phi_r} + \bar{A}_r(\tau) e^{-i\phi_r}, \tag{4.48}$$

where $\bar{A}_r$ is the complex conjugate of A_r that is given by the polar form

$$A_r(\tau) = \frac{1}{2} a_r(\tau) e^{i\beta_r(\tau)}, \tag{4.49}$$

where a_r and β_r are real. Using (4.48) and (4.43) in (4.47), with $f_r(\tau, \tilde{\omega}_r \frac{\partial z_{r0}}{\partial \phi_r})$ expanded in a Fourier series, one obtains the following equation

$$\begin{aligned} \tilde{\omega}_r^2\left(\tfrac{\partial^2 z_{r1}}{\partial \phi_r^2} + z_{r1}\right) = -i(2\tilde{\omega}_r A_r' + \tilde{\omega}_r' A) e^{i\phi_r} + \textstyle\sum_{n=-\infty}^{\infty} f_{rn}(A_r, \bar{A}_r, \tau) e^{in\phi_r} + \\ k_r e^{i(\phi_r + \vartheta_r)} + cc, \end{aligned} \tag{4.50}$$

where

$$f_{rn}(A_r, \bar{A}_r, \tau) = \frac{1}{2\pi} \int_0^{2\pi} f_r(A_r, \bar{A}_r, \tau, \phi_r) e^{-in\phi_r} d\phi_r, \tag{4.51}$$

and cc denotes the complex conjugate of the preceding terms. The condition for the elimination of the secular terms in (4.50) is

$$-i(2\tilde{\omega}_r A_r' + \tilde{\omega}_r' A) + f_{r1}(A_r, \bar{A}_r, \tau) + k_r e^{i\vartheta_r} = 0, \tag{4.52}$$

where

$$f_{r1}(A_r, \bar{A}_r, \tau) = \frac{1}{2\pi}\int_0^{2\pi} f_r(A_r, \bar{A}_r, \tau, \phi_r)e^{-i\phi_r}d\phi_r. \tag{4.53}$$

By expressing A_r in the polar form in equation (4.52), by separating the result into its real and imaginary parts, and also by denoting

$$\psi_r = \vartheta_r - \beta_r, \tag{4.54}$$

one obtains the following set

$$\begin{array}{l} a_r' = -\frac{1}{2}\frac{\tilde{\omega}_r'}{\tilde{\omega}_r}a_r - \frac{1}{2\pi\tilde{\omega}_r}\int_0^{2\pi} f_r(\tau, -a_r\tilde{\omega}_r\sin\theta_r)\sin\theta_r d\theta_r + \frac{k_r}{\tilde{\omega}_r}\sin\psi_r, \\ \psi_r' = \sigma_r(\tau) + \frac{1}{2\pi\tilde{\omega}_r a_r}\int_0^{2\pi} f_r(\tau, -a_r\tilde{\omega}_r\sin\theta_r)\cos\theta_r d\theta_r + \frac{k_r}{\tilde{\omega}_r a_r}\cos\psi_r, \end{array} \tag{4.55}$$

where $\theta_r = \phi_r + \beta_r$. Using (4.39) in (4.55) leads to

$$\begin{array}{l} a_r' = -\frac{1}{2}\left\{\frac{\tilde{\omega}_r'}{\tilde{\omega}_r} - \frac{1}{m_r^v(\tau)}\left[\begin{array}{c} EA\frac{L_{v0}}{V_c}\Lambda_{rr}(\tau) - 2l'C_{rr}^v(\tau) - \\ M_S l'\left(\frac{1}{L_c} - \frac{M_S}{m}\gamma_r^2(\tau)\right)\end{array}\right] - \frac{L_{v0}}{V_c}\mu_2\right\}a_r + \frac{k_r}{\tilde{\omega}_r}\sin\psi_r, \\ \psi_r' = \sigma_r(\tau) + \frac{k_r}{\tilde{\omega}_r a_r}\cos\psi_r. \end{array} \tag{4.56}$$

Following the expansion (4.40), the first approximation to the solution is obtained when (4.54) together with (4.43) are used in (4.48). This results in

$$z_r = a_r\cos(\tilde{\Omega}T - \psi_r) + O(\varepsilon), \tag{4.57}$$

with a_r and ψ_r given by (4.56).

4.4 Longitudinal Damping Parameters

The longitudinal damping force is defined by equation (3.66) with the damping operator $\mathcal{C}_u$ given by (3.67). In this model, which was also assumed in the analysis presented by

Thomas & Brillhart [1987], the damping coefficient μ_1 represents internal damping effects, that are proportional to the rate of strain in the cable, and the second damping coefficient μ_2 accommodates the external damping in the system.

The coefficient μ_1 is usually assumed to be a function of some cable parameters, which may be established from an appropriate experiment. Goroshko & Savin [1971] showed that this coefficient is independent of the amplitude of oscillations in the cable dynamic tension, but depends on the mean (quasi-static) value of the cable tension. Namely, μ_1 decreases with increasing mean tension. This effect was also observed by Mankowski and Cox [1986]. It can be argued that when the tension is increased, the wire strands are more readily locked, and the inter-strand relative motion is constrained, resulting in the coefficient μ_1 being decreased. This agrees with an earlier observation by Vanderveldt and Gilheany [1970] who found that the velocity of propagation of a longitudinal pulse in wire ropes increases with increasing applied tension load, and postulated that this was due to the cable approaching the geometry of a solid bar due to a gradual tightening of the wires and strands. Greenway [1989] extracted the damping coefficient μ_1 from the measurement of the logarithmic measurement of the fundamental longitudinal mode performed on a mine hoist installation. It was shown that the damping coefficient increased in proportion to the rope length. Constancon [1993] analyzed the results of damping measurements via drop tests carried out at Elandsrand Mine, R.S.A. In these tests, a conveyance was clamped between the guides, loaded with a dead weight, and released. The response was monitored with an accelerometer, and the modal damping ratios were extracted from the measurements using standard parameter estimation procedures. A strong dependency of the fundamental mode ratio on the mean rope tension was recorded. It was evident that the damping ratio decreased approximately linearly with the tension. However, in the final model the relative damping coefficient μ_1 was assumed to depend on the cable length, as proposed earlier by Greenway.

Taking into account the existing strong evidence, the dependency of the damping coefficient μ_1 on the mean tension is accommodated in the present analysis. The model proposed by Savin and Goroshko [1971] is adopted. In this approach, based on experimental data, the damping coefficient is defined as

$$\mu_1 = (0.5 + \frac{23000}{3500 + 0.75 \times 10^{-5}\sigma_v^i}) \times 10^{-4}, \tag{4.58}$$

where σ_v^i denotes the mean stress in the cable in N/m^2 and is given as

$$\sigma_v^i = \frac{T_v^i}{A}, \tag{4.59}$$

with the mean tension T_v^i in the vertical rope determined from equation (3.37).

The external damping effects, such as air damping, friction at conveyance guides, and damping at the sheave wheel bearings, may be represented by the coefficient μ_2. The order of this coefficient was established by the drop tests conducted at Elandsrand Gold Mine, and its value can be estimated from the corresponding test results.

4.5 Numerical Example and Results

4.5.1 Overall Dynamic Response

The total longitudinal dynamic behaviour of the system is described by the set of linear ordinary differential equations (4.23), and the solution of these equations, combined with the expansion (4.14), gives the overall longitudinal response. The coefficients in the system (4.23) are slowly time-varying, and the system is referred to as linear time-varying system [D'Angelo,1970]. In general, it is not feasible to obtain an exact closed-form solution to time-varying coupled systems of ordinary differential equations. Traditionally, approximate analytical studies to predict the response of these system have been carried out by the pertur-

Number of longitudinal modes N_{long}	4
Total winding cycle time $[s]$	163
Acceleration/deceleration time $[s]$	26
Nominal hoisting velocity $V_c\left[\frac{m}{s}\right]$	16
Total hoisted mass $M\,[kg]$	23649
Sheave wheel moment of inertia I $[kgm^2]$	25689
Winder drum radus R_d $[m]$	2.77
Sheave wheel radius R $[m]$	2.77
Coil cross-over arc β $[rad]$	0.1
Cable diameter d $[m]$	48×10^{-3}
Cable linear density m $\left[\frac{kg}{m}\right]$	9.75
Cable effective steel area A $[m^2]$	1.053×10^{-3}
Cable effective Young's Modulus E $\left[\frac{N}{m^2}\right]$	1.25×10^{11}
Catenary length $L_c\,[m]$	73
Maximum depth of winding $L_{v\,\max}\,[m]$	2204
Relative damping coefficient $\mu_1\,[s]$	given by (4.58)
Absolute damping coefficient μ_2 $[s^{-1}]$	0.159

Table 1. Elandsrand Simulation Parameters

bation methods, as discussed earlier in Chapter 2. However, the algebra in these techniques is quite involved. An alternative method was presented by Shahruz & Tan [1989], who found an approximate closed-form solution to the response of linear slowly varying systems under external excitations using the technique of freezing slowly varying parameters. This technique, however, is not suitable for the general case when the eigenvalues of the frozen system cannot be obtained explicitly in terms of the frozen time parameter. Thus, the most convenient approach to solving the system of equations (4.23) is by direct numerical integration.

The numerical simulation requires the definition of necessary input data, which are shown in Table 1. These data are based on the winder and rope parameters of the double drum rock winder at Elandsrand Gold Mine [CSIR, 1995; Van Zyl, 1998], and can be considered typical for a deep mine hoisting system operating in South Africa.

The boundary excitation u_l present in equation (4.23) is assumed in the harmonic form given by equation (4.27) with the amplitude u_0 prescribed by the geometry of a mechanism

employed to implement the coiling process. The Elandsrand Mine winder drum is equipped with $180^0 - 180^0$ Lebus arrangement to achieve a repetitive coiling pattern during a winding cycle. In this mechanism, the winder drum surface is covered by parallel circular grooves with two diametrically opposed cross-over zones per drum circumference, as shown in Figure 9. Each zone offsets the grooves by half a cable diameter and when the cable passes through a cross-over an additional axial displacement relative to the nominal transport motion occurs. The magnitude of this displacement can be calculated as approximately equal to the difference between the arc length transversed through the cross-over and the corresponding diametrical arc [Mankowski, 1982], which gives the amplitude

$$u_0 = \sqrt{(R_d\beta)^2 + \frac{d^2}{4}} - R_d\beta, \tag{4.60}$$

where R_d is the drum radius, d represents the cable diameter, and β is the angle defining the diametrical arc corresponding to the cross over region. As the cross-over occurs twice per drum revolution the frequency of the excitation is equal to twice that of drum frequency, namely $\Omega = 2\omega_d$.

Since the highest dynamic forces in hoisting cables occur during the up-wind, the simulation is carried out for the ascending cycle, when a fully loaded conveyance is being raised from the bottom of the shaft. This winding cycle consists of three main phases: the acceleration phase, the constant velocity phase, and the deceleration phase. The natural frequencies of the system vary slowly during the entire wind due to the slowly varying length of the vertical rope. This is illustrated in Figure 10, where the first four up-wind longitudinal natural frequencies, determined from the transcendental equation (4.16), are plotted against the vertical cable length. Frequencies of the excitation Ω, corresponding to various winding velocity V_c, are also shown in this diagram. As one can observe, the natural frequencies increase with the shortening length of the vertical rope. For the nominal winding velocity of 16 m/s, a transition through resonance occur twice: at the beginning of the cycle when

the excitation frequency coincides with the third natural frequency at approximately $L_v = 1950\,m$, and later during the wind when a passage through the second natural frequency takes place at approximately $L_v = 950\,m$.

The system (4.23) demonstrates features of a *stiff* problem [Nikravesh, 1988]. It can be seen from the frequency diagram in Figure 10, that the eigenvalues are widely spread, especially at the end of the wind, and therefore the complete solution to the problem will consist of slow and fast components. Hence, if the numerical solution is to return the entire transient response of the system over a long time interval, integration must be performed using relatively large time step to cover the slow components. However, the time step must be also small enough to capture the fast components, and to keep the numerical solution within acceptable bounds. Thus, due to these requirements integration methods not designed for stiff problems are ineffective, and lead to unstable results when applied to stiff equations. The problem of numerical integration of systems of stiff ordinary differential equations has attracted considerable attention, and a number of efficient integration algorithms that allow relatively large time steps, and that guarantee stability and bounded numerical error are available [Hairer & Wanner, 1991; Shampine, 1994]. Multistep methods based on backward differentiation formulas (BDF's), (also known as Gear's method), have been the most prominent and most widely used for solving stiff problems. Recently a new family of formulas called the numerical differentiation formulas (NDF's) have been developed and implemented in the MATLAB ODE suite [Shampine & Reichelt, 1996]. They are more efficient than the BDF's, though the higher order formulas in this family are somewhat less stable. Both BDF's and NDF's codes are available from the ode15s MATLAB solver. Another stiff solver, namely ode23s, based on Rosenbrock formula of order 2, is also provided with the MATLAB ODE suite. It is a one-step method and is especially effective at crude tolerances.

The non-stationary modal equations (4.23) are integrated numerically in the MATLAB 5 computing environment. First the equations are written in the *standard form*, namely as

$$\dot{\mathbf{y}}(t) = \mathbf{A}(t)\,\mathbf{y}(t) + \mathbf{F}(t), \tag{4.61}$$

where $\mathbf{y} = \left[\mathbf{z}^T, \dot{\mathbf{z}}^T\right]^T$, is the $2N_{long}$-dimensional modal state vector, with $\mathbf{z} = \left[z_1, z_2, \ldots, z_{N_{long}}\right]^T$, $\mathbf{A}(t)$ is the $2N_{long} \times 2N_{long}$ system matrix, and $\mathbf{F}(t)$ is the $2N_{long}$-dimensional excitation vector. The time-varying system matrix is defined as

$$\mathbf{A}(t) = \begin{bmatrix} \mathbf{0} & \mathbf{I} \\ -\mathbf{K}^{\mathbf{v}} & -\mathbf{C}^{\mathbf{v}} \end{bmatrix}, \tag{4.62}$$

where

$$\begin{aligned} \mathbf{K}^{\mathbf{v}} &\equiv [K^v_{rn}]_{(N_{long}\times N_{long})} = diag\left[\omega_r^2\right] + \\ &\left[\frac{1}{m_r^v}\left(\dot{l}^2 D^v_{rn} + \ddot{l} C^v_{rn} - EA\dot{l}B^v_{rn} + \mu_2 \dot{l} C^v_{rn} + M_S \dot{l}^2 \Gamma_n\right)\right], \\ \mathbf{C}^{\mathbf{v}} &\equiv [C^v_{rn}]_{(N_{long}\times N_{long})} = \mu_2 \mathbf{I} + \\ &\left[\frac{1}{m_r^v}\left\{2\dot{l} C^v_{rn} - EA\Lambda_{rn} + M_S \dot{l}\left(\frac{1}{L_c} - \frac{M_S}{m}\gamma_n^2\right)\right\}\right], \end{aligned} \tag{4.63}$$

and $\mathbf{0}$ and $\mathbf{I}$ are $N_{long} \times N_{long}$ null and identity matrices, respectively. The excitation vector $\mathbf{F}$ is given as

$$\mathbf{F}(t) = \begin{bmatrix} \mathbf{0}_{(N_{long}\times 1)} \\ [g_r + Z_r]_{(N_{long}\times 1)} \end{bmatrix}. \tag{4.64}$$

Next, the equation (4.61) is coded in a MATLAB ODE file, and the ode15s solver with the default numerical differentiation formulas, with the default *relative accuracy tolerance* and *absolute error tolerances* of 10^{-3} and of 10^{-6} respectively, is applied to simulate the system on the total winding cycle time interval. The time-varying natural frequencies and coefficients are calculated prior to the simulation, and are assembled in look-up tables as functions of the length parameter l. The linear interpolation is later applied to determine the actual values of the natural frequencies and of the coefficients during the simulation.

The simulation results are shown in Figures 11 -14. The generalized modal co-ordinates z_n, $n = 1, \ldots, 4$, are plotted against the vertical rope length L_v in Figure 11. The displacements at the sheave and at the conveyance, given as

$$u_S = \sum_{n=1}^{4} Y_n(L_1, l)\, z_n(t), \tag{4.65}$$

$$u_M = \sum_{n=1}^{4} Y_n(L_0, l)\, z_n(t), \tag{4.66}$$

respectively, are shown in Figure 12. The plots of the total catenary tension T_c, and of the total vertical rope tension T_S at the sheave and T_M at the conveyance, together with the tension ratio across the sheave, versus L_v are presented in Figure 13. In these plots the tensions are determined as follows. The total catenary tension is calculated as

$$T_c(t) = T_c^i(t) + k_c \left[\sum_{n=1}^{4} z_n(t) - u_l(t) \right], \tag{4.67}$$

where the catenary mean tension T_c^i is given by (3.36). The vertical rope tension is defined as

$$T_v(s,t) = T_v^i(s) + T_{vd}(s,t), \tag{4.68}$$

where the dynamic component T_{vd} is expressed using the Kelvin-Voigt viscoelastic model, whereby the normal stress is related to the strain and strain rate, namely

$$T_{vd}(s,t) = EA\left[u_{v,s} + \mu_1(s)\, u_{v,ts}\right], \tag{4.69}$$

and the mean tension T_v^i is defined by equation (3.37). Hence, the rope tensions at the sheave and at the conveyance are given as $T_S = T_v(L_1, t)$, and $T_M = T_v(L_0, t)$, respectively. The catenary dynamic tension is defined as

$$T_{cd} = k_c \left[\sum_{n=1}^{4} z_n(t) - u_l(t) \right], \tag{4.70}$$

the vertical rope dynamic tension are given as $T_{Sd} = T_{vd}(L_1, t)$ at the sheave and $T_{Md} = T_{vd}(L_0, t)$ at the conveyance, and are plotted against L_v in Figure 14.

The results demonstrate various transient vibration phenomena that occur during the wind. Significant response due to the initial acceleration / final deceleration inertial loads at the beginning, and at the end of the cycle respectively, is predicted. This response is prominent both at the sheave and at the conveyance. Referring to the modal co-ordinate plots, it is evident that the fundamental mode dominates in the resulting transient oscillations, as recorded in the co-ordinate z_1 plot shown in Figure 11. As anticipated earlier in the frequency diagram (Figure 10), passages through resonance are manifested in the response plots. This is can be seen in Figure 11, where the co-ordinate z_2 displays resonance behaviour in the region $\Omega = \omega_2$, and z_3 demonstrates transition through the resonance condition $\Omega = \omega_3$. These resonance phenomena affect especially the sheave response, which can be seen in Figure 12(a).

The cable tensions reflect the system dynamics during the wind. The dynamic components oscillate about the corresponding mean values, that for the catenary and at the sheave increase with the vertical length. The tension ratio across the sheave is close to unity over the entire cycle, demonstrating a small increase at the end of the wind, but remaining in the limits of approximately $0.94 - 1.05$. This indicates that frictional slip will not occur[8]. The influence of acceleration/deceleration, and of transitions through resonance on the cable tensile forces is better illustrated in Figure 14. It can be seen, that significant oscillations in the

[8] Skalmierski [1979] discussed the equilibrium between a rope and a Koepe pulley in hoisting machines. It was shown that the equation governing the impending slipping of the rope around the pulley may be written in the classical form $T_2 = T_1 e^{-\mu\alpha}$, where T_1, T_2 are the larger tensile force and the smaller tensile force, respectively, in the two parts of the rope not in contact with the pulley, μ is the coefficient of friction, and α denotes the angle of contact. This relationship can be used to formulate a criterion for no slip between the cable and the headsheave in the hoisting system, requiring that $e^{-\mu\alpha} < \frac{T_c}{T_s} < e^{\mu\alpha}$. A similar criterion was used earlier by Perry & Smith [1932], and was adopted by Mankowski [1982] and Constancon [1993]. Using for example the average value of $\mu = 0.25$, and the angle $\alpha = 135^0$, this criterion shows that the tension ratio must be within the limits [0.5559, 1.8023] for slip not to occur.

dynamic tensions are predicted during the initial and final stages of winding due to the acceleration/deceleration inertial loads. Also, at the depth of approximately $700 - 1000\,m$, the resonance condition $\Omega = \omega_2$ produces substantial tension oscillations. The effect of the main resonance on the system dynamics is discussed in more detail in what follows.

4.5.2 Response at the resonance region

The single-mode response of the system near the resonance is given by equations (4.25), and (4.57), with the slowly varying amplitude and the phase determined by the system of first order differential equations (4.56). These autonomous ordinary differential equations with variable coefficients do not easily lend themselves to an analytical solution. Analytical methods for analysis of problems this type are very few and tend to be either difficult to apply or limited in application to a small class of systems. For example, Raman, Bajaj & Davies [1996] treated analytically classical non-linear vibratory systems in the presence of non-stationary excitation. They discussed passage through primary resonance in the forced Duffing's oscillator, described by the averaged first order equations for the amplitude and phase. An analytical study of the response was presented using matched asymptotic expansions. This technique is however applicable only within a small neighbourhood of the instability region, and various beating phenomena associated with the passage cannot be predicted by this approach. As shown by Nayfeh & Mook [1979], direct numerical integration of non-stationary amplitude-phase equations is perhaps the most convenient approach. This technique was also successfully used by Cveticanin [1991], who analyzed the passage through resonance in a textile machine rotor with variable mass. The amplitude a_r and phase ψ_r governed by equations (4.56) are slowly varying functions, and the system can be solved numerically without difficulty using standard integration methods. The MATLAB ode23

solver based on an explicit Runge-Kutta $(2,3)$ pair of Bogacki and Shampine [Shampine, 1994] is used to determine the solution in what follows.

The accuracy of this solution and of the first approximation given by equation (4.57) can be verified by comparison with the overall response obtained earlier from the system of equations (4.23). This comparison is shown in Figure 15, where passage through resonance region $\Omega = \omega_2$ (that is for $r = 2$) in the Elandsrand system operating at the nominal hoisting velocity $V_c = 16\ \frac{m}{s}$ is illustrated. In Figure $15(a)$ the response envelope, determined as $a_S = Y_2(L_1, l)\, a_2$, is superimposed on the sheave response obtained from equation (4.65). The rope dynamic tensions T_{Sd} at the sheave and T_{Md} at the conveyance, calculated using the expansion (4.14) and equation (4.69), with superimposed tension envelopes are shown in Figure $15(b)$ and Figure $15(c)$, respectively. The tension envelopes are determined from equation (4.69) using the single-mode representation (4.25) together with the approximation (4.57), and are given by

$$E_{vd}(s,\tau) = EA\sqrt{A_r^2 + B_r^2}, \tag{4.71}$$

where

$$A_r(s,\tau) = \left(\frac{\partial Y_r}{\partial s} + \mu_1 \frac{\partial^2 Y_r}{\partial s \partial l} V_c\right) a_r + \mu_1 \varepsilon \omega_0 \frac{\partial Y_r}{\partial s} a_r', \tag{4.72}$$

$$B_r(s,\tau) = \mu_1 \left(\varepsilon \omega_0 \psi_r' - \Omega\right) \frac{\partial Y_r}{\partial s} a_r. \tag{4.73}$$

It can be seen that in the resonance region the single-mode solution approximates well the overall response and tension curves.

Transition through the resonance region $\Omega = \omega_2$ is further illustrated in Figure 16. In Figure $16(a)$ the non-stationary frequency-response curves are shown, with the amplitudes a_2 plotted against the detuning parameter σ_2, and in Figure $16(b)$ these amplitudes are shown against the vertical length (depth) L_v, for four winding velocities, namely $V_c = 12, 14, 16,$ and $18\ m/s$. It should be noted, that these amplitudes represent directly the maximum sheave motions, as the resonant modes Y_r in equation (4.25) are normalized to the unity at the sheave

end. It can be seen that the resonance region is reached at higher depths for lower values of the winding velocities, while the detuning parameter σ_2 decreases when making a single passage through zero. This is consistent with the frequency diagram shown in Figure 10, where the resonance regions for the corresponding velocities can be identified against the depth. The amplitudes start growing when the resonance region is approached, and near the resonance ($\sigma_r \approx 0$) they increase rapidly, and decline afterwards due to damping, developing damped beat phenomena. The period of the beats decreases with time. It can be observed that the higher the winding velocity, the higher the maximum value of the corresponding amplitude. A different pattern of behaviour can be identified at the conveyance end, which is illustrated in Figure 17(a), and 17(b). In this figure, the conveyance amplitude envelope curves, determined as $a_M = Y_r(L_0, l)\, a_2$, are represented against the frequency detuning parameter and against the depth, respectively. As one can see, in this case higher maximum values of amplitudes are recorded for lower winding velocities.

The upper envelopes of the dynamic tensions, namely E_{cd} of the catenary cable , E_{Sd} of the rope at the sheave and E_{Md} at the conveyance, are plotted against the detuning parameter and the vertical length in Figures 18, 19 and 20. The catenary tension envelopes are determined using equation (4.70) where the single-mode solution (4.57) is applied, so that

$$E_{cd} = k_c \sqrt{(a_r \cos\psi_r - u_0)^2 + (a_r \sin\psi_r)}. \tag{4.74}$$

The rope tension envelopes are found from equation (4.71). It is evident from the tension envelope plots that the tension amplitudes increase rapidly during the passage through resonance, declining slowly afterwards. Both in the catenary and in the vertical rope the tension amplitudes demonstrate the tendency to reach higher values for higher velocities.

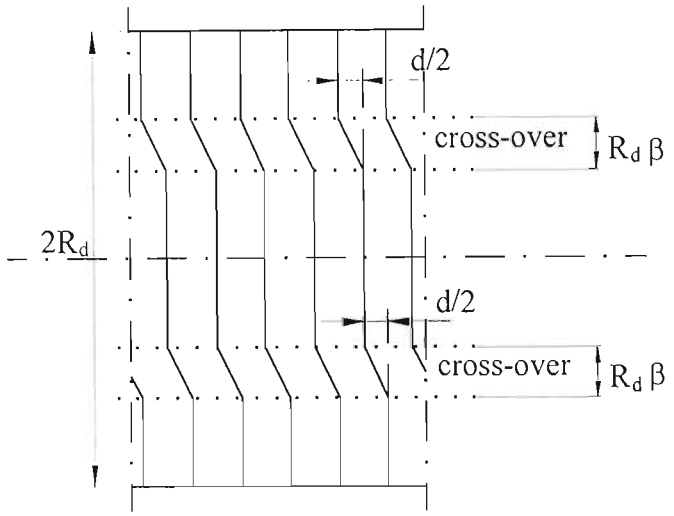

Figure 9. Cross-over zones of the Lebus system.

4.6 Summary and Conclusions: Longitudinal Dynamics

The overall longitudinal dynamic behaviour of a hoisting cable system is demonstrated in the numerical simulation of the double drum winder system at Elandsrand Gold Mine. The simulation results illustrate a transient response due to the acceleration/deceleration inertial load and passages through primary longitudinal resonances, when the frequency of the excitation due to a coiling mechanism at the winding drum coincides with the natural frequencies during the cycle. Also, significant dynamic fluctuations in the cable tensions are predicted. The tension ratio across the sheave is close to the unity which indicates that frictional slip will not occur.

The effect of transitions through the primary resonances is investigated using a combined perturbation and numerical technique. A single-mode model is applied to represent the system during a passage through resonance. It accommodates the fundamental feature of the system, namely its non-stationary nature, and adequately represents the main type of

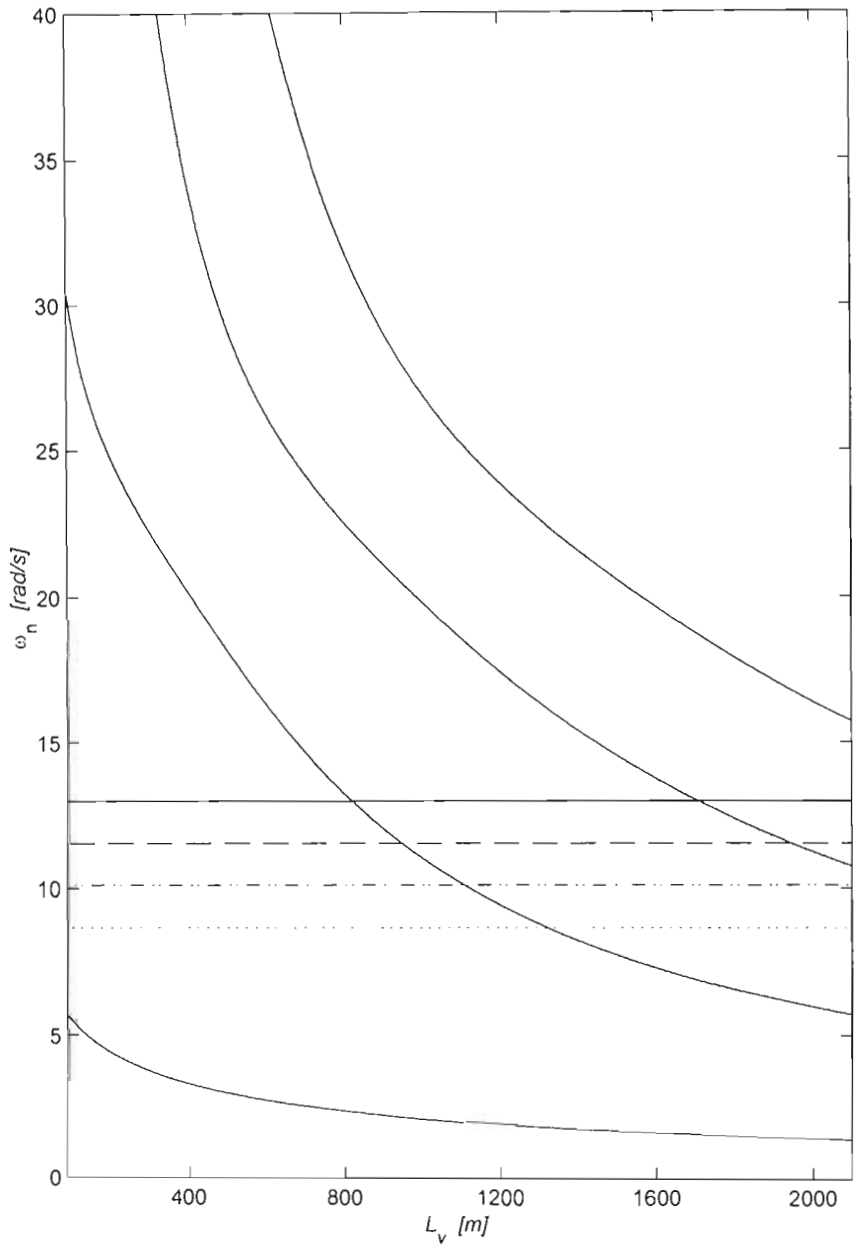

Figure 10. Longitudinal frequency curves for Elandsrand Mine winder, with horizontal lines denoting the frequency of excitation Ω, corresponding to various nominal winding velocities: $V_c = 12$ $(\cdots)$, 14 $(- \cdot -)$, 16 $(--)$, and 18 $(—)$ m/s.

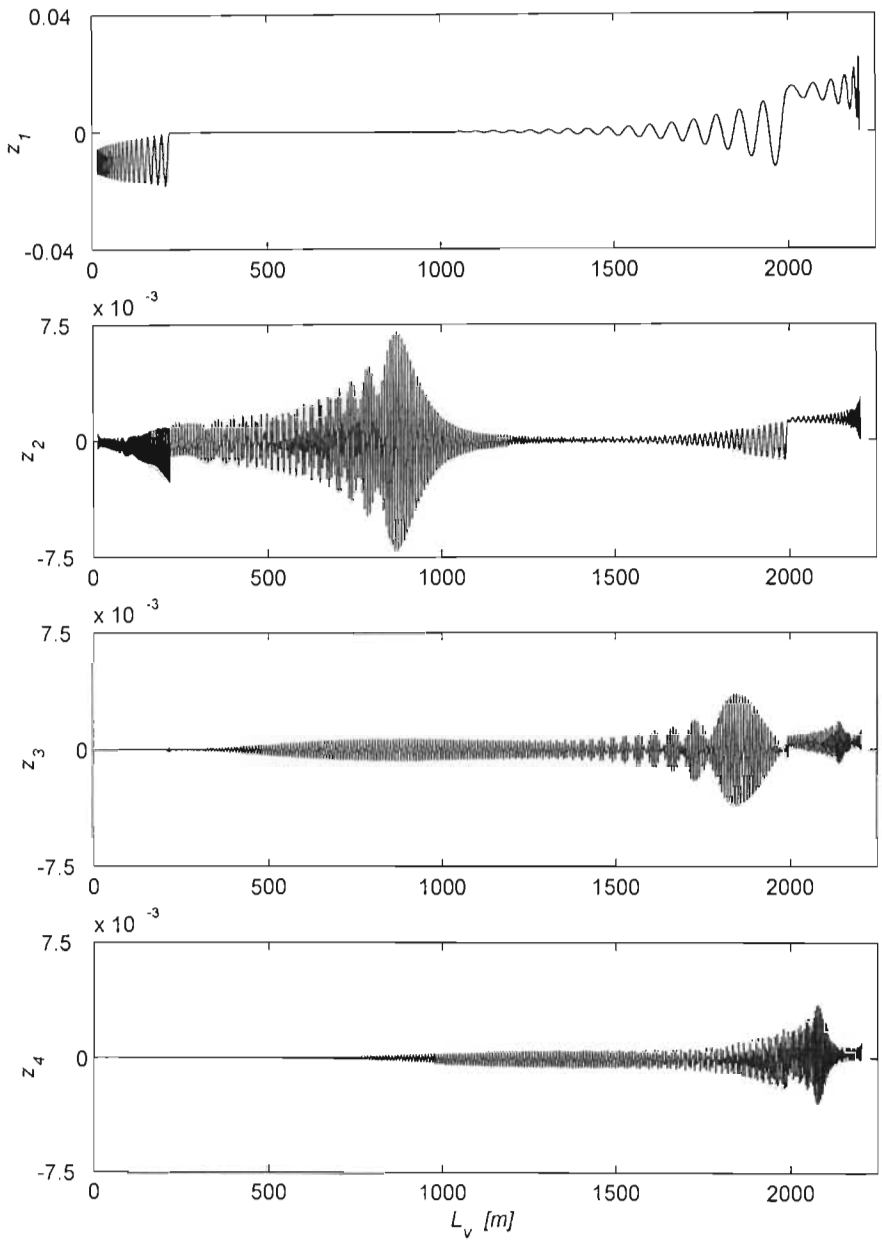

Figure 11. Longitudinal modal co-ordinates for Elandsrand Mine simulation at the nominal winding velocity $V_c = 16\ m/s$.

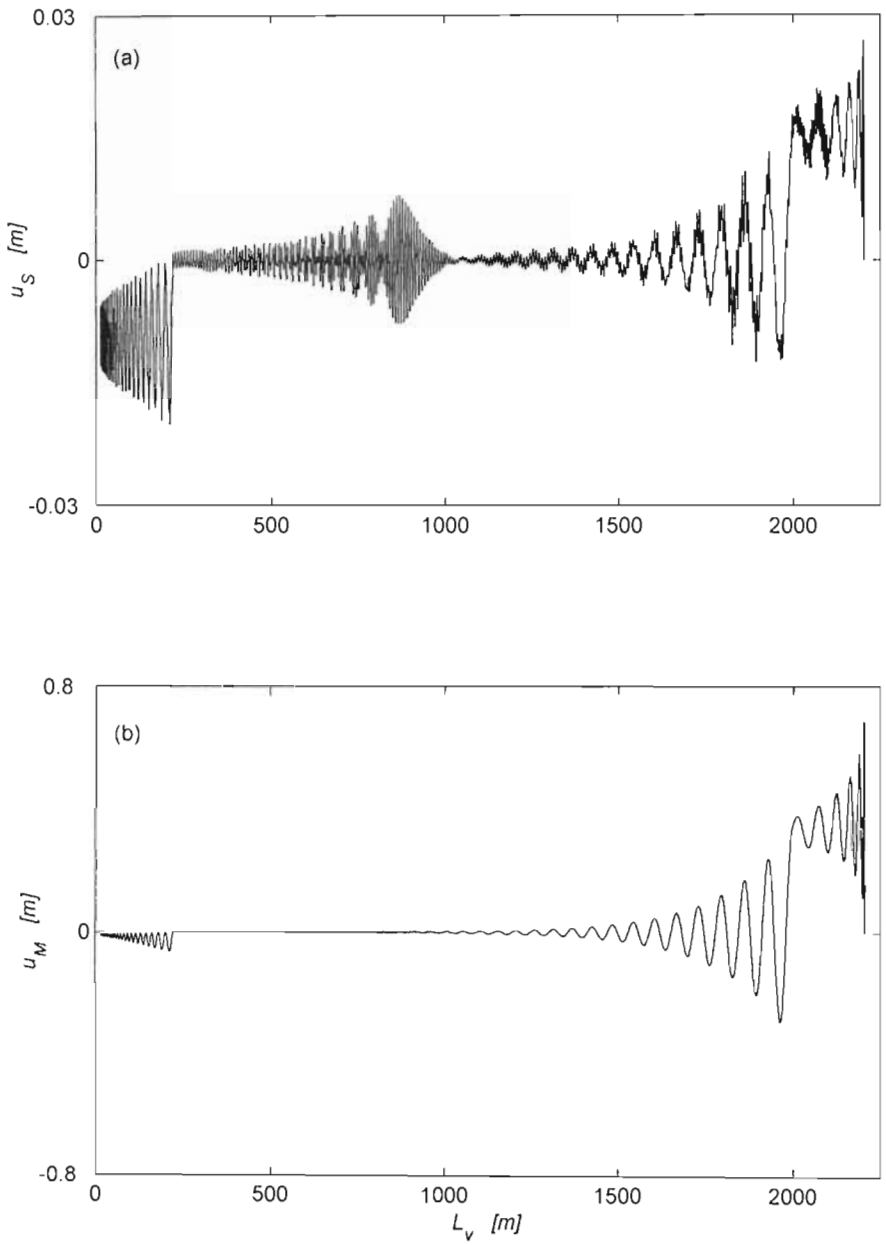

Figure 12. Longitudinal response of the Elandsrand system at the nominal winding velocity $V_c = 16\ m/s$: (a) at the sheave; (b) at the conveyance.

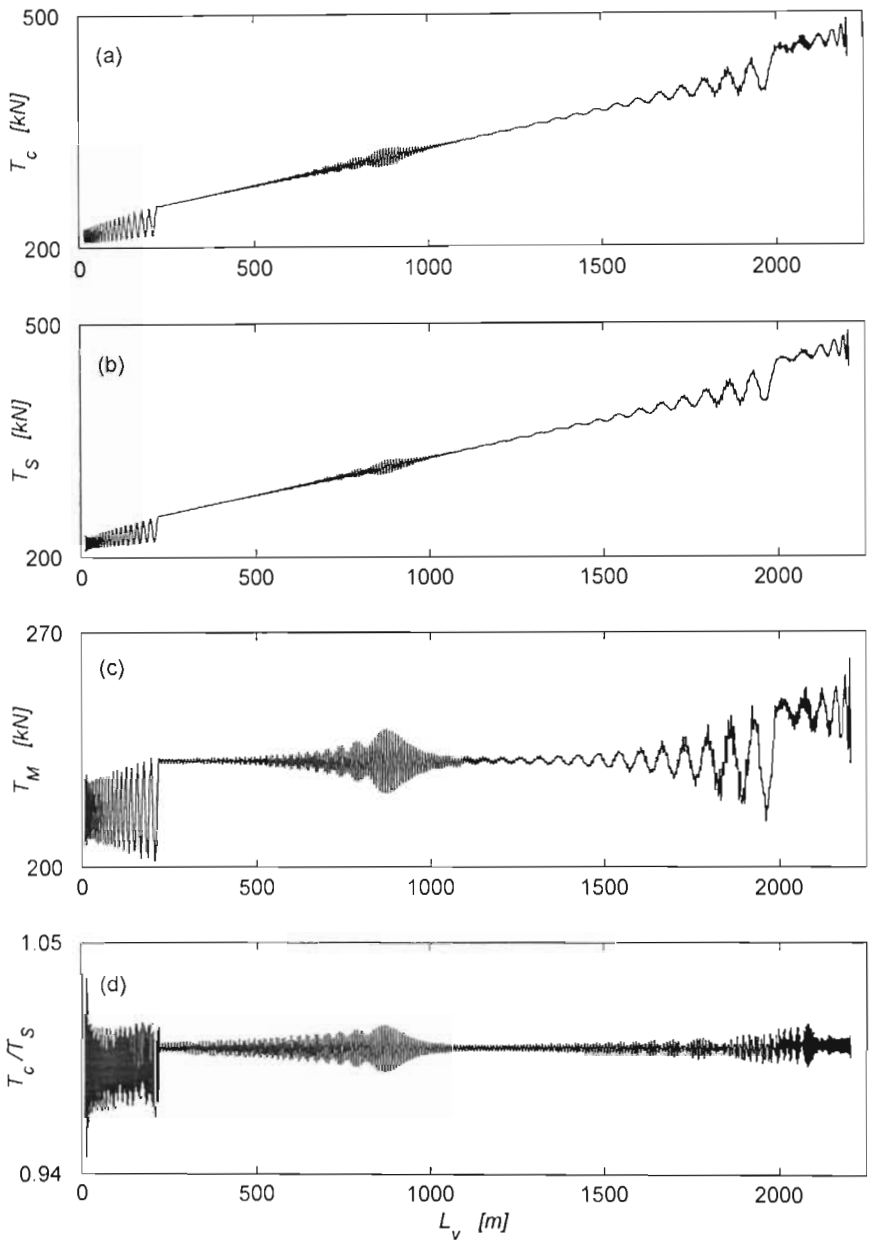

Figure 13. Total cable tensions for Elandsrand Mine winder at the nominal velocity $V_c = 16\ m/s$: (a) the catenary tension T_c; (b) the vertical rope tension T_S at the sheave; (c) the vertical rope tension T_M at the conveyance; (d) the tension ratio across the sheave T_c/T_S.

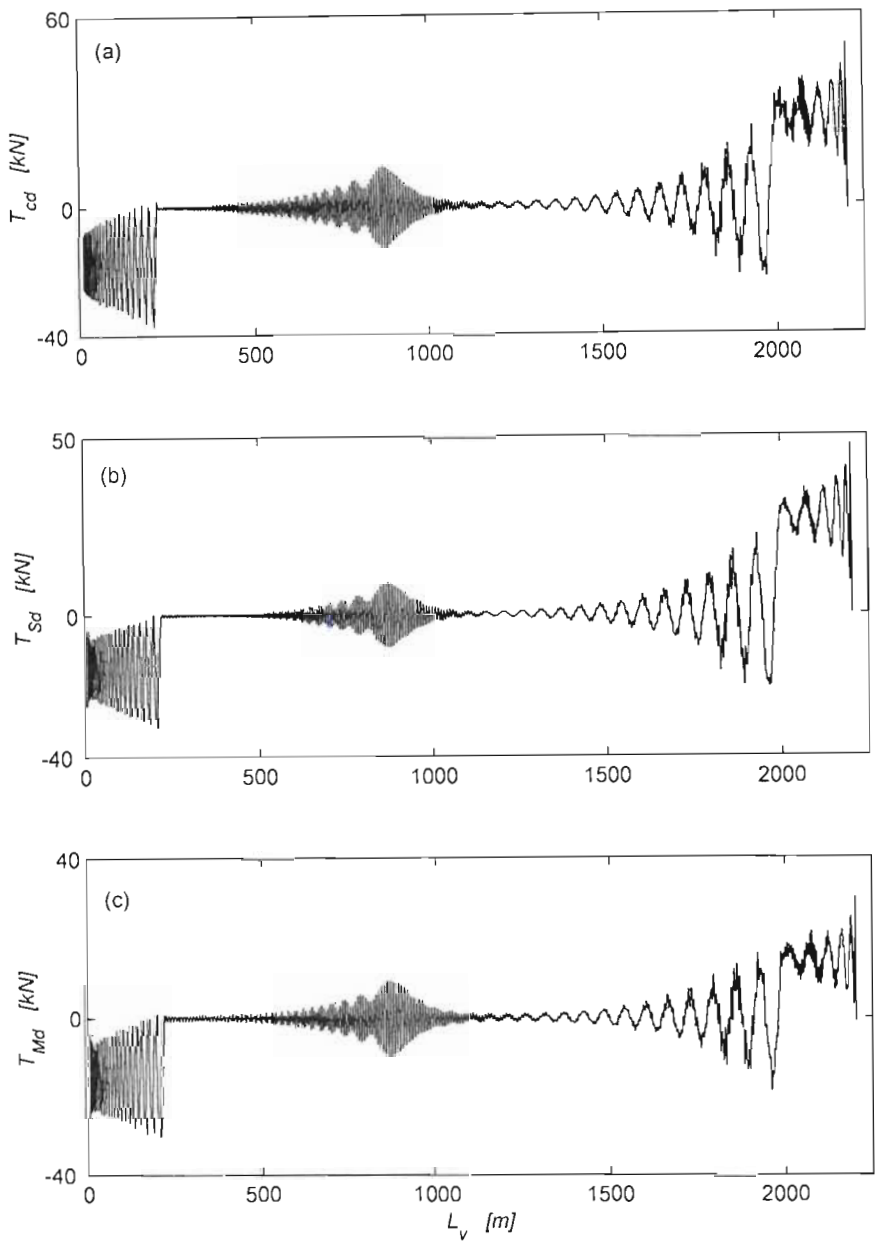

Figure 14. Dynamic cable tensions for Elandsrand Mine winder at the nominal velocity $V_c = 16\ m/s$: (a) the catenary dynamic tension T_{cd}; (b) the vertical rope dynamic tension T_{Sd} at the sheave; (c) the vertical rope dynamic tension T_{Md} at the conveyance.

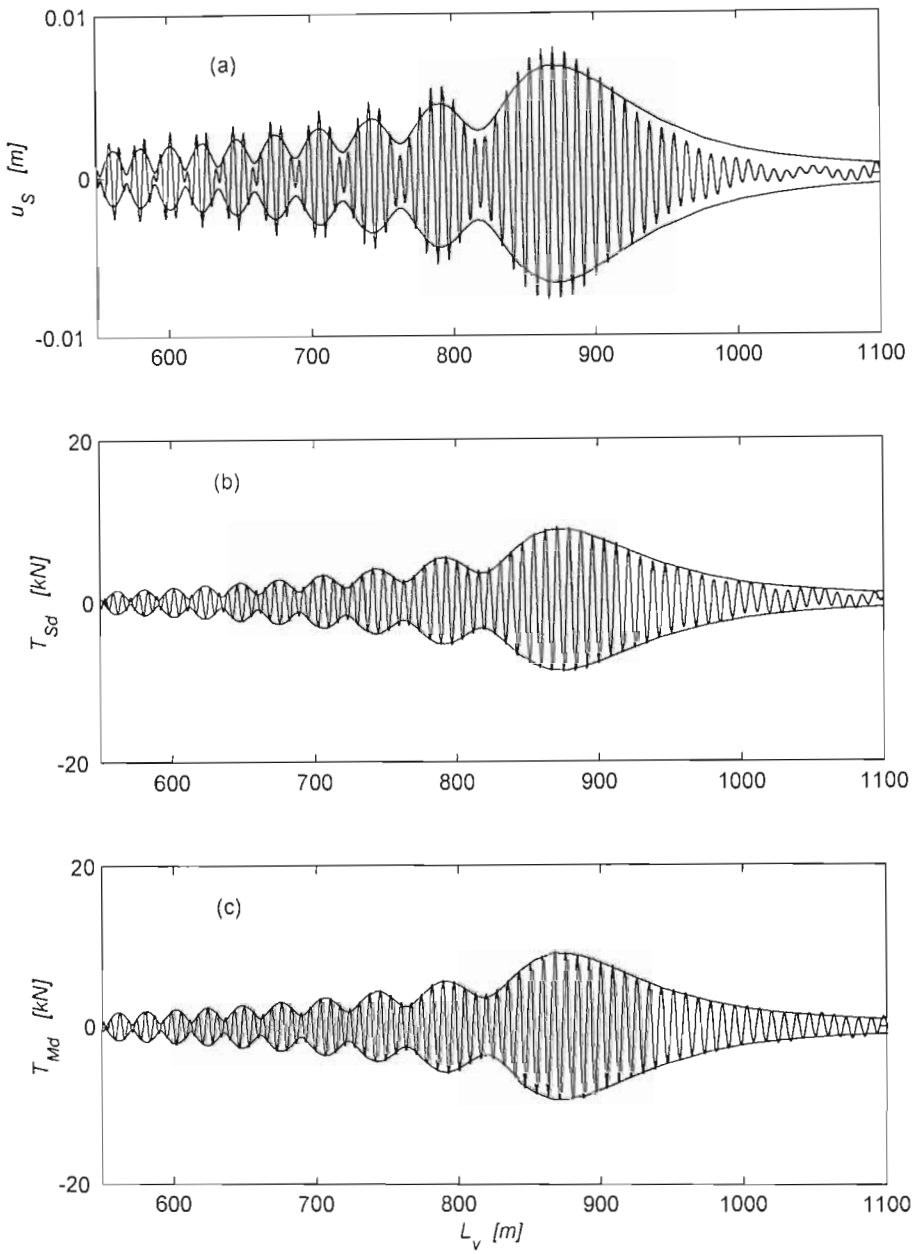

Figure 15. Overall response and dynamic cable tensons for Elandsrand Mine winder at the nominal velocity $V_c = 16\ m/s$ with superimposed envelope curves obtained from the multiple scales model at the resonance region: (a) the sheave response; (b) the rope tension at the sheave; (c) the rope tension at the conveyance.

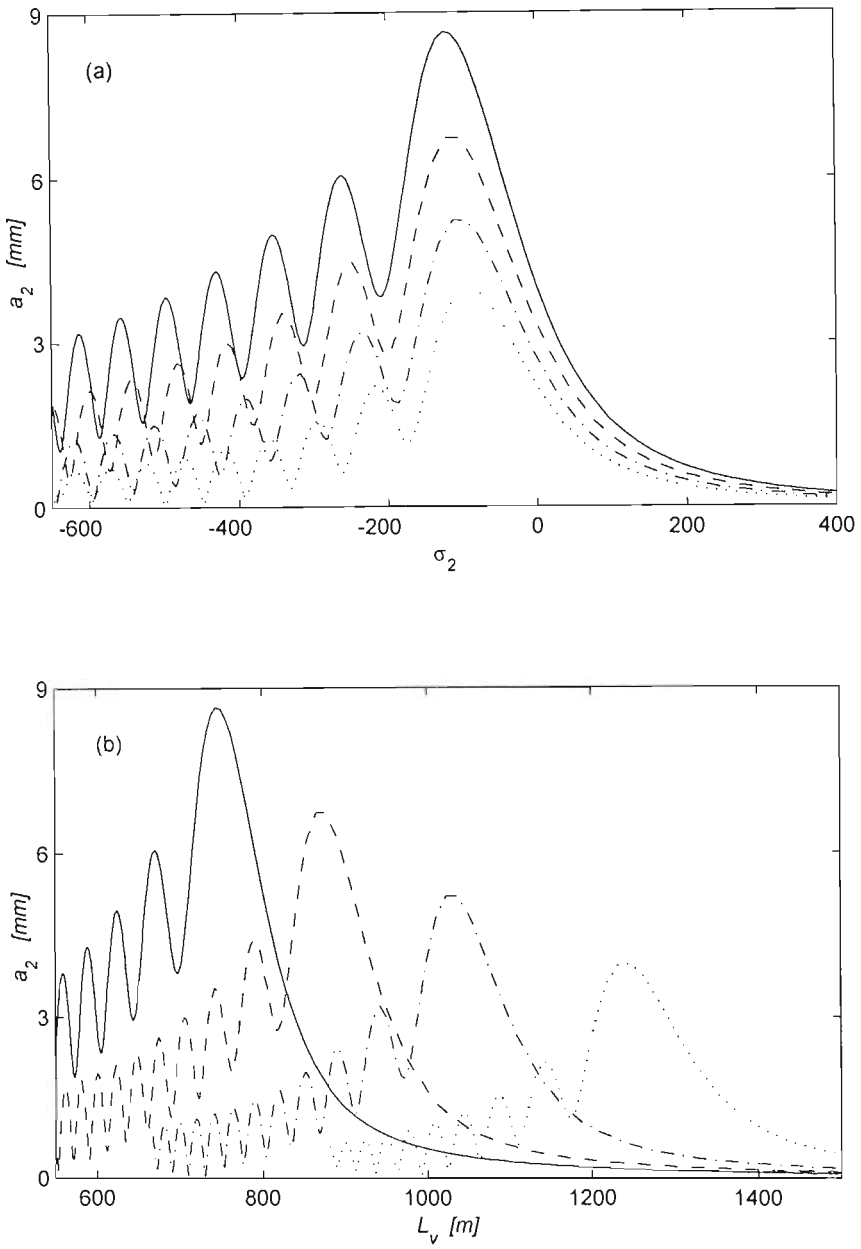

Figure 16. Non-stationary amplitude response during passage through resonance in Elandsrand Mine system: (a) the frequency-response curves; (b) amplitudes against the vertical length, for the winding velocities $V_c = 12\ (\cdots)$, $14\ (- \cdot -)$, $16\ (--)$, and $18\ (—)\ m/s$.

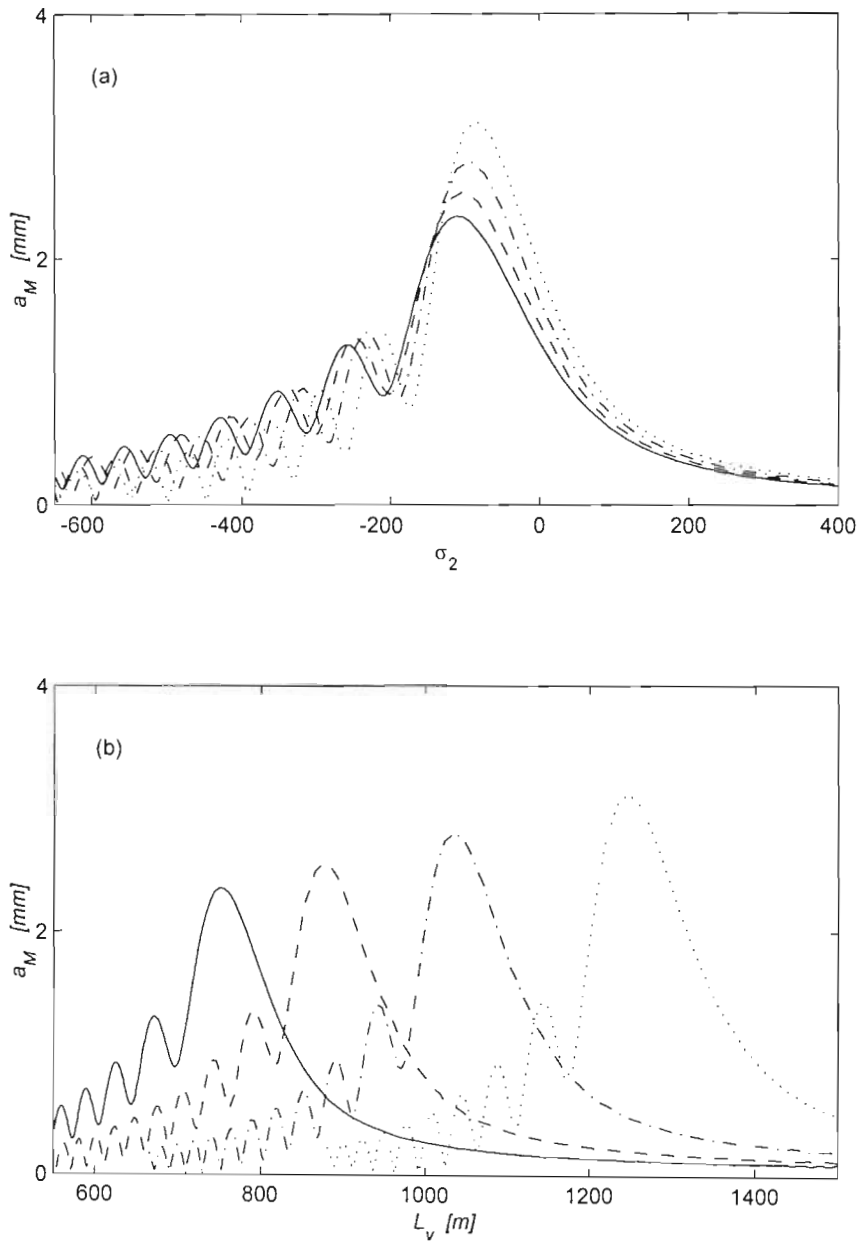

Figure 17. Conveyance amplitude response during passage through resonance in Elandsrand Mine system: (a) the non-stationary frequency-response curves; (b) amplitudes against the vertical length, for the winding velocities $V_c = 12$ $(\cdots)$, 14 $(- \cdot -)$, 16 $(--)$, and 18 $(—)$ m/s.

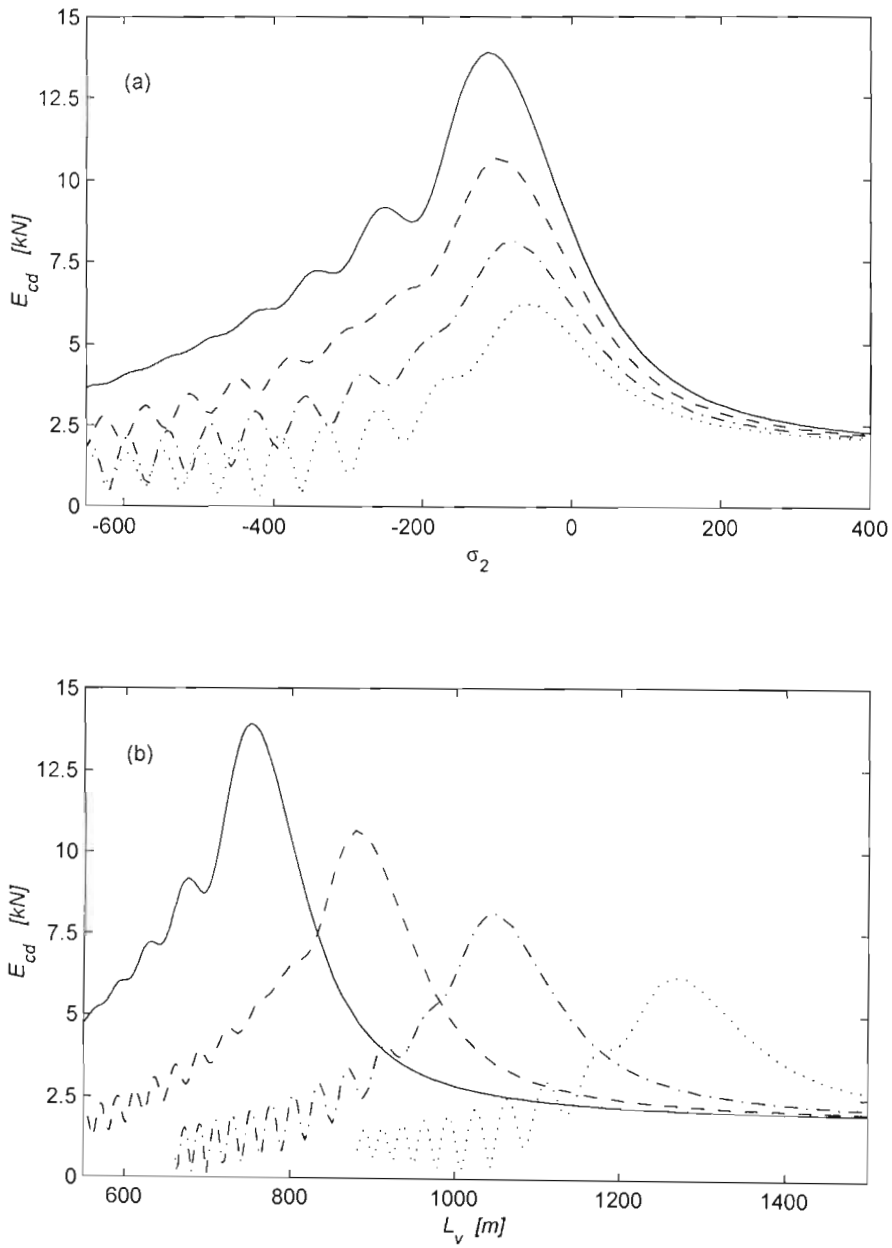

Figure 18. Catenary dynamic tension envelopes during passage through resonance in Elandsrand Mine system shown (a) against the frequency detuning parameter; (b) against the vertical length, for the winding velocities $V_c = 12\ (\cdots)$, $14\ (- \cdot -)$, $16\ (--)$, and $18\ (—)\ m/s$.

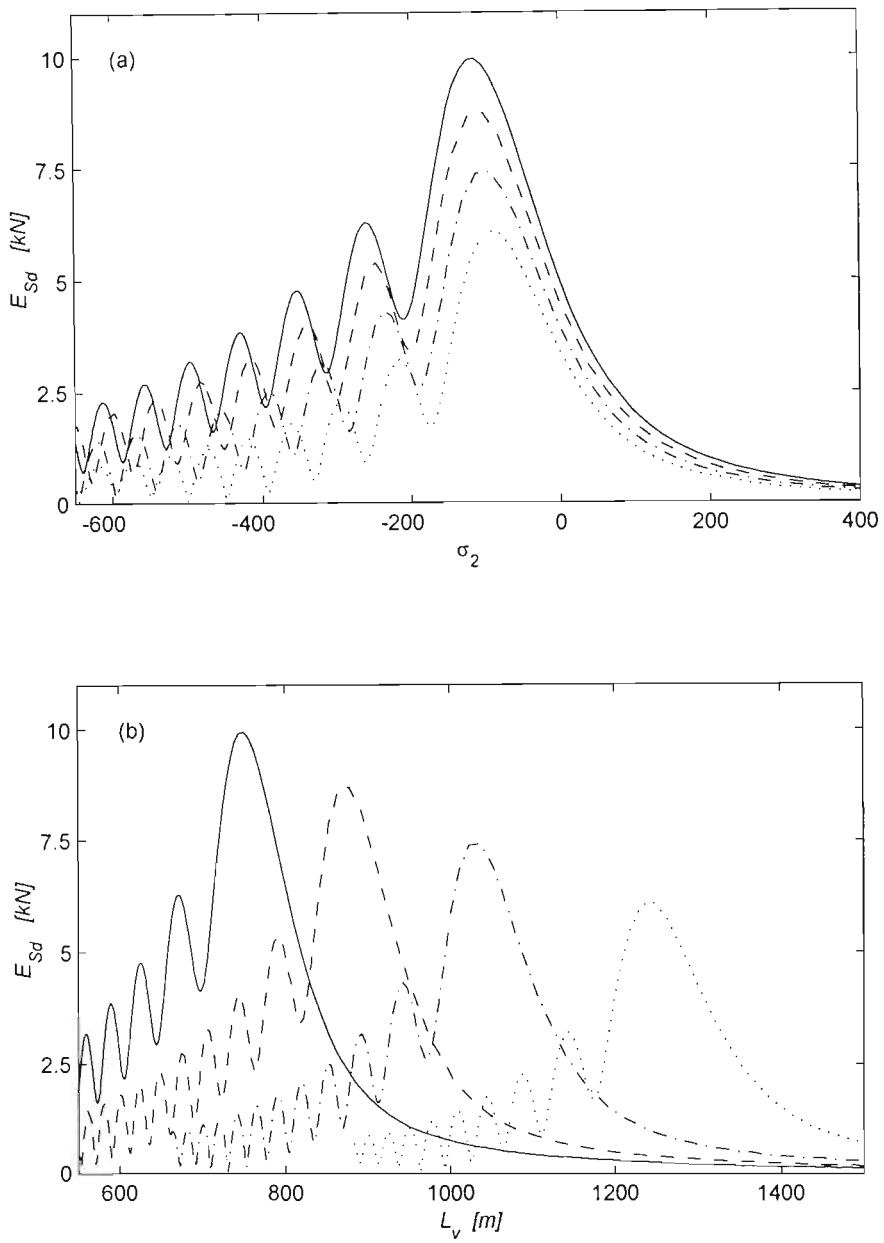

Figure 19. Sheave dynamic tension envelopes during passage through resonance in Elandsrand Mine system shown (a) against the frequency detuning parameter; (b) against the vertical length, for the winding velocities $V_c = 12\ (\cdots)$, $14\ (-\cdot-)$, $16\ (--)$, and $18\ (—)$ m/s.

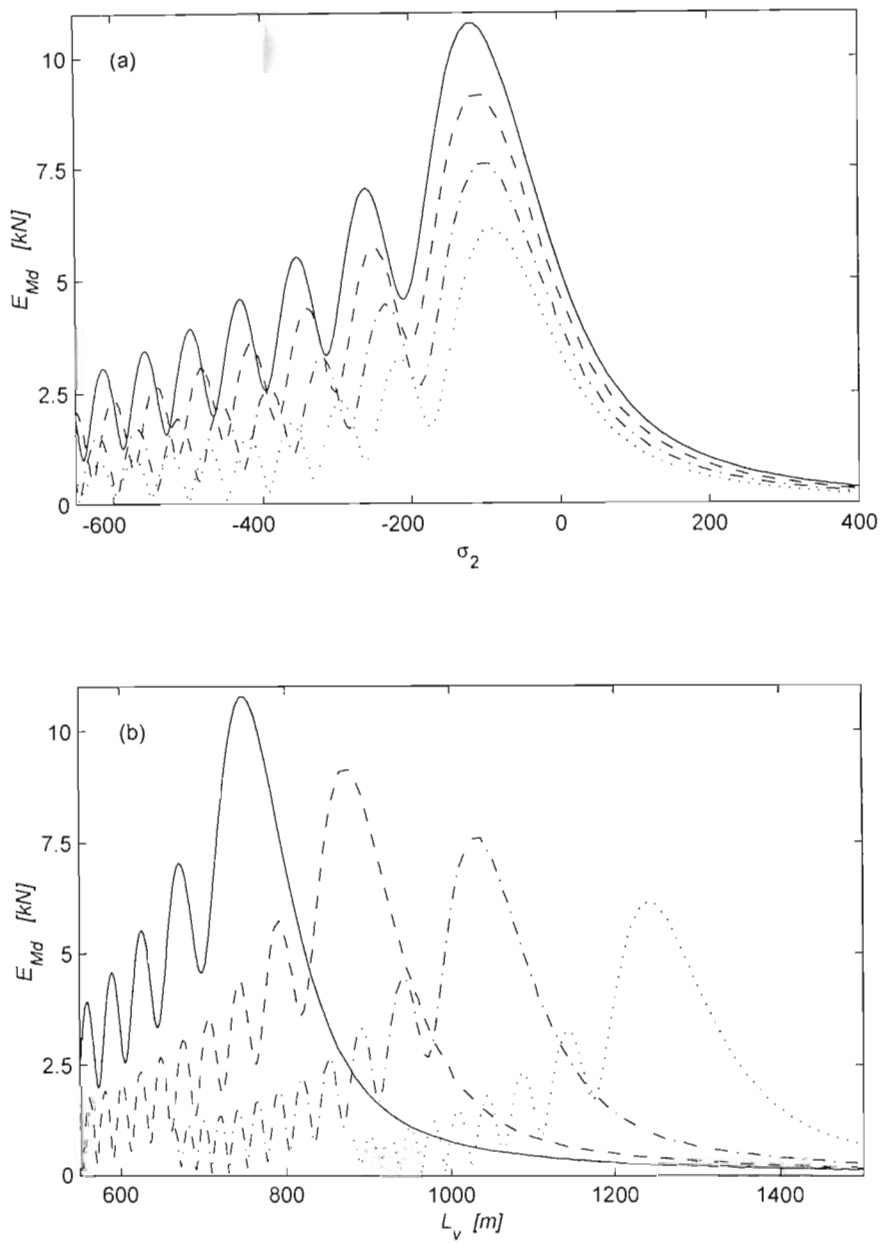

Figure 20. Conveyance dynamic tension envelopes during passage through resonance in Elandsrand Mine system shown (a) against the frequency detuning parameter; (b) against the vertical length, for the winding velocities $V_c = 12$ $(\cdots)$, 14 $(- \cdot -)$, 16 $(--)$, and 18 $(—)$ m/s.

vibration occurring in the system. The multiple scales method is used which leads to a system of first order ordinary differential equations for the amplitude and phase of the response. These are slowly varying functions and the system can be solved numerically without difficulty. The accuracy of this solution is verified against the overall response obtained from a numerical simulation of the original second order ordinary differential equations of motion. It is shown that the single-mode model approximates well the system in the main resonance region.

The analysis demonstrates that the main resonance is reached at higher depths for lower values of hoisting velocities. The amplitude plots reveal that the more rapid the passage through resonance, the smaller the maxima of the conveyance response, and the higher the maxima of the response at the sheave. The amplitudes decline after the passage due to damping developing beat phenomena. The dynamic cable tensions also grow rapidly during the passage, and reach higher levels for higher hoisting velocities.

Chapter 5
Non-Linear Interactions in a Hoisting Cable System

The dynamic behaviour of hoisting cables demonstrates a strongly non-linear character which was reported in published research [Dimitriou & Whiller, 1979; Mankowski, 1982; Constancon, 1993]. This non-linear behaviour includes *ballooning* or *whip* in long catenaries. Namely, conditions exist in mine hoist installations under which the lateral catenary motion becomes unstable and the cable begins to whirl like a jump rope. This phenomenon was observed also in many other string or cable systems [Nayfeh & Mook, 1979].

A non-linear model of the catenary-vertical rope system is given in terms of the partial differential equations (3.68), (3.69), and (3.70). The source of non-linearity in this system is the large displacement catenary approximation, and therefore is geometric in nature. Besides, the equations are defined over time dependent spatial domain rendering the problem non-stationary. Hence, the exact solution to this problem is not available, and recourse must be made to an approximate analysis. In what follows, the spatial variation of displacements is assumed in terms of the linear slowly varying undamped natural modes of the system, and the Rayleigh-Ritz procedure is employed to obtain non-linear, non-stationary, coupled second-order ordinary-differential equations describing the temporal behaviour. These equations are later analyzed numerically.

5.1 Discrete Model

The equations of motion (3.68), (3.69), and (3.70) can be discretised by applying the Rayleigh-Ritz procedure. Hence, the dynamic response of the catenary (lateral) system is approximated by the following expansions

$$\bar{v} = \sum_{n=1}^{N_{lat}} \Phi_n(s,l)p_n(t), \tag{5.1a}$$

$$\bar{w} = \sum_{n=1}^{N_{lat}} \Phi_n(s,l)q_n(t), \tag{5.1b}$$

where p_n and q_n are generalized (modal) coordinates, and Φ_n, are linear free-oscillation modes of the corresponding undamped stationary system. The in-plane and the out-of-plane modes Φ_n are assumed to be identical, and equivalent to those of a taut string, which in the co-ordinate system used are given as

$$\Phi_n = \sin[\frac{n\pi}{L_c}(s-l)]. \tag{5.2}$$

The corresponding natural frequencies are defined as $\bar{\omega}_n(l) = \frac{n\pi}{L_c}\bar{c}$, where $\bar{c} = \sqrt{\frac{T_c^i(l)}{m}}$, with the mean tension T_c^i given by equation (3.36) An approximate dynamic response of the vertical (longitudinal) system is represented by the series (4.14), with the shape functions Y_n defined by equation (4.15), and with the eigenvalues determined from the transcendental expression (4.16).

The expansions (5.1a) and (5.1b) result in the following expressions for partial derivatives of the lateral displacement functions

$$\bar{v}_{,t} = \sum_{n=1}^{N_{lat}} \left(\frac{\partial \Phi_n}{\partial l}\dot{l}p_n + \Phi_n \dot{p}_n \right), \ \bar{w}_{,t} = \sum_{n=1}^{N_{lat}} \left(\frac{\partial \Phi_n}{\partial l}\dot{l}q_n + \Phi_n \dot{q}_n \right), \tag{5.3}$$

$$\bar{v}_{,s} = \sum_{n=1}^{N_{lat}} \Phi_n' p_n, \ \bar{w}_{,s} = \sum_{n=1}^{N_{lat}} \Phi_n' q_n, \tag{5.4}$$

$$\bar{v}_{,tt} = \sum_{n=1}^{N_{lat}} \left[\left(\frac{\partial^2 \Phi_n}{\partial l^2}\dot{l}^2 + \frac{\partial \Phi_n}{\partial l}\ddot{l} \right) p_n + 2\frac{\partial \Phi_n}{\partial l}\dot{l}\dot{p}_n + \Phi_n \ddot{p}_n \right], \tag{5.5a}$$

$$\bar{w}_{,tt} = \sum_{n=1}^{N_{lat}} \left[\left(\frac{\partial^2 \Phi_n}{\partial l^2} \dot{l}^2 + \frac{\partial \Phi_n}{\partial l} \ddot{l} \right) q_n + 2 \frac{\partial \Phi_n}{\partial l} \dot{l} \dot{q}_n + \Phi_n \ddot{q}_n \right], \tag{5.5b}$$

$$\bar{v}_{,ss} = \sum_{n=1}^{N_{lat}} \Phi_n'' p_n, \ \bar{w}_{,ss} = \sum_{n=1}^{N_{lat}} \Phi_n'' q_n, \tag{5.6}$$

$$\bar{v}_{,st} = \sum_{n=1}^{N_{lat}} \left(\frac{\partial \Phi_n'}{\partial l} \dot{l} p_n + \Phi_n' \dot{p}_n \right), \ \bar{w}_{,st} = \sum_{n=1}^{N_{lat}} \left(\frac{\partial \Phi_n'}{\partial l} \dot{l} q_n + \Phi_n' \dot{q}_n \right), \tag{5.7}$$

$$\bar{v}_{,sst} = \sum_{n=1}^{N_{lat}} \left(\frac{\partial \Phi_n''}{\partial l} \dot{l} p_n + \Phi_n'' \dot{p}_n \right), \ \bar{w}_{,sst} = \sum_{n=1}^{N_{lat}} \left(\frac{\partial \Phi_n''}{\partial l} \dot{l} q_n + \Phi_n'' \dot{q}_n \right). \tag{5.8}$$

where the primes denote partial derivatives with respect to s.

By substituting the series (5.4) into the expression (3.56) the discretised form of the catenary strain e can be obtained. This is accomplished by finding directly from the expansions (5.1a) and (5.1b) that

$$\bar{v}_{,s}^2 = \sum_{i=1}^{N_{lat}} \sum_{j=1}^{N_{lat}} p_i p_j \Phi_i' \Phi_j', \tag{5.9a}$$

$$\bar{w}_{,s}^2 = \sum_{i=1}^{N_{lat}} \sum_{j=1}^{N_{lat}} q_i q_j \Phi_i' \Phi_j', \tag{5.9b}$$

so that, when the orthogonality properties of the lateral modes are applied, the following results

$$\int_l^{L_1} (\bar{v}_{,s}^2 + \bar{w}_{,s}^2) ds = \frac{\pi^2}{2L_c} \sum_{n=1}^{N_{lat}} n^2 (p_n^2 + q_n^2). \tag{5.10}$$

Noting also that

$$\int_l^{L_1} \bar{v}_{,s} = \int_l^{L_1} \bar{w}_{,s} = 0, \tag{5.11}$$

and applying the series (4.14) with the eigenfunctions (4.15) to express the deflection at the sheave as $u_v(L_1,t) = \sum_{n=1}^{N_{long}} z_n$, the following expression for the catenary strain results

$$e(t) = F_l(t) + \frac{1}{L_c}\sum_{n=1}^{N_{long}} z_n + \sum_{n=1}^{N_{lat}} \beta_n^2(p_n^2 + q_n^2), \tag{5.12}$$

where $F_l(t) = \frac{1}{L_c}\left\{\frac{1}{2L_c}[v_l^2(t) + w_l^2(t)] - u_l(t)\right\}$, and $\beta_n = \frac{n\pi}{2L_c}$.

By substituting the expansions (5.3)-(5.8) together with the strain (5.12) into the differential equations of motion (3.68) and (3.69), and by applying the Rayleigh-Ritz procedure, the discretised lateral equations in the following form are obtained

$$\begin{aligned}\ddot{p}_k + 2\bar{\zeta}_k\bar{\omega}_k\dot{p}_k + \bar{\omega}_k^2\left[1 + \left(\tfrac{c}{\bar{c}}\right)^2 F_l(t)\right] p_k = -\tfrac{2}{m_k}\dot{l}\textstyle\sum_{n=1}^{N_{lat}} C_{kn}\dot{p}_n - \\ \tfrac{1}{m_k}\textstyle\sum_{n=1}^{N_{lat}}\left(\dot{l}^2 D_{kn} + \ddot{l}C_{kn} - \lambda_1\dot{l}T_c^i B_{kn} + \lambda_2\dot{l}C_{kn}\right) p_n - \\ \left(\tfrac{c}{\bar{c}}\right)^2\bar{\omega}_k^2\left[\tfrac{1}{L_c}\textstyle\sum_{n=1}^{N_{long}} z_n + \sum_{n=1}^{N_{lat}}\beta_n^2(p_n^2+q_n^2)\right] p_k + P_k(t),\end{aligned} \tag{5.13}$$

$$\begin{aligned}\ddot{q}_k + 2\bar{\zeta}_k\bar{\omega}_k\dot{q}_k + \bar{\omega}_k^2\left[1 + \left(\tfrac{c}{\bar{c}}\right)^2 F_l(t)\right] q_k = -\tfrac{2}{m_k}\dot{l}\textstyle\sum_{n=1}^{N_{lat}} C_{kn}\dot{q}_n - \\ \tfrac{1}{m_k}\textstyle\sum_{n=1}^{N_{lat}}\left(\dot{l}^2 D_{kn} + \ddot{l}C_{kn} - \lambda_1 T_c^i\dot{l}B_{kn} + \lambda_2\dot{l}C_{kn}\right) q_n - \\ \left(\tfrac{c}{\bar{c}}\right)^2\bar{\omega}_k^2\left[\tfrac{1}{L_c}\textstyle\sum_{n=1}^{N_{long}} z_n + \sum_{n=1}^{N_{lat}}\beta_n^2(p_n^2+q_n^2)\right] q_k + Q_k(t),\end{aligned} \tag{5.14}$$

where $k = 1, 2, \ldots, N_{lat}$, and

$$\bar{\zeta}_k = \frac{1}{2}\left(\lambda_1\bar{\omega}_k + \frac{\lambda_2}{\bar{\omega}_k}\right), \tag{5.15a}$$

$$m_k = m\int_l^{L_1}\Phi_k^2 ds, \tag{5.15b}$$

$$B_{kn} = \int_l^{L_1}\Phi_k\frac{\partial\Phi_n''}{\partial l}ds, \tag{5.15c}$$

$$C_{kn} = m\int_l^{L_1}\Phi_k\frac{\partial\Phi_n}{\partial l}ds, \tag{5.15d}$$

$$D_{kn} = m\int_l^{L_1}\Phi_k\frac{\partial^2\Phi_n}{\partial l^2}ds, \tag{5.15e}$$

$$P_k = \frac{1}{m_k}\int_l^{L_1}\Phi_k F_v(s,t)ds, \tag{5.15f}$$

$$Q_k = \frac{1}{m_k}\int_l^{L_1} \Phi_k F_w(s,t)ds. \tag{5.15g}$$

Similarly, the nonlinear longitudinal equation of motion (3.70) is discretised by using the expansion (4.14) together with (5.1a), and (5.1b). Noting that this transforms equation (3.58) into the form

$$f_c(t) = \frac{1}{2L_c}\left[\sum_{n=1}^{N_{lat}} \frac{n^2\pi^2}{2}(p_n^2+q_n^2) + v_l^2 + w_l^2\right], \tag{5.16}$$

the Rayleigh-Ritz method yields the following equation

$$\begin{aligned}\ddot{z}_r + \mu_2\dot{z}_r + \omega_r^2 z_r = &-\tfrac{1}{m_r^v}\textstyle\sum_{n=1}^{N_{long}}\left[2\dot{l}C_{rn}^v - EA\Lambda_{rn} + M_S\dot{l}\left(\tfrac{1}{L_c} - \tfrac{M_S}{m}\gamma_n^2\right)\right]\dot{z}_n - \\ &\tfrac{1}{m_r^v}\textstyle\sum_{n=1}^{N_{long}}\left(\dot{l}^2 D_{rn}^v + \ddot{l}C_{rn}^v - EA\dot{l}B_{rn}^v + \mu_2\dot{l}C_{rn}^v + M_S\dot{l}^2\Gamma_n\right)z_n - \\ &\tfrac{EA}{m_r^v}\left[\textstyle\sum_{n=1}^{N_{lat}}\beta_n^2(p_n^2+q_n^2) + F_l(t)\right] + Z_r,\end{aligned} \tag{5.17}$$

where $r = 1, 2, \ldots, N_{long}$, and the non-stationary coefficients m_r^v, B_{rn}^v, C_{rn}^v, D_{rn}^v, Γ_n, Λ_{rn}, and the excitation term Z_r are defined by the expressions (4.24a)-(4.24g).

The lateral coefficients and excitation terms (5.15b)-(5.15g) can be determined directly, and are given as

$$m_k = \frac{1}{2}mL_c, \tag{5.18a}$$

$$B_{kn} = \left\{ \begin{array}{l} -\left(\frac{\pi}{L_c}\right)^2 \frac{rn^3\left[(-1)^{k+n}-1\right]}{k^2-n^2},\ k \neq n \\ 0,\ k = n \end{array} \right\}, \tag{5.18b}$$

$$C_{kn} = \left\{ \begin{array}{l} m\frac{rn\left[(-1)^{k+n}-1\right]}{k^2-n^2},\ k \neq n \\ 0,\ k = n \end{array} \right\}, \tag{5.18c}$$

$$D_{kn} = \left\{ \begin{array}{l} 0,\ k \neq n \\ -m\frac{n^2\pi}{2L_c},\ k = n \end{array} \right\}, \tag{5.18d}$$

$$P_k = -\frac{2}{k\pi}\left\{\ddot{v}_l - \left(2\dot{v}_l\frac{\dot{l}}{L_c} + v_l\frac{\ddot{l}}{L_c}\right)\left[(-1)^k - 1\right]\right\}, \tag{5.18e}$$

$$Q_k = -\frac{2}{k\pi}\left\{\ddot{w}_l - \left(2\dot{w}_l\frac{\dot{l}}{L_c} + w_l\frac{\ddot{l}}{L_c}\right)\left[(-1)^k - 1\right]\right\}. \tag{5.18f}$$

The longitudinal coefficients and excitation terms appearing in the longitudinal equation (5.17) depend on the non-stationary eigenvalues γ_n, and must be calculated numerically following the procedure outlined in Appendix B, as indicated earlier in Chapter 4.

It should be noted that the lateral natural frequency in equations (5.13) and (5.14), as well as the longitudinal natural frequency and coefficients in (5.17) depend on the non-stationary parameter l, and are varying slowly. Hence, their variation can be observed on a slow time scale, and following the formulation used Chapter 4 this scale is defined as $\tau = \varepsilon T$, where ε is a small parameter. T denotes the fast scale given by equation (4.28), and a variation of the generalized co-ordinates p_k, q_k, and z_r are observed on this fast scale. By assuming that the damping is small, the longitudinal damping coefficients are ordered as in the expressions (4.36) and (4.37). Similarly, the lateral damping coefficients are arranged as

$$\lambda_1 = \varepsilon\lambda_1^*, \tag{5.19a}$$

$$\lambda_2 = \varepsilon\lambda_2^*, \tag{5.19b}$$

so that

$$\bar{\zeta}_k = \varepsilon\bar{\zeta}_k^*. \tag{5.20}$$

Therefore, by substituting the expressions (4.32)-(4.35) together with the time derivatives of the in- and out-of-plane temporal co-ordinates given as

$$\dot{p}_k = \omega_0\frac{dp_k}{dT},\ \ddot{p}_k = \omega_0\frac{d^2p_k}{dT^2}, \tag{5.21a}$$

$$\dot{q}_k = \omega_0\frac{dq_k}{dT},\ \ddot{q}_k = \omega_0\frac{d^2q_k}{dT^2}, \tag{5.21b}$$

for $k = 1, 2, \ldots, N_{lat}$, respectively, into equations (5.13), (5.14), and (5.17), the following results

$$\frac{d^2p_k}{dT^2} + \hat{\omega}_k^2(\tau)\left[1 + \left(\frac{c}{\bar{c}}\right)^2 F_l(T)\right] p_k = \varepsilon f_k^p(\tau, \frac{dp_1}{dT}, \ldots, \frac{dp_{N_{lat}}}{dT}) -$$
$$\left(\frac{c}{\bar{c}}\right)^2 \hat{\omega}_k^2(\tau)\left[\frac{1}{L_c}\sum_{n=1}^{N_{long}} z_n + \sum_{n=1}^{N_{lat}} \beta_n^2(p_n^2 + q_n^2)\right] p_k + \hat{P}_k(\tau, T) + O(\varepsilon^2), \quad (5.22)$$

$$\frac{d^2q_k}{dT^2} + \hat{\omega}_k^2(\tau)\left[1 + \left(\frac{c}{\bar{c}}\right)^2 F_l(T)\right] q_k = \varepsilon f_k^q(\tau, \frac{dq_1}{dT}, \ldots, \frac{dq_{N_{lat}}}{dT}) -$$
$$\left(\frac{c}{\bar{c}}\right)^2 \hat{\omega}_k^2(\tau)\left[\frac{1}{L_c}\sum_{n=1}^{N_{long}} z_n + \sum_{n=1}^{N_{lat}} \beta_n^2(p_n^2 + q_n^2)\right] q_k + \hat{Q}_k(\tau, T) + O(\varepsilon^2), \quad (5.23)$$

where $k = 1, 2, \ldots, N_{lat}$, $\hat{\omega}_k = \frac{\bar{\omega}_k}{\omega_0}$, $\hat{P}_k = \frac{P_k}{\omega_0^2}$, $\hat{Q}_k = \frac{Q_k}{\omega_0^2}$, and

$$\frac{d^2z_r}{dT^2} + \tilde{\omega}_r^2(\tau) z_r = \varepsilon f_r^z(\tau, \frac{dz_1}{dT}, \ldots \frac{dz_{N_{long}}}{dT}) -$$
$$\frac{EA}{\omega_0^2 m_r^v(\tau)}\left[\sum_{n=1}^{N_{lat}} \beta_n^2(p_n^2 + q_n^2) + F_l(T)\right] + \hat{Z}_r(\tau, T) + O(\varepsilon^2), \quad (5.24)$$

where $r = 1, 2, \ldots, N_{long}$, $\hat{Z}_r = \frac{Z_r}{\omega_0^2}$, and

$$f_k^p = -2\left[\frac{l'}{m_k}\sum_{n=1}^{N_{lat}} C_{kn}\frac{dp_n}{dT} + \bar{\zeta}_k^* \hat{\omega}_k \frac{dp_k}{dT}\right], \quad (5.25a)$$

$$f_k^q = -2\left[\frac{l'}{m_k}\sum_{n=1}^{N_{lat}} C_{kn}\frac{dq_n}{dT} + \bar{\zeta}_k^* \hat{\omega}_k \frac{dq_k}{dT}\right], \quad (5.25b)$$

$$f_r^z = -\frac{1}{m_r^v(\tau)}\sum_{n=1}^{N_{long}}\left[2l' C_{rn}^v(\tau) - \frac{EA}{\omega_0}\Lambda_{rn}^* + M_S l'\left(\frac{1}{L_c} - \frac{M_S}{m}\gamma_n^2\right)\right]\frac{dz_n}{dT}$$
$$-\frac{\mu_2^*}{\omega_0}\frac{dz_r}{dT}, \quad (5.25c)$$

where $\Lambda_{rn}^*(\tau) = \int_{L_1}^{L_0} \mu_1^* Y_r Y_n'' ds$.

The discrete model equations (5.22)-(5.24) form a non-linear slowly varying ordinary-differential equation system. It describes the interactions of lateral oscillations of the catenary cable and of longitudinal oscillations of the vertical rope in the hoisting cable system. In the catenary (lateral) system a quadratic coupling between the lateral and the longitudinal modes exists, and a cubic coupling arises between the in- and out-of-plane lateral modes. In the vertical rope (longitudinal) system a quadratic coupling with the lateral modes results. The lateral and longitudinal natural frequencies change with time, and linear coupling terms due to the non-stationary nature of the natural modes arise. The lateral system equations contain parametric excitation terms. Terms representing the inertial load due to the axial transport motion, and the cross-over external excitation are present in both systems.

5.2 Damping Parameters

The equivalent proportional viscous damping has been assumed in the non-linear model to represent both the lateral and longitudinal overall damping effort in the system. The longitudinal damping parameters have already been discussed and defined in the analysis presented in Chapter 4. The choice of the cable lateral damping parameters requires attention.

There is not much published research available concerning the lateral damping in wire cables. The basic nature of internal damping in stranded structural cables and its influence on transverse vibration was studied by Yu [1952]. In this study, static and dynamic experimental tests on 7-wire cable specimens were performed, from which the deformation and energy relationships were developed. It was established that interstrand dry friction is the main source of internal damping in wire cables, and energy dissipation per cycle (damping capacity) is a linear function of amplitude. Factors that may influence internal damping were also identified, namely, that the test results indicated the increase of damping capacity with the reduction of lay length; the increase of this capacity with the increase of number of wires

in strands of comparable sizes; and the reduction of the capacity with prestressing of cables over yield point. It was also shown that cables with wires in which the twist was formed before they were stranded together (*preformed* cables) possess less damping capacity that non-preformed ones.

Vanderveldt, Chung & Reader [1973] also conducted damping studies in wire ropes of various types, and determined the lateral equivalent viscous damping coefficient from measurement of the logarithmic decrement. The results of this investigation showed that the damping coefficient increases with increasing axial load applied to the rope. It was concluded that this increasing tensile load contributes to the friction effects between individual wires and strands, and that Coulomb damping is responsible for a major portion of the equivalent damping coefficient. Furthermore, it was also established, that the geometry and construction of a wire rope has a significant influence on the damping coefficient.

Irvine [1981] studied the dynamic response of a flat-sag suspended cable making provision for lateral viscous damping through modal damping, introduced in the discrete model of the cable. He stated that the internal damping in wire cables, represented by λ_1 in (3.65), is affected by the lay of the strands and is usually small, resulting due to rubbing between individual wires. He quoted also that the internal damping could be expected to be larger in slack cables rather than in taut cables, with the corresponding damping ratios $\zeta = 4\,\%$ and $\zeta = 0.4\,\%$, respectively. The air (external) damping, represented by λ_2, was identified as negligible in still air, but as contributing substantially to the energy dissipation in strong winds, with the suggested damping ratio up to $4\,\%$.

Mankowski [1988] proposed an empirical formula for quantifying the damping mechanism occurring in mine hoisting cables undergoing non-planar lateral motion. He expressed the power dissipation in terms of the amplitude and frequency of vibration, the cable span, and two experimentally determined coefficients, namely the damping capacity coefficient, and the curvature characteristic. A mathematical relationship was developed that enabled

the amount of internal power loss due to damping to be assessed. Furthermore, it was established that a critical cable curvature exists above which the internal power loss increased linearly with increasing amplitude-to-span ratio. The results of this research were extended and applied to assess the effects of internal friction occurring at the wavefront of travelling transverse disturbances on mine hoisting cable [Mankowski, 1990].

Constancon [1993] used this damping model and converted Mankowski's results into equivalent viscous damping coefficients, and consequently determined the corresponding equivalent damping ratios ζ, which were identified to be very small, namely ranging from $0.007\,\%$ to $0.017\,\%$. He indicated that aerodynamic effects may be significant in the lateral damping mechanism, and determined the corresponding equivalent viscous damping coefficients in terms of the air density, cable diameter and span, and the amplitude and frequency of vibration. The corresponding damping ratios were calculated for the same parameters as used by Mankowski, and were found to be between $0.04\,\%$ to $0.1\,\%$.

Due to the lack of any other reliable lateral damping data, Mankowski's test results are used as the basis of the lateral damping model in the present analysis. Consequently, the lateral damping is represented by ratios $\bar{\zeta}_r$ in the equations of motion (5.13) and (5.14), and the order of these ratios is established following the calculations summarized in Appendix E.

5.3 Excitation Definition

The cross-over excitation represented by periodic functions $v_l(t)$, $w_l(t)$, and $u_l(t)$ is imparted to the system during the winding cycle. Typically a repetitive coiling pattern during a winding cycle in hoist systems is achieved via a symmetrical 180° Lebus liner as discussed earlier and shown in Figure 9.

The lateral out-of–plane excitation w_l occurs due to a traverse motion of the cable in the cross-over zone across the drum through a distance of a half its diameter, relative to the entry position. As multiple layers are required to wind the cable, the direction of this motion is reversed after the layer change which represents a 180^o phase shift in the excitation relative to that of the previous layer. The cross-over excitation v_l in the lateral in-plane direction takes place on the second and higher layers, and represents a radial shift of the cable over underlying coils of the previous layer. An additional axial displacement relative to the nominal transport motion is also applied to the cable in the cross-over region. As stated earlier, this is a consequence of the increase in the axial velocity of the cable to compensate for the difference between the arc length covered through a cross-over, and that which would be covered without a cross-over. This effect is represented by the excitation component u_l.

These excitation functions can be defined in terms of the geometry of the system and the transport velocity. Mankowski]1982] proposed a definition by means of versine functions. During the constant velocity phase the excitation functions are given by the following equations

$$v_l = \left\{ \begin{array}{ll} \frac{1}{2}v_0^n \left[1 - \cos(2\nu t)\right], & 0 \leq t \leq t_\beta \\ 0, & t_\beta \leq t \leq \tau \end{array} \right\}, \tag{5.26}$$

$$w_l = \left\{ \begin{array}{ll} \frac{1}{2}w_0 \left[1 - \cos(\nu t)\right], & 0 \leq t \leq t_\beta \\ \frac{d}{2}, & t_\beta \leq t \leq \tau \end{array} \right\}, \tag{5.27}$$

$$u_l = \left\{ \begin{array}{ll} \frac{1}{2}u_0 \left[1 - \cos(\nu t)\right], & 0 \leq t \leq t_\beta \\ u_0(\tau - t)/(\tau - t_\beta), & t_\beta \leq t \leq \tau \end{array} \right\}, \tag{5.28}$$

where v_0, w_0, and u_0 are determined from the geometry of a cross-over as

$$v_0^n = (n-1)(1 - \frac{\sqrt{3}}{2})d, n = 1, 2, 3, 4, \tag{5.29}$$

$$w_0 = \frac{d}{2}, \tag{5.30}$$

$$u_0 = R_d\beta \left[\sqrt{1 + \left(\frac{d}{2R_d\beta}\right)^2 + \left(\frac{2v_0^n}{R_d\beta}\right)^2} - 1 \right], \tag{5.31}$$

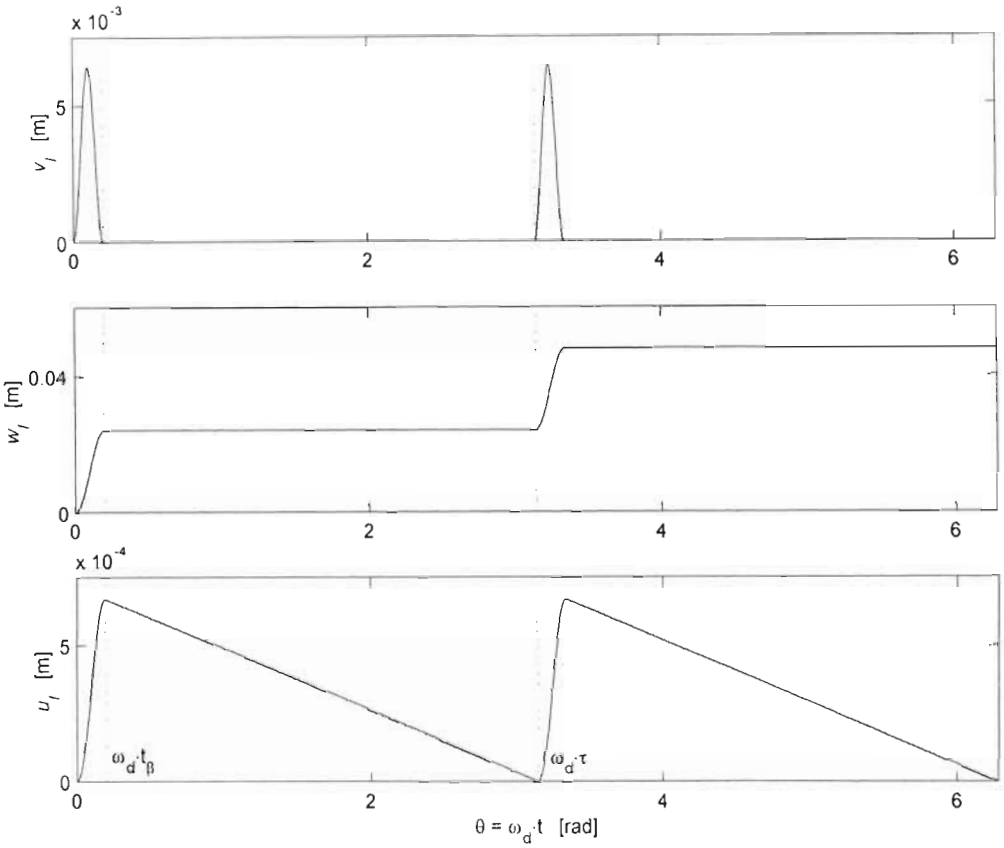

Figure 21. Boundary excitation functions

in which n denotes the layer number, d is the cable diameter, R_d is the drum radius, β is the angle defining the cross-over diametrical arc, and where $t_\beta = \beta/\omega_d$, with $\omega_d = V_c/R_d$, represents the duration of the cross-over pulse, $\tau = \pi/\Omega$, where $\Omega = 2\omega_d$, is the period of the excitation, V_c denotes the nominal transport velocity, and $\nu = \pi/t_\beta$. The boundary excitation functions for the values of $d = 0.048\,m$, $R_d = 2.14\,m$, $V_c = 15\,m/s$, and $\beta = 0.2\,rad$, are shown in Figure 21

5.4 Numerical Simulation and Results

The non-linearly coupled equations (5.22)-(5.24) describing the temporal behaviour and interactions in the catenary-vertical rope system, are of a complicated nature, and cannot be solved exactly. An approximate solution can be sought using asymptotic (perturbation) methods. However, the strictly non-stationary nature of this system, namely the fact that both the system parameters and excitation are time-varying, introduces a substantial complication to an asymptotic analysis of the system. This complication, combined with the non-linear nature of the system, leads to involved algebraic manipulations, and to a situation intractable to perturbation analysis. Thus, a numerical analysis is applied in what follows in order to predict the dynamic behaviour of the system.

In this analysis the system (5.22)-(5.24) is represented in the matrix form given by the equation

$$\dot{\mathbf{y}} = \mathbf{A}\left(T, \tau; \varepsilon\right) \mathbf{y} + \mathbf{N}\left(\tau, \mathbf{y}\right) + \mathbf{F}\left(T, \tau\right), \tag{5.32}$$

where $\mathbf{y} = \left[\mathbf{p}^T, \mathbf{q}^T, \mathbf{z}^T, \dot{\mathbf{p}}^T, \dot{\mathbf{q}}^T, \dot{\mathbf{z}}^T\right]^T$ is the $2\left(2N_{lat} + N_{long}\right)$-dimensional modal state vector, with $\mathbf{p} = \left[p_1, p_2, \ldots, p_{N_{lat}}\right]^T$, $\mathbf{q} = \left[q_1, q_2, \ldots, q_{N_{lat}}\right]^T$, and $\mathbf{z} = \left[z_1, z_2, \ldots, z_{N_{long}}\right]^T$, and dots denote differentiation with respect to fast time, $\mathbf{A}\left(T, \tau; \varepsilon\right)$ is $2\left(2N_{lat} + N_{long}\right)$ $\times 2\left(2N_{lat} + N_{long}\right)$ -dimensional slowly varying linear coefficient matrix, $\mathbf{N}\left(\tau, \mathbf{y}\right)$ represents the $2\left(2N_{lat} + N_{long}\right)$-dimensional vector of non-linear coupling terms, and $\mathbf{F}\left(T, \tau\right)$ is the $2\left(2N_{lat} + N_{long}\right)$-dimensional external excitation vector. The non-stationary coefficient matrix is given as

$$\mathbf{A}\left(T, \tau; \varepsilon\right) = \begin{bmatrix} \mathbf{0} & \mathbf{I} \\ -\mathbf{K}\left(T, \tau\right) & -\mathbf{C}\left(\tau; \varepsilon\right) \end{bmatrix}, \tag{5.33}$$

where $\mathbf{0}$ and $\mathbf{I}$ are $\left(2N_{lat} + N_{long}\right) \times \left(2N_{lat} + N_{long}\right)$ null and identity matrices, respectively, and $\mathbf{K}$ and $\mathbf{C}$ are $\left(2N_{lat} + N_{long}\right) \times \left(2N_{lat} + N_{long}\right)$ matrices. These matrices are defined as

$$\mathbf{K}\left(T, \tau\right) = \begin{bmatrix} \mathbf{K}^{lat}\left(T, \tau\right) & \mathbf{0} & \mathbf{0} \\ \mathbf{0} & \mathbf{K}^{lat}\left(T, \tau\right) & \mathbf{0} \\ \mathbf{0} & \mathbf{0} & \mathbf{K}^{long}\left(\tau\right) \end{bmatrix}, \tag{5.34}$$

$$\mathbf{C}(\tau;\varepsilon)=\begin{bmatrix} \mathbf{C}^{lat}(\tau;\varepsilon) & 0 & 0 \\ 0 & \mathbf{C}^{lat}(\tau;\varepsilon) & 0 \\ 0 & 0 & \mathbf{C}^{long}(\tau;\varepsilon) \end{bmatrix} \tag{5.35}$$

where $\mathbf{K}^{lat}$, $\mathbf{C}^{lat}$ are diagonal $N_{lat} \times N_{lat}$ matrices, and $\mathbf{K}^{long}$, $\mathbf{C}^{long}$ are diagonal $N_{long} \times N_{long}$ matrices. When terms $O(\varepsilon^2)$ are neglected in equations (5.22)-(5.24), these matrices are determined as

$$\mathbf{K}^{lat}(T,\tau)=\left[1+\left(\frac{c}{\bar{c}}\right)^2 F_l(T)\right] diag\left[\hat{\omega}_k^2(\tau)\right], \tag{5.36}$$

$$\mathbf{C}^{lat}(\tau)=\left[C_{kn}^{lat}\right]=2\varepsilon\left\{diag\left[\bar{\zeta}_k^*\hat{\omega}_k(\tau)\right]+\frac{2l'}{mL_c}\left[C_{kn}\right]\right\}, \tag{5.37}$$

$$\mathbf{K}^{long}(\tau)=diag\left[\tilde{\omega}_r^2(\tau)\right], \tag{5.38}$$

$$\mathbf{C}^{long}(\tau)=\left[C_{rn}^{long}\right]=\varepsilon\frac{\mu_2^*}{\omega_0}\mathbf{I}+ \\ \frac{\varepsilon}{m_r^v(\tau)}\left[2l'C_{rn}^v(\tau)-\frac{EA}{\omega_0}\Lambda_{rn}^*+M_S l'\left(\frac{1}{L_c}-\frac{M_S}{m}\gamma_n^2\right)\right], \tag{5.39}$$

where $\mathbf{I}$ is $N_{long} \times N_{long}$ identity matrix. The non-linear vector $\mathbf{N}(\tau,\mathbf{y})$ is given as

$$\mathbf{N}(\tau,\mathbf{y})=\left[\mathbf{N}^{v^T}(\tau,\mathbf{y}),\mathbf{N}^{w^T}(\tau,\mathbf{y}),\mathbf{N}^{u^T}(\tau,\mathbf{y})\right]^T, \tag{5.40}$$

where

$$\mathbf{N}^v(\tau,\mathbf{y})=\left[N_k^v\right]_{(N_{lat}\times 1)}=-\left(\frac{c}{\bar{c}}\right)^2\left\{\hat{\omega}_k^2(\tau)\left[\frac{1}{L_c}\sum_{n=1}^{N_{long}} z_n+\sum_{n=1}^{N_{lat}}\beta_n^2(p_n^2+q_n^2)\right]p_k\right\}, \tag{5.41}$$

$$\mathbf{N}^w(\tau,\mathbf{y})=\left[N_k^w\right]_{(N_{lat}\times 1)}=-\left(\frac{c}{\bar{c}}\right)^2\left\{\hat{\omega}_k^2(\tau)\left[\frac{1}{L_c}\sum_{n=1}^{N_{long}} z_n+\sum_{n=1}^{N_{lat}}\beta_n^2(p_n^2+q_n^2)\right]q_k\right\}, \tag{5.42}$$

$$\mathbf{N}^u(\tau,\mathbf{y})=\left[N_r^u\right]_{(N_{long}\times 1)}=-\frac{EA}{\omega_0^2}\left[\frac{1}{m_r^v(\tau)}\sum_{n=1}^{N_{lat}}\beta_n^2(p_n^2+q_n^2)\right]. \tag{5.43}$$

The excitation vector $\mathbf{F}$ is in the form

$$\mathbf{F}(\tau, T) = \begin{bmatrix} 0_{\left[\left(2N_{lat}+N_{long}\right)\times 1\right]} \\ \begin{bmatrix} \hat{P}_r \\ \hat{Q}_r \\ \hat{Z}_r - \frac{EA}{m_r^v} \end{bmatrix}_{\left[\left(2N_{lat}+N_{long}\right)\times 1\right]} \end{bmatrix}. \tag{5.44}$$

5.4.1 The Kloof Gold Mine Winding System

Problematic dynamic behaviour of hoisting cables was reported to occur during the normal operating conditions on the two main rock winders of No 1 Shaft of Kloof Gold Mine in South Africa [Dimitriou & Whillier, 1973; Mankowski, 1982; Constancon, 1993].

The Kloof winder is a double-drum Blair multi-rope (BMR) system with two conveyances (skips) attached via compensating sheaves on bridles. A schematic diagram showing the arrangement of cables in this system is presented in Figure 22. In this installation the underlay cable 1 wound onto the underlay drum D_1 passes over the headsheaves H_1 and H_2 and supports the underlay skip S_1, forming two catenary sections and two vertical ropes. Similarly, two catenaries and vertical ropes are formed by the overlay cable 2 wound onto the overlay drum D_2 and supporting the underlay skip S_2. Fundamental parameters of the system are summoned in Table 2 [Dimitriou & Whillier, 1973].

The dynamic behaviour of cables in the Kloof winding plant were under regular observation over many years, and the vibration phenomena occurring in this system were recorded. Dimitriou & Whillier [1973] documented these observations and gave a thorough description of the cable vibrations during the ascending cycle, when a full conveyance was being raised. The parameters of modern mine hoist systems are similar to those of the Kloof arrangement, and the observations made by Dimitriou and Whillier are still pertinent.

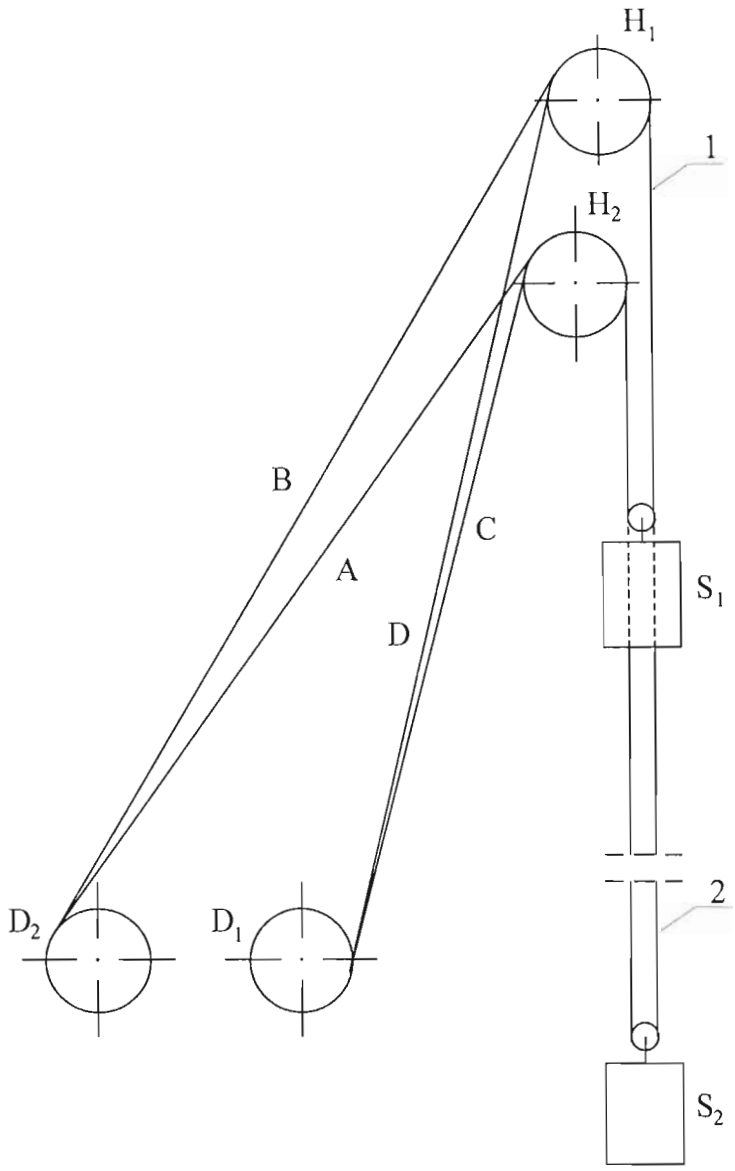

Figure 22. Schematic arrangement of cables in the BMR Kloof winder [Dimitriou & Whillier, 1973].

Maximum hoisting velocity $[\frac{m}{s}]$	15
Weight of skip and bridle $[kN]$	180
Load on skip $[kN]$	165 ± 10
Winder drum diameter $[m]$	4.27
Sheave wheel diameter $[m]$	4.27
Cable diameter $[m]$	48×10^{-3}
Cable linear density $\left[\frac{kg}{m}\right]$	8.49
Cable type	6-strand Lang's lay
Number of layers on winder drum	4
Length of catenaries A, B, C, D $[m]$	74.4, 79.6, 69.8, 75.3
Maximum depth of wind $[m]$	2085

Table 2. Fundamental parameters of No 1 Shaft Kloof Gold Mine winder.

Two distinct phases were identified, namely *Phase 1* of duration approximately 20 s, starting when the conveyance is around 900 m below the headsheave, which corresponds to about $t = 110$ s, and *Phase 2* starting at the third to the fourth layer cross-over on the drum (at the depth of around 550 m) and ending at the top of the winding cycle. The main characteristics of the vibrations are as follows.

1. Except during Phases 1 and 2 the catenary vibrations are of no clearly defined modes and are of small amplitudes. Smaller amplitudes and higher frequencies are recorded at higher depths, when the conveyance is near the bottom of the shaft.

2. During Phase 1, the amplitudes increase and the second mode (full sine-wave) is clearly identified, both in the in-plane and out-of-plane motion of the catenaries. The amplitude of the out-of-plane vibration is usually larger and is judged to be of the order of 1 m.

3. Sometimes these vibrations continue through Phase 2, with a gradual change in mode shape, but no appreciable change in amplitude.

4. Lateral vibrations in vertical ropes also occur during Phase 1, and continue throughout Phase 2. The maximum amplitude of these vibrations is about 0.1 m. Photographic evidence exists which indicates that the main wavelength is approximately the same as the wavelength of the catenaries. The main frequency is estimated as 2 Hz.

Number of lateral modes N_{lat}	4
Number of longitudinal modes N_{long}	4
Total winding cycle time $[s]$	156
Acceleration/deceleration time $[s]$	19.7
Nominal hoisting velocity $V_c\ [\frac{m}{s}]$	15
Total hoisted mass $M\ [kg]$	17584
Sheave wheel moment of inertia $I\ [kgm^2]$	15200
Winder drum radus $R_d\ [m]$	2.14
Sheave wheel radius $R\ [m]$	2.13
Coil cross-over arc $\beta\ [rad]$	0.2
Cable diameter $d\ [m]$	48×10^{-3}
Cable linear density $m\ [\frac{kg}{m}]$	8.4
Cable effective steel area $A\ [m^2]$	1.028×10^{-3}
Cable effective Young's Modulus $E\ [\frac{N}{m^2}]$	1.1×10^{11}
Catenary length $L_c\ [m]$	74.95
Maximum depth of winding $L_{v\,\max}\ [m]$	2100
Lateral modal damping ratio $\zeta\ \%$	0.05
Relative damping coefficient $\mu_1\ [s]$	given by (4.58)
Absolute damping coefficient $\mu_2\ [s^{-1}]$	0.159

Table 3. Kloof Simulation Parameters

5. At times, at the beginning of Phase 2, the in-plane catenary vibrations reach amplitudes exceeding 2 m. It was recorded that this motion exhibits the first mode shape pattern.

6. The reduction of the winding velocity from 15 m/s to 14 m/s at the beginning of Phase 1 is sufficient to decrease significantly the amplitude of vibrations throughout both Phase 1 and Phase 2.

7. None of the above vibration phenomena were observed during the descending winding cycle.

5.4.2 Kloof Simulation Model

The parameters of one of the Kloof winders are chosen in the numerical simulation of equations (5.22)-(5.24), and are presented in Table 3. It should be noted that a single overlay, or underlay, arrangement with one conveyance is analyzed in what follows. In this model a single equivalent catenary and equivalent vertical rope, supporting one half of the full weight of the conveyance, represent the two actual catenaries and two vertical ropes. An ascending cycle of this equivalent cable system is considered. Both the longitudinal and lateral natural frequencies of the system vary slowly during this cycle, as shown in Figure 23. The first four longitudinal and lateral natural frequencies of the system are plotted versus the vertical rope length, and the first and the second harmonics of the excitation frequency at the nominal winding velocity $V_c = 15\ m/s$ together with the cable layer change locations are shown in this figure. The longitudinal frequencies increase, and the lateral frequencies decrease, with the decreasing length of the rope, and conditions arise for primary longitudinal and lateral resonances, as well as for combination, internal (autoparametric) and parametric resonances during the up-wind.

It must be noted that the natural modes are widely spaced throughout the entire winding cycle, and the that system is stiff. Thus, an appropriate integration strategy is required in the numerical simulation, as discussed earlier in Section 4.5. Thus, equation (5.32) is coded in a MATLAB ODE file (the code is presented in Appendix F), and the ode15s stiff solver function is applied to the problem. The solver is invoked with the numerical differentiation formulas (NDF's) chosen to implement the integration. The relative accuracy tolerance $RelTol = 10^{-4}$ and the default absolute error tolerance $AbsTol = 10^{-6}$ are used to monitor and control the error of each integration step. In order to improve the efficiency of the calculations the total time span of the simulation is broken into a number of smaller pieces[9]. The

[9] The solver uses as many time points as necessary to produce a smooth solution. If the ODE function changes on a time scale that is very short compared to the simulation time span, then the solver will use a large

natural frequencies, the time-varying coefficients, and the excitation parameters are determined in advance and are made available in look-up tables as functions of length l. The actual values of these non-stationary characteristics are determined at each step of the integration by means of the linear interpolation.

5.4.3 Kloof Simulation results

Nominal winding velocity

The primary simulation results for an ascending cycle with the nominal winding velocity $V_c = 15\ m/s$ are presented in Figures 64-66, and assembled in Appendix G. These results have been further processed, and the resulting graphs are shown in Figures 24-38. The modal phase space trajectories with associated power spectra are illustrated in Figures 24-32. The displacement response plots are given in Figure 33, where the lateral motions at the first quarter point of the catenary cable, and the longitudinal motions at the sheave and at the conveyance vs. the vertical length are presented. The whirling motion of the catenary cable is further illustrated in Figures 34-36. The lateral motion at the first quarter point of the catenary against the vertical length is presented in Figure 34. The trajectory of this point is illustrated in more detail in eight different time windows in Figures 35-36. The total cable tension plots vs. the vertical length, together with the tension ratio across the sheave plot, are shown in Figure 37. This is followed by the dynamic cable tension plots given in Figure 38.

The simulation results demonstrate the dynamic phenomena occurring during the wind. When the conveyance accelerates from the bottom of the shaft, the acceleration inertial load results in a transient response, evident in the longitudinal modal co-ordinate plots and in the

number of time steps. This is the case in the present problem, as the simulation time span of the entire winding cycle is long, and for the nominal velocity of $V_c = 15\ m/s$ it exceeds 156 s.

longitudinal displacement plots. A similar effect can be noted when the conveyance is decelerated to rest at the end of the wind. The effect of transition from the acceleration phase to the constant velocity phase, and from the constant velocity phase to the deceleration phase, is clearly visible as a rapid change in the mean value of the longitudinal response. The catenary response is planar between the start of the wind and the first layer change, evident in the in-plane lateral response at approximately $L_v = 1600\ m$. The longitudinal co-ordinates and displacements exhibit drifts in agreement with the overall lateral out-of-plane cable motion across the winding drum. This means that the longitudinal motions digress in a negative direction during the first layer, and go off in the opposite during the second layer. This pattern repeats itself throughout the wind.

Taking into consideration the quadratic coupling between the longitudinal and lateral modes, and the cubic coupling between the in- and out-of-plane lateral modes, a number of resonance conditions arise during the wind. One-to-one $(1:1)$ lateral internal resonances occur throughout the wind since the in- and out-of-plane lateral natural frequencies are the same. Upon close examination of the frequency chart given in Figure 23, one can notice that interesting frequency tunings occur in the depth region $L_v = 900 - 700\ m$. At the depth $L_v \approx 900\ m$ the fourth longitudinal and the second lateral natural frequencies are in the ratio $2:1$, and a two-to-one $(\omega_4 \approx 2\bar{\omega}_2)$ internal resonance condition takes place. A primary external resonance exists simultaneously with this condition, since at this level the second harmonic of the Lebus cross-over motion directly excites the fourth longitudinal mode $(\Omega_2 = \omega_4)$.

Furthermore, at the depth $L_v \approx 750$ the second longitudinal frequency is near twice that of the first lateral natural frequency $(\omega_2 \approx 2\bar{\omega}_1)$, so that another two-to-one internal resonance arises. At the same, time the second longitudinal frequency is tuned closely to the second lateral frequency $(\omega_2 \approx \bar{\omega}_2)$, implicating also a one-to-one internal resonance. At this depth the model is also involved in primary external resonances, since the first harmonic

of the cross-over excitation is near the second longitudinal natural frequency and the second lateral frequency ($\Omega_1 \approx \omega_2 \approx \bar{\omega}_2$), and also the second harmonic of the excitation is near the fourth lateral natural frequency ($\Omega_2 \approx \bar{\omega}_4$). Principal parametric resonances of the first and of the second lateral modes occur at the same time, namely the resonances $\Omega_1 \approx 2\bar{\omega}_1$ and $\Omega_2 \approx 2\bar{\omega}_2$, and also the summed combination resonance $\Omega_2 \approx \omega_2 + \bar{\omega}_2$ exists. In addition to these conditions, the primary resonances $\Omega_1 \approx \omega_3$ at $L_v \approx 1550\ m$, and $\Omega_2 \approx \omega_3$ at $L_v \approx 500\ m$ occur during the wind.

The response plots vs. the depth L_v along with phase plots and associated frequency power spectra illustrate the problematic dynamic behaviour of the system, when a passage through the regions of instability occurs due to the above resonance conditions. The fundamental excitation frequency corresponding to the nominal winding speed of 15 m/s is 2.23 Hz, and this frequency together with its harmonics are evident in the system response, as shown in the power spectra presented in Figures 24-32. The associated phase portraits show crossings/twisting of the phase trajectories demonstrating the complexity of the motions.

Considering the depth region $L_v = 1000 - 800\ m$, the primary resonance $\Omega_2 = \omega_4$ is apparent in the fourth longitudinal modal co-ordinate plot of Figure 66, and in the power spectrum presented in Figure 26. At the same time, a passage through the autoparametric resonance $\omega_4 \approx 2\bar{\omega}_2$ of the second lateral mode shows in the corresponding lateral co-ordinate response plots.

In the depth region $L_v = 800 - 600\ m$ large lateral motions and substantial longitudinal response occur. At this stage of the winding cycle, the system passes through the primary resonances $\Omega_1 \approx \omega_2 \approx \bar{\omega}_2$ and $\Omega_2 \approx \bar{\omega}_4$. It should be noted that the out-of-plane lateral motions are strongly excited, with the in-plane excitation being much smaller throughout the wind. It is interesting to observe that in this instability region the second mode of the in-plane response continues to grow after the out-of-plane response has reached its peak value. Hence, it is evident that the large in-plane response is a direct consequence of the

autoparametric 1 : 1 resonance and of the energy exchange between the lateral modes, with the out-of-plane motion being essentially a parametric excitation for the in-plane motion.

The lateral response remains large beyond the 600 m depth level, due to cascading energy exchanges among the modes. This is evident from a visual inspection of response plots shown in Figure 33, and also from the illustration of the tubular motion at the first quarter point of the catenary given in Figure 34. The trajectory plots of lateral motion at this point presented in Figures 35-36 show that up to the level $L_v \approx 1000\ m$ the catenary response is small. Afterwards it grows, and in the region of approximately $800 - 600\ m$ the cable begins to whirl, and consequently a full ballooning motion is developed in the region of $600 - 400\ m$, which persists till the end of the simulation.

The dynamic behaviour of the system is further demonstrated in the cable tension plots. From an inspection of the total cable tension plots given in Figure 37, it is evident that the mean catenary tension and the mean vertical rope tension at the sheave decrease during the up-wind due to the decreasing length of the vertical rope. Significant oscillations in the tensions occur at the beginning of the ascending cycle. These oscillations, caused by the initial acceleration inertial load, are of low frequency and become small after approximately $1500\ m$ depth level. Large tension fluctuations begin to take place from the $1000\ m$ level and continue till the end of the wind. They result due to the non-linear modal interactions and resonance phenomena occurring in the system. It should be noted, however, that the tension ratio across the sheave does not exceed the limits for no slip [10]. The tension oscillations are better illustrated in Figure 38. It can be seen that the most severe tension oscillations occur in the catenary cable, and are caused by large lateral motions of this cable.

---

[10] Following the considerations presented earlier in Subsection 4.5.1, these limits can be assumed as [0.5559, 1.8023]. Consequentely, the model assumptions are not violated during the simulation.

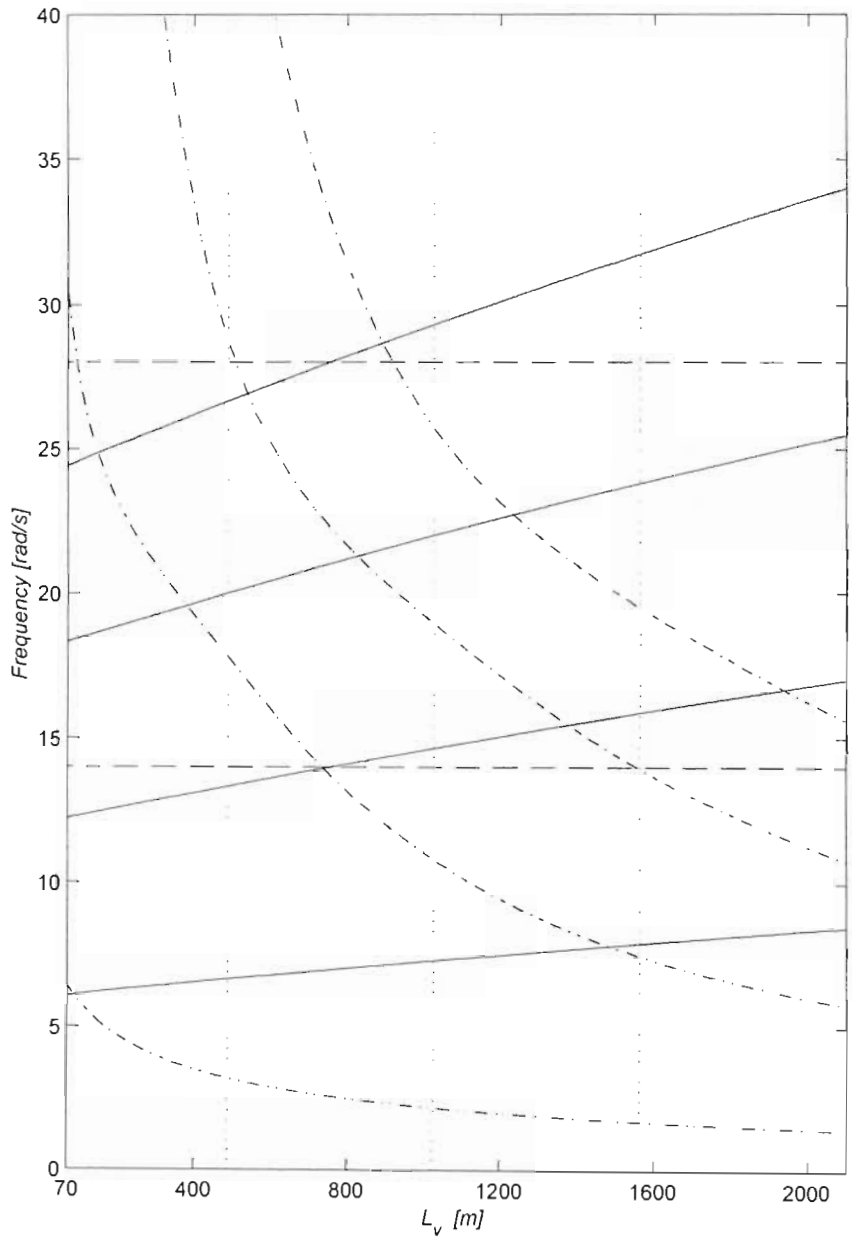

Figure 23. Longitudinal frequency ω_n $(- \cdot -)$ and lateral frequency $\bar{\omega}_n$ (—) curves for Kloof Gold Mine winder (ascending cycle), with horizontal lines $(--)$ denoting the first and the second harmonics of the excitation frequency at the nominal winding velocity $V_c = 15$ m/s. Vertical lines $(\cdots)$ indicate the layer change locations.

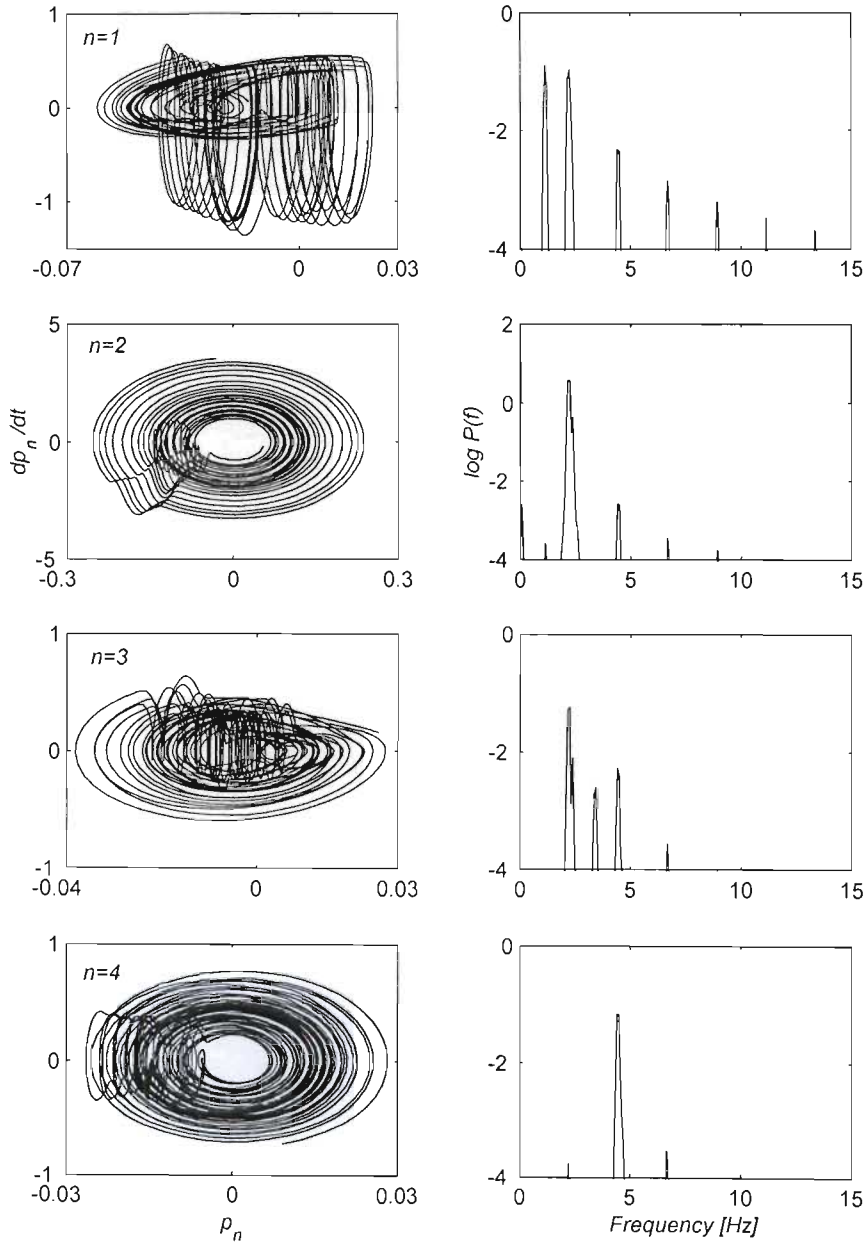

Figure 24. Phase space trajectories and the power spectra of the catenary lateral in-plane modal co-ordinates during the ascending Kloof cycle at $V_c = 15\ m/s$ within the interval $L_v = 1000 - 800\ m$

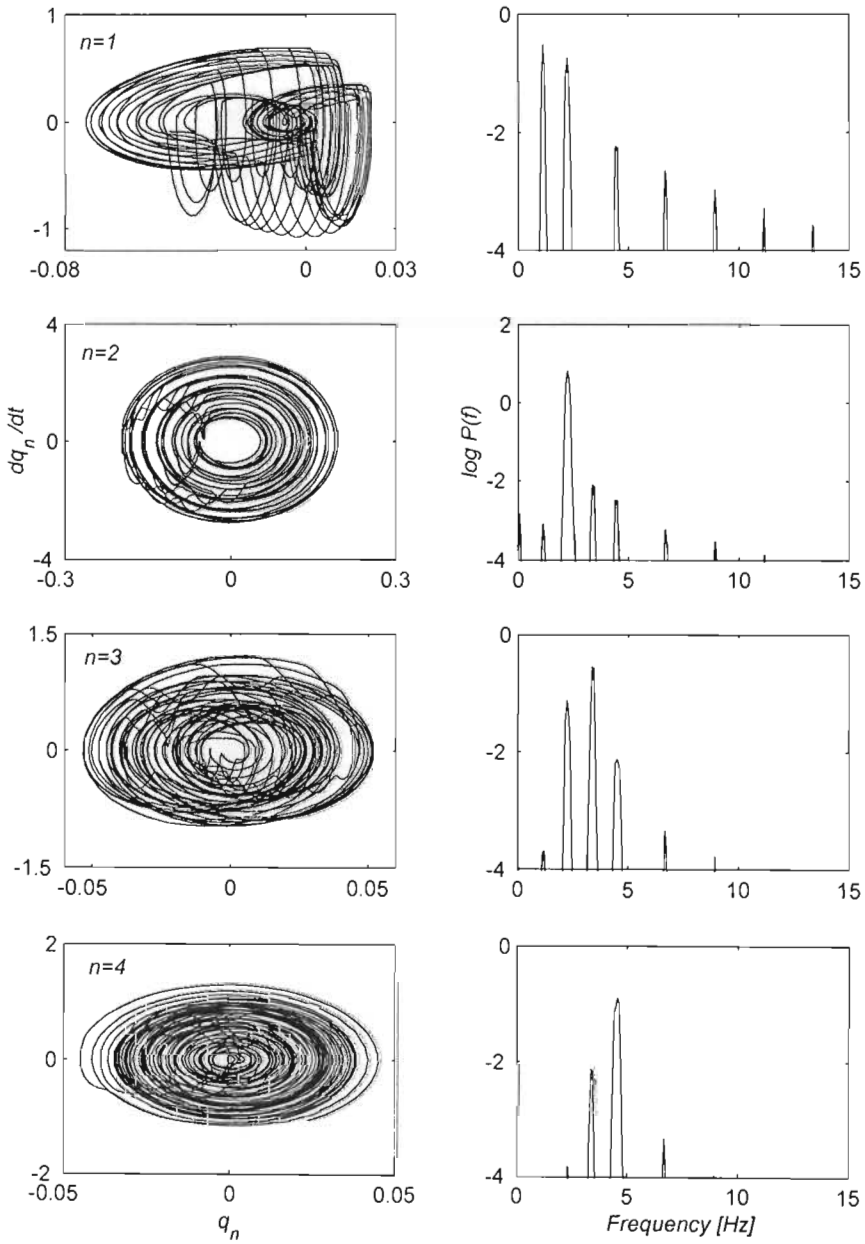

Figure 25. Phase space trajectories and the power spectra of the catenary lateral out–of-plane modal co-ordinates during the ascending Kloof cycle at $V_c = 15\ m/s$ within the interval $L_v = 1000 - 800\ m$.

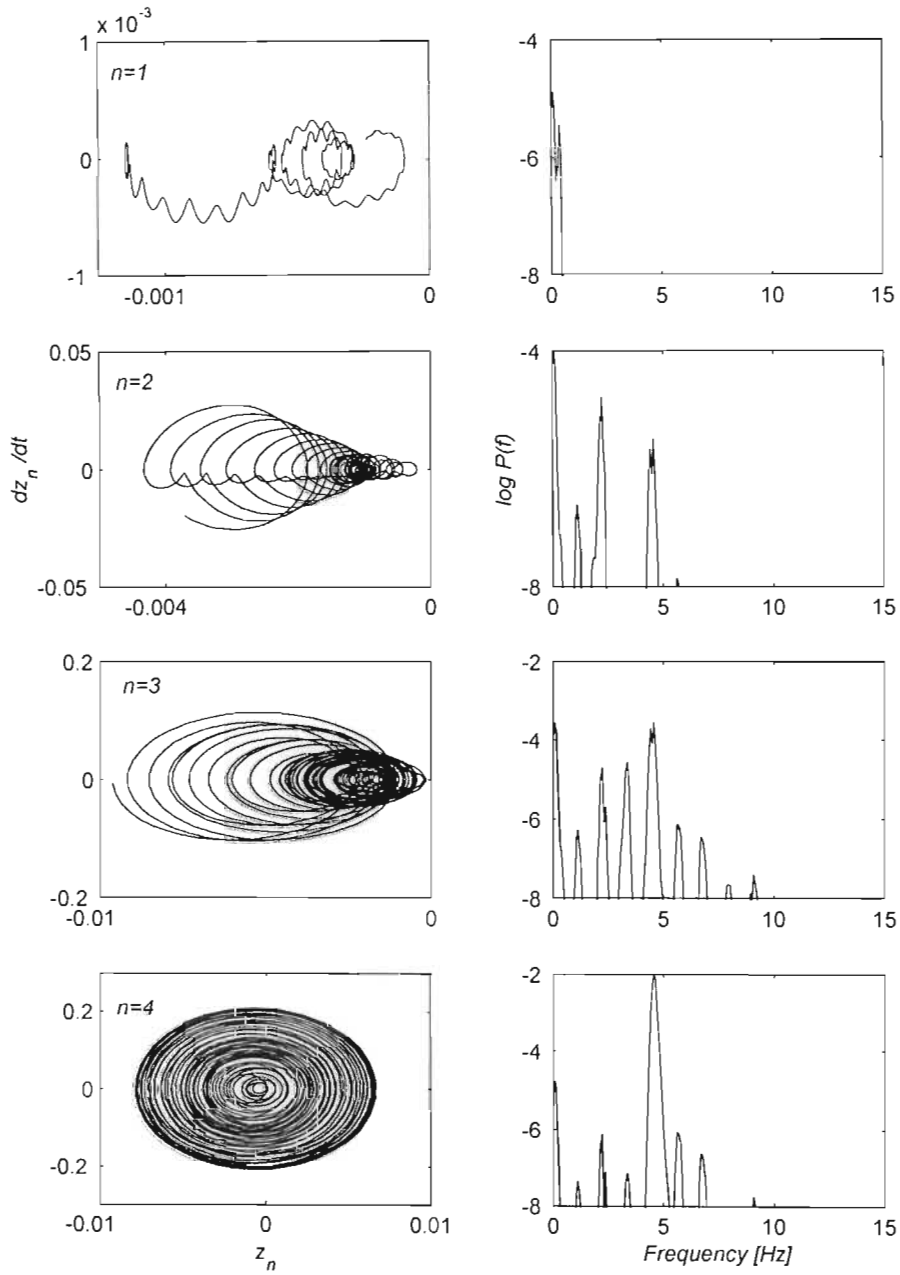

Figure 26. Phase space trajectories and the power spectra of the vertical rope longitudinal modal co-ordinates during the ascending Kloof cycle at $V_c = 15\ m/s$ within the interval $L_v = 1000 - 800\ m$.

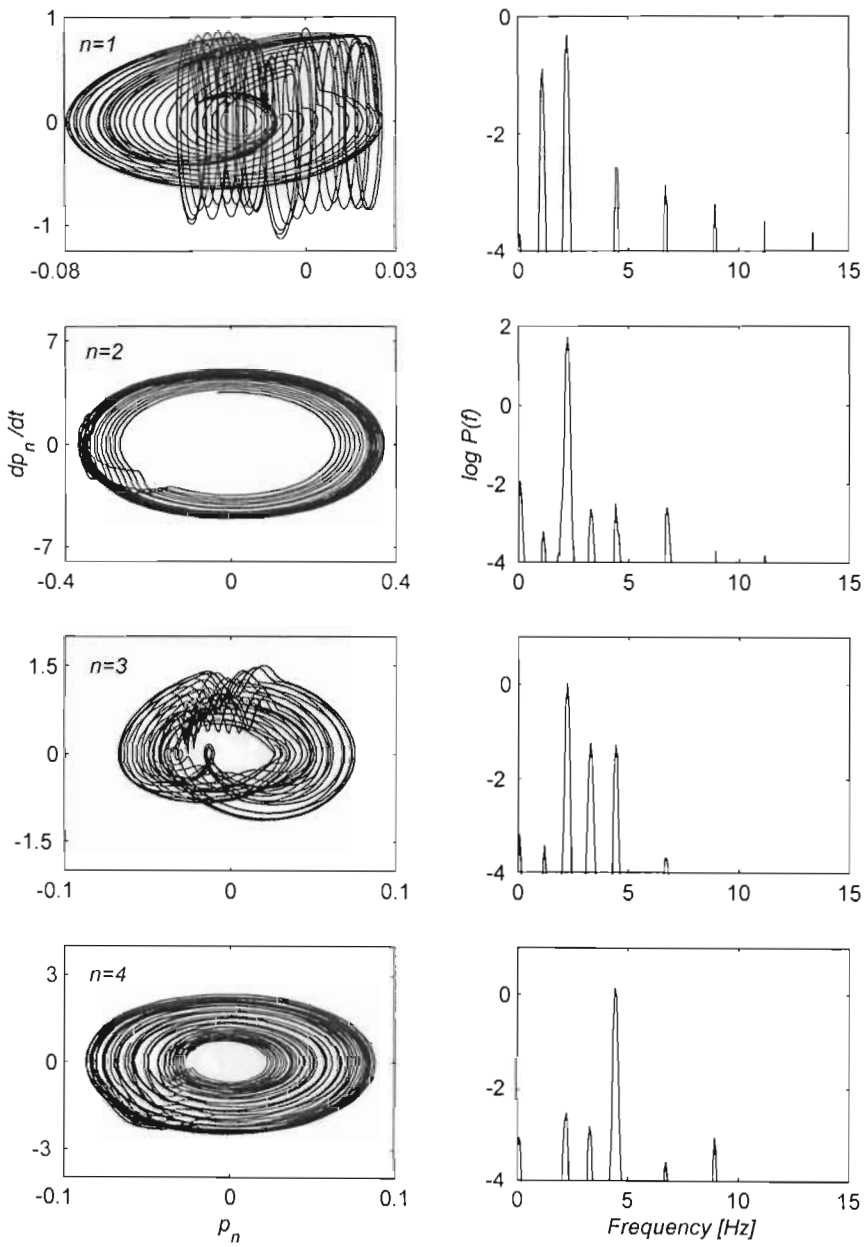

Figure 27. Phase space trajectories and the power spectra of the catenary lateral in-plane modal co-ordinates during the ascending Kloof cycle at $V_c = 15\ m/s$ within the interval $L_v = 800 - 600\ m$.

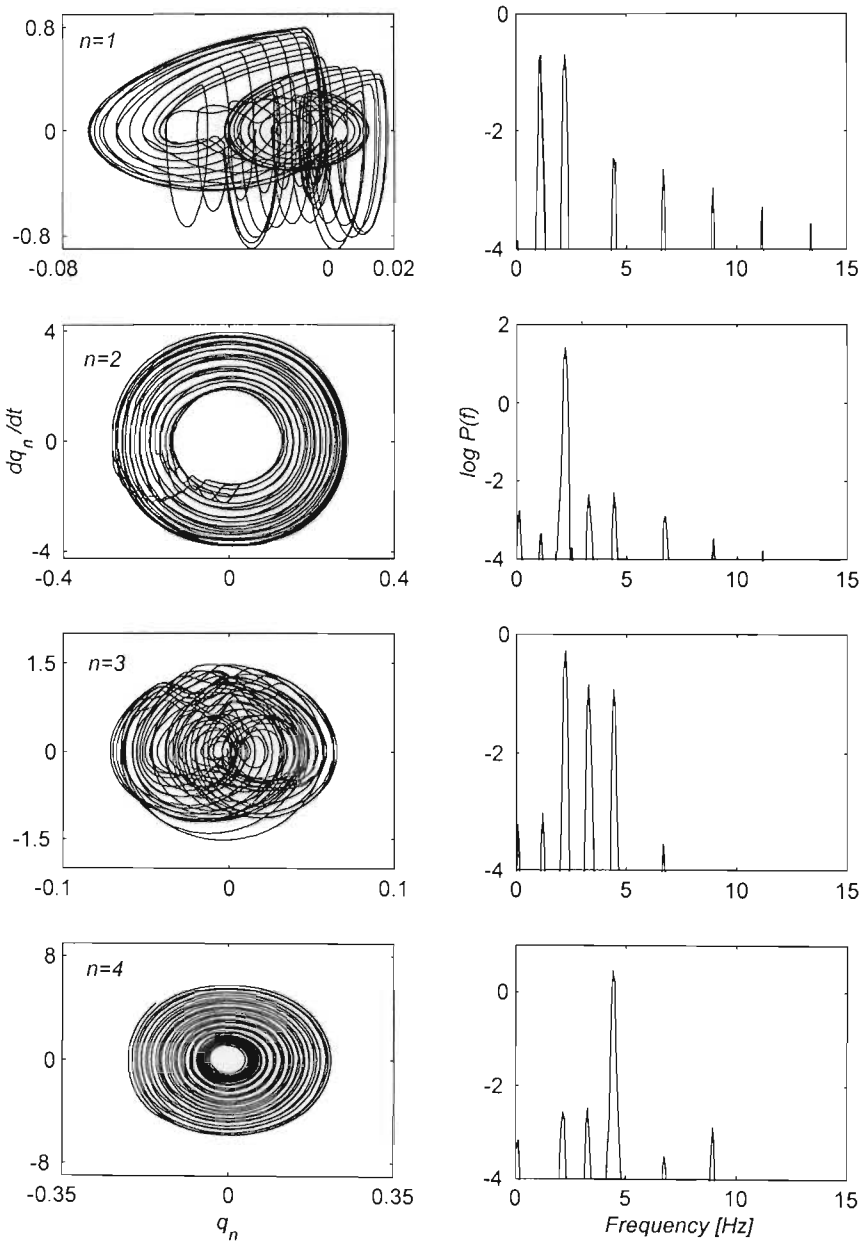

Figure 28. Phase space trajectories and the power spectra of the catenary lateral out–of-plane modal co-ordinates during the ascending Kloof cycle at $V_c = 15\ m/s$ within the interval $L_v = 800 - 600\ m$.

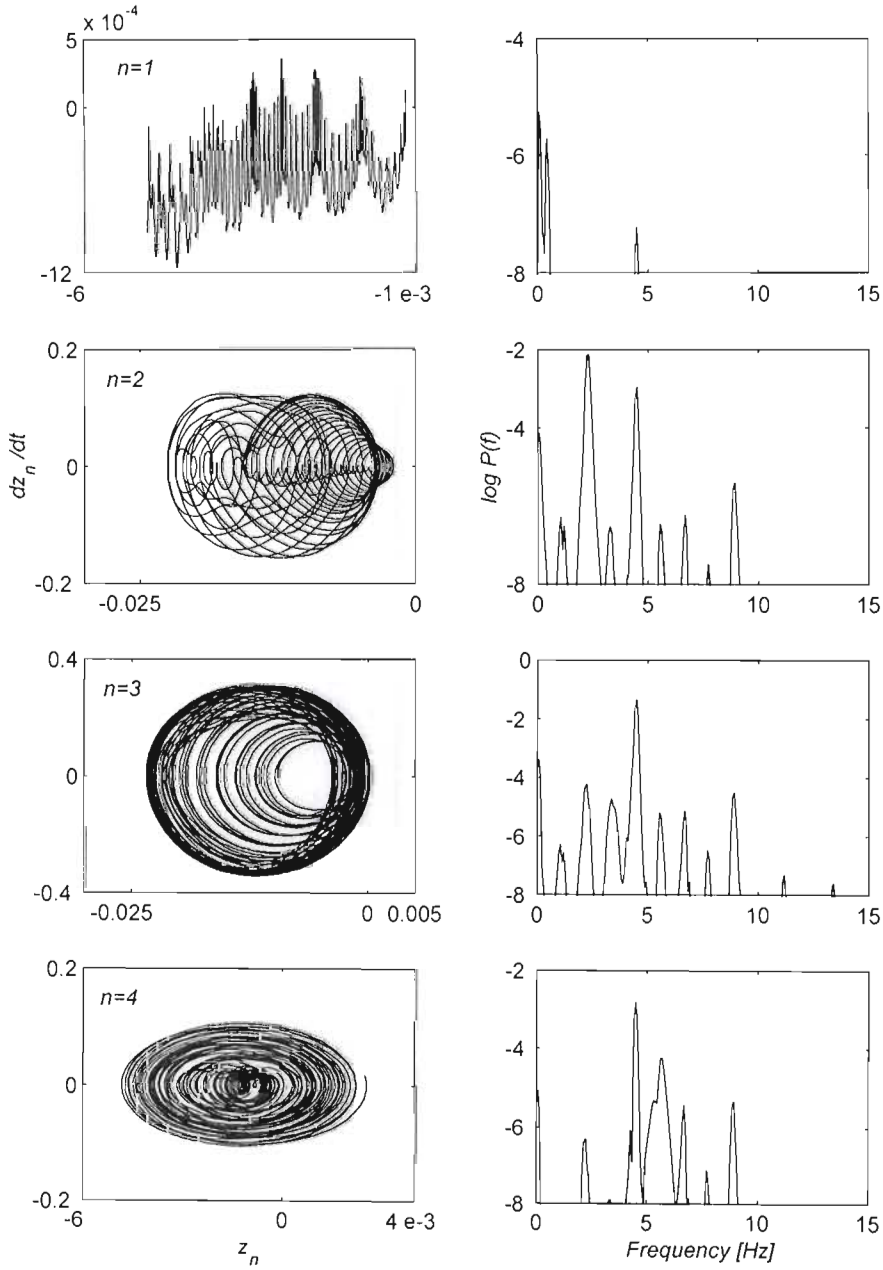

Figure 29. Phase space trajectories and the power spectra of the vertical rope longitudinal modal co-ordinates during the ascending Kloof cycle at $V_c = 15\ m/s$ within the interval $L_v = 800 - 600\ m$.

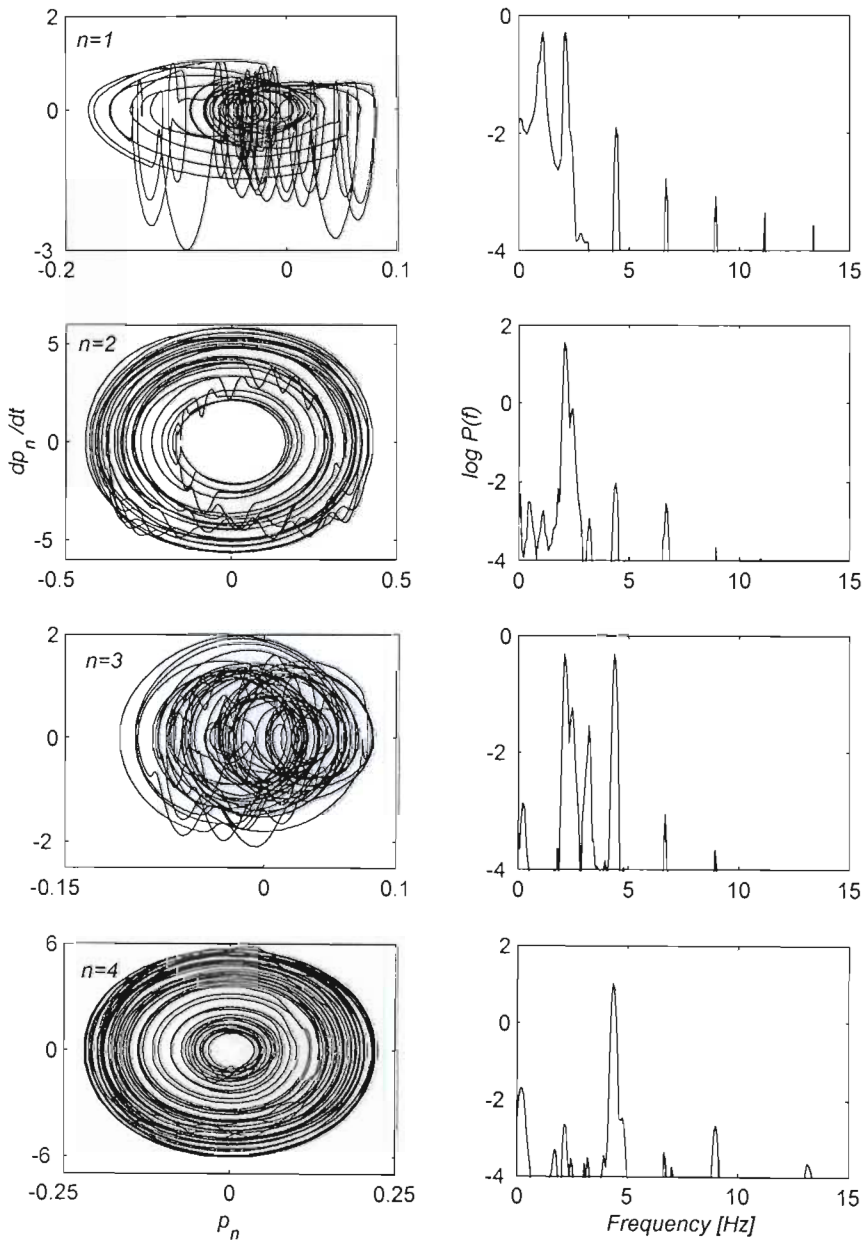

Figure 30. Phase space trajectories and the power spectra of the catenary lateral in-plane modal co-ordinates during the ascending Kloof cycle at $V_c = 15\ m/s$ within the interval $L_v = 600 - 400\ m$.

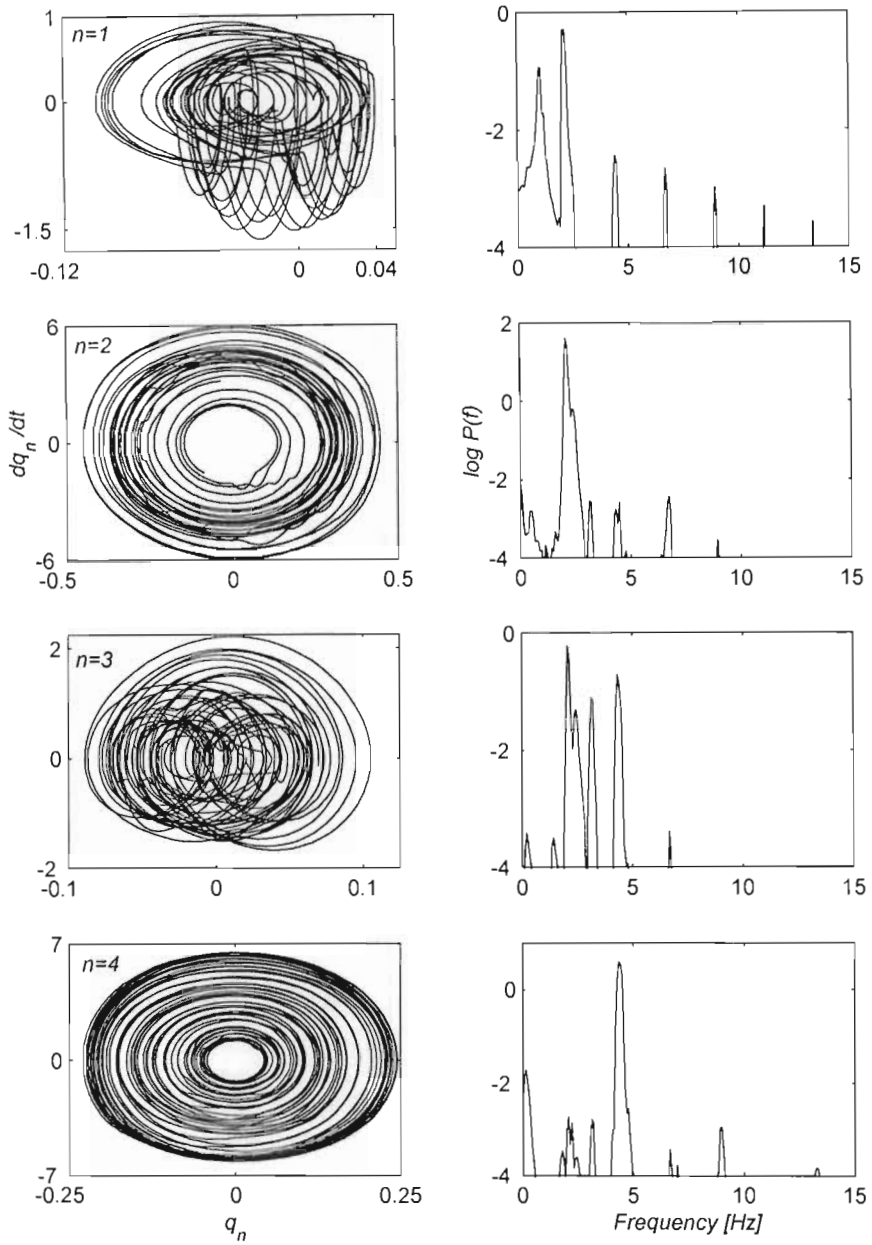

Figure 31. Phase space trajectories and the power spectra of the catenary lateral out–of-plane modal co-ordinates during the ascending Kloof cycle at $V_c = 15\ m/s$ within the interval $L_v = 600 - 400\ m$.

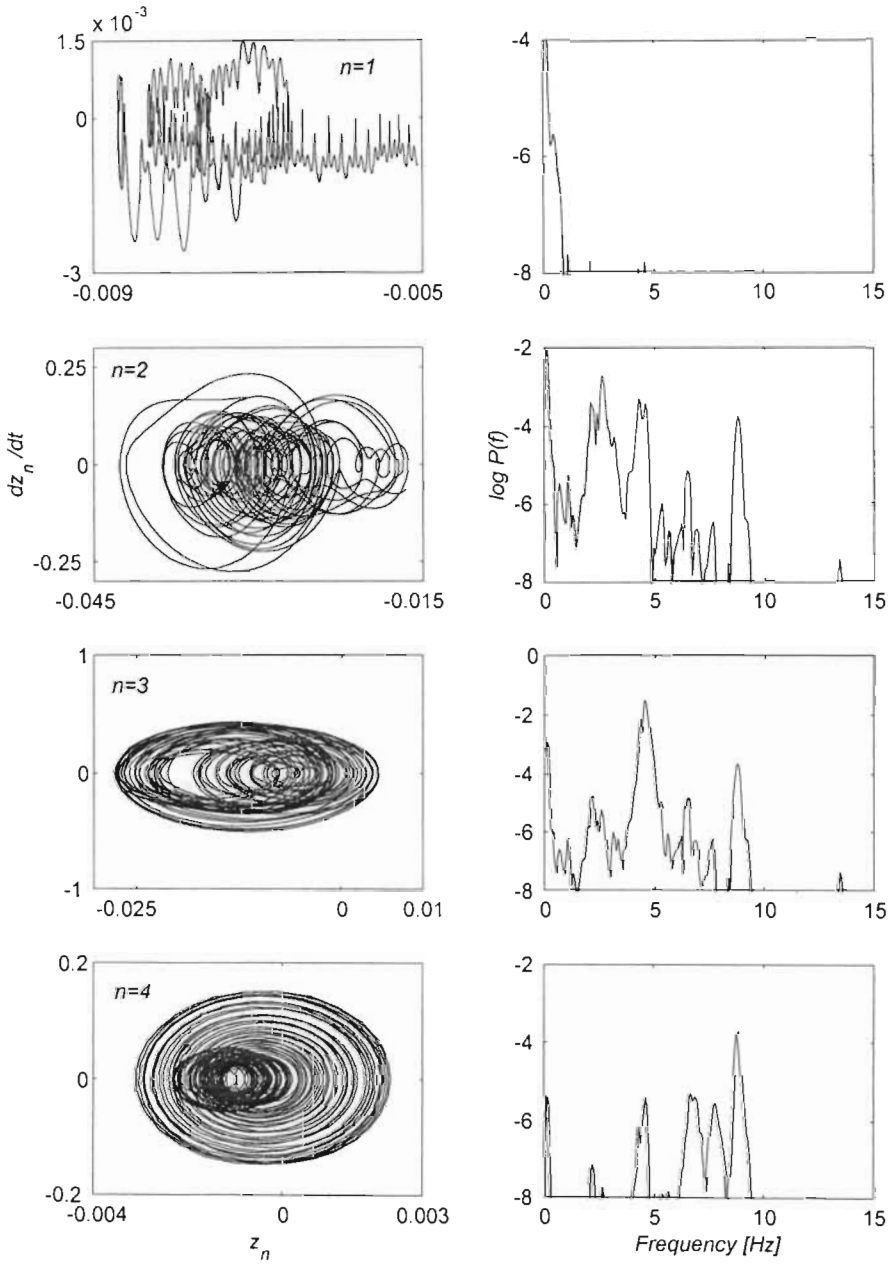

Figure 32. Phase space trajectories and the power spectra of the vertical rope longitudinal modal co-ordinates during the ascending Kloof cycle at $V_c = 15\ m/s$ within the interval $L_v = 600 - 400\ m$.

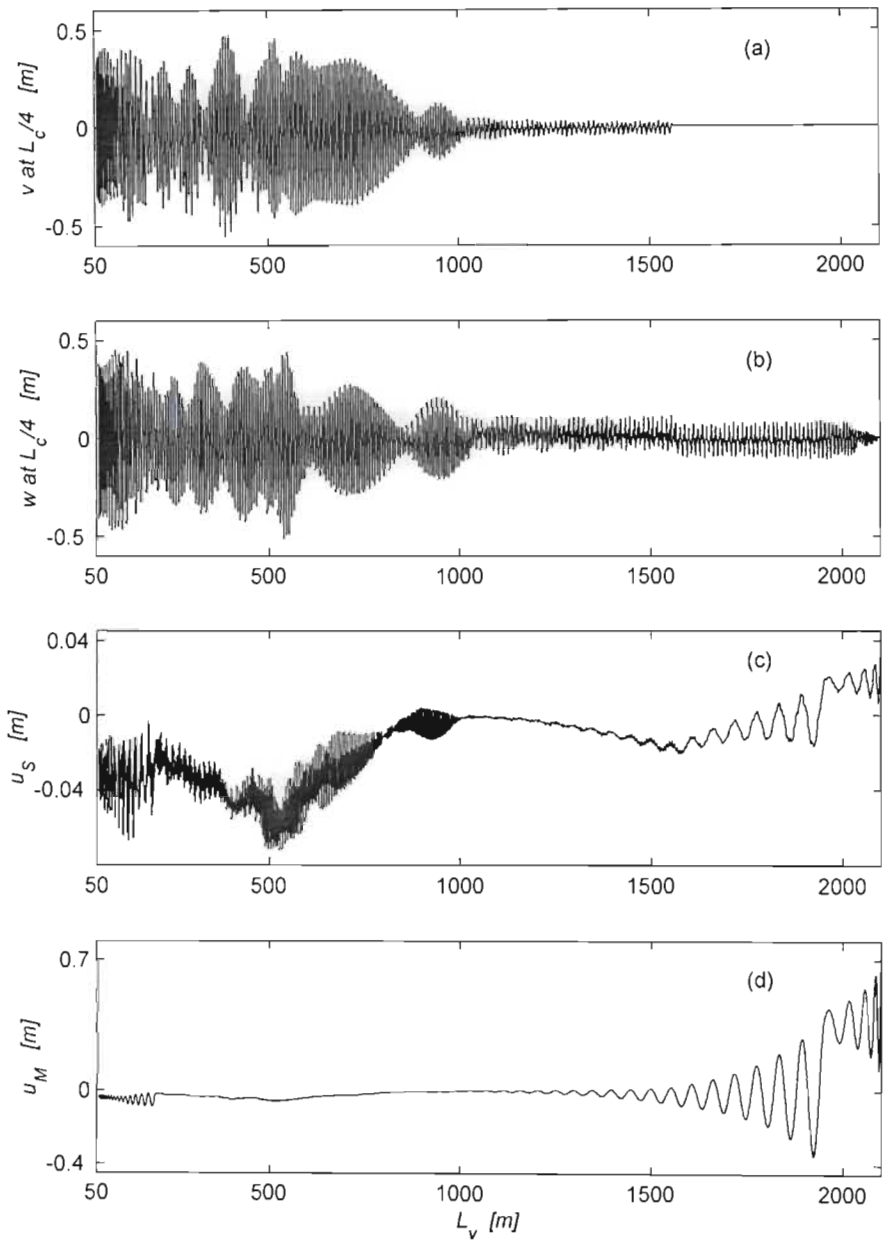

Figure 33. Displacement response of Kloof Mine winding cables for $V_c = 15\ m/s$: lateral (a) in-plane and (b) out-of-plane motions at the first quarter of the catenary; longitudinal responses (c) at the sheave and (d) at the conveyance.

Other Winding Velocity Regimes

Changes in the winding velocity can shift the resonance locations. Hence, the winding velocity is the most important parameter of the system. In order to investigate and to predict the system response under various winding velocity regimes simulations were carried out for other than the nominal velocity values.

The simulation results for the winding velocity $V_c = 14\ m/s$ are presented in Figures 70-72 in Appendix G. The corresponding linear frequency map, showing the relationship between the natural frequencies of the system, and the first two harmonics of the cross-over excitation, is given in Figure 43. The actual displacements in the system are presented in Figures 44. As one can observe, the system develops a large dynamic response after a depth of approximately $500\ m$. An inspection of the linear frequency map reveals that at a depth of $L_v = 400\ m$ the second lateral mode is tuned to the fundamental harmonic of the excitation, and simultaneously the fourth lateral mode is tuned to the second harmonic of the excitation. Hence, the primary resonances $\Omega_1 \approx \bar{\omega}_2$ and $\Omega_2 \approx \bar{\omega}_4$ take place. Since the second lateral natural frequency is twice the first lateral natural frequency ($\bar{\omega}_2 = 2\bar{\omega}_1$), and the fourth lateral natural frequency is twice the second lateral natural frequency ($\bar{\omega}_4 = 2\bar{\omega}_2$), the catenary cable is simultaneously involved in the principal parametric resonances $\Omega_1 \approx 2\bar{\omega}_1$ and $\Omega_2 \approx 2\bar{\omega}_2$. Autoparametric interactions between the in- and out-of-plane lateral modes also occur, and these resonance conditions produce large catenary ballooning motions. As one can see from plots given in Figures 44 and 45, the amplitudes of these motions approach $1\ m$. This large lateral catenary response affects the longitudinal response significantly. This effect can be observed in the first, the second and in the third modal longitudinal co-ordinate plots presented in Figure 72, and in the displacement response at the sheave and at the conveyance shown in Figure 44. Besides, passages through longitudinal primary resonances occur during the wind. In particular, the third longitudinal mode is directly activated by the fundamental

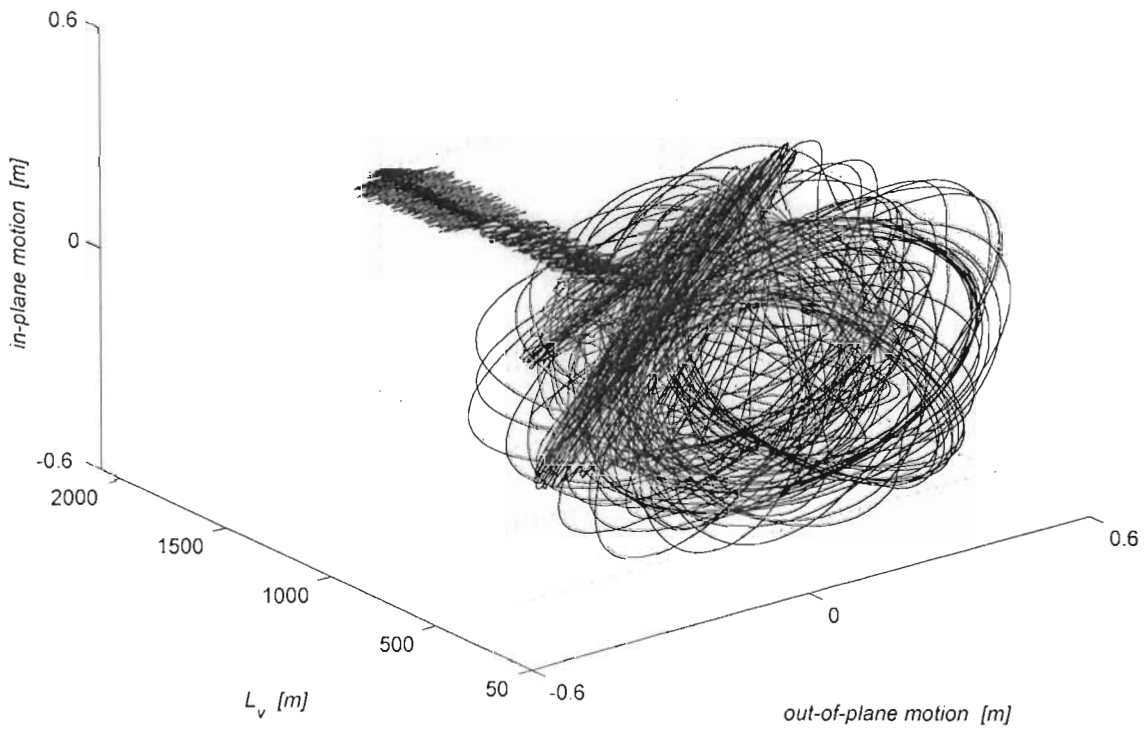

Figure 34. Lateral cable motion at the first quarter point of the catenary in the Kloof system at $V_c = 15\ m/s$.

harmonic of the excitation at the depth level $L_v \approx 1700\ m$, and later by the second harmonic of the excitation at $L_v \approx 550\ m$. Also, at $L_v \approx 1000\ m$ the fourth longitudinal mode tunes to the second harmonic of the excitation, and at $L_v \approx 800\ m$ the second longitudinal mode tunes to the fundamental harmonic of the excitation. To conclude this set of results, the total cable tension plots are presented in 46. As expected, significant oscillations in the cable tensions arise in the catenary resonance region. However, the limits for no slip are not exceeded.

The frequency relationship map for a winding cycle with the velocity $V_c = 16\ m/s$ is shown in Figure 47. This is followed by the simulation results given in Figures 48-50. The primary and parametric catenary resonances are shifted towards the halfway depth level, and occur at $L_v \approx 1150\ m$. As in the previous simulations, amplitude modulated whirling motions result, which promote a significant longitudinal response at the sheave. The system also passes through a number of primary longitudinal resonances, which are noticeable in the tension plots. However the tension ratio across the sheave remains within the no slip range.

Interesting dynamic phenomena can be observed when the winding velocity is increased to 18 m/s. The frequency map given in Figure 51 shows that the catenary resonance is then shifted further towards the beginning of the wind, and takes place at a depth of $L_v \approx 2000\ m$, during the initial acceleration phase. At this level the system has not yet reached the full winding speed, and the resonance phenomena are delayed until the level of approximately 1900 m is attained. This is evident from the response plots presented in Figures 52-54. As one can see, large catenary whirling motions are developed which exceed 1 m. These motions coincide with a significant longitudinal response at the sheave, and at the conveyance. Large dynamic tension fluctuations arise, and the tension ratio across the sheave exceeds the limits for no slip condition in the depth region $L_v \approx 800 - 1200\ m$.

Catenary resonance can be avoided throughout the main part of the ascending cycle if the winding velocity is further raised. This is illustrated in Figure 55, where the system frequency map for a velocity of 19.5 m/s is presented. The simulation results for this case are shown in Figures 56-58. It can be noticed that the system response remains small for the most part of the wind, with an increase taking place only at the end of the cycle. This increase can be attributed to the fact that at the end of the wind the fundamental harmonic of the excitation becomes close to the third lateral natural frequency, namely is $\Omega_1 \approx \bar{\omega}_3$. Also, several longitudinal resonances occur during the wind and are manifested in the longitudinal modal co-ordinate plots. It is not possible to evade the longitudinal resonances within the winding cycle, and they contribute to the cable tension fluctuations, as can be seen in Figure 58.

It is evident from the results for $V_c = 14$, 15, 16 and 18 m/s that when the even lateral modes are resonant at some stage of the wind, a large response occurs in the system. In the Kloof installation this can be avoided if the velocity is increased above 19 m/s. However, if the winding velocity is lowered, for example to 12 m/s, only the third lateral mode is directly excited by the second harmonic of the excitation at a depth of approximately 1200 m, as can be seen in Figure 39. The simulation results for this winding velocity are presented in Figures 40-42, and, as one can notice, the response remains small throughout the wind.

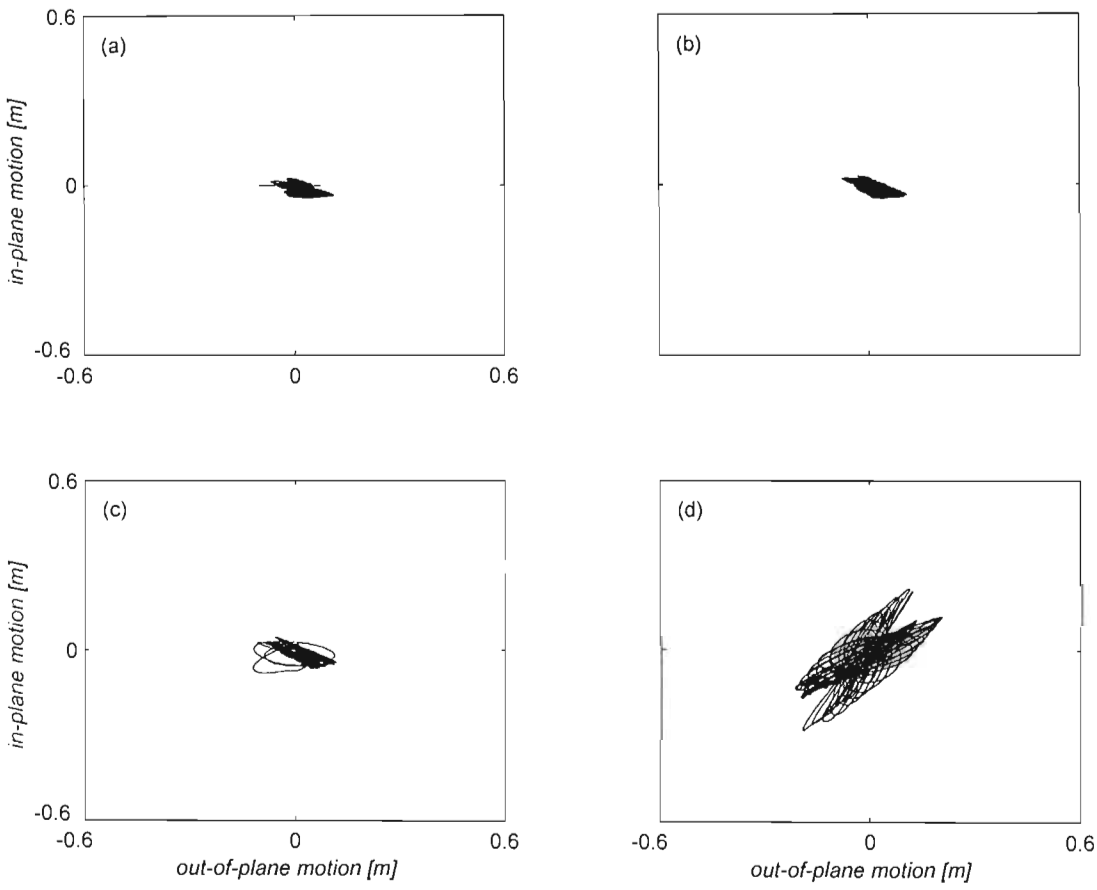

Figure 35. The trajectory of the first quarter point of the catenary during various stages of the ascending cycle in the Kloof system at $V_c = 15\ m/s$: $(a)\ L_v = 1600 - 1400\ m$, $(b)\ L_v = 1400 - 1200\ m$, $(c)\ L_v = 1200 - 1000\ m$, $(d)\ 1000 - 800\ m$.

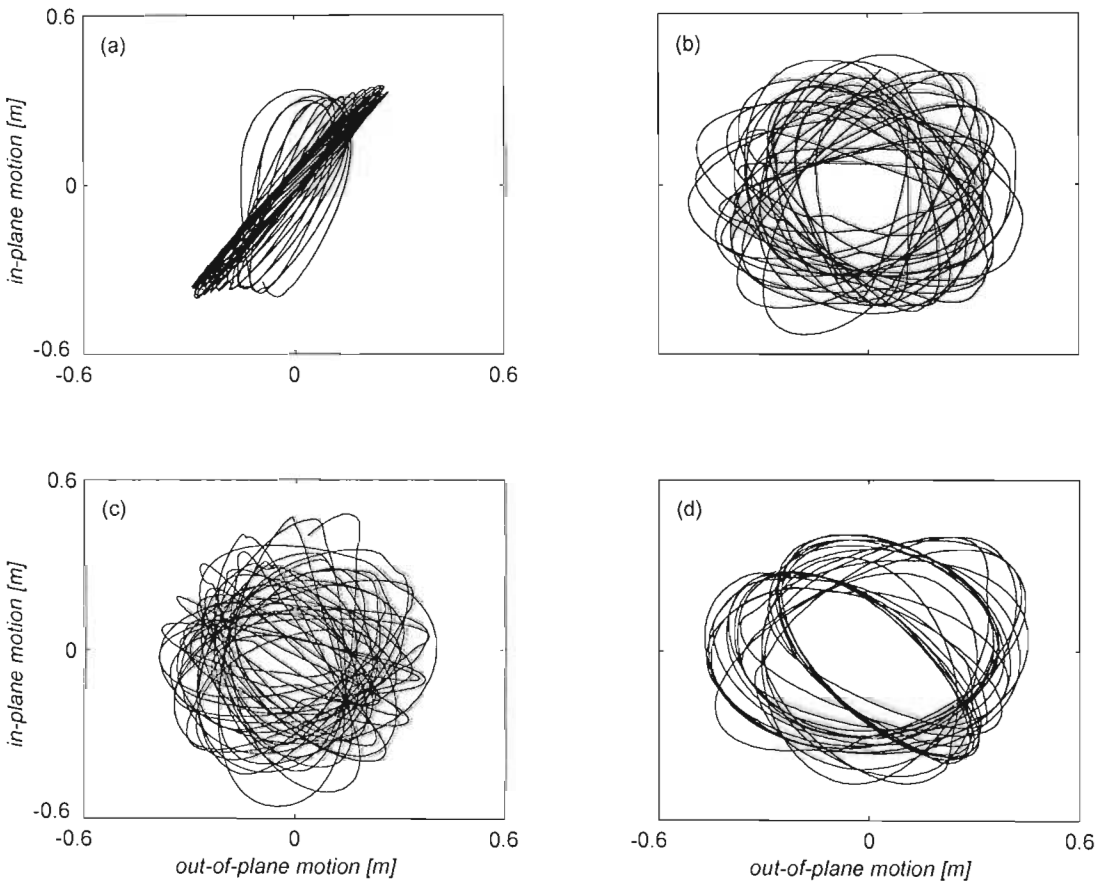

Figure 36. The trajectory of the first quarter point of the catenary during various stages of the ascending cycle in the Kloof system at $V_c = 15\ m/s$ - continued: $(a)\ L_v = 800 - 600\ m$, $(b)\ L_v = 600 - 400\ m$, $(c)\ L_v = 400 - 150\ m$, $(d)\ 150 - 60\ m$.

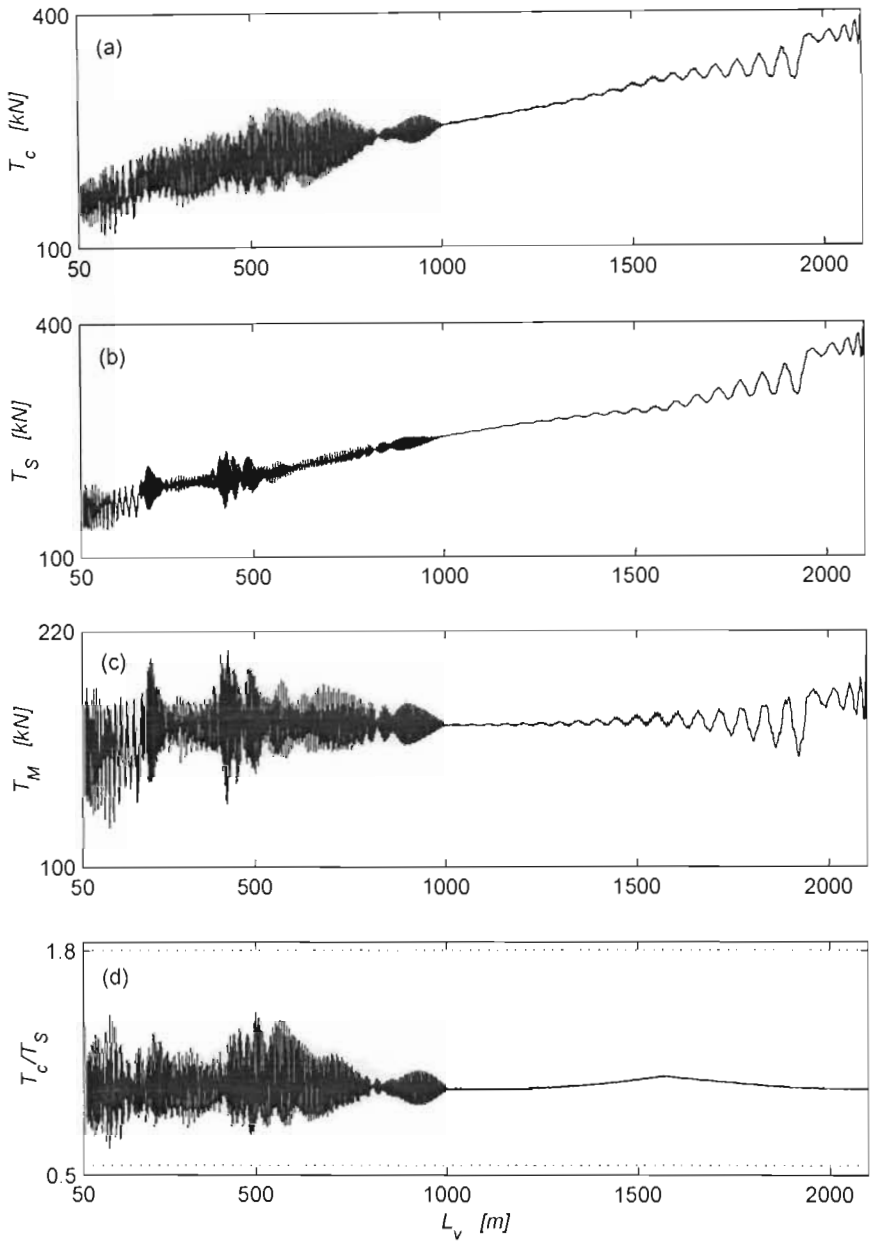

Figure 37. Total tensions in Kloof Mine winding cables at the nominal velocity $V_c = 15$ m/s: (a) the catenary tension T_c; (b) the vertical rope tension T_S at the sheave; (c) the vertical rope tension T_M at the conveyance; (d) the tension ratio across the sheave T_c/T_S.

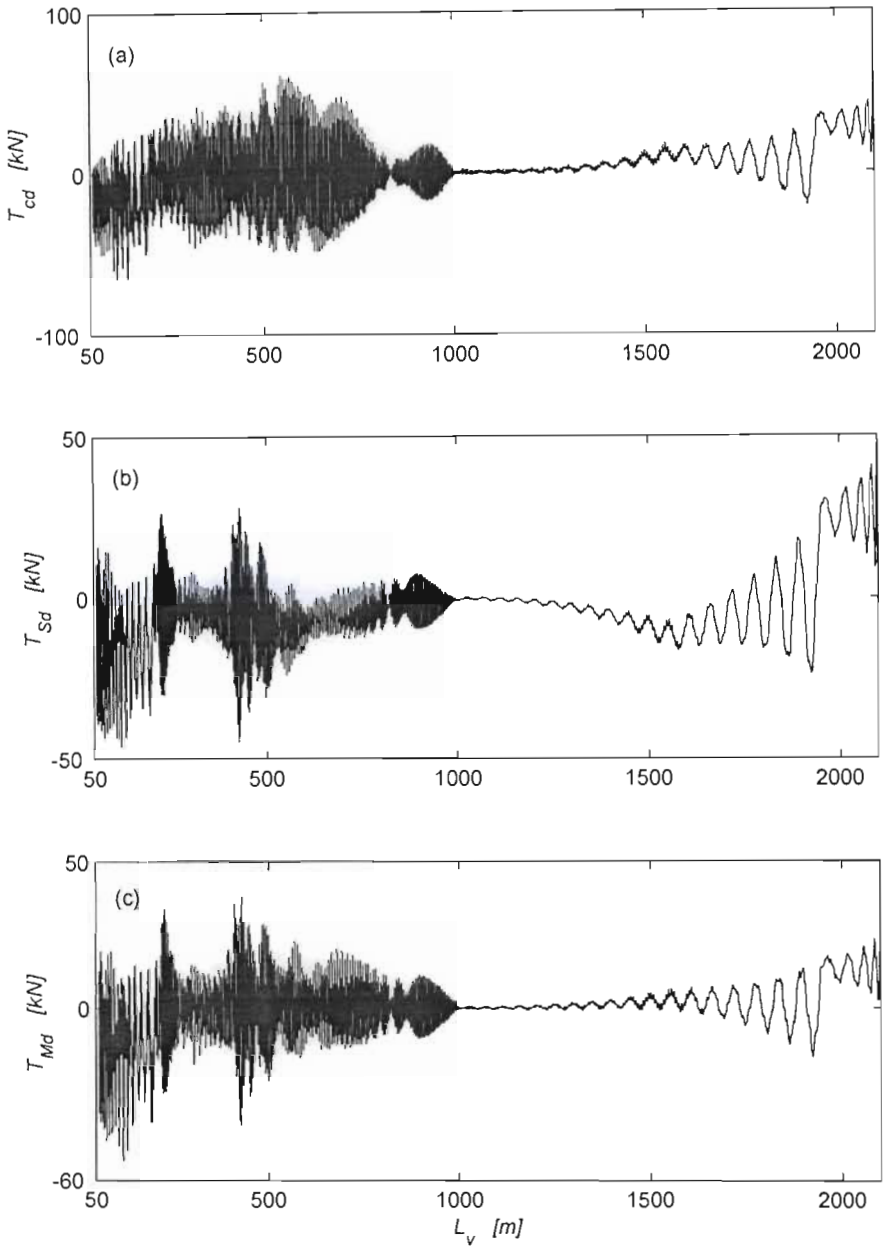

Figure 38. Dynamic tensions in Kloof Mine winding cables at the nominal speed $V_c = 15$ m/s: (a) the catenary dynamic tension T_{cd}; (b) the vertical rope dynamic tension T_{Sd} at the sheave; (c) the vertical rope dynamic tension T_{Md} at the conveyance.

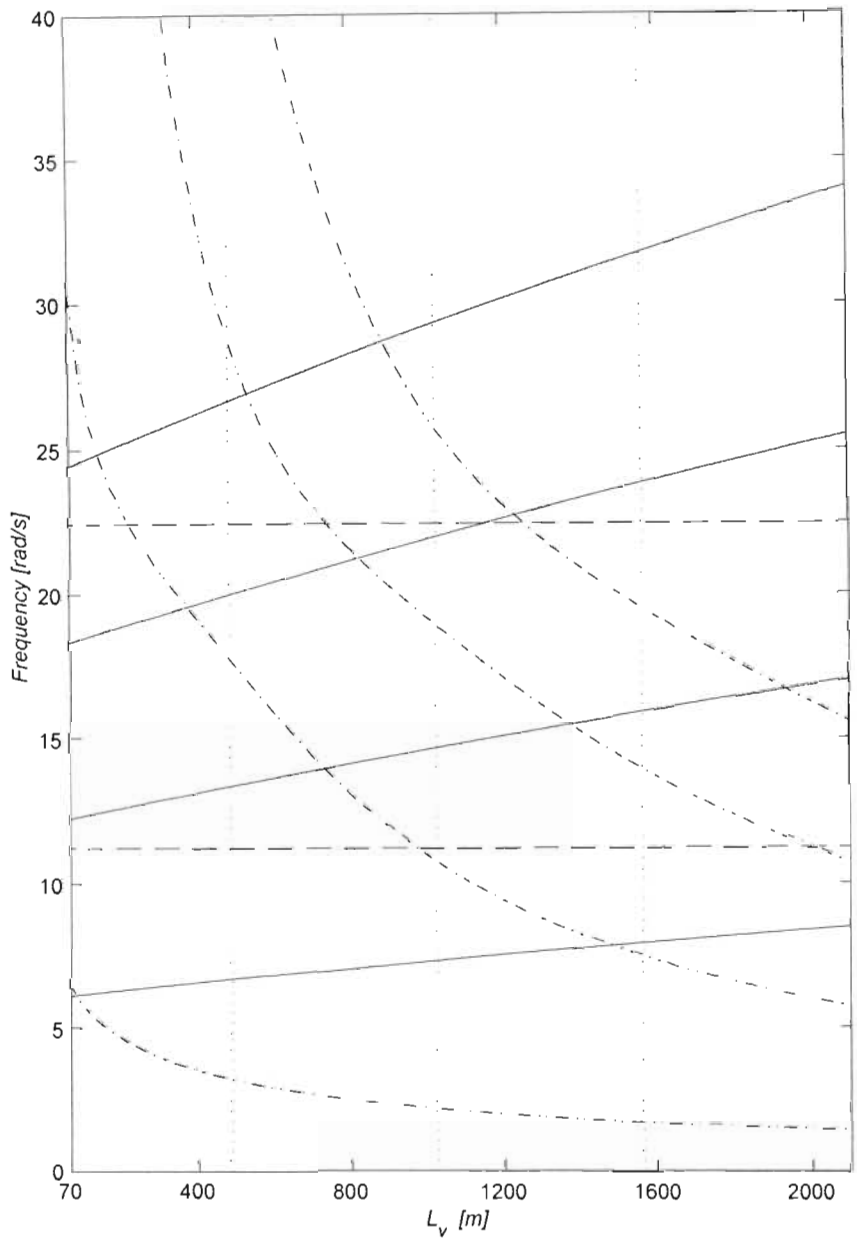

Figure 39. Longitudinal frequency ω_n $(- \cdot -)$ and lateral frequency $\bar{\omega}_n$ (—) curves for Kloof Gold Mine winder (ascending cycle), with horizontal lines $(--)$ denoting the first and the second harmonics of the excitation frequency at the winding velocity $V_c = 12\ m/s$. Vertical lines $(\cdots)$ indicate the layer change locations.

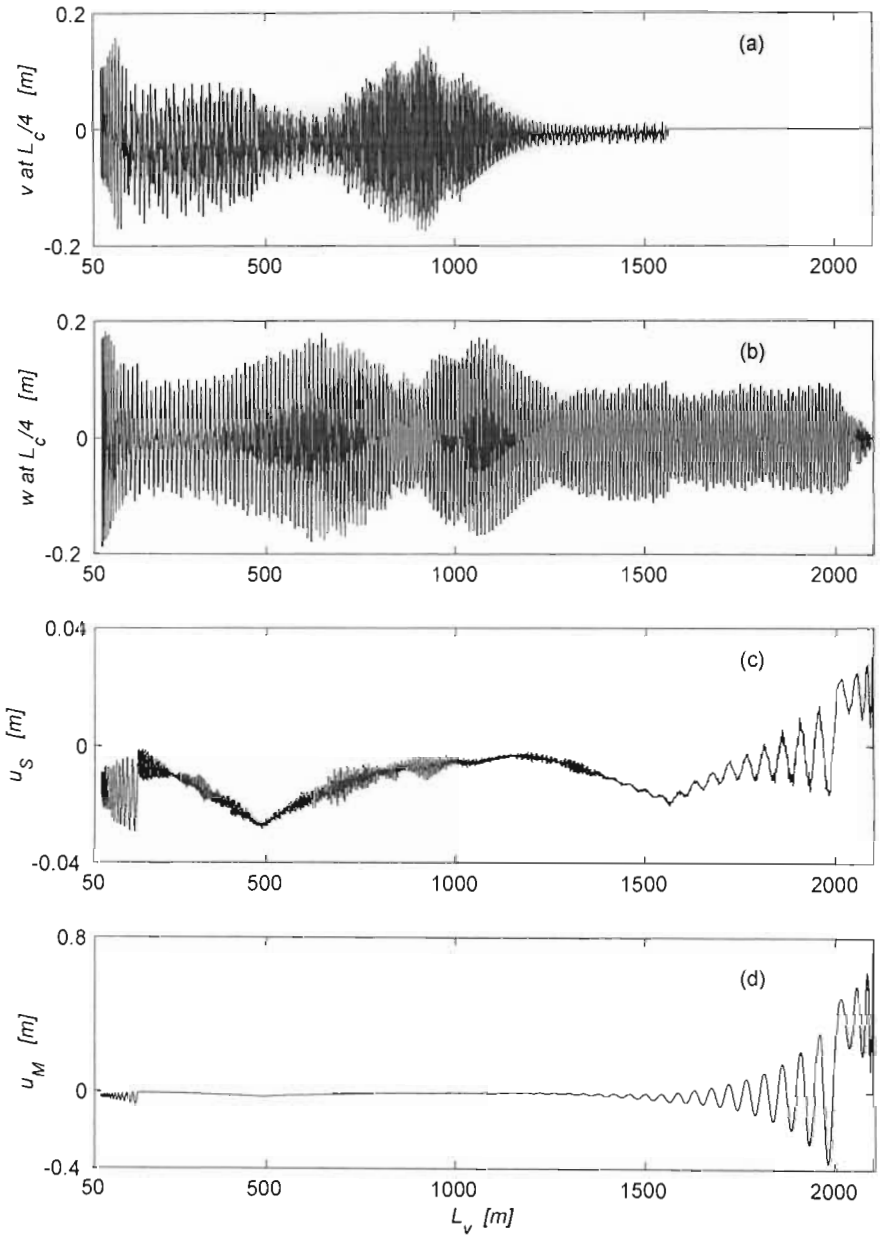

Figure 40. Displacement response of Kloof Mine winding cables for $V_c = 12\ m/s$: lateral (a) in-plane and (b) out-of-plane motions at the first quarter of the catenary; longitudinal responses (c) at the sheave and (d) at the conveyance.

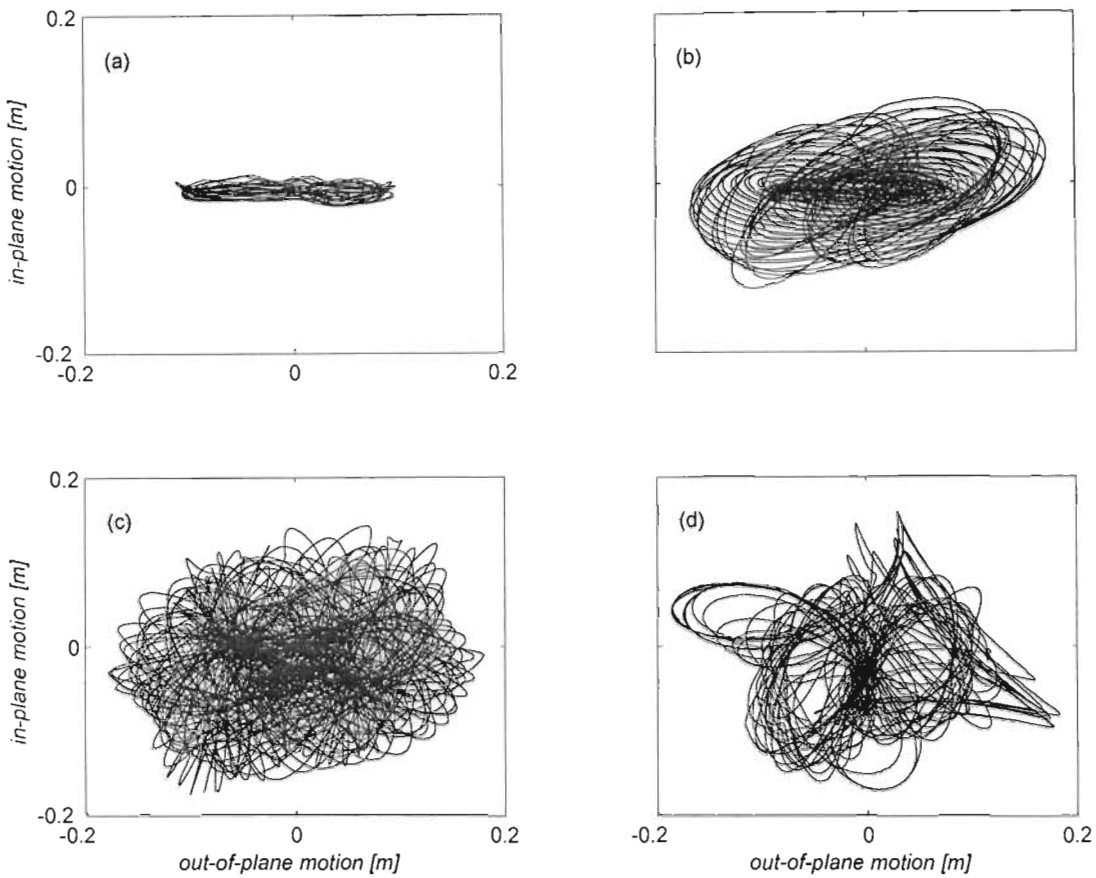

Figure 41. The trajectory of the first quarter point of the catenary during various stages of the ascending cycle in the Kloof system at $V_c = 12\ m/s$: $(a)\ L_v = 1600 - 1400\ m$, $(b)\ L_v = 1400 - 1000\ m$, $(c)\ L_v = 1000 - 400\ m$, $(d)\ 400 - 70\ m$.

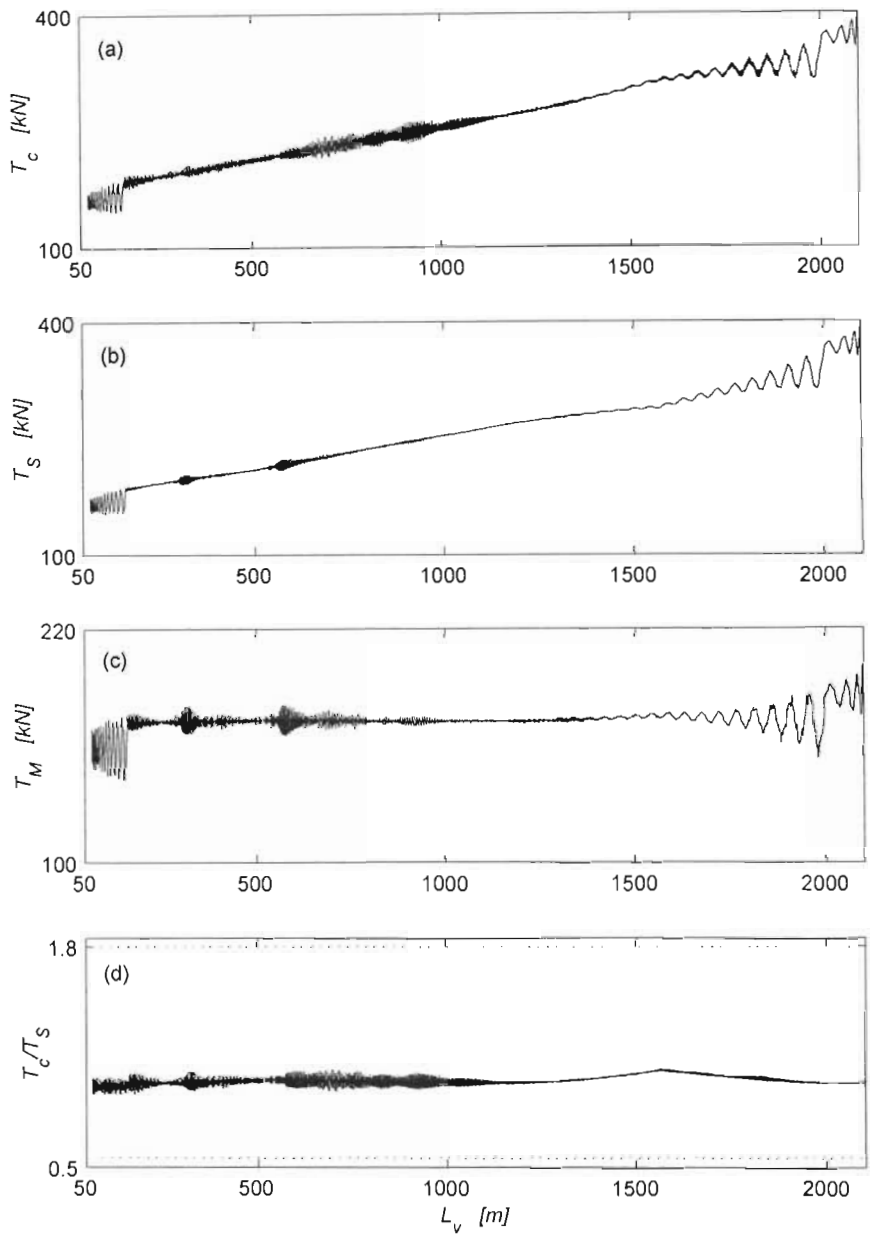

Figure 42. Total tensions in Kloof Mine winding cables at the winding velocity $V_c = 12$ m/s: (a) the catenary tension T_c; (b) the vertical rope tension T_S at the sheave; (c) the vertical rope tension T_M at the conveyance; (d) the tension ratio across the sheave T_c/T_S.

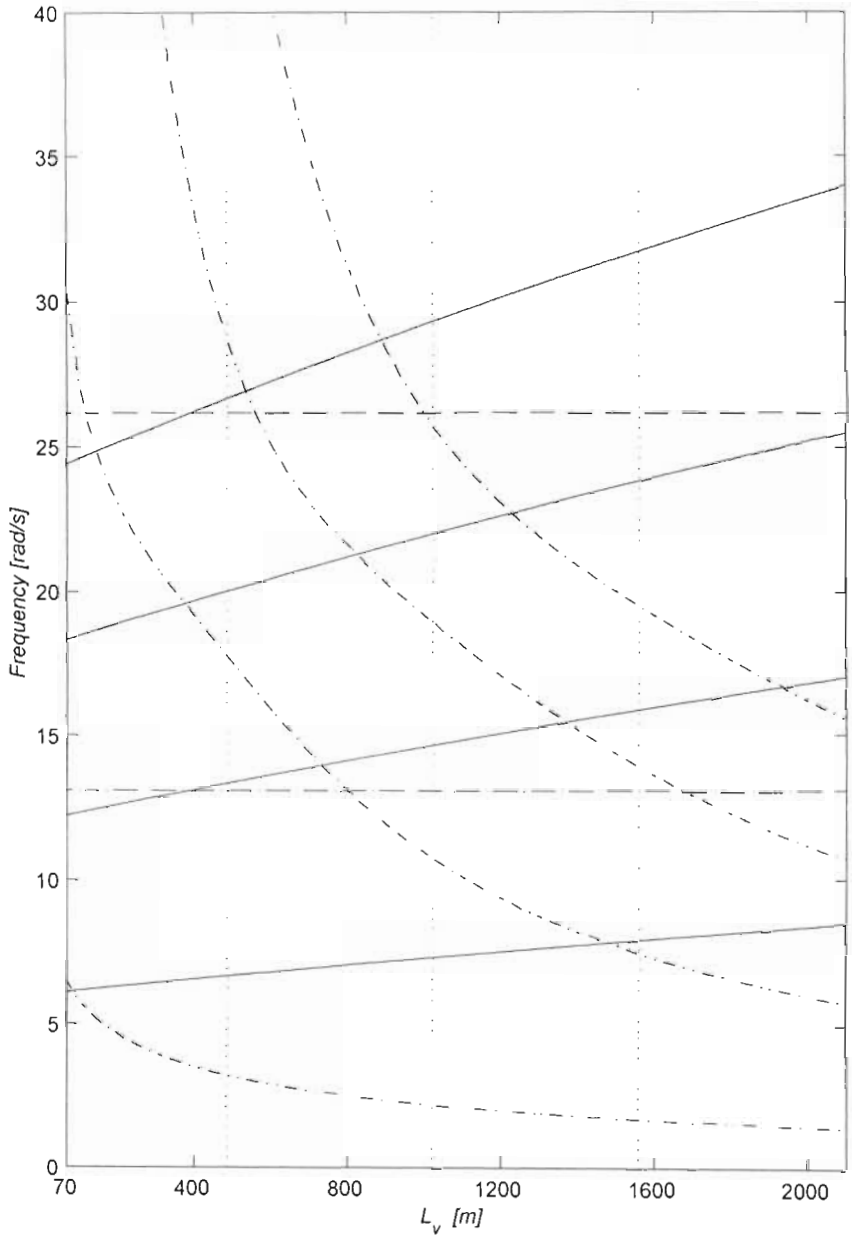

Figure 43. Longitudinal frequency ω_n $(- \cdot -)$ and lateral frequency $\bar{\omega}_n$ (—) curves for Kloof Gold Mine winder (ascending cycle), with horizontal lines $(--)$ denoting the first and the second harmonics of the excitation frequency at the winding velocity $V_c = 14\ m/s$. Vertical lines $(\cdots)$ indicate the layer change locations.

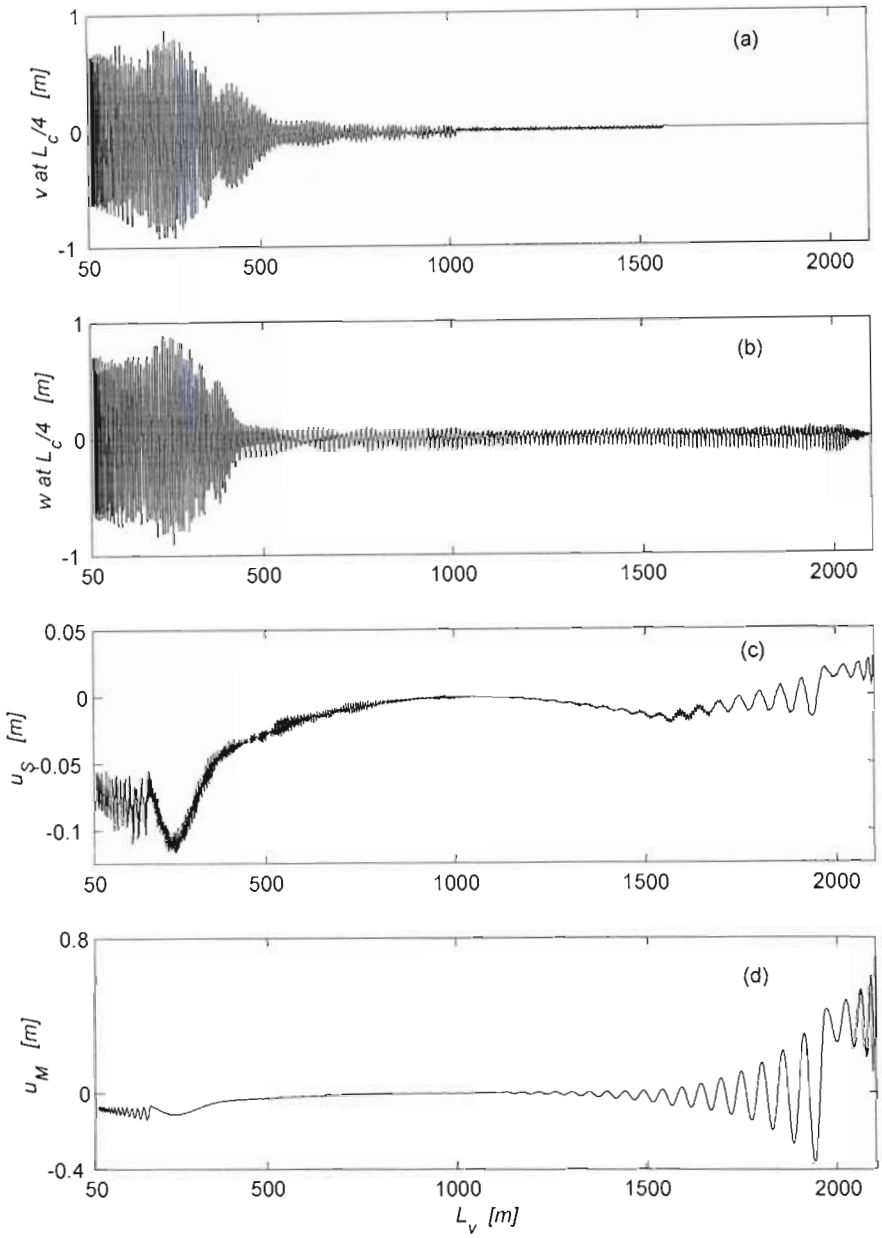

Figure 44. Displacement response of Kloof Mine winding cables for $V_c = 14\ m/s$: lateral (a) in-plane and (b) out-of-plane motions at the first quarter of the catenary; longitudinal responses (c) at the sheave and (d) at the conveyance.

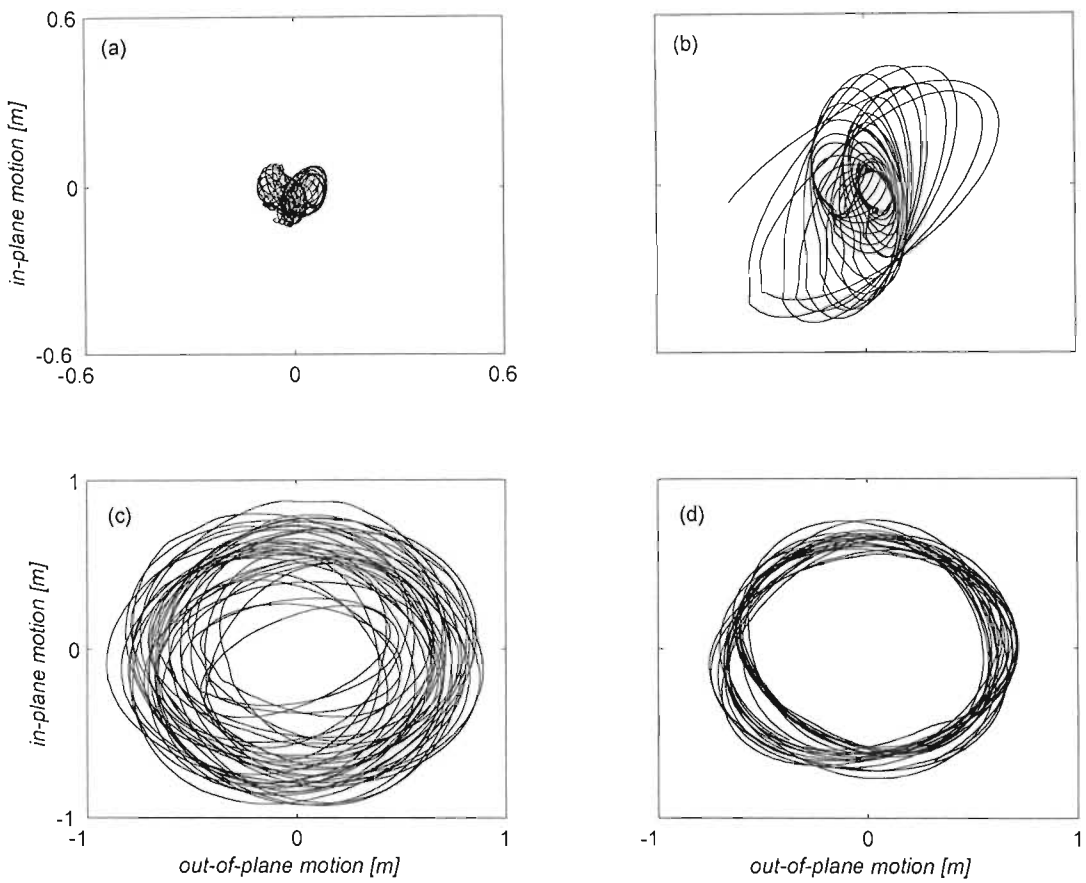

Figure 45. The trajectory of the first quarter point of the catenary during various stages of the ascending cycle in the Kloof system at $V_c = 14\ m/s$: $(a)\ L_v = 800 - 600\ m$, $(b)\ L_v = 600 - 400\ m$, $(c)\ L_v = 400 - 150\ m$, $(d)\ 150 - 60\ m$.

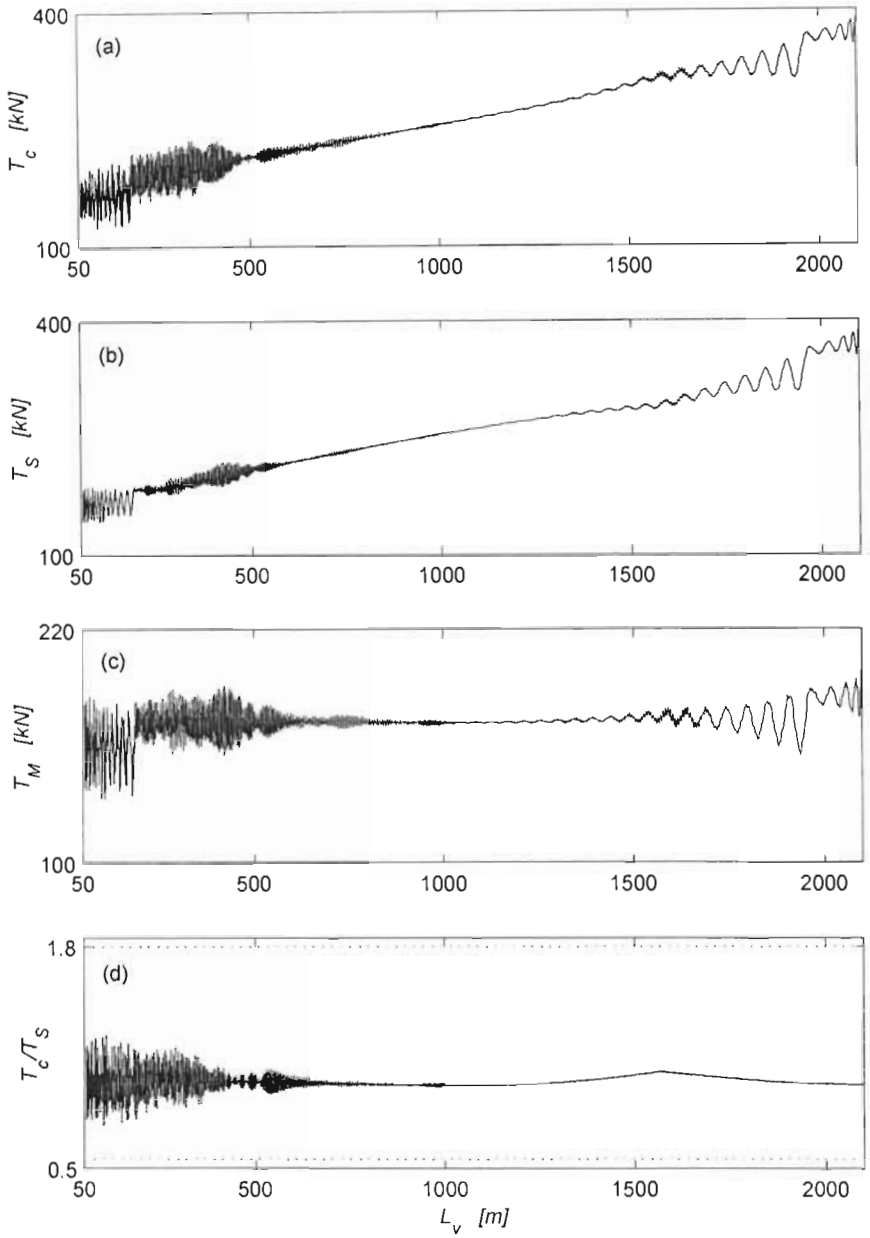

Figure 46. Total tensions in Kloof Mine winding cables at the winding velocity $V_c = 14$ m/s: (a) the catenary tension T_c; (b) the vertical rope tension T_S at the sheave; (c) the vertical rope tension T_M at the conveyance; (d) the tension ratio across the sheave T_c/T_S.

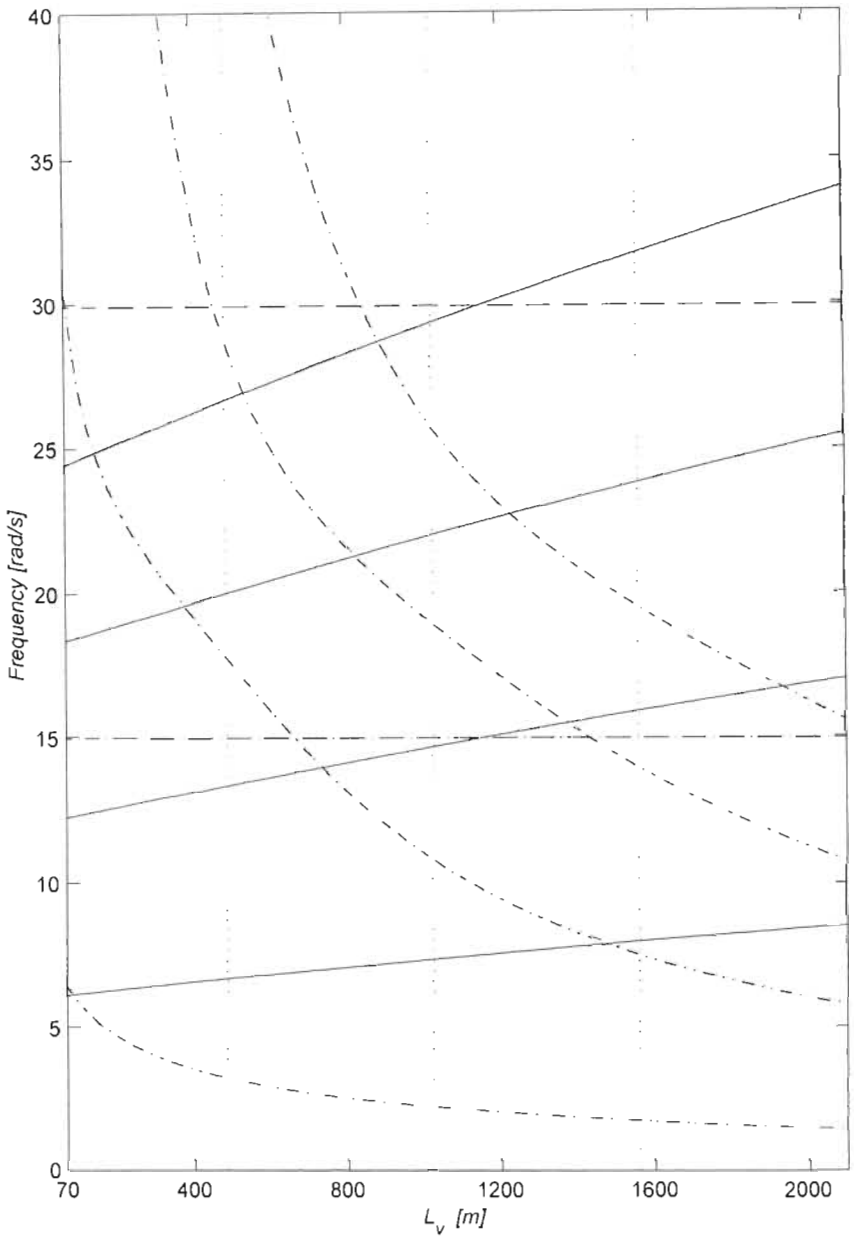

Figure 47. Longitudinal frequency ω_n $(- \cdot -)$ and lateral frequency $\bar{\omega}_n$ (—) curves for Kloof Gold Mine winder (ascending cycle), with horizontal lines $(--)$ denoting the first and the second harmonics of the excitation frequency at the winding velocity $V_c = 16\ m/s$. Vertical lines $(\cdots)$ indicate the layer change locations.

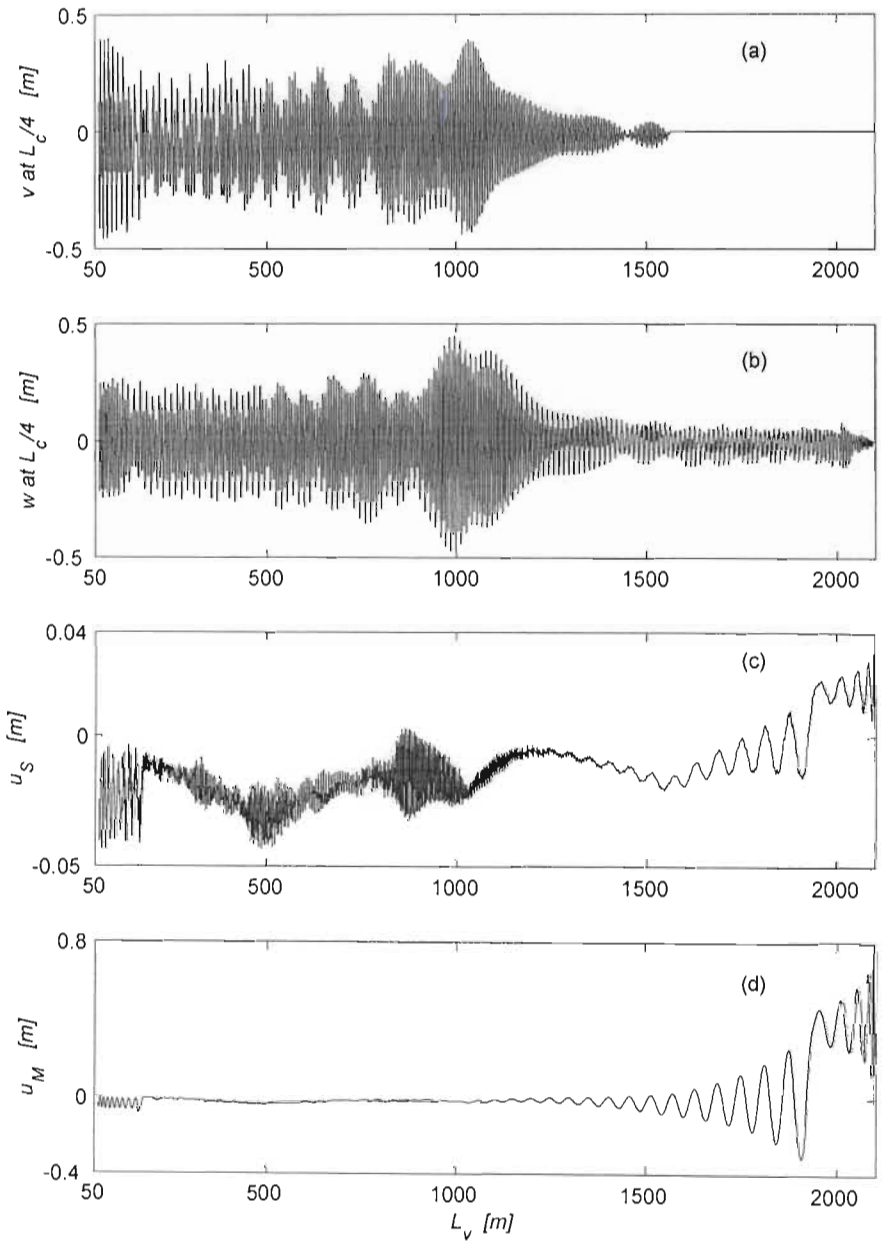

Figure 48. Displacement response of Kloof Mine winding cables for $V_c = 16\ m/s$: lateral (a) in-plane and (b) out-of-plane motions at the first quarter of the catenary; longitudinal responses (c) at the sheave and (d) at the conveyance.

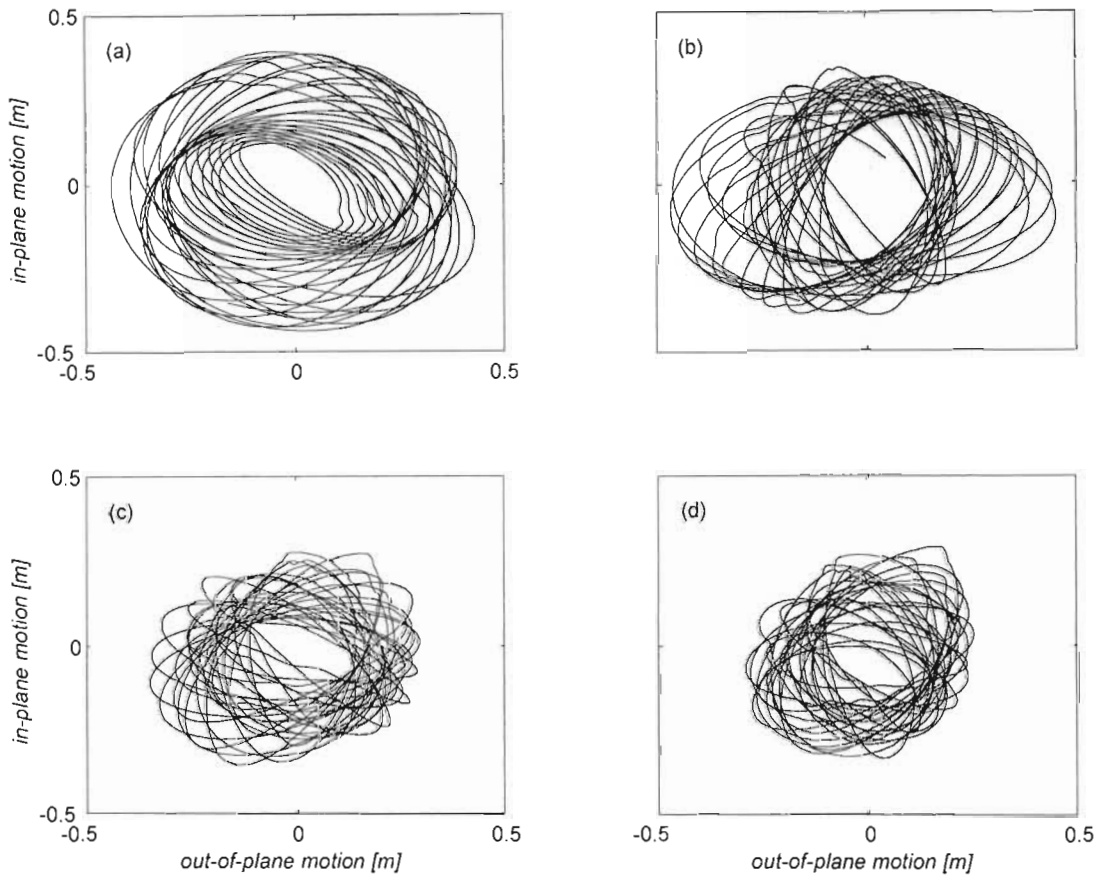

Figure 49. The trajectory of the first quarter point of the catenary during various stages of the ascending cycle in the Kloof system at $V_c = 16\ m/s$: $(a)\ L_v = 1200 - 1000\ m$, (b) $L_v = 1000 - 800\ m$, $(c)\ L_v = 800 - 600\ m$, $(d)\ 600 - 400\ m$.

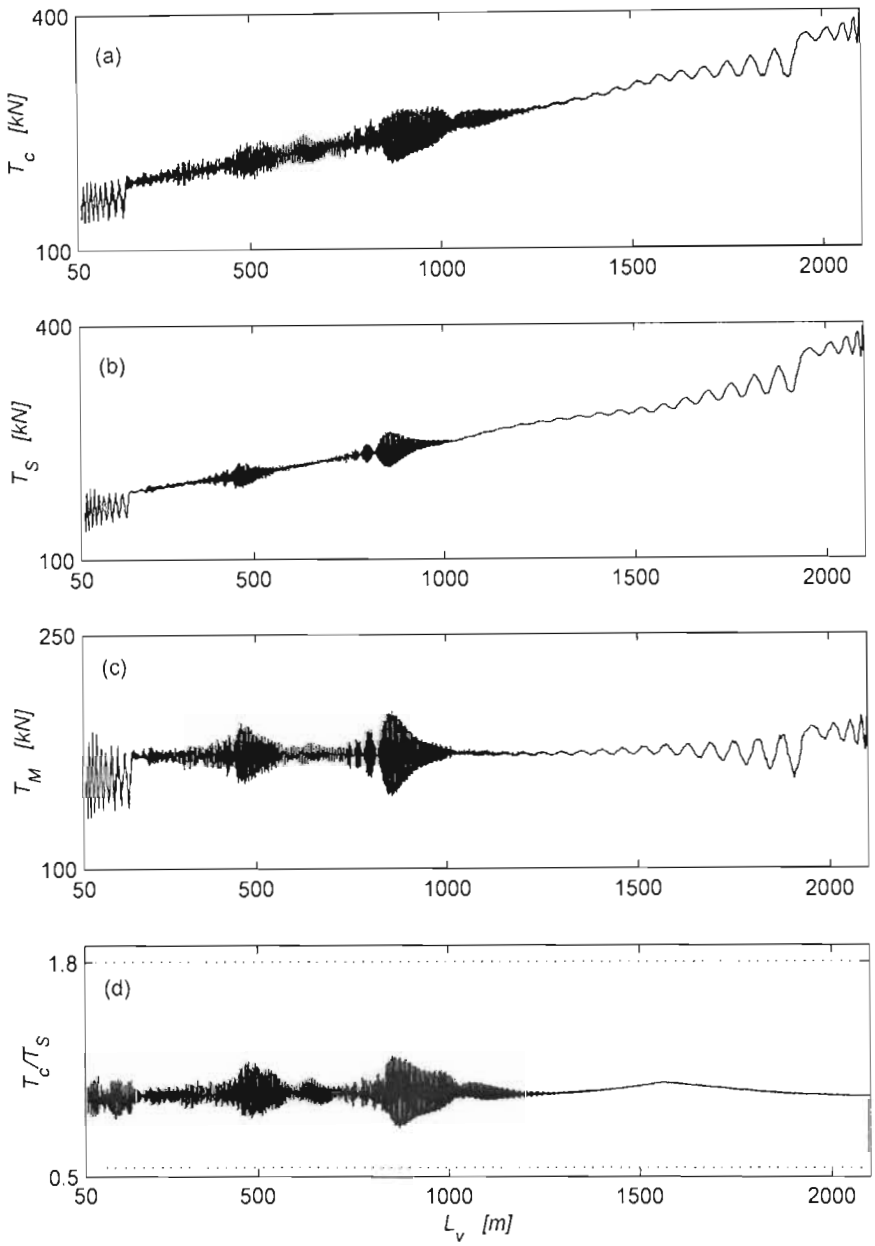

Figure 50. Total tensions in Kloof Mine winding cables at the winding velocity $V_c = 16$ m/s: (a) the catenary tension T_c; (b) the vertical rope tension T_S at the sheave; (c) the vertical rope tension T_M at the conveyance; (d) the tension ratio across the sheave T_c/T_S.

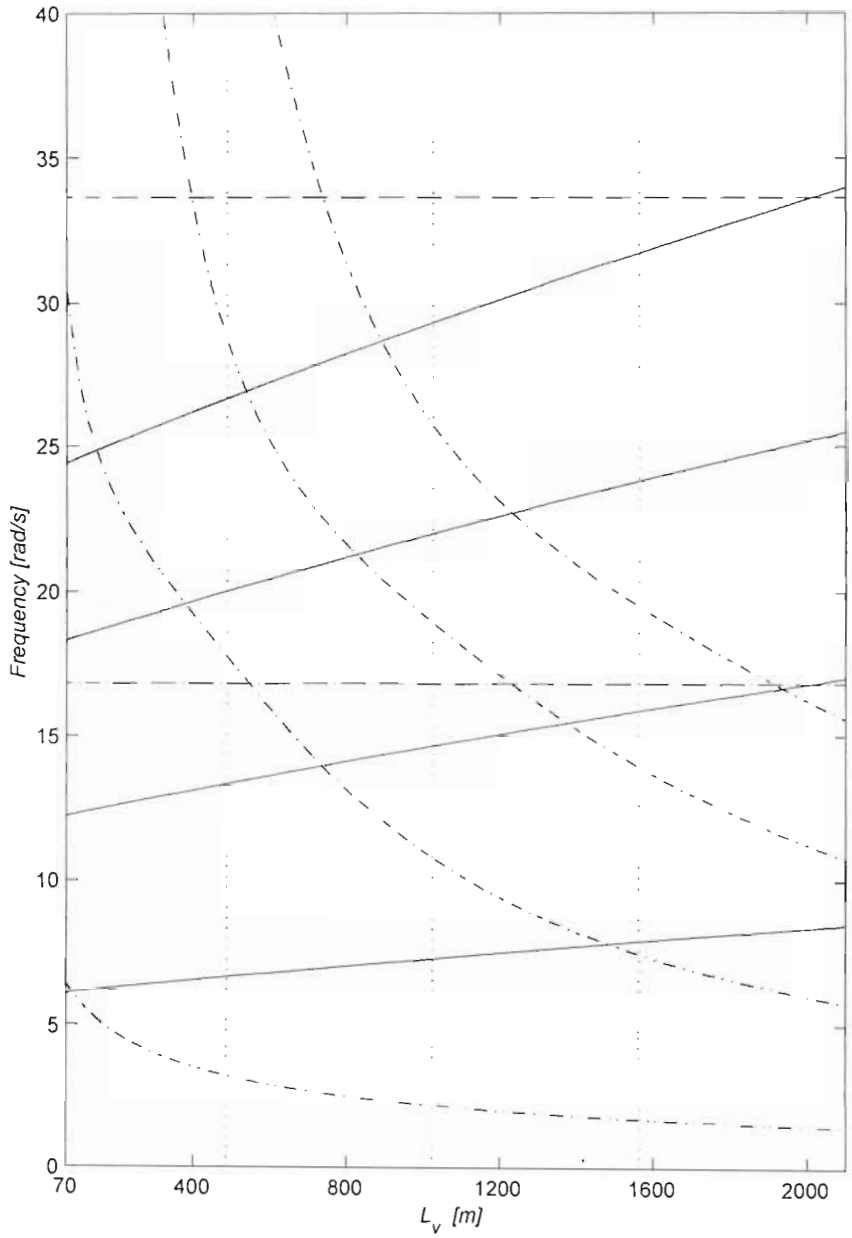

Figure 51. Longitudinal frequency ω_n $(- \cdot -)$ and lateral frequency $\bar{\omega}_n$ (—) curves for Kloof Gold Mine winder (ascending cycle), with horizontal lines $(--)$ denoting the first and the second harmonics of the excitation frequency at the winding velocity $V_c = 18\ m/s$. Vertical lines $(\cdots)$ indicate the layer change locations.

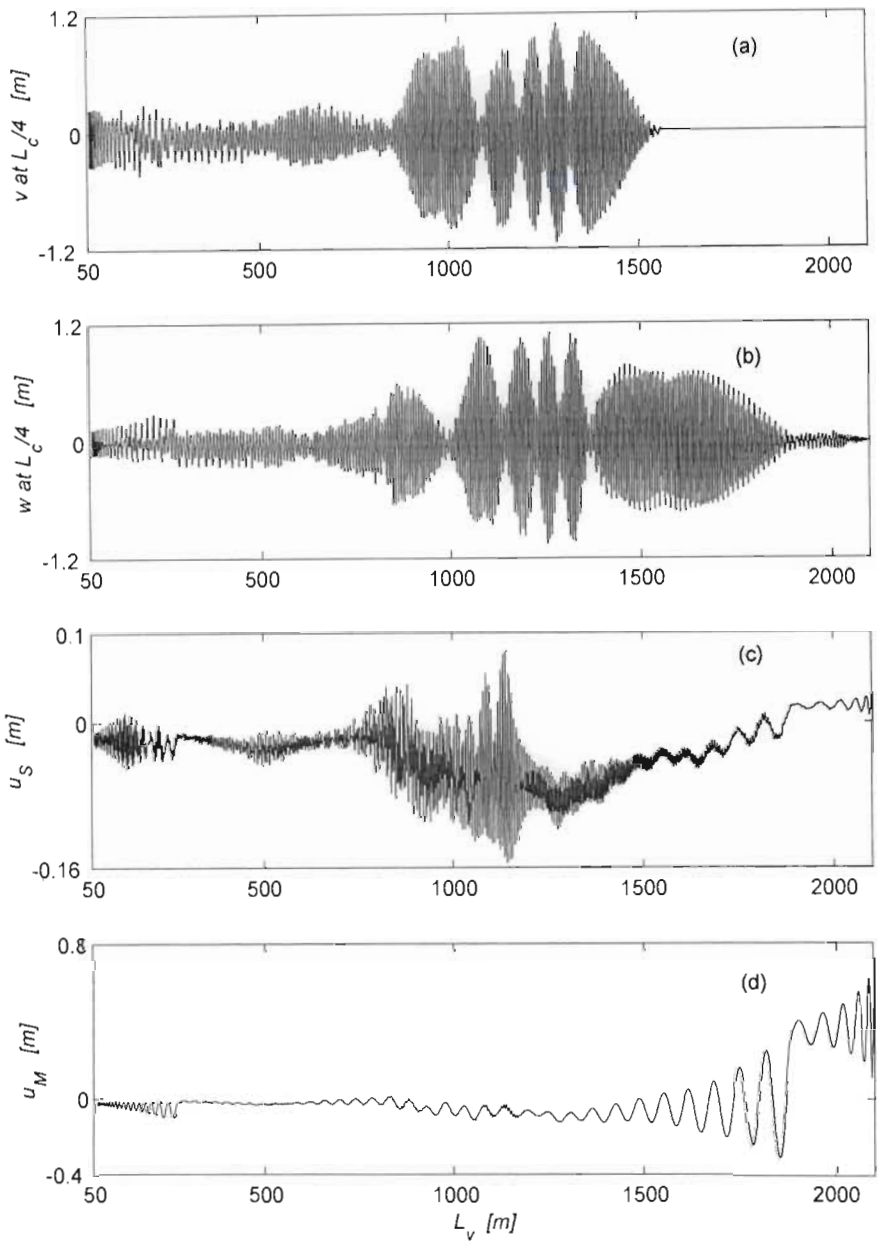

Figure 52. Displacement response of Kloof Mine winding cables for $V_c = 18\ m/s$: lateral (a) in-plane and (b) out-of-plane motions at the first quarter of the catenary; longitudinal responses (c) at the sheave and (d) at the conveyance.

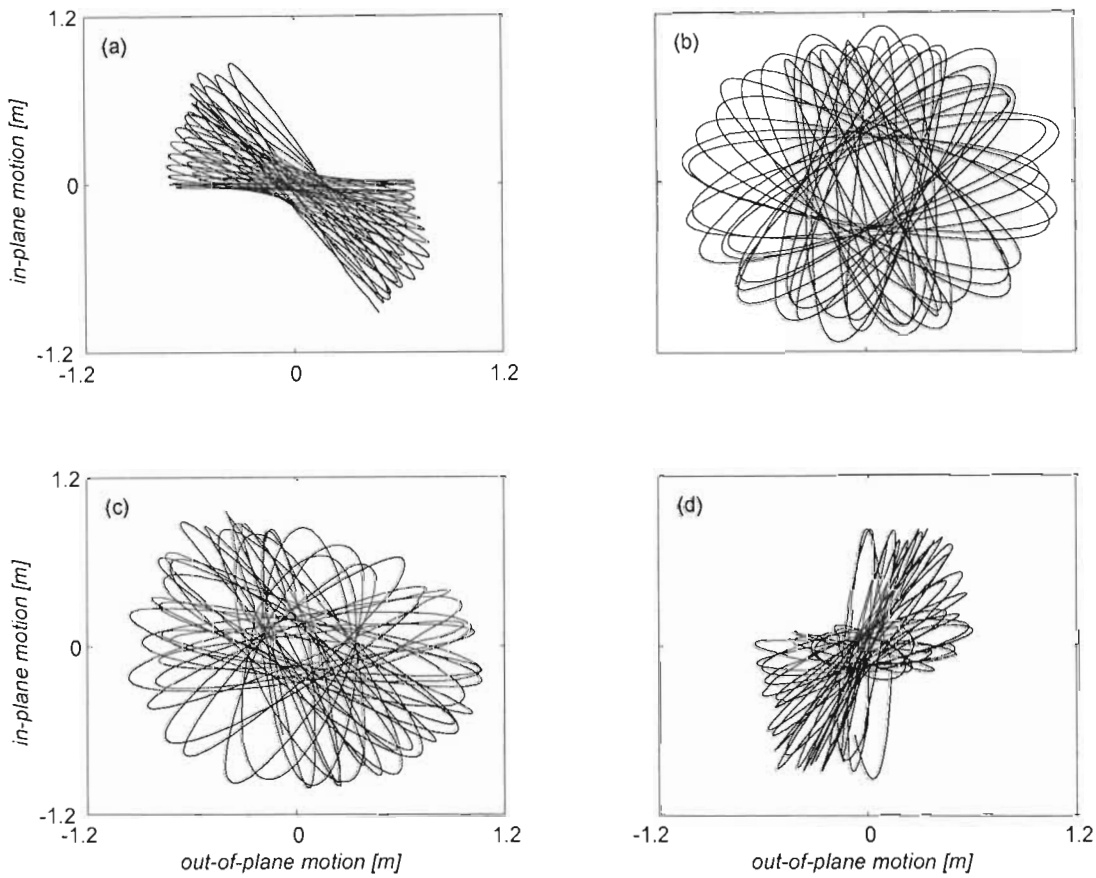

Figure 53. The trajectory of the first quarter point of the catenary during various stages of the ascending cycle in the Kloof system at $V_c = 18\ m/s$: $(a)\ L_v = 1600 - 1400\ m$, $(b)\ L_v = 1400 - 1200\ m$, $(c)\ L_v = 1200 - 1000\ m$, $(d)\ 1000 - 800\ m$.

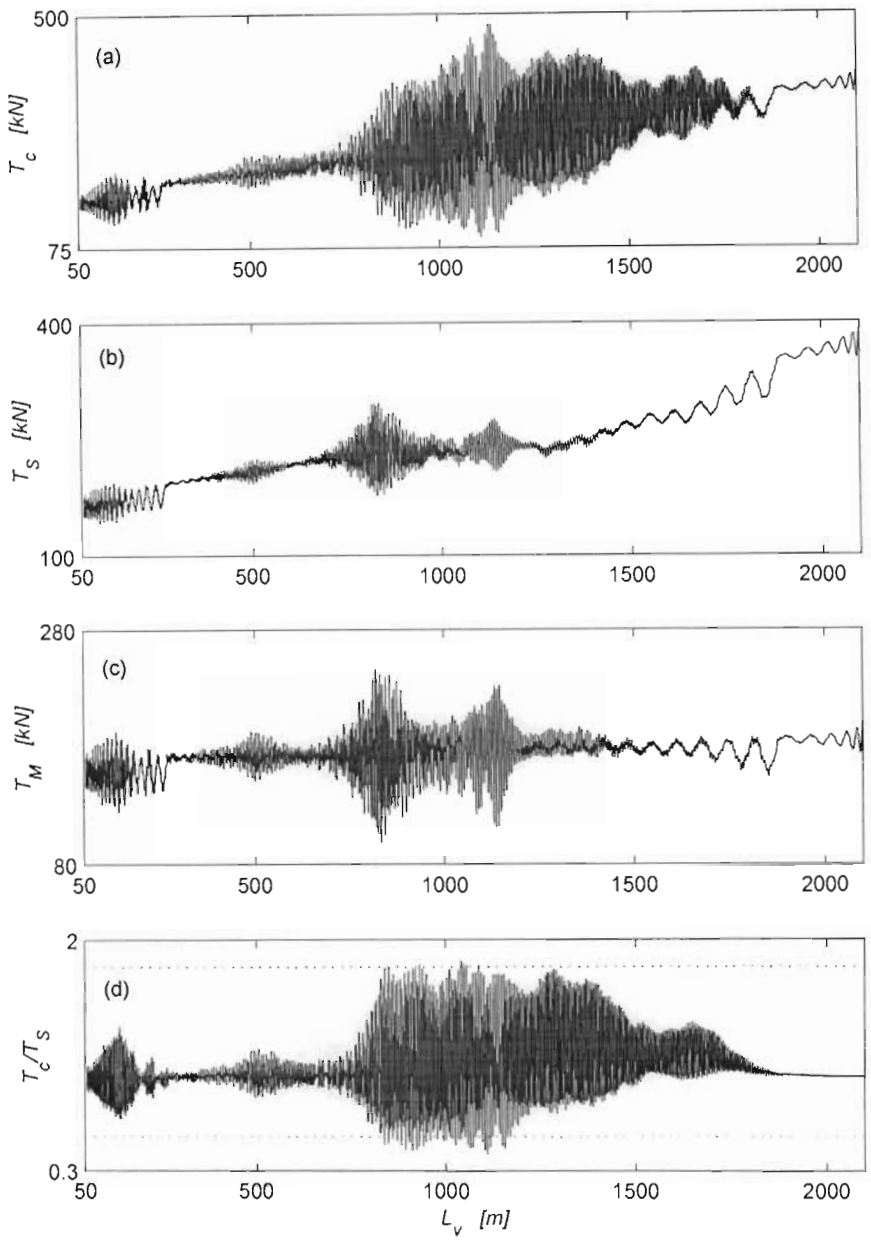

Figure 54. Total tensions in Kloof Mine winding cables at the winding velocity $V_c = 18$ m/s: (a) the catenary tension T_c; (b) the vertical rope tension T_S at the sheave; (c) the vertical rope tension T_M at the conveyance; (d) the tension ratio across the sheave T_c/T_S.

5.4.4 Elandsrand Simulation

The non-linear response of the Elandsrand Mine winding cables, with parameters presented earlier in Table 1, has also been simulated. The results for the nominal ascending cycle with a winding velocity of 16 m/s are presented in Figures 60-61. It is evident from the frequency plot given in Figure 59 that the second harmonic of the excitation is near the third lateral frequency at approximately $L_v \approx 800\ m$. This resonance does not produce a significant increase in the response, as can be seen in the lateral co-ordinate plots and in the displacement response plots. However, at the beginning of the wind a passage through the fundamental lateral resonance takes place, which can observed in the out-of-plane response curves. The effects of this resonance are damped out soon and, in general, the response is small throughout the main part of the cycle. It is interesting to observe a significant growth in the fundamental in-plane lateral mode at the end of the wind. Rope tension fluctuations occur due to the passage through the longitudinal resonances, but the limits for no slip across the sheave are never reached. Hence, the wind can be mostly considered as trouble-free, and this resembles the Kloof cycle at the winding velocity 12 m/s, when also a passage through the third lateral resonance occurred, but large catenary amplitude modulated motions and energy exchanges were absent.

5.5 Summary and Conclusions: Non-Linear Interactions

The results of numerical simulations of a number of ascending cycles for the non-linear model of a hoisting cable system, based on the parameters of the Kloof Mine winding plant, show a vast range of interesting and potentially dangerous non-linear dynamic phenomena.

The nominal cycle simulation with winding velocity $V_c = 15\ m/s$ demonstrates problematic dynamic behaviour from the depth level of approximately 900 m. The results of

this simulation principally corroborate the observations recorded during the operation of the Kloof winding plant presented earlier in Subsection 5.4.1. The adverse dynamic behaviour of the system is caused largely by the primary catenary even (second and fourth) resonances, and by the autoparametric interactions between the in- and out-of-plane catenary modes. Principal parametric resonances of the lateral modes also occur, and conditions for autoparametric interactions between the lateral and longitudinal modes arise. Additionally, a transition through a number of primary longitudinal resonances takes place during the wind. It should also be noted that the adverse dynamic motions in the system promote large oscillations in the cable tension. These oscillations must be considered significant with respect to fatigue of the cable.

The phase space trajectories and associated power spectra further illustrate the complexity of motions during passages through the resonance regions. A more advanced analytical analysis would be required to predict and to investigate possible bifurcation phenomena arising during the slow transitions across the points of dynamic instability. Many interesting dynamic phenomena have recently been reported as occurring in resonant motions of strings which can be pertinent to the catenary dynamic behaviour. These include torus doubling bifurcations and the destruction of the torus, leading to a strange attractor, and to chaotic vibrations [Johnson & Bajaj, 1988; Molteno & Tufillaro, 1990, O'Reilly & Holmes, 1992]. However, the non-stationary nature of the catenary-vertical rope system complicates the problem significantly, as the bifurcations do not occur at the bifurcation points in the stationary response: they are delayed [Raman, Bajaj & Davies, 1996].

When the winding velocity is changed the resonance locations are shifted. The simulation of the winding cycle at $14\ m/s$ demonstrates that the primary catenary resonances are moved towards the end of the wind, and thus the catenary response is decreased throughout the main part of the cycle. The strategy of decreased winding velocity had often been applied in practice in the Kloof winding installation, as reported in the observations documented by

Dimitriou & Whillier [1973]. However, the simulation predicts large catenary whirling motions at the end of the wind. The simulation results for 16 m/s and 18 m/s further clarify the role of the location of the primary catenary resonances, and confirm the autoparametric nature of the system. Hence, it is evident that the catenary resonances can be avoided, to a large extent, if the winding velocity is increased to an appropriate level. For example, in the Kloof winding plant a velocity of about 19.5 m/s could be applied on the ascending cycle in order to achieve suitable resonance shifts. The simulation results for this velocity confirm the benefits of this strategy.

The Kloof simulation with the winding velocity decreased to 12 m/s demonstrates that the adverse dynamic response of the system can be largely suppressed if the even lateral primary resonances are avoided during the wind. This is further confirmed in the Elandsrand Mine parameter simulation at the nominal velocity of 16 m/s. In both cases only third lateral modes are directly excited during the constant velocity phase of the up-wind. It is known that the Elandsrand system have not experienced major vibration problems during its nominal operational regimes, and this corroborates the simulation results.

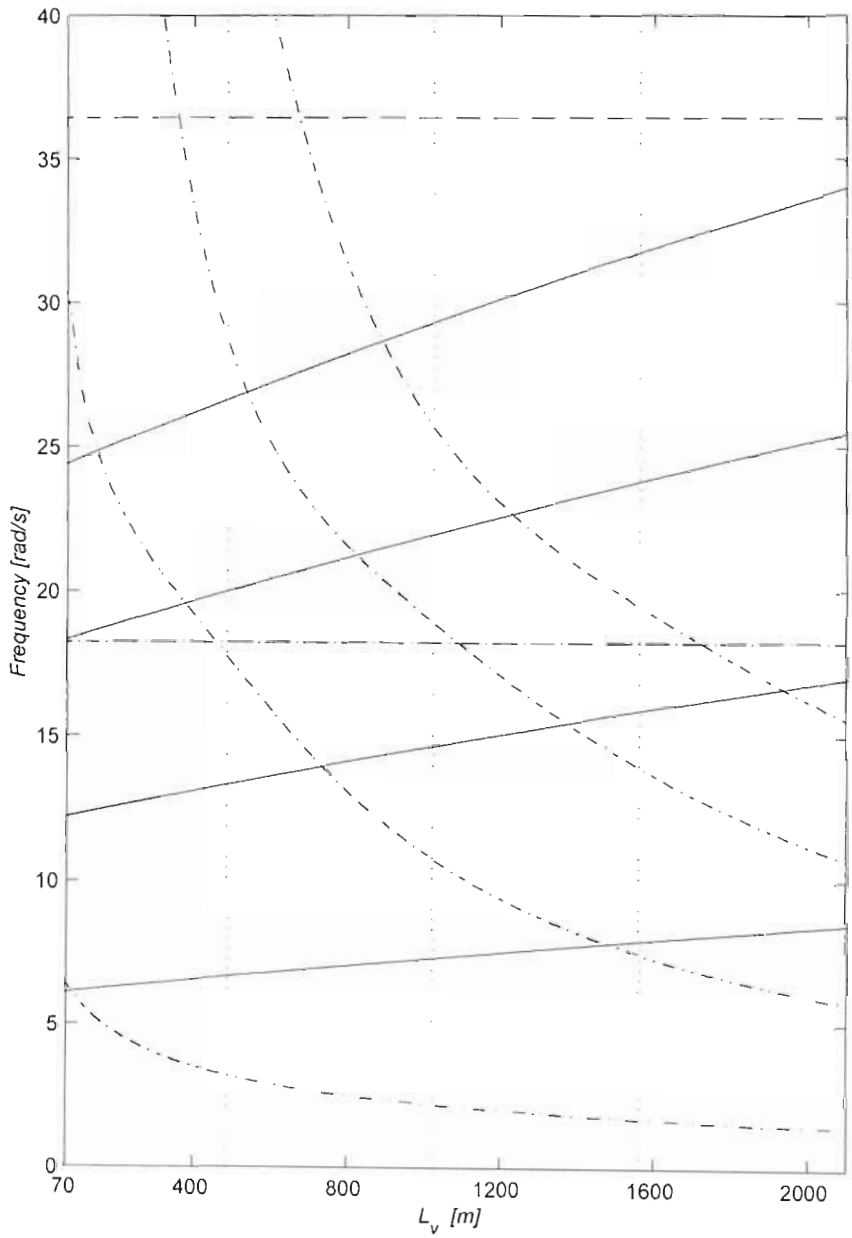

Figure 55. Longitudinal frequency ω_n $(- \cdot -)$ and lateral frequency $\bar{\omega}_n$ (—) curves for Kloof Gold Mine winder (ascending cycle), with horizontal lines $(--)$ denoting the first and the second harmonics of the excitation frequency at the winding velocity $V_c = 19.5$ m/s. Vertical lines $(\cdots)$ indicate the layer change locations.

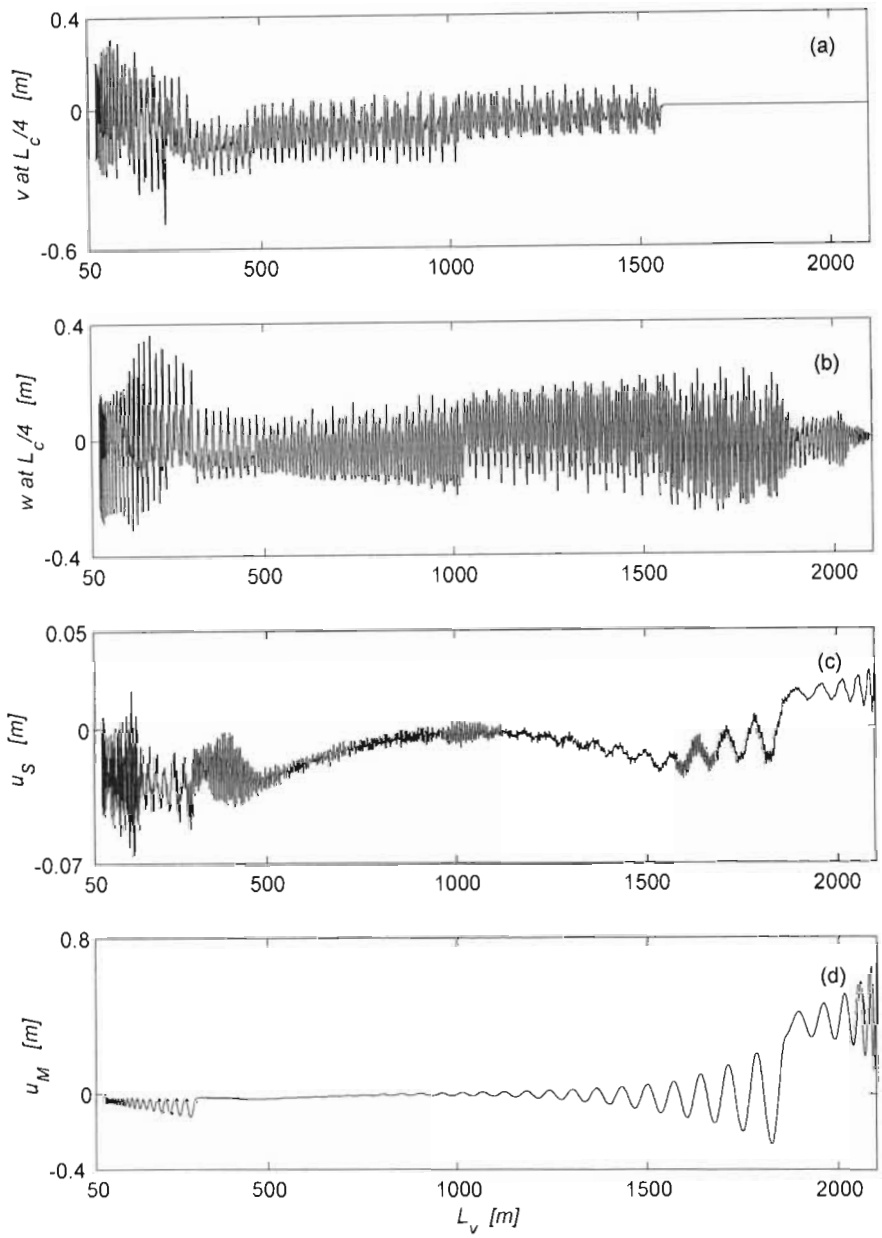

Figure 56. Displacement response of Kloof Mine winding cables for $V_c = 19.5\ m/s$: lateral (a) in-plane and (b) out-of-plane motions at the first quarter of the catenary; longitudinal responses (c) at the sheave and (d) at the conveyance.

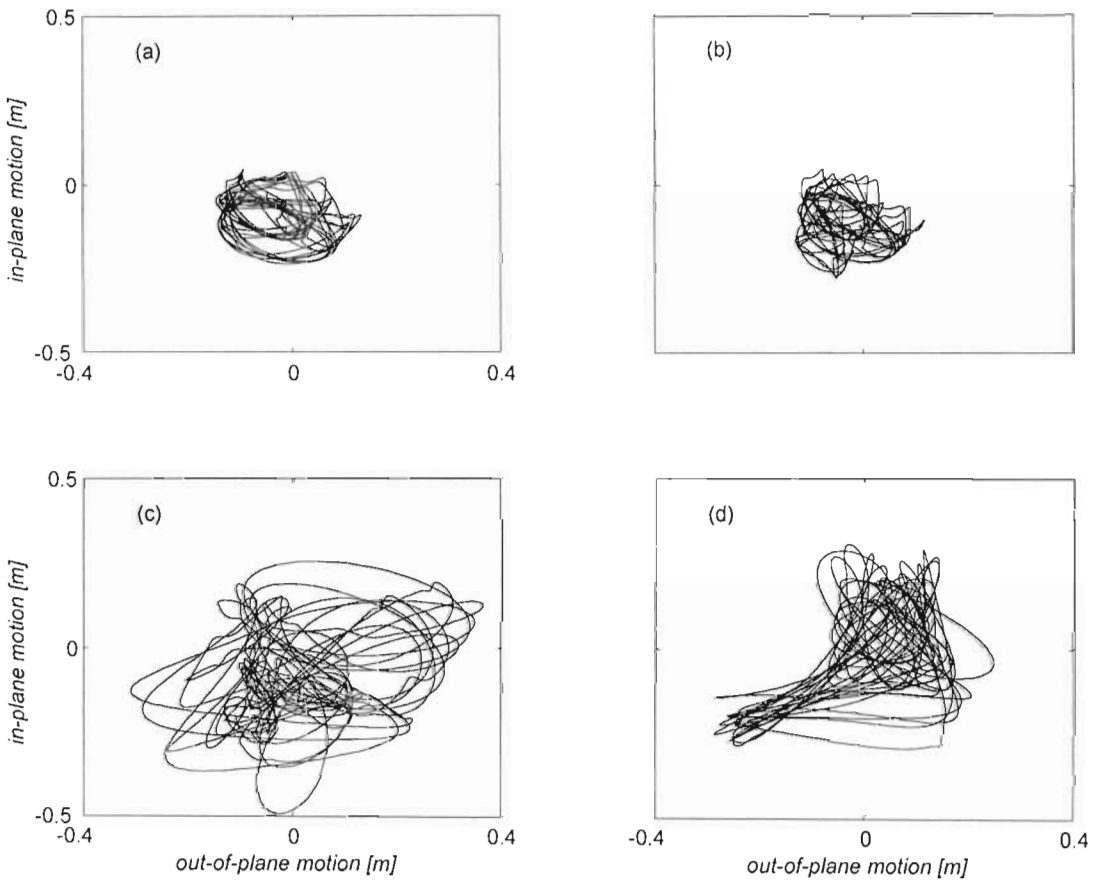

Figure 57. The trajectory of the first quarter point of the catenary during various stages of the ascending cycle in the Kloof system at $V_c = 19.5\ m/s$: $(a)\ L_v = 800 - 600\ m$, (b) $L_v = 600 - 400\ m$, $(c)\ L_v = 400 - 150\ m$, $(d)\ 150 - 70\ m$.

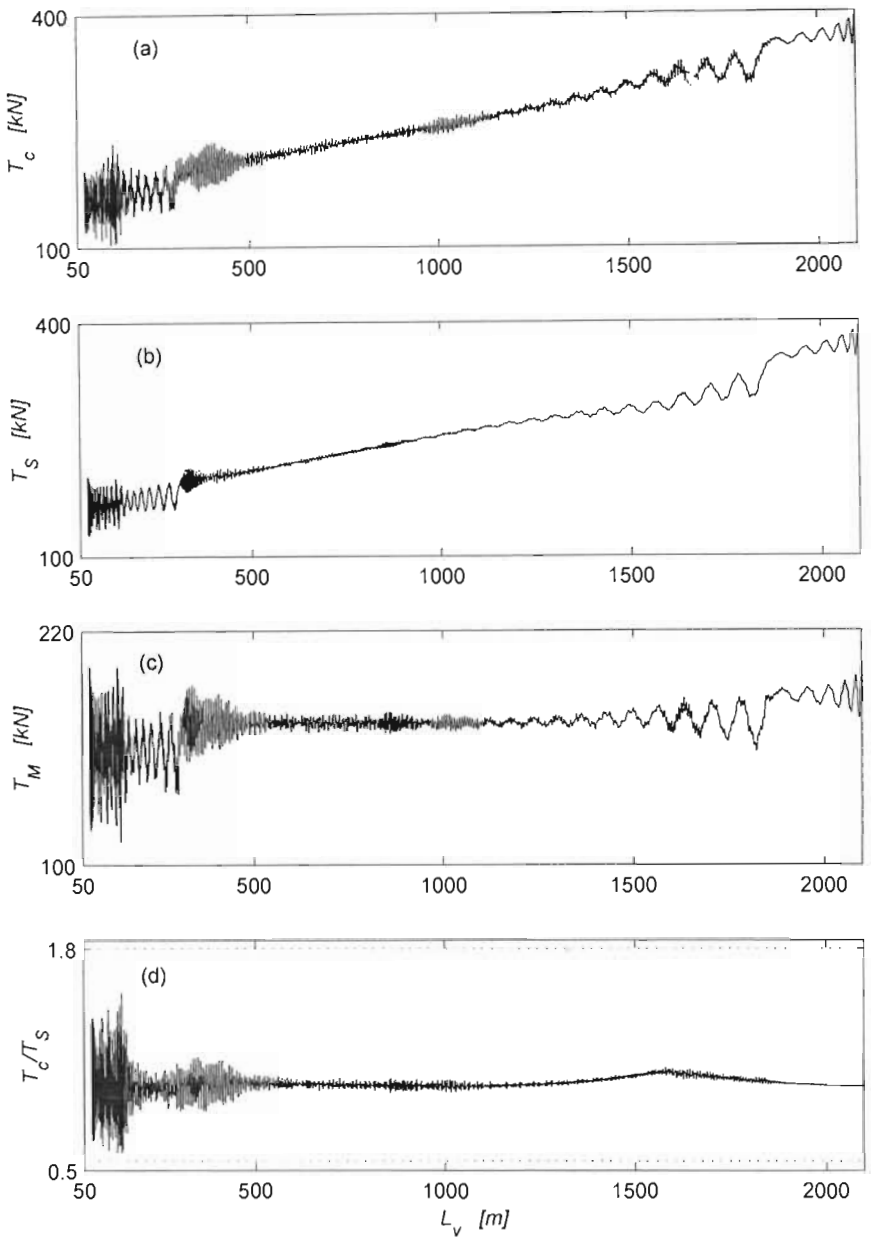

Figure 58. Total tensions in Kloof Mine winding cables at the winding velocity $V_c = 19.5$ m/s: (a) the catenary tension T_c; (b) the vertical rope tension T_S at the sheave; (c) the vertical rope tension T_M at the conveyance; (d) the tension ratio across the sheave T_c/T_S.

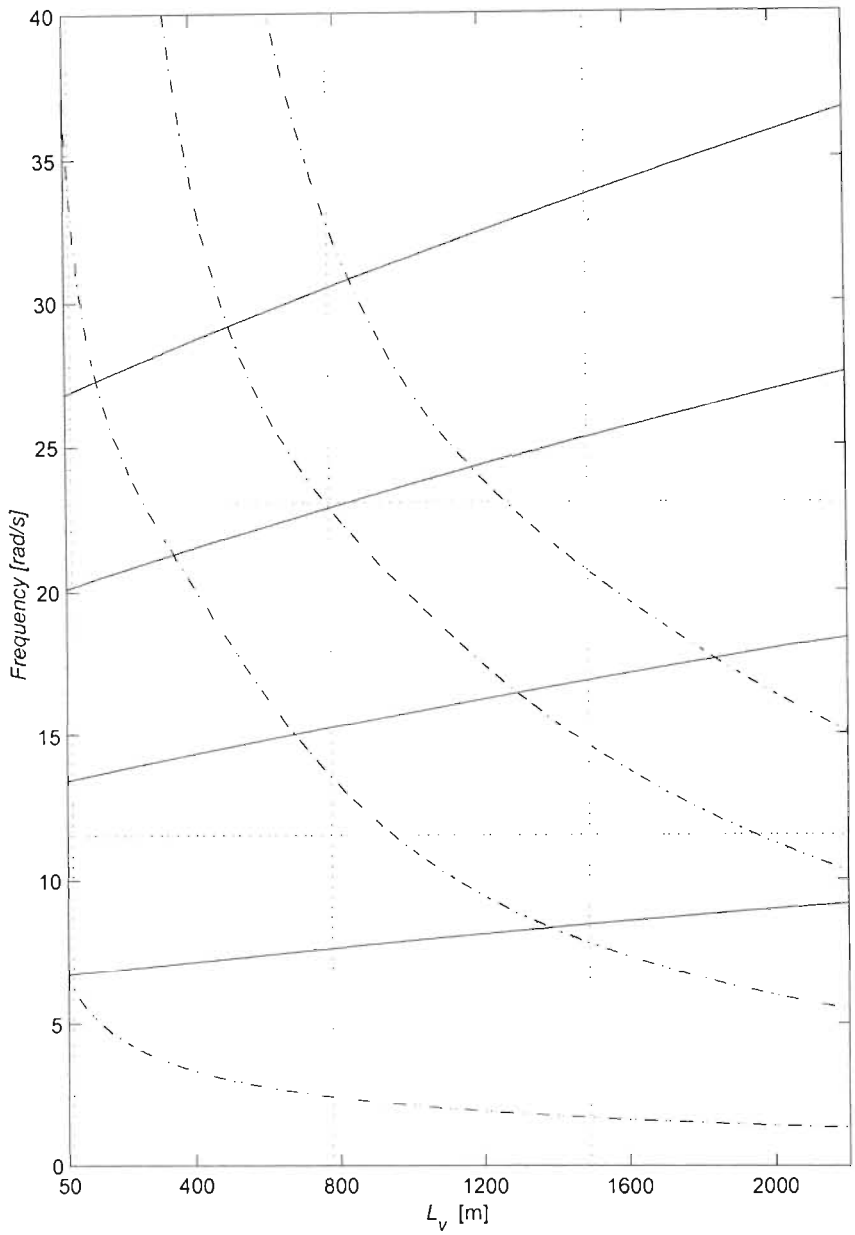

Figure 59. Longitudinal frequency ω_n $(- \cdot -)$ and lateral frequency $\bar{\omega}_n$ (—) curves for Elandsrand Gold Mine winder (ascending cycle), with horizontal lines $(--)$ denoting the first and the second harmonics of the excitation frequency at the winding velocity $V_c = 16$ m/s. Vertical lines $(\cdots)$ indicate the layer change locations.

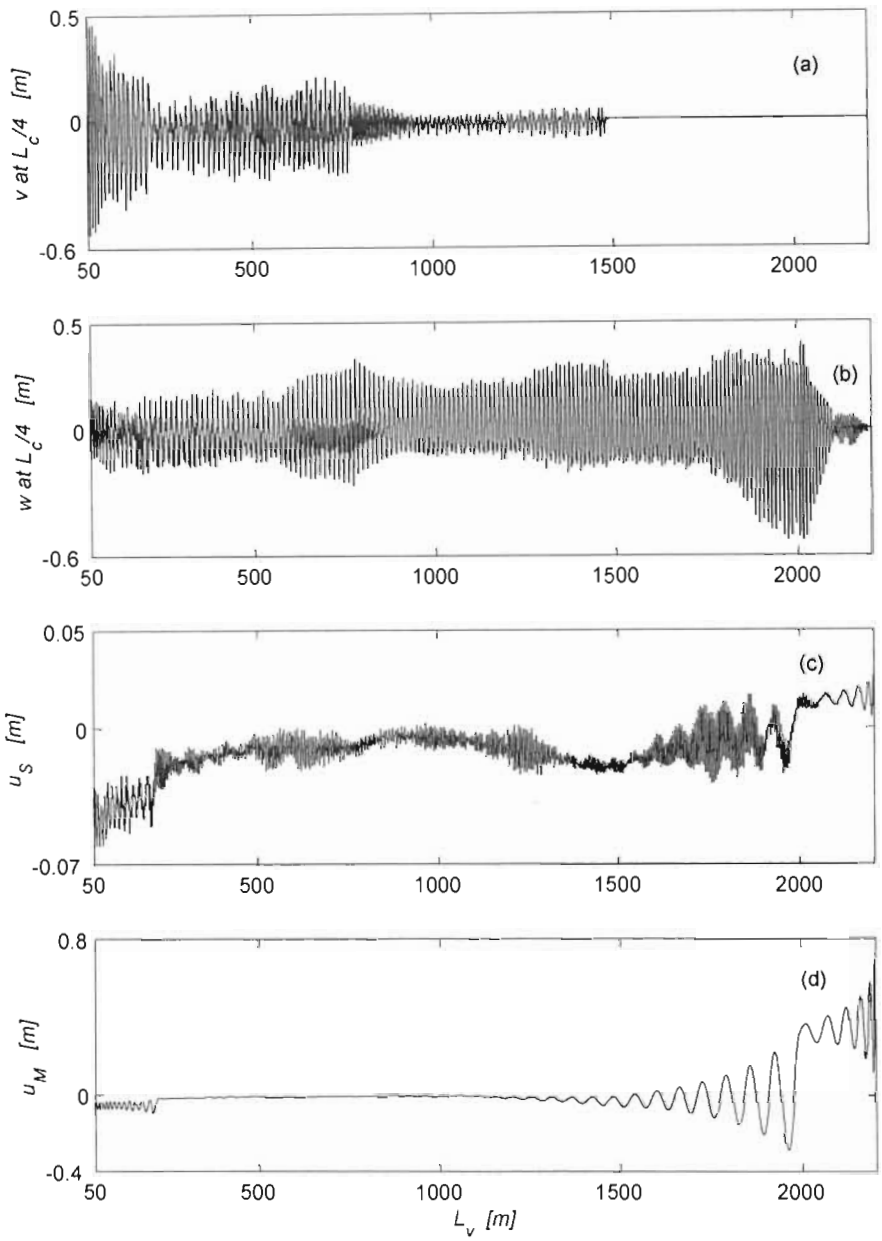

Figure 60. Displacement response of Elandsrand Mine winding cables for $V_c = 16\ m/s$: lateral (a) in-plane and (b) out-of-plane motions at the first quarter of the catenary; longitudinal responses (c) at the sheave and (d) at the conveyance.

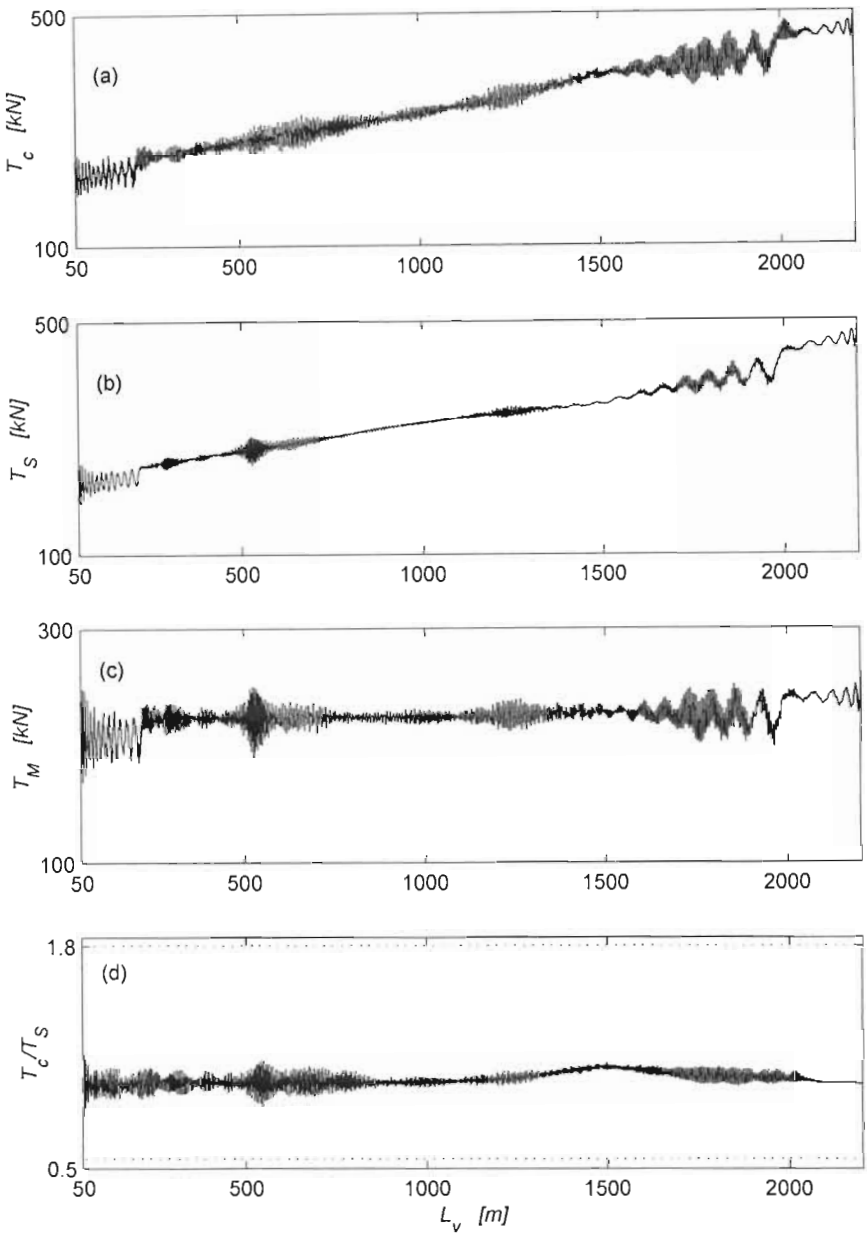

Figure 61. Total tensions in Elandsrand Mine winding cables at the winding velocity $V_c = 16\ m/s$: (a) the catenary tension T_c; (b) the vertical rope tension T_S at the sheave; (c) the vertical rope tension T_M at the conveyance; (d) the tension ratio across the sheave T_c/T_S.

Chapter 6
Conclusion

6.1 Summary of Conclusions of Preceding Chapters and Final Recommendations

An extensive analytical and numerical dynamic analysis of hoisting cable systems is presented in this thesis. The emphasis is put on the non-stationary nature of these systems, with hoisting cables being treated as one-dimensional continua with slowly varying length, which have been introduced in Chapter 2. Thus, hoisting installations are represented as non-stationary oscillatory systems with slowly varying natural frequencies and mode shapes. Furthermore, non-stationary characteristics of excitations in these systems are also accounted for in the numerical studies. This non-stationary aspect is important in mine hoist systems where a mechanism applied on the winder drum surface to ensure a uniform coiling pattern forms a source of cross-over excitation, which consists of lateral and longitudinal pulses. The frequency of these pulses varies during the acceleration/deceleration phases, as it is directly related to the drum frequency. Also, the phase of this excitation is altered by 180^0 following the layer change, when the rope changes its traverse direction.

Following the concepts introduced by Goroshko & Savin [1971] and using the classical moving frame approach, the non-stationary parameters of hoisting cable systems are accounted for via a slowly varying length parameter l representing a time-varying length of the cable section coiled onto the winder drum. Applying the Lagrangian representation of motion an original mathematical model of a typical industrial hoisting cable installation has been derived and formulated in Chapter 3. This non-linear dynamic model of the

catenary-vertical rope system describes the lateral motions of the catenary cable, coupled with the longitudinal motion of the vertical rope, when acted upon by an inertial load due to the transport motion, and subjected to boundary cross-over excitation.

This formulation has a number of advantages, and has facilitated an extension of the research work conducted by Mankowski [1982] and Constancon [1993] to simulate the dynamic behaviour of cables in deep mine hoist winding plants. The use of the Lagrangian representation rather than the Eulerian representation of motion has simplified substantially the partial differential equations of motion of the system. The introduction of the non-stationary parameter l has enabled the non-stationary effects in the system, due to the time-varying natural frequencies and mode shapes, to be efficiently accounted for. Furthermore, the dependency of the longitudinal damping parameters on the mean tension of the vertical rope has been accommodated in the analysis.

A simplified longitudinal model of the hoisting system has been analyzed in Chapter 4. This model enables one to investigate the longitudinal uncoupled non-stationary response of the system, and to study passages through primary resonances which occur during a winding cycle. The overall longitudinal dynamic response of the hoisting cable system is determined through direct numerical integration of the longitudinal discrete model obtained from the Rayeligh-Ritz approximation. Since the hoisting cable system represents a stiff problem, the numerical differentiation formulas (NDF's) are applied to carry out the simulation. Parameters of the double drum rock winder at Elandsrand Gold Mine are used in this simulation. The results illustrate a transient response due to the acceleration/deceleration inertial load and passages through primary longitudinal resonances, when the frequency of the excitation due to a coiling mechanism at the winding drum coincides with the natural frequencies during the cycle. These passages are further investigated using a combined perturbation and numerical technique applied to a single-mode model of the system. The influence of the winding velocity on the response amplitude, and on the cable tensions has been established. It has been shown that the more rapid the passage through resonance, the smaller the maxima of the conveyance response, and the higher the maxima of the response at the sheave.

Also, it has been demonstrated that dynamic cable tension grows rapidly during the passage, and reaches higher levels for higher hoisting velocities.

In Chapter 5 attention has been turned to non-linear dynamic interactions arising in the catenary-vertical rope system. The numerical simulation of differential equations of motion describing the dynamics of the system has corroborated the problematic dynamic behaviour of hoisting cables at the Kloof Mine winding plant during the nominal ascending cycle with a winding velocity of 15 m/s. During this cycle, the catenary even lateral modes become resonant at a depth of approximately 750 m, and the results of the simulation indicate that energy exchanges among the in- and out-of-plane modes take place, resulting in amplitude modulating whirling motions. Also, conditions for autoparametric interactions between the longitudinal and lateral modes arise. However, these interactions are not clearly evident in the simulation results. Perhaps the amplitudes of the longitudinal response are not large enough to excite autoparametrically the lateral modes at this stage of the winding cycle. A more advanced study would be required to investigate the longitudinal-lateral internal resonance in detail, as previous research [Kumaniecka & Niziol.1994] revealed that in emergencies, the longitudinal amplitude was sufficiently high to promote transverse-longitudinal resonance in a vertical rope. Also, a possibility exists that energy exchanges among widely spaced modes take place due to a mechanism which is neither a classical internal resonance nor an external or parametric resonance involving the low-frequency mode [Nayfeh & Mook, 1995]. Rather, slow modulation of the amplitude and phase of the high-frequency modes allows for the energy to be transferred to the low-frequency modes. Favourable conditions for such an exchange arise at the end of ascending cycles, when the longitudinal modes are excited by the second harmonic of the excitation, with their frequencies becoming very high and with the lateral frequencies being low.

It has become evident from simulations carried out, for other than the nominal regimes, that a suitable change of winding velocity can eliminate the main catenary resonances. It has

been demonstrated that in the Kloof system this effect can be achieved when the winding velocity is raised to approximately 19.5 m/s. Alternatively, the possibility of elimination of the catenary resonances should be considered at the design stage. The simulation results revealed also that in the case of a single catenary resonance the dynamic response of the system remains small. This has been demonstrated, both in the Kloof, and in the Elandsrand non-linear simulations.

The non-linear simulation has revealed that the non-linear interactions in the catenary-vertical rope hoisting system lead to adverse dynamic behaviour of the entire installation. The Elandsrand simulation demonstrates the significant difference between the uncoupled longitudinal behaviour studied in Chapter 4, and the non-linear response. Therefore, it should be appreciated that the longitudinal dynamics studies are limited only to systems where the catenary lateral dynamics plays a lesser role.

The non-linear simulation of ascending winding cycles has proved to be a challenging task. This has been due to reach modal interactions taking place during the winding and due to the stiff character of the problem. Thus, a suitable modelling approach[11], and an appropriate numerical integration strategy has had to be used to ensure that the necessary numerical tolerances were maintained during the simulation. Eventually, this has proved to be a success, largely due the correct choice of an efficient numerical algorithm with a suitable set of the ODE solver parameters.

---

[11] It is important how the vertical system is modelled. Constancom [1993] represented the vertical rope as a linearly unconstrained subsystem, and applied unrestrained normal modes in his model. This approach leads to an overestimation of the response at lower depths during ascending cycles [Kaczmarczyk, 1997c]. Consequently, the simulation results become unrealistic from a depth of approximately 300 m during the Kloof nominal cycle.

6.2 Suggestions for Future Work

It is appreciated that results of a numerical and/or analytical study alone may not be, and often are not a sufficient source from which to draw correct conclusions. In the present study available publications, observations and reports from industry has provided suitable reference material to corroborate the results. More actual experimental evidence would be required. However, experimental activities on operating shafts are restricted and difficult due to production restraints. Thus, a need exists for a suitable laboratory rig to be designed , which sufficiently represents the non-stationary catenary-vertical rope system. This laboratory model should accommodate slowly varying characteristics of the actual system, namely time-varying catenary tension and variable mass and stiffness of the vertical subsystem. Some aspects of a feasible experimental laboratory simulation have already been discussed [Constancon, E-mail communication, 1995], and some measurement arrangements and techniques tested under the author's supervision [Carter-Brown, 1996]. Hence, this work would form an interesting and important avenue for future research.

Furthermore, as has already been stated, the non-linear simulation results should be supported by more advanced analytical studies. The non-stationary multiple scales analysis applied to the longitudinal model could be extended to a simplified multi-degree-of-freedom model with slowly varying parameters. Also, the techniques described by Kevorkian [1987] would be applicable to the non-stationary perturbation analysis of the system. It would be advantageous if this future research incorporates using symbolic manipulation programming systems such as MAPLE or MATHEMATICA.

Scope exists for further work to include lateral modes of the vertical rope into the non-stationary analysis. The current simulation results show that the in-plane catenary modes remain dormant during the first layer coiling. In the present model the in-plane modes become directly excited only from the second layer onwards, and the existing non-linear coupling has

not resulted in lateral in-plane motions during the initial stage of winding. However, small in-plane motions have been observed in practice during the first layer winding. Hence, an additional coupling must exist in the system, and this coupling may involve the lateral motions of the vertical rope. Also, the headgear structure is not perfectly rigid, and its flexible motions could be accounted for in order to provide further clarification.

Further limitation of the current hoist system model is the assumption that the winder drum represents an ideal source of energy. Consequently, the inertial effects of the drum are not considered. Investigation into the response of the system by including these effects would represent a further extension to the non-stationary analysis. Some aspects of this problem have already been considered by the author, and it was shown that the problem involved the electrical characteristics of the winder motor being taken into account [Kaczmarczyk, 1994].

References

Ablowitz, M J, Funk, B A & Newell , A C, (1973), "Semi-Resonant Interactions and Frequency Dividers", *Studies in Applied Mathematics*, Vol.L11, No.1, p.51-74.

Agrawal, B N, (1975), "Nonstationary and Nonlinear Vibration Analysis and its Application", *The Shock and Vibration Digest,* Vol.7, p.77-87

Agrawal, B N, & Evan-Iwanowski, R M, (1973), "Resonances in Nonstationary, Nonlinear, Multidegree-of-Freedom Systems", *AIAA Journal,* Vol.11, No.7 p.907-912.

Bogolubov, N N, & Mitropolskii, Y A, (1961), "Asymptotic Methods in the Theory of Non-linear Oscillations", Delhi, Hindustan Publishing Corporation (India).

Bosley, D L, (1996), "An Improved Matching Procedure for Transient Resonance Layers in Weakly Nonlinear Oscilatory systems", *SIAM Journal of Applied Mathematics*, Vol.56, No.2, p.420-445.

Bosley, D L, & Kevorkian, J, (1991), "Sustained Resonance in Very Slowly Varying Oscillatory Hamiltonian Systems", *SIAM Journal of Applied Mathematics*, Vol.51, No.2, p.439-471.

Bosley, D. L & Kevorkian, J, (1992) "Adiabatic Invariance and Transient Resonance in Very Slowly Varying Oscillatory Hamiltonian Systems", *SIAM Journal of Applied Mathematics,* Vol.52, p.494-527.

Carter-Brown, P J, (1996), "Optical Displacement Probe for Non-Contact Vibration Measurement", *Final Year Design and Research Project,* Durban, Department of Mechanical Engineering, University of Natal.

Cartmell, M & Lawson, J, (1994), "Performance Enhancement of an Autoparametric Vibration Absorber by Means of Computer Control", *Journal of Sound and Vibration,* Vol.177, No.2, p.173-195.

Cartmell, M P & Roberts, J W, (1988), "Simultaneous Combination Resonances in Autoparametrically Resonant System", *Journal of Sound and Vibration,* Vol.123, No.1, p.81-101.

Costello, G A, (1990), "Theory of Wire Rope", New York, Springer-Verlag.

Constancon, C P, (1993), "The Dynamics of Mine Hoist Catenaries", *PhD Thesis,* Johannesburg, Faculty of Engineering, University of the Witwatersrand.

Constancon, C P, (1995), "Communication on Non-Stationary Fulcrum System", *E-mail communication*, 16 February 1995.

CSIR, (1995), "Mine Hoisting", Site Visit and Presentation at the Mine Hoisting, Metallurgical & Corrosion Services, CSIR, Johannesburg, 25 January 1995.

Cveticanin, L, (1991), "The Oscillations of a Textile Machine Rotor on Which the Textile is Wound up", *International Journal of Mechanism and Machine Theory*, Vol.26, No.3, p.253-260.

Czaja, J, (1977), "Determination of the Forces in Head and Tail Ropes in a Hoist Installation During the Overwind Arresting of Conveyances", *Zeszty Naukowe Politechniki Slaskiej, Mining,* Z.80. p.77–93 (in Polish).

D'Angelo, A, (1970), "Linear Time-Varying Systems: Analysis and Synthesis", Boston, Allyn and Bacon, Inc.

de Jalon, J G & Bayo, E, (1994), "Kinematic and Dynamic Simulation of Multibody Systems", New York Springer-Verlag.

Dimitriou, C & Whillier, A, (1973), "Vibrations in Winding Ropes: an Appraisal.", Conference Proceedings, *SAIMechE Hoisting Conference,* SAIMechE, Johannesburg, *16-20* October *1973*

Evan-Iwanowski, R M, (1976) "Resonance Oscillations in Mechanical Systems", Amsterdam, Elsevier Scientific Publishing Company.

Géradin, M & Rixen, D, (1994), "Mechanical Vibrations. Theory and Application to Structural Dynamics", New York, John Wiley & Sons Ltd.

Gerald, C F & Wheatley, P O, (1989), "Applied Numerical Analysis", Reading Massachusetts, Addison-Wesley Publishing Company.

Glushko, M F, (1966), "Steel Hoisting Cables", Kiev, Technika (in Russian).

Goroshko, O A & Savin, G N, (1962), "The Dynamics of Threads with Variable Length. Applications in Mine Hoist Systems", Kiev, The Ukrainian Academy of Sciences (in Russian).

Goroshko, O A & Savin, G N, (1971) "Introduction to Mechanics of One-Dimensional Bodies with Variable Length", Kiev, Naukova Dumka (in Russian).

Goroshko, O A & Titova, L D, (1971), "Approximate Solutions to Problems on Transverse Vibrations of a Cable at Medium Velocities", *Steel Ropes*, Vol.8, p.212-216 (in Russian).

Greenway, M E, (1989), "Dynamic Loads in Winding Ropes - an Analytical Approach", *Internal Report,* Johannesburg, Anglo American Corporation.

Greenway, M. E., (1990a), A Simple Static and Dynamic Analysis of Coupled Extensional-Torsional Behaviour of Winding Rope, *Report No. 90-T 22*, Johannesburg, Anglo American Corporation.

Greenway, M. E., (1990b), "Dynamic Rope Loads due to Cage Loading", *Report No.90-T 09*, Johannesburg, Anglo American Corporation.

Greenway, M E, (1990c), "An Engineering Evaluation of the Limits to Hoisting from Great Depth", *Conference: Technical Challenges in Deep Level Mining,* Johannesburg, SAIMM.

Haddow, A G, Barr, A D & Mook, D T, (1984), "Theoretical and Experimental Study of Modal Interactions in a Two-Degree-of-Freedom Structure", *Journal of Sound and Vibration*, Vol.97, No.3, p.451-473.

Hairer, E, & Wanner, G, (1991), "Solving Ordinary Differential Equations II. Stiff and Differential -Algebraic Problems", Berlin Heidelberg, Springer-Verlag.

Hamilton, R S & Greenway, M E, (1991), "A Finite Element Study of the Coupled Extensional-Torsional Behaviour of Winding Ropes", *Report, No. 91-T-16*, Johannesburg, Anglo American Corporation.

Harvey, T & Laubscher, P S, (1965), "'Escort' - a winder braking system", *The Transactions of the Institute of Electrical Engineers,* Vol.56, Part 2, p.37-50.

Hitchen, H, (1963), "Ropes for Drum and Koepe Friction Hoists", *The Canadian Mining and Metallurgical Bulletin,* Vol.56, No.610, p.122-130.

Hsu, C S, (1963), "On the Parametric Excitation of a Dynamic System Having Multiple Degrees of Freedom", *Transactions of ASME: Journal of Applied Mechanics*, Vol.30, p.367-372.

Inman, D J, (1996), "Engineering Vibration", New Jersey, Prentice-Hall International, Inc.

Irvine, H M, (1981), "Cable Structures", Cambridge, Massachusetts, The MIT Press.

Johnson, J M & Bajaj, A K, (1989), "Amplitude Modulated and Chaotic Dynamics in Resonant Motion of Strings", *Journal of Sound and Vibration*, Vol.128, No.1, p.87-107.

Kaczmarczyk, S, (1994), "Nonstationary Oscillations of Mine Hoisting Cables", *Proceedings of Thirteenth Machinery Dynamics Seminar,* Canadian Machinery Vibration Association, 12 - 13 September, 1994, Toronto, Ontario, p.252-261.

Kaczmarczyk, S, (1997a), "Transient Resonance in a Hoisting Cable System with a Periodic Excitation", *R&D Journal,* Vol.13, No.1, p.31-40.

Kaczmarczyk, S, (1997b),"The Passage Through Resonance in a Catenary-Vertical Cable Hoisting System with Slowly Varying Length", *Journal of Sound and Vibration,* Vol.208, No.2, p.243-269.

Kaczmarczyk, S, (1997c), "Nonstationary Vibrations in a Catenary-Vertical Hoisting Cable System", *Proceedings of Fifth International Congress of Sound and Vibration,* December 16 - 18, 1997, University of Adelaide, South Australia, p.1821-1828.

Kevorkian, J, (1971), "Passage Through Resonance For a One-Dimensional Oscillator with Slowly Varying Frequency", *SIAM Journal of Applied Mathematics, Vol.*20, No.3, p.364-373.

Kevorkian, J, (1974), "On a Model for Reentry Roll Resonance", *SIAM Journal of Applied Mathematics,* Vol.26, No.3, p.638-669.

Kevorkian, J, (1980), "Resonance in a Weakly Nonlinear System with Slowly Varying Parameters", *Studies in Applied Mathematics,* 62, p.23-67.

Kevorkian, J, (1982), "Adiabatic Invariance and Passage Through Resonance for Nearly Periodic Hamiltonian Systems", *Studies in Applied Mathematics,* 66, p.95-119.

Kevorkian, J, (1987), "Perturbation Techniques for Oscillatory Systems with Slowly Varying Coefficients", *SIAM Review,* Vol.29, p.391-461.

Kevorkian, J & Li, H K, (1984), "Resonant Modal Interactions and Adiabatic Invariance for a Nonlinear Wave Equation in a Variable Domain, *Studies in Applied Mathematics,* 71, p1-64.

Klich, A, (1981), "The Methods of Calculations of Normal Operating and Emergency Loads in Mine Hoists with Deep Shafts", *Selected Problems in Mining and Mechanical Processing,* Mining 21, p.3-15.

Kotera, T, (1978), "Vibrations of String with Time-Varying Length.", *Bulletin of the JSME,* Vol.21, p.1469-1474.

Kruszewski, J, Gawronski, W, Ostachowicz, W, Tarnowski, J & Wittbrodt, E, (1984), "Finite Element Method in Dynamics of Structures", Warsaw, Arkady (in Polish).

Kumaniecka, A & Niziol, J, (1994), "Dynamic Stability of a Rope with Slow Variability of the Parameters", *Journal of Sound and Vibration,* Vol.178, No.2, p.211-226.

Lanczos, C, (1962), "The Variational Principles of Mechanics", Toronto, University of Toronto Press.

Lewin, L & Kevorkian, J, (1978), "On the Problem of Sustained Resonance", *SIAM Journal of Applied Mathematics,* Vol.35, No.4, p.738-754.

Luongo, A, Rega, G & Vestroni, F, (1984), "Planar Non-Linear Free Vibrations of an Elastic Cable", *International Journal of Non-Linear Mechanics,* Vol 19, No.1, p.39-52.

Mankowski, R R, (1982), "A Study of Nonlinear Vibrations Occurring in Mine Hoisting Cables", *PhD Thesis,* Johannesburg, Faculty of Engineering, University of the Witwatersrand.

Mankowski, R R, (1988), "Internal Damping Characteristics of a Mine Hoist Cable Undergoing Non-Planar Transverse Vibration", *Journal of the South African Institute of Mining and Metallurgy*, Vol.88, No.12, p.401-410.

Mankowski, R R, (1990), "Internal Power Losses Occurring at the Wavefront of Travelling Transverse Disturbances on Mine Hoisting Cables", *Journal of the South African Institute of Mining and Metallurgy*, Vol.90, No.12, p. 339-344.

Mankowski, R R & Cox, F J, (1986), "Response of Mine Hoisting Cables to Longitudinal Shock Loads", *Journal of the South African Institute of Mining and Metallurgy*, Vol.86, p.51-60.

Marczyk, S & Niziol, J, (1979), "Transverse-Longitudinal Vibrations of Ropes with Time-Varying Length", *Engineering Transactions,* Vol.27, N0.3, p.403-415.

Meirovitch, L, (1990), "Dynamics and Control of Structures", New York, John Wiley & Sons.

Mitropolskii, Y A, (1965), "Problems of the Asymptotic Theory of Nonstationary Vibrations", Jerusalem, Israel Program for Scientific Translations Ltd..

Molteno, T C A & Tufillaro, N B, (1990), "Torus Doubling and Chaotic String Vibrations: Experimental Results", *Journal of Sound and Vibration,* Vol.137, No.2, p.327-330.

Neal, H L & Nayfeh, A H, (1990), "Response of a Single-Degree-of-Freedom System to a Non-Stationary Principal Parametric Excitation, *International Journal of Non-Linear Mechanics*, Vol.25, No.2/3, p.275-284.

Nayfeh, A H, (1973) "Perturbation Methods", New York, John Wiley & Sons.

Nayfeh, A H & Asfar, K R, (1988), "Non-Stationary Parametric Oscillations", *Journal of Sound and Vibration,* Vol.124, No.3, p.529-537.

Nayfeh, A H & Balachandran, B, (1989), "Modal Interactions in Dynamical and Structural Systems", *Applied Mechanics Reviews*, Vol.42, No.11, p.175-201.

Nayfeh, A H, Mook, D T & Lobitz, D W, (1974), "Numerical-Perturbation Method for the Nonlinear Analysis of Structural Vibrations", *AIAA Journal*, Vol.12, No.9, p.1222-1228.

Nayfeh, A H, Mook, D T & Marshall L R,, (1973), "Nonlinear Coupling of Pitch and Roll Modes in Ship Motions", *Journal of Hydronautics,* Vol.7, No.4, p.145-152.

Nayfeh, A H & Mook, D T, (1979), "Nonlinear Oscillations", New York: John Wiley & Sons.

Nayfeh, A H & Mook, D T, (1995), "Energy Transfer from High-Frequency to Low-Frequency Modes in Structures", *Transactions of the ASME Special 50th Anniversary Design Issue*, Vol.117, p.186-195.

Nayfeh, S A & Nayfeh, A H, (1993), "Nonlinear Interactions Between Two Widely Spaced Modes - External Excitation", *International Journal of Bifurcation and Chaos,* Vol.3, No.2, p.417-427.

Nayfeh, S A & Nayfeh, A H, (1994), "Energy Transfer from High- to Low-Frequency Modes in a Flexible Structure via Modulation", *Journal of Vibration and Acoustics*, Vol.116, p.203-207.

Nikravesh, P E, (1988), "Computer-Aided Analysis of Mechanical Systems", Englewood Cliffs, Prentice-Hall, Inc.

O'Reilly, O & Holmes, P J, (1992), "Non-Linear, Non-Planar and Non-Periodic Vibrations of a String", *Journal of Sound and Vibration,* Vol.153, No.3, p.413-435.

Ostachowicz, W, (1979), "Rigid Finite Element Models of Mechanical Systems with Periodic Stiffness", *Engineering Transactions,* 3, p.432-440.

Ögüt, T, (1978), "Berechnung der transversalen Schwingungen herabhängender schwerer Ketten veränderlicher Länge mit angehängter sowie geführter Einzellast", *Fortschritt-Berichte der VDI Zeitschriften,* Reiche *11,* Nr. 30, p.13-134.

Perkins, N C, (1992), "Modal Interactions in the Non-Linear Response of Elastic Cables under Parametric/External Excitation", *International Journal of Non-Linear Mechanics,* Vol. 27, No. 2, pp.233-250.

Perkins, N C & Mote Jr, C D, (1987), "Three-Dimensional Vibration of Travelling Elastic Cable", *Journal of Sound and Vibration,* Vol.114, No.2, p.325-340.

Perry, J, (1906), "Winding Ropes in Mines", *Phil. Mag.,* Ser.6, Vol.11, p.107-117.

Perry, J F & Smith, D M, (1932), "Mechanical Breaking and its Influence on Winding Equipment", *Proceedings of the Institution of Mechanical Engineers*, Vol. 123, p.537-620.

Pollock, P J & Alexander, G W, (1950), "Dynamic Stresses in Wire Ropes for Use on Vertical Shafts", *Wire Ropes in Mines,* Paper No.12, p.445-462.

Ram, Y M & Caldwell, J, (1996), "Free Vibration of a String with Moving Boundary Conditions by the Method of Distorted Images", *Journal of Sound and Vibration,* Vol.194, No.1, p.35-47.

Raman, A, Bajaj, A K & Davies, P, (1996), "On the Slow Transition Across Instabilities in Nonlinear Dissipative Systems", *Journal of Sound and Vibration,* Vol.192, No.4, p.835-865.

Roberts, J W & Cartmell, M P, (1984), "Forced Vibration of a Beam System with Autoparametric Coupling Effects", *Strain*, Vol.20, p.123-131.

Rubenfeld, L A, (1977), "The Passage of Weakly Coupled Nonlinear Oscillators through Internal Resonance", *Studies in Applied Mathematics"*, Vol.57, p.77-92.

Savin, G N, (1963), "Dynamics of an Anelastic String of Variable Length", *Stress Waves in Anelastic Solids*, Kolsky/Prager (Editors), IUTAM Symposium, Providence, p.78-86.

Savin, G N & Goroshko, O A, (1965), "On Parametric Resonance in Mine Hoist Installations", *Steel Ropes*, Vol.2, p.15-20 (in Russian).

Savin, G N & Kayuk, I F, (1965), "The Differential Equations of Dynamics of a String with Varying Length in the Case of Physical and Geometric Nonlinearity", *Steel Ropes*, Vol.2, p.31-41 (in Russian).

Shampine, L F, (1994), "Numerical Solution of Ordinary Differential Equations", New York, Chapman & Hall.

Shampine, L F & Reichelt, M W, (1996), "The Matlab ODE suite", in the MATLAB Version 5 Software Package, the MathWorks Inc.

Shahruz, S M & Tan, C A, (1989), "Response of Linear Slowly Varying Systems Under External Excitations", *Journal of Sound and Vibration,* Vol.131, No.2, p.239-247.

Skalmierski, B, (1979), "Mechanics and Strength of Materials", Warsaw, PWN - Amsterdam, Elsevier.

Stühler, W, (1978), "Berechnung der rheonomen transversalen Seilschwingungen von Schachtförderanlagen", *VDI-Berichte,* Nr. 320, p.133-141.

Szemplinska-Stupnicka, W, (1990), "The Behavior of Nonlinear Vibrating Systems", Dordrecht, Kluver Academic Publishers.

Szklarski, R, (1977), "Theoretical Problems on Winding Machines", Warsaw, PWN.

Tagata, G, (1983), "A Parametrically Driven Harmonic Analysis of a Non-Linear Stretched String with Time-Varying Length", *Journal of Sound and Vibration,* Vol.87, No.3, p.493-511.

Terumichi, Y, Ohtsuka, M, Yoshizawa, M, Fukawa, Y & Tsujioka, Y, (1997), "Nonstationary Vibrations of a String with Time-Varying Length and a Mass-Spring System Attached at the Lower End", *Nonlinear Dynamics,* Vol. 12, p.39-55.

Thomas, G R & Brillhart, R D, (1987), "Final Report on an Investigation into the Dynamic Rope Loads in Drum Winder Systems", San Diego, SDRC INC, California.

Timoshenko, S, Young, D H & Weaver, W, (1974), "Vibration Problems in Engineering", New York: John Wiley & Sons, fourth edition.

Tran, M H & Evan-Iwanowski, R M, (1990), "Non-Stationary Responses of Self-Excited Driven systems", *International Journal of Non-Linear Mechanics*, Vol.25, No.2/3, p.285-297.

Tse, F S, Morse, I E & Hinkle, R T, (1978), "Mechanical Vibrations. Theory and Applications",Boston, Allyn and Bacon, Inc.

Vanderveldt, H H, Chung, B S & Reader, W T, (1973), "Some Dynamic Properties of Axially Loaded Wire Ropes", *Experimental Mechanics* Vol.13, p.24-30.

Vanderveldt, H H & Gilheany, J J, (1970), "Propagation of a Longitudinal Pulse in Wire Ropes under Axial Loads", *Experimental Mechanics* Vol.10, p.401-407.

Vaughan, J A, (1904), "An Investigation Regarding the Effect of Kinetic Shocks on Winding Ropes in Vertical Shafts", *The South African Association of Engineers, Minutes of Proceedings, General Meeting, March 30th, 1904,* p.217-245.

Vesnitzky, A I, & Potapov, A I, (1975), "On Some Characteristics of Wave Processes in One-Dimensional Mechanical Systems with Variable Length", *Prikladnaya Mekhanika,* Vol.XI, No.4, p.98-103.

Watzky, A, (1992), "Non-Linear Three-Dimensional Large-Amplitude Damped Free Vibration of a Stiff Elastic Stretched String", *Journal of Sound and Vibration,* Vol.153, No.1, p.125-142.

Wojnarowski, J & Tejszerska, D, (1977), "Modelling of Mine Hoist Machines", *Zeszty Naukowe Politechniki Slaskiej, Mining,* Z.81. p.165-179 (in Polish).

Wojnarowski, J & Meder A, (1977), "On Numerical Modelling of Vibrations in Multi-Rope Mine Hoisting Systems", *Zeszty Naukowe Politechniki Slaskiej, Mining,* Z.81. p.139–154 (in Polish).

You, A, (1952), "Vibration Damping of Stranded Cable", *SESA Proceedings,* Vol.9, No.2, p.141-157.

Van Zyl, M, (1998), "Elandsrand Gold Mine Winder Data", Personal Communication, Mike Van Zyl Inc. 17 April 1998.

Zajaczkowski, J & Lipinski, J, (1979), "Instability of the Motion of a Beam of Periodically Varying Length", *Journal of Sound and Vibration,* Vol.63, p.9-18.

Zajaczkowski, J & Yamada, G, (1980), "Further Results of Instability of Motion of a Beam of Periodically Varying Length", *Journal of Sound and Vibration,* Vol.68, p.173-180.

Appendix A
The Longitudinal Eigenvalue Problem

The differential equation for the stationary free longitudinal motion of the unconstrained system shown in Figure 8 can be written as

$$u_{v,tt} - c^2 u_{v,yy} = 0, \tag{A.1}$$

which must be satisfied over the domain $0 < y < L_v$, and where $y = s - L_1$. In addition, u_v must satisfy the boundary conditions

$$M_S u_{v,tt}(0,t) - EAu_{v,y}(0,t) = -k_c u_v(0,t), \tag{A.2a}$$

$$Mu_{v,tt}(L_v,t) + EAu_{v,y}(L_v,t) = 0. \tag{A.2b}$$

Using the separation of variables method, the displacement u is expressed as

$$u_v(y,t) = Y(y)f(t), \tag{A.3}$$

where f is a harmonic function of time with the frequency ω, so that $u_{v,tt} = -\omega^2 Y(y)f(t)$. The eigenvalue problem (A.1)-(A.2b) is then reduced to

$$Y'' + \gamma^2 Y = 0, \tag{A.4}$$

where the prime designates differentiation with respect to y. Thus, the boundary conditions assume the following form

$$\left(k_c - M_S\omega^2\right) Y(0) - EAY'(0) = 0, \tag{A.5a}$$

$$-M\omega^2 Y(L_v) + EAY'(L_v) = 0. \tag{A.5b}$$

The solution of (A.4) is

$$Y(z) = C\cos\gamma y + D\sin\gamma y, \tag{A.6}$$

so that the conditions (A.5a)-(A.5b) yield

$$\begin{bmatrix} k_c - M_s\omega^2 & -EA\gamma \\ -(M\omega^2\cos\gamma L_v + EA\gamma\sin\gamma L_v) & EA\gamma\cos\gamma L_v - M\omega^2\sin\gamma L_v \end{bmatrix} \begin{bmatrix} C \\ D \end{bmatrix} = 0. \tag{A.7}$$

Therefore, a nontrivial solution is possible only if the determinant of the coefficient matrix in (A.7) vanishes, which results in the following form

$$\left(\frac{1}{L_c} - \frac{M_s}{m}\gamma^2\right)(\cos\gamma L_v - \frac{M}{m}\gamma\sin\gamma L_v) - \gamma\left(\frac{M}{m}\gamma\cos\gamma L_v + \sin\gamma L_v\right) = 0. \quad \text{(A.8)}$$

The eigenfunction coefficients C, D can be obtained from (A.7). Scaling $C = 1$, the mode shapes are given as

$$Y_n = \cos\gamma_n y + \left(\frac{1}{L_c\gamma_n} - \frac{M_S}{m}\gamma_n\right)\sin\gamma_n y. \quad \text{(A.9)}$$

The orthogonality properties of the eigenfunctions (A.9) can be examined by considering modes i and j of the eigenvalue problem as the following equations

$$EAY_i'' = -m\omega_i^2 Y_i, \quad \text{(A.10a)}$$

$$EAY_j'' = -m\omega_j^2 Y_j. \quad \text{(A.10b)}$$

Multiplying the first of these equations by Y_j and the second by Y_i, and integrating over the length L_v gives

$$EA\int_0^{L_v} Y_j Y_i'' dy = -m\omega_i^2\int_0^{L_v} Y_j Y_i dy, \quad \text{(A.11a)}$$

$$EA\int_0^{L_v} Y_i Y_j'' dy = -m\omega_j^2\int_0^{L_v} Y_i Y_j dy. \quad \text{(A.11b)}$$

The first boundary condition (A.5a) for modes i and j may be written as the following expressions:

$$EAY_j(0)\,Y_i'(0) = \left(k_c - M_S\omega_i^2\right)Y_j(0)\,Y_i(0), \quad \text{(A.12a)}$$

$$EAY_i(0)\,Y_j'(0) = \left(k_c - M_S\omega_j^2\right)Y_i(0)\,Y_j(0), \quad \text{(A.12b)}$$

where the first expression has been multiplied by $Y_j(0)$, and the second by $Y_i(0)$. Similarly, the second boundary condition (A.5a) for modes i and j may be written as

$$EAY_j(L_v)\,Y_i'(L_v) = M\omega_i^2 Y_j(L_v)\,Y_i(L_v), \quad \text{(A.13a)}$$

$$EAY_i(L_v)\,Y_j'(L_v) = M\omega_j^2 Y_i(L_v)\,Y_j(L_v). \quad \text{(A.13b)}$$

Adding (A.12a) to equation (A.11a) and subtracting (A.13a) from the resulting expression gives

$$\begin{aligned} &EA\int_0^{L_v} Y_jY_i''dy + EAY_j(0)\,Y_i'(0) - EAY_j(L_v)\,Y_i'(L_v) = \\ &k_cY_j(0)\,Y_i(0) - \omega_i^2[m\int_0^{L_v} Y_jY_idy + \\ &M_SY_j(0)\,Y_i(0) + MY_j(L_v)\,Y_i(L_v)]. \end{aligned} \tag{A.14a}$$

Similarly, adding (A.13a) to equation (A.11b) and subtracting (A.13b) from the result yields

$$\begin{aligned} &EA\int_0^{L_v} Y_iY_j''dy + EAY_i(0)\,Y_j'(0) - EAY_i(L_v)\,Y_j'(L_v) = \\ &k_cY_i(0)\,Y_j(0) - \omega_j^2[m\int_0^{L_v} Y_iY_jdy + \\ &M_SY_j(0)\,Y_i(0) + MY_j(L_v)\,Y_i(L_v). \end{aligned} \tag{A.15a}$$

Evaluating the integrals on the left in (A.14a) and (A.15a) by parts produces the combined relationships

$$\begin{aligned} -EA\textstyle\int_0^{L_v} Y_j'Y_i'dy = \;& k_cY_j(0)\,Y_i(0) - \\ & \omega_i^2[m\int_0^{L_v} Y_jY_idy + M_SY_j(0)\,Y_i(0) \\ & +MY_j(L_v)\,Y_i(L_v)], \end{aligned} \tag{A.16a}$$

$$\begin{aligned} -EA\textstyle\int_0^{L_v} Y_i'Y_j'dy = \;& k_cY_i(0)\,Y_j(0) - \\ & \omega_j^2[m\int_0^{L_v} Y_iY_jdy + M_SY_j(0)\,Y_i(0) \\ & +MY_j(L_v)\,Y_i(L_v)]. \end{aligned} \tag{A.16b}$$

Subtracting equation (A.16b) from equation (A.16a) yields

$$(\omega_j^2 - \omega_i^2)\left[m\int_0^{L_v} Y_iY_jdy + M_SY_j(0)\,Y_i(0) + MY_j(L_v)\,Y_i(L_v)\right] = 0. \tag{A.17}$$

Since $i \neq j$, equation (A.17) gives the orthogonality relationship

$$m\int_0^{L_v} Y_iY_jdy + M_SY_j(0)\,Y_i(0) + MY_j(L_v)\,Y_i(L_v) = 0, \tag{A.18}$$

or

$$\int_0^{L_v} \rho(y) Y_i Y_j dy = 0, \tag{A.19}$$

where $\rho = m + M_S \delta(y)\, M\delta(y - L_v)$. For the case when $i = j$ the second term in (A.17) may be an arbitrary constant, so that one can choose

$$\int_0^{L_v} \rho(y) Y_j^2 dy = m_{jj}. \tag{A.20}$$

It can also be seen that when the orthogonality property (A.18) is used in (A.14a) the following relationship for $i \neq j$ results

$$EA\left[\int_0^{L_v} Y_j Y_i'' dy + Y_j(0)\, Y_i'(0) - Y_j(L_v)\, Y_i'(L_v)\right] - k_c Y_j(0)\, Y_i(0) = 0. \tag{A.21}$$

When $i = j$ and the eigenfunctions are normalized to satisfy the (A.20), equation (A.14a) gives

$$EA\left[\int_0^{L_v} Y_j Y_j'' dy + Y_j(0)\, Y_j'(0) - Y_j(L_v)\, Y_j'(L_v)\right] - k_c Y_j(0)\, Y_j(0) = -m_{jj}\omega_j^2. \tag{A.22}$$

Appendix B
Coefficients of Multi-Degree-of-Freedom Longitudinal Model

The coefficients and excitation terms appearing in the system (4.23) depend on the non-stationary parameter l, and are defined by equations (4.24a)-(4.24g) in terms of the eigenvalues γ_n, the eigenfunctions Y_n, and their derivatives. The eigenvalues γ_n are found from the transcendental frequency equation (4.16) which is solved using the modified *regula falsi* method [Gerald & Wheatley, 1989]. The partial derivatives of Y_n with respect to l are given as

$$\begin{aligned}\frac{\partial Y_n}{\partial l} &= \left(\frac{d\gamma_n}{dl}y-\gamma_n\right)\left[\left(\frac{1}{L_c\gamma_n}-\gamma_n\frac{M_S}{m}\right)\cos\gamma_n y-\sin\gamma_n y\right]- \\ &\quad \left(\frac{1}{L_c\gamma_n^2}+\frac{M_S}{m}\right)\frac{d\gamma_n}{dl}\sin\gamma_n y, \end{aligned} \tag{B.1a}$$

$$\begin{aligned}\frac{\partial^2 Y_n}{\partial l^2} &= \left(2\frac{\partial\gamma_n}{\partial l}-\frac{d^2\gamma_n}{dl^2}y\right)\{\frac{d\gamma_n}{dl}\left(\frac{1}{L_c\gamma_n^2}+\frac{M_S}{m}\right)\cos\gamma_n y- \\ &\quad \left(\frac{d\gamma_n}{dl}y-\gamma_n\right)\left[\left(\frac{1}{L_c\gamma_n}-\gamma_n\frac{M_S}{m}\right)\sin\gamma_n y+\cos\gamma_n y\right]\}- \\ &\quad \{\left[\left(\frac{1}{L_c\gamma_n^2}+\frac{M_S}{m}\right)\frac{d^2\gamma_n}{dl^2}-\frac{2}{L_c\gamma_n^3}\left(\frac{d\gamma_n}{dl}\right)^2\right]\sin\gamma_n y+ \\ &\quad \left(\frac{d\gamma_n}{dl}y-\gamma_n\right)\left(\frac{1}{L_c\gamma_n^2}+\frac{M_S}{m}\right)\frac{d\gamma_n}{dl}\cos\gamma_n y\}. \end{aligned} \tag{B.2a}$$

The derivatives of the eigenvalues γ_n with respect to l are obtained through differentiation of the frequency equation (4.16), and are calculated as

$$\frac{d\gamma_n}{dl}=\frac{N_n(l)}{D_n(l)}, \tag{B.3}$$

$$\frac{d^2\gamma_n}{dl^2}=\frac{1}{D_n^2}(\frac{dN_n}{dl}D_n-N_n\frac{dD_n}{dl}), \tag{B.4}$$

where

$$N_n = \gamma_n \left\{ \left[\frac{1}{L_c} - (M_S + M) \frac{\gamma_n^2}{m} \right] \sin \gamma_n L_v + \gamma_n \left[\left(\frac{1}{L_c} - \frac{M_S}{m} \gamma_n^2 \right) \frac{M}{m} + 1 \right] \cos \gamma_n L_v \right\}, \tag{B.5}$$

$$\begin{aligned} D_n \;=\; & \left[\frac{1}{L_c} \left(L_v + \frac{M}{m} \right) - 3 \frac{M_S M}{m^2} \gamma_n^2 - (M_S + M) \frac{\gamma_n^2}{m} L_v + 1 \right] \sin \gamma_n L_v + \\ & \left\{ 2 (M_S + M) \frac{\gamma_n}{m} + \left[\left(\frac{1}{L_c} - \frac{M_S}{m} \gamma_n^2 \right) \frac{M}{m} + 1 \right] \gamma_n L_v \right\} \cos \gamma_n L_v, \end{aligned} \tag{B.6}$$

$$\begin{aligned} & \frac{dN_n}{dl} = \frac{d\gamma_n}{dl} \{ \left[\frac{1}{L_c} - (M_S + M) \frac{\gamma_n^2}{m} \right] \sin \gamma_n L_v + \\ & \gamma_n \left[\left(\frac{1}{L_c} - \frac{M_S}{m} \gamma_n^2 \right) \frac{M}{m} + 1 \right] \cos \gamma_n L_v \} \\ & + \gamma_n \{ \left[\frac{1}{L_c} - (M_S + M) \frac{\gamma_n^2}{m} \right] \left(\frac{d\gamma_n}{dl} L_v - \gamma_n \right) \cos \gamma_n L_v - \\ & 2 \frac{M_S + M}{m} \gamma_n \frac{d\gamma_n}{dl} \sin \gamma_n L_v \\ & + \frac{d\gamma_n}{dl} \left[\left(\frac{1}{L_c} - \frac{M_S}{m} \gamma_n^2 \right) \frac{M}{m} + 1 \right] \cos \gamma_n L_v - \\ & \gamma_n \{ \left[2 \frac{M_S M}{m^2} \gamma_n \frac{d\gamma_n}{dl} \cos \gamma_n L_v + \left(\frac{1}{L_c} - \frac{M_S}{m} \gamma_n^2 \right) \frac{M}{m} + 1 \right] \cdot \\ & \left(\frac{d\gamma_n}{dl} L_v - \gamma_n \right) \sin \gamma_n L_v \} \}, \end{aligned} \tag{B.7}$$

$$\begin{aligned} & \frac{dD_n}{dl} = - \left[6 \frac{M_S M}{m^2} \gamma_n \frac{d\gamma_n}{dl} + \frac{1}{L_c} + \frac{M_S + M}{m} \gamma_n \left(2 \frac{d\gamma_n}{dl} L_v - \gamma_n \right) \right] \sin \gamma_n L_v + \\ & \left[\frac{1}{L_c} \left(L_v + \frac{M}{m} \right) - 3 \frac{M_S M}{m^2} \gamma_n^2 - \frac{M_S + M}{m} \gamma_n^2 L_v + 1 \right] \left(\frac{d\gamma_n}{dl} L_v - \gamma_n \right) \cos \gamma_n L_v + \\ & \{ \frac{2}{m} \frac{d\gamma_n}{dl} \left(M_S + M - \frac{M_S M}{m} \gamma_n^2 L_v \right) + \\ & \left[\left(\frac{1}{L_c} - \frac{M_S}{m} \gamma_n^2 \right) \frac{M}{m} + 1 \right] \left(\frac{d\gamma_n}{dl} L_v - \gamma_n \right) \} \cos \gamma_n L_v \\ & - \left\{ 2 \frac{M_S + M}{m} \gamma_n + \left[\left(\frac{1}{L_c} - \frac{M_S}{m} \gamma_n^2 \right) \frac{M}{m} + 1 \right] \gamma_n L_v \right\} \cdot \\ & \left(\frac{d\gamma_n}{dl} L_v - \gamma_n \right) \sin \gamma_n L_v. \end{aligned} \tag{B.8}$$

Finally, noting that

$$Y_n'' = -\gamma_n^2 Y_n, \tag{B.9}$$

$$\frac{\partial Y_n''}{\partial l} = -\gamma_n \left(2\frac{d\gamma_n}{dl} Y_n + \gamma_n \frac{\partial Y_n}{\partial l} \right), \tag{B.10}$$

the expressions (4.24a)-(4.24g) are evaluated numerically.

Appendix C
The Perturbation Procedure of Multiple Scales

Many physical problems exhibit features which preclude exact analytical solutions. In dynamic and vibration problems these features include for example non-linearities, variable coefficients, and unknown boundaries. In order to obtain information about solutions of equations governing these problems special methods must be adopted. Usually numerical methods, approximation methods, or a combination of both are applied. The approximation methods include perturbation (asymptotic) methods, in which the solution is represented by the first few terms of an asymptotic expansion [Nayfeh, 1973]. Usually *parameter perturbations* are used, and expansions are carried out in terms of a small parameter which appears naturally in the equations, or which is introduced artificially for convenience.

Often the problem is represented by the non-homogeneous differential equation

$$\mathcal{L}(u, t, \varepsilon) = F(t) \tag{C.1}$$

where $u = u(t)$, $\mathcal{L}$ represents a differential operator of a general nature, containing linear and non-linear terms in u and its derivatives; ε is a small parameter, and $F(t)$ is the non-homogeneous part of the equation, with harmonic terms.

C..1 Stationary System Analysis

Generally the problem (C.1) cannot be solved exactly. Consider the case when the operator $\mathcal{L}$ is of constant coefficients, with the assumption that for $\varepsilon = 0$ the problem can be solved exactly, and the general solution is $u_0(t)$.

The fundamental perturbation technique, referred to as the straightforward expansion, can then be used, in which a solution of equation (C.1) is expressed in the form of a power

series in ε, namely

$$u(t;\varepsilon) = u_0(t) + \varepsilon u_1(t) + \varepsilon^2 u_2(t) + \cdots \tag{C.2}$$

where u_n is independent of ε. This series is in turn substituted into equation (C.1), and one collects coefficients of each power of ε. Equating each of the coefficients to zero yields simpler equations for u_n, which can be solved successively. However, the solutions of these equations contain terms that grow indefinitely with time, referred to as *secular terms*. In addition to the secular terms, the solutions contain terms whose denominators may be very small, referred to as *small-divisor terms*, *and* occurring at resonant frequencies. Therefore, the straightforward expansions are *non-uniform* and break down for extended periods of time, and are often referred to as *pedestrian expansions*.

More advanced perturbation techniques exist that yield approximate solutions free of secular and small-divisor terms. The method of multiple scales is one the most widely applied to formulate uniformly valid perturbation expansions for dynamic problems of the form (C.1), and has been used to treat various resonance phenomena. The solution is then represented by an expansion having the form

$$u(t;\varepsilon) = u_0(T_0, T_1, T_2, \cdots) + \varepsilon u_1(T_0, T_1, T_2, \cdots) + \varepsilon^2 u_2(T_0, T_1, T_2, \cdots) + \cdots, \tag{C.3}$$

where

$$T_n = \varepsilon^n t, \quad n = 0, 1, 2, \cdots \tag{C.4}$$

represent different time scales. Because ε is a small parameter, T_0 represents a fast scale, T_1 represents a slower scale, T_2 denotes a more slower scale, and so on. Hence, the behaviour of u is observed on the different time scales. Consider equation (C.1) in the following form

$$\ddot{u} + \omega^2 u = \varepsilon f(u, \dot{u}) + F(t), \tag{C.5}$$

where the overdot designates differentiation with respect to time, ω denotes the natural frequency, $F(t)$ represents a monofrequency excitation

$$F(t) = K \cos \Omega t, \tag{C.6}$$

and f is a function which accounts for damping and nonlinear effects in the system. As $u(t,\varepsilon) = \hat{u}(T_0, T_1, T_2, \cdots; \varepsilon)$, the time derivatives of u are expressed as

$$\dot{u} = \frac{\partial u}{\partial T_0} + \varepsilon \frac{\partial u}{\partial T_1} + \varepsilon^2 \frac{\partial u}{\partial T_2} + \cdots \tag{C.7a}$$

$$\ddot{u} = \frac{\partial^2 u}{\partial T_0^2} + 2\varepsilon \frac{\partial^2 u}{\partial T_0 \partial T_1} + \varepsilon^2 \left(2\frac{\partial^2 u}{\partial T_0 \partial T_2} + \frac{\partial^2 u}{\partial T_1^2} \right) + \cdots \tag{C.7b}$$

It can be noted that when equations (C.7a)-(C.7b) are substituted into (C.5), the original ordinary differential equation is replaced by a partial differential equation. However, this complication does not present a problem, and is far outweighed by the advantages of the method in analysis of various resonance phenomena. Substituting the expansion (C.3) into (C.7a)-(C.7b), inserting the resulting expressions into equation (C.5), and equating coefficients of the same power of ε, yields a set of partial differential equations for the approximations u_n. In resonant cases so called detuning parameters are introduced to transform small-divisor terms into terms that lead to secular terms, and the partial differential equations are solved in succession by using the conditions, referred to as the *solvability conditions*, for the elimination of the secular terms.

For example, in order to investigate a primary or main resonance in the system (C.5), a detuning parameter σ, describing the nearness of Ω to ω, is introduced as follows

$$\Omega = \omega + \varepsilon\sigma. \tag{C.8}$$

In order to determine the first approximation to the solution of equation (C.5) two time scales, namely the scales T_0 and T_1, are sufficient. Accordingly, the solution is expressed as

$$u(t;\varepsilon) = u_0(T_0, T_1) + \varepsilon u_1(T_0, T_1) + \cdots \tag{C.9}$$

By applying equation (C.8) the excitation is also expressed in terms of the two scales as

$$F(t) = 2\varepsilon k \cos\left(\omega T_0 + \sigma T_1\right), \tag{C.10}$$

where the amplitude K is ordered so that the excitation will appear at $O(\varepsilon)$ where the function f representing damping and nonlinear terms first appear. This will ensure that a uniformly valid approximate solution to the problem is obtained, as the actual response of the system is limited by the damping and the non-linearity. Substituting (C.9) and (C.10)

into (C.5) gives

$$\begin{aligned}&\frac{\partial^2 u_0}{\partial T_0^2}+\varepsilon\frac{\partial^2 u_1}{\partial T_0^2}+2\varepsilon\frac{\partial^2 u_0}{\partial T_0\partial T_1}+\cdots+\omega\left(u_0+\varepsilon u_1+\cdots\right)=\\&\varepsilon f\left[u_0+\varepsilon u_1+\cdots,\frac{\partial u_0}{\partial T_0}+\varepsilon\left(\frac{\partial u_1}{\partial T_0}+\frac{\partial u_0}{\partial T_1}\right)+\cdots\right]+\\&2\varepsilon k\cos\left(\omega T_0+\sigma T_1\right).\end{aligned}\tag{C.11a}$$

Equating the coefficients of like powers of ε yields

$$\frac{\partial^2 u_0}{\partial T_0^2}+\omega^2 u_0=0,\tag{C.12a}$$

$$\frac{\partial^2 u_1}{\partial T_0^2}+\omega^2 u_1=-2\frac{\partial^2 u_0}{\partial T_0\partial T_1}+f(u_0,\frac{\partial u_0}{\partial T_0})+2k\cos\left(\omega T_0+\sigma T_1\right).\tag{C.12b}$$

The general solution of (C.12a) is given as

$$u_0=A(T_1)e^{i\omega T_0}+\bar{A}(T_1)e^{-i\omega T_0},\tag{C.13}$$

where $\bar{A}$ is the complex conjugate of A, that can be expressed in the polar form

$$A(T_1)=\frac{1}{2}a(T_1)e^{i\beta(T_1)},\tag{C.14}$$

where a and β represent real amplitude and phase angle, respectively. Expressing the excitation term in complex form, namely

$$2k\cos\left(\omega T_0+\sigma T_1\right)=ke^{i(\omega T_0+\sigma T_1)}+cc,\tag{C.15}$$

substituting (C.13) into equation (C.12b), noting that

$$\frac{\partial u_0}{\partial T_0}=i\omega A(T_1)e^{i\omega T_0}+cc,\tag{C.16a}$$

$$\frac{\partial^2 u_0}{\partial T_0\partial T_1}=i\omega A'e^{i\omega T_0}+cc,\tag{C.16b}$$

where the prime denotes the derivative with respect to T_1, and cc designates the complex conjugate of the preceding terms, leads to

$$\begin{aligned}\frac{\partial^2 u_1}{\partial T_0^2}+\omega^2 u_1 \;=\;& -2i\omega A'e^{i\omega T_0}+ke^{i(\omega T_0+\sigma T_1)}+cc+\\&f\left(Ae^{i\omega T_0}+cc,i\omega e^{i\omega T_0}+cc\right).\end{aligned}\tag{C.17a}$$

All particular solutions of equation (C.17a), which depend on A, contain secular terms, namely terms proportional to $T_0e^{\pm i\omega T_0}$. Therefore, the component εu_1 can grow without

bounds as t increases, and the expansion (C.9) is not uniformly valid. However the function $A(T_1)$ can be chosen so that the secular terms vanish. from the particular solution of (C.17a). To this end it can be noted that f is periodic and its Fourier expansion is

$$f = \sum_{n=-\infty}^{\infty} f_n e^{in\Phi}, \tag{C.18}$$

where $\Phi = \omega T_0$, and

$$f_n(A, \bar{A}) = \frac{1}{2\pi} \int_0^{2\pi} f e^{-in\Phi} d\Phi. \tag{C.19}$$

Thus, the solvability condition is

$$2i\omega A' - k e^{i\sigma T_1} - f_1(A, \bar{A}) = 0. \tag{C.20}$$

Expressing A in the polar form (C.14), separating the transformed form (C.20) into its real and imaginary parts, and also denoting $\psi = \sigma T_1 - \beta$, leads to

$$a' = \frac{k}{\omega} \sin\psi - \frac{1}{2\pi\omega} \int_0^{2\pi} f(a\cos\theta, -a\omega\sin\theta) \sin\theta d\theta, \tag{C.21a}$$

$$\psi' = \sigma + \frac{k}{a\omega} \cos\psi + \frac{1}{2\pi a\omega} \int_0^{2\pi} f(a\cos\theta, -a\omega\sin\theta) \cos\theta d\theta, \tag{C.21b}$$

where $\theta = \omega T_0 + \beta(T_1)$. Therefore, the first approximation to the steady-state response is given by

$$u = a\cos(\Omega t - \psi) + O\left(\varepsilon^2\right), \tag{C.22}$$

where a and ψ are solutions of equations (C.21a) and (C.21b), respectively.

C..2 Non-stationary Vibrations

The procedure of multiple scales can be extended to analyze systems having components that are time dependent (i.e. are non-stationary). Physically, these components may be the amplitude or frequency of excitation, mass and length parameters, stiffness and material properties, or damping coefficients. Usually it can be assumed that these components are slowly varying, and the non-stationary studies are concerned with the modification of the response near the resonance conditions called *passage through resonance* [Nayfeh & Mook, 1979]. Two cases can be distinguished in these resonance studies [Kevorkian, 1987]. In the first case the resonant behaviour is of short duration and is referred to as *transient*

resonance. This resonance phenomenon occur in systems in which the rate of slow variation of parameters is considered to be equivalent to the order of the weak damping or weak non-linearity. Namely, if the strength of the damping or the nonlinear coupling is of order $O(\varepsilon)$, then the parameter variation can be observed on a slow scale defined as

$$\tau = \varepsilon t. \tag{C.23}$$

The second case concerns systems in which the parameters vary more slowly relative to the order of the damping or non-linearity, which remains $O(\varepsilon)$. The variation of the parameters is then observed on a *very slow* time scale $\tau^* = \varepsilon^2 t$, and the resonance, referred to as *sustained resonance*, persists for long times [Bosley & Kevorkian, 1991].

In this study systems with slowly varying components are considered. These non-stationary systems can generally be described by

$$\mathcal{L}(u, t, \varepsilon t, \varepsilon) = F(t, \varepsilon t), \tag{C.24}$$

where the operator $\mathcal{L}$ has slowly varying coefficients, and the excitation term is of slowly varying amplitude and frequency. Nayfeh [1979] considered transient resonance in a system with constant parameters, and with non-stationary excitation. The problem is described by equation (C.5) with the excitation term given by

$$F(t, \varepsilon t) = 2\varepsilon k(\varepsilon t)\cos\left[\theta(t, \varepsilon t)\right], \tag{C.25}$$

where $\dot{\theta}$, the frequency of the excitation, is close to the natural frequency ω during a short time interval. The method of multiple scales, with a fast scale T_0 and a slow scale T_1, is used to find an approximate solution in the form of the expansion (C.9). The nearness of the frequency of the excitation to the natural frequency is quantified by a slowly varying detuning parameter $\sigma(T_1)$, so that

$$\dot{\theta} = \omega + \varepsilon\sigma(T_1), \tag{C.26}$$

and consequently $\theta(T_0, T_1) = \omega T_0 + \nu(T_1)$, with $\frac{d\nu}{dT_1} = \sigma(T_1)$. Following the standard procedure of substituting the asymptotic series (C.9) into the differential equation (C.5), and of collecting coefficients of each power of ε leads to the solution for u_0 given by

equation (C.13), and consequently to a partial differential equation for u_1 of the form

$$\frac{\partial^2 u_1}{\partial T_0^2} + \omega^2 u_1 = -2i\omega A' e^{i\omega T_0} + k(T_1) e^{i[\omega T_0 + \nu(T_1)]} + cc + f\left(Ae^{i\omega T_0} + cc, i\omega e^{i\omega T_0} + cc\right). \tag{C.27a}$$

With f expanded in a Fourier series according to (C.18), the solvability condition is given by

$$2i\omega A' - k\left(T_1\right) e^{i\nu(T_1)} - f_1(A, \bar{A}) = 0, \tag{C.28}$$

where f_1 is found from (C.19). Denoting $\psi = \nu(T_1) - \beta(T_1)$, it is found eventually that the response during the transition through the main resonance is given by

$$u = a\cos\left(\theta - \psi\right) + O\left(\varepsilon^2\right), \tag{C.29}$$

where a and ψ are given by differential equations having the same form as for the stationary case, namely by equations (C.21a) and (C.21b), respectively. However in the non-stationary case k and σ are slowly varying, consequently steady-state solutions do not exist, and the response is aperiodic.

Resonances in non-stationary systems with slowly varying parameters, namely systems described by equation (C.24) with $\mathcal{L}$ having slowly varying coefficients, can also be treated by the multiple scales procedure. Consider a system with non-stationary parameters and stationary excitation described by

$$\ddot{u} + \omega^2\left(\tau\right) u = \varepsilon f^*(u, \dot{u}, \tau) + F(t), \tag{C.30}$$

where F is given by (C.6), τ is a slow scale defined by (C.23), the natural frequency ω is varying slowly, and f^* represents damping and nonlinear terms, and additional reactive effects due to the variation of mass or length in the system. The solution to equation (C.30) is sought in terms of the slow and fast scales in the form

$$u = u_0\left(\phi, \tau\right) + \varepsilon u_1\left(\phi, \tau\right) + \cdots, \tag{C.31}$$

where ϕ denotes the fast scale defined as

$$\phi = \int_0^t \omega\left(\varepsilon\xi\right) d\xi. \tag{C.32}$$

Thus, the time derivatives of u in terms of the two scales become

$$\frac{du}{dt} = \omega\frac{\partial u}{\partial \phi} + \epsilon\frac{\partial u}{\partial \tau}, \tag{C.33a}$$

$$\frac{d^2u}{dt^2} = \omega^2\frac{\partial^2 u}{\partial \phi^2} + \epsilon(2\omega\frac{\partial^2 u}{\partial \phi \partial \tau} + \omega'\frac{\partial u}{\partial \phi}) + \epsilon^2\frac{\partial^2 u}{\partial \tau^2}, \tag{C.33b}$$

where the prime denotes the derivative with respect to τ. Using the series (C.31) in (C.33a)-(C.33b), and in (C.30) yields

$$\begin{aligned}
&\omega^2(\frac{\partial^2 u_0}{\partial \phi^2} + u_0) + \varepsilon\left(\omega^2\frac{\partial^2 u_1}{\partial \phi^2} + 2\omega\frac{\partial^2 u_0}{\partial \phi \partial \tau} + \omega'\frac{\partial u_0}{\partial \phi} + \omega^2 u_1\right) + \\
&\varepsilon^2\left(2\omega\frac{\partial^2 u_1}{\partial \phi \partial \tau} + \omega'\frac{\partial u_1}{\partial \phi} + \frac{\partial^2 u_0}{\partial \tau^2}\right) + \cdots = \\
&\varepsilon f\left[u_0 + \varepsilon u_1, \omega\frac{\partial u_0}{\partial \phi} + \varepsilon\left(\omega\frac{\partial u_1}{\partial \phi} + \frac{\partial u_0}{\partial \tau}\right) + \cdots\right] + K\cos\Omega t.
\end{aligned} \tag{C.34a}$$

When transient resonance is of concern, values of the slowly varying natural frequency are near Ω, so that

$$\Omega = \omega(\tau) + \varepsilon\sigma(\tau), \tag{C.35}$$

where $\sigma(\tau)$ is a slowly varying detuning parameter. Using the definition (C.32), it follows from (C.35) that

$$\Omega t = \phi + \vartheta(\tau), \tag{C.36}$$

where

$$\vartheta = \varepsilon\int_0^t \sigma(\varepsilon\xi)\, d\xi. \tag{C.37}$$

Thus, ordering the amplitude of the excitation as $K = 2\varepsilon k$, applying the expression (C.36), and equating the coefficients of ε^0 and ε on both sides of equation (C.34a) gives

$$\omega^2\left(\frac{\partial^2 u_0}{\partial \phi^2} + u_0\right) = 0, \tag{C.38a}$$

$$\begin{aligned}
\omega^2(\frac{\partial^2 u_1}{\partial \phi^2} + u_1) = &-2\omega\frac{\partial^2 u_0}{\partial \phi \partial \tau} - \omega'\frac{\partial u_0}{\partial \phi} + f\left(u_0, \omega\frac{\partial u_0}{\partial \phi}, \tau\right) + \\
&2k\cos[\phi + \vartheta(\tau)].
\end{aligned} \tag{C.38b}$$

The general solution of (C.38a) is given as

$$u_0 = a(\tau)\cos[\phi + \beta(\tau)], \tag{C.39}$$

which alternatively can be written in a complex form

$$u_0 = A(\tau)e^{i\phi} + \bar{A}(\tau)e^{-i\phi}, \tag{C.40}$$

where

$$A(\tau) = \frac{1}{2}a(\tau)e^{i\beta(\tau)}. \tag{C.41}$$

Using the solution (C.40) together with the excitation term expressed in a complex form in (C.38b) yields

$$\begin{aligned}\omega^2\left(\frac{\partial^2 u_1}{\partial\phi^2} + u_1\right) &= -i\left(2\omega A' + \omega' A\right)e^{i\phi} + ke^{i(\phi+\vartheta)} + cc + \\ &\quad f\left(Ae^{i\phi} + cc, i\omega Ae^{i\phi} + cc, \tau\right).\end{aligned} \tag{C.42a}$$

When f is expanded into a Fourier series

$$f^*\left(\phi, \tau, A, \bar{A}\right) = \sum_{n=\infty}^{\infty} f_n^*\left(\tau, A, \bar{A}\right)e^{in\phi}, \tag{C.43}$$

where

$$f_n^*\left(\tau, A, \bar{A}\right) = \frac{1}{2\pi}\int_0^{2\pi} f^*\left(\phi, \tau, A, \bar{A}\right)e^{-in\phi}d\phi, \tag{C.44}$$

the solvability condition can be written as

$$-i(2\omega A' + \omega' A) + ke^{i\vartheta} + f_1^*(\tau, A, \bar{A}) = 0. \tag{C.45}$$

Expressing A in polar form in equation (C.45), separating the result into the real and imaginary parts, denoting $\psi = \vartheta - \beta$, and $\theta = \phi + \beta$, leads to

$$a' = -\frac{1}{2}\frac{\omega'}{\omega}a - \frac{1}{2\pi\omega}\int_0^{2\pi} f^*(\tau, a\cos\theta, -a\omega\sin\theta)\sin\theta d\theta + \frac{k}{\omega}\sin\psi, \tag{C.46a}$$

$$\psi' = \sigma + \frac{1}{2\pi\omega a}\int_0^{2\pi} f^*(\tau, a\cos\theta, -a\omega\sin\theta)\cos\theta d\theta + \frac{k}{\omega a}\cos\psi. \tag{C.46b}$$

The response is then given by

$$u = a\cos\left(\Omega t - \psi\right) + O\left(\varepsilon^2\right), \tag{C.47}$$

where a and ψ are determined from the first order system (C.46a)-(C.46b). It is evident that, as in the case with non-stationary excitation, the response is aperiodic. It can be also noted that when ω and σ are constant, and the non-stationary reactive effects are neglected, so that $f^* \equiv f$, the system (C.46a)-(C.46b) is reduced to the stationary form given by equations (C.21a) and (C.21b).

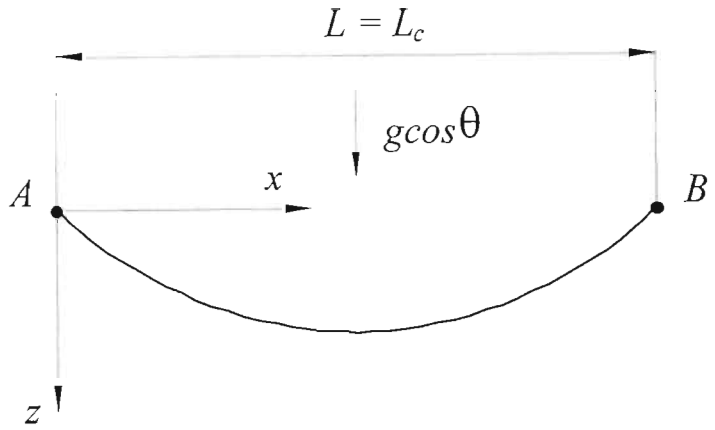

Figure 62. Catenary supported at equal elevation.

Appendix D
The Profile of a Catenary Cable

In a typical hoisting system, the catenary cable is inclined at an angle θ. Due to the high tension the catenary profile lies closely to the chord between the sheave and drum, and it is of interest to determine an approximate solution to this profile.

Constancon [1993] based this solution on a model with the horizontal catenary, with the corrected gravitational constant $g\cos\theta$, as shown in Figure 62, with the co-ordinate frame (x, z). Using the results derived by Irvine [1981], the profile in this configuration is governed by the following differential equation

$$H\frac{d^2z}{dx^2} + \left[1 + \left(\frac{dz}{dx}\right)^2\right]^{\frac{1}{2}} mg\cos\theta = 0, \tag{D.1}$$

where H denotes the horizontal component of cable tension, and m is the cable mass per unit length. If the profile is flat, namely the ratio of sag to span is 1:8 or less, the derivative $\frac{dz}{dx}$ is considered sufficiently small for its square to be ignored, and equation (D.1) reduces to

$$H\frac{d^2z}{dx^2} = -mg\cos\theta, \tag{D.2}$$

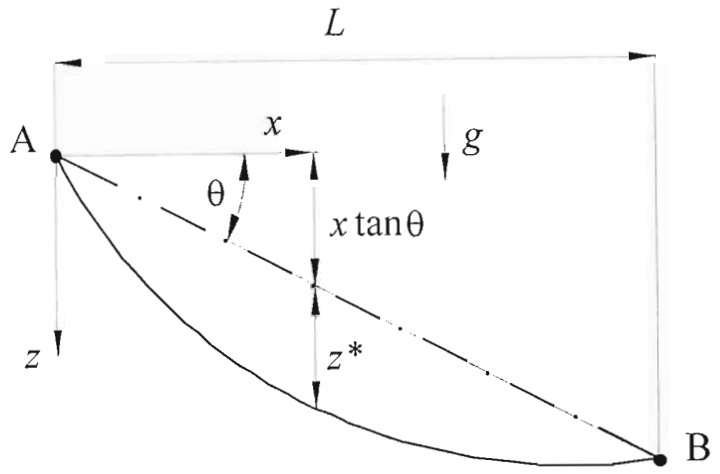

Figure 63. Inclined catenary cable.

for which the exact solution is

$$\bar{z} = \frac{1}{2}\bar{x}\left(1 - \bar{x}\right), \tag{D.3}$$

where $\bar{z} = z/mgL^2\cos\theta/H$, $\bar{x} = x/L$, in which L is the span of the cable. Thus, noting that the flat profile curvature is approximated as $\kappa = \frac{d^2z}{dx^2}$, it can be concluded from equation (D.2) that the catenary equilibrium curvature is constant and defined as

$$\kappa = \frac{mg\cos\theta}{H}. \tag{D.4}$$

Irvine [1981] showed that the differential equation governing the equilibrium configuration of an inclined catenary shown in Figure 63 is

$$H\frac{d^2z^*}{dx^2} + \left[1 + \left(\tan\theta + \frac{dz^*}{dx}\right)^2\right]^{\frac{1}{2}} mg = 0, \tag{D.5}$$

where z^* denotes the dip of the profile below the chord. This non-linear equation cannot be solved exactly, and an approximate solution is sought in the form of a straightforward expansion

$$\bar{z}^*\left(\bar{x};\varepsilon\right) = \bar{z}_0^*\left(\bar{x}\right) + \varepsilon\bar{z}_1^*(\bar{x}) + \cdots, \tag{D.6}$$

where $\bar{z}^* = z^*/\left(mgL^2/H\cos\theta\right)$, and ε is a small parameter defined as

$$\varepsilon = mgL\sin\theta/H. \tag{D.7}$$

Substituting the series (D.6) into equation (D.5), and collecting the coefficients of ε^0 and ε yields

$$\frac{d^2\bar{z}_0^*}{d\bar{x}^2} = -1, \tag{D.8}$$

$$\frac{d^2\bar{z}_1^*}{d\bar{x}^2} = -\frac{d\bar{z}_0^*}{d\bar{x}}, \tag{D.9}$$

where $\bar{z}_0^*$ and $\bar{z}_1^*$ must satisfy zero boundary conditions at A $(\bar{x}=0)$, and at $B.(\bar{x}=1)$. These equations are solved successively to produce $\bar{z}_0^* = \frac{1}{2}\bar{x}\,(1-\bar{x})$ and $\bar{z}_1^* = \frac{1}{12}\bar{x}\,(1-\bar{x})\,(1-2\bar{x})$, respectively, so that

$$\bar{z}^* = \frac{1}{2}\bar{x}\,(1-\bar{x})\left[1+\frac{\varepsilon}{6}\,(1-2\bar{x})\right] + O\left(\varepsilon^2\right). \tag{D.10}$$

It can be noted that this profile is asymmetric with respect to the mid span. However, for small ε equations (D.3) and (D.10) yield similar results. Hence, if $\varepsilon \ll 1$ the catenary profile can be approximated by a symmetric parabola.

Using equation (D.3) or (D.10), together with equation (D.4), one can prove that for a typical industrial hoisting installation the catenary profile lies very close to the chord, and has negligible curvature. For example, in the case of a typical mine hoist system, with the mass of a loaded conveyance $M = 17500$ kg, the cable mass per unit length $m = 8.5$ kg/m, the length of vertical rope $L_v = 10 \div 2100$ m, the catenary length $L_c = 75$ m, and with the angle of inclination $\theta = 45^0$, where the equilibrium tension H is defined as

$$H = (M + mL_v)\,g, \tag{D.11}$$

the maximum sag varies between 0.12 to 0.24 m, so that the corresponding sag to span ratios are between $1:312$ and $1:625$, respectively. Furthermore, the curvature range is $(1.7003 \div 3.4179) \times 10^{-4}$. Hence, as these values are very small, the catenary in a typical industrial hoisting system can be treated as a taut flat cable, or string element. Consequently, the catenary strain measure is assumed in the form (3.10), which is the basis for a non-linear string equation.

Appendix E
Equivalent Viscous Damping Considerations

E..3 Fundamental Considerations

Various types of damping may be represented by *equivalent viscous damping*. In this approach, one can approximate the response of the actual system with damping forces of a complicated nature with the solution of a viscously damped system that dissipates an equivalent amount of energy per cycle. Damping effects are the most important at resonance regions in systems with periodic excitation. Consider a linear viscously damped single-degree-of-freedom system subjected to harmonic excitation with frequency Ω, defined by

$$m\ddot{q} + c\dot{q} + kq = F_0 \cos \Omega t, \tag{E.1}$$

where m denotes mass, c is the coefficient of damping, and k represents stiffness properties of the system. The steady-state response is of the form

$$q = X \cos(\Omega t - \varphi), \tag{E.2}$$

where φ denotes the phase shift due to damping. The energy dissipated in this system per cycle of motion is given by

$$\Delta E = \oint c\dot{q} dq = \int_{\varphi/\Omega}^{T+\varphi/\Omega} c\dot{q}^2 dt, \tag{E.3}$$

where $T = 2\pi/\Omega$. Using equation (E.2) in (E.3) and integrating yields

$$\Delta E = \pi c \Omega X^2. \tag{E.4}$$

When the energy loss given by equation (E.4) is equated to the energy dissipation associated with another form of damping, an equivalent viscously damped system can be created. For example, if the single-degree-of-freedom system under consideration is subjected to *quadratic damping* the equation of motion becomes

$$m\ddot{q} + \alpha \dot{q}^2 sgn(\dot{q}) + kq = F_0 \cos \Omega t. \tag{E.5}$$

This type of damping can be used to model the air damping, for example [Inman, 1996]. Noting that the steady-state response is of the form given by equation (E.2), the energy dissipated per cycle in this case of damping is determined as

$$\Delta E = \alpha \oint \dot{q}^2 sgn\left(\dot{q}\right) dq = \alpha \int_{\varphi/\Omega}^{T+\varphi/\Omega} \dot{q}^3 sgn\left(\dot{q}\right) dt. \tag{E.6}$$

so that

$$\Delta E = -\alpha X^3 \Omega^2 \int_0^{2\pi} \sin^3\theta sgn\left(\dot{q}\right) d\theta = \frac{8}{3}\alpha X^3 \Omega^2. \tag{E.7}$$

Equating the energy loss given by equation (E.7) to the energy loss for viscous damping given by equation (E.4) yields the equivalent viscous damping coefficient

$$c_{eq} = \frac{8}{3\pi}\alpha X \Omega. \tag{E.8}$$

The corresponding equivalent damping ratio is then determined as

$$\zeta_{eq} = \frac{c_{eq}}{2m\omega}, \tag{E.9}$$

so that the equivalent viscously damped system is described by

$$\ddot{q} + 2\zeta_{eq}\omega\dot{q} + \omega q = f_0 \cos\Omega t, \tag{E.10}$$

where $\omega = \sqrt{k/m}$, and $f_0 = F_0/m$.

E..4 Equivalent Lateral Viscous Damping

Mankowski [1988] conducted studies to determine the internal energy loss arising from inter-wire/strand friction in a wire cable undergoing non-planar transverse motion. It was established through experimental tests that the internal power loss P_n in W, corresponding to the cable n^{th} transverse vibration mode is given by

$$P_n = 2nR_{SS}f_nC_1\left(1 + C_2X_n\right), \tag{E.11}$$

where R_{SS} denotes the sag to span ratio, f_n is the n^{th} natural frequency in Hz, X_n is the amplitude of the n^{th} mode in m, and C_1, C_2 are the cable characteristics. Namely, C_1 is the damping capacity in J, and C_2 denotes the curvature characteristic in m^{-1}. Mankowski used equation (E.11) to analyze the power losses in a single catenary cable of the Blair double-drum winding plant installed in No. 1 Shaft at Kloof Gold Mine. The resonant

Mode No. n	Frequency f_n Hz / $\bar{\omega}_n$ $\frac{rad}{s}$	Ampliude X_n m	Power Loss W	Modal Damping Ratio ζ_{eq}^n %	Modal Damping Ratio ζ_{eqair}^n %
1	1.12 / 7.0372	1.0	3.4218	0.0031	0.1314
2	2.24 / 14.0743	0.575	14.0430	0.0048	0.0755
3	3.36 / 21.1115	0.5	40.3341	0.0054	0.0657
4	4.48 / 28.1487	0.375	69.1004	0.0069	0.0493

Table 4. Estimations of Lateral Equivalent Modal Damping Ratios - Kloof Gold Mine

conditions were chosen in this analysis, namely when the cable natural lateral frequencies are tuned to the integer multiplies of the fundamental drum frequency during normal operations. The worst-case amplitudes of vibration were used in calculations, with the cable characteristic constants $C_1 = 42.75\ J$ and $C_2 = 0.34\ m^{-1}$, and span $L_c = 75\ m$.

The results obtained from this analysis can be employed to determine the equivalent viscous damping coefficients and damping ratios corresponding to each vibration mode. Namely, by using equation (E.4), one can equate the energy losses as follows

$$\pi c_{eq}^n \bar{\omega}_n X_n^2 = P_n T_n, \tag{E.12}$$

where $\bar{\omega}_n$ is the lateral natural frequency and $T_n = 2\pi/\bar{\omega}_n$, so that the equivalent viscous damping coefficient corresponding to the n^{th} mode is given by

$$c_{eq}^n = \frac{2P_n}{X_n^2 \bar{\omega}_n^2}. \tag{E.13}$$

Noting that the modal mass of the catenary cable is given by equation (5.18a), the equivalent modal damping ratio is determined as

$$\zeta_{eq}^n = \frac{2P_n}{mL_c X_n^2 \bar{\omega}_n^3}. \tag{E.14}$$

The modal damping ratios calculated using equations (E.11) and (E.14) are presented in Table 4.

Constancon [1993] considered the influence of air damping on the lateral catenary vibration. It has been assumed that the air damping can be represented as quadratic damping with the coefficient α given as

$$\alpha = \frac{1}{2} C \rho A, \tag{E.15}$$

where C is the air drag coefficient, ρ denotes the air density, and A is the cross-sectional area of the moving object. Recalling that damping effects are the most important at the

resonance region, when the cable response demonstrates a single-mode behoviour, a planar air damping force per unit length of the cable corresponding to the resonance mode r can be represented as

$$F_d^r = \frac{1}{2} C\rho d V_r^2 sgn\left(V_r\right), \tag{E.16}$$

where d is the cable diameter, and V_r denotes the cable velocity. When, for instance, the out -of-plane motion is considered the velocity is given by

$$V_r = \Phi_r \dot{q}_r, \tag{E.17}$$

where $\Phi_r = \sin(\frac{r\pi}{L_c} y)$, $0 < y < L_c$, so that equation (E.16) assumes the form

$$F_d^r = \frac{1}{2} C\rho d \dot{q}_r^2 \sin^2\left(\frac{r\pi}{L_c} y\right) sgn\left(\dot{q}_r\right). \tag{E.18}$$

The corresponding modal damping force is defined as

$$Q_d^r = \int_0^{L_c} F_d^r \Phi_r dy = \frac{1}{2} r C\rho d \dot{q}_r^2 sgn\left(\dot{q}_r\right) \int_0^{L_c/r} \sin^3\left(\frac{r\pi}{L_c} y\right) dy, \tag{E.19}$$

and integrating yields

$$Q_d^r = \frac{2}{3\pi} C\rho d L_c \dot{q}_r sgn\left(\dot{q}_r\right). \tag{E.20}$$

During the steady-state motion at resonance the response q_r is of the form given by equation (E.2), namely $q_r = X_r \cos\left(\bar{\omega}_r t - \varphi_r\right)$, and the energy loss can be calculated as in equation (E.6)

$$\Delta E = \oint Q_d^r dq_r = \frac{2}{3\pi} C\rho d L_c \int_{\varphi_r/\bar{\omega}_r}^{T_r + \varphi_r/\bar{\omega}_r} \dot{q}_r^3 sgn\left(\dot{q}_r\right) dt. \tag{E.21}$$

Consequently integrating gives

$$\Delta E = \frac{16}{9\pi} C\rho d L_c X_r^3 \bar{\omega}_r^2. \tag{E.22}$$

Equating the energy loss given by equation (E.22) to the energy loss for viscous damping given by equation (E.4), in which one uses $X = X_r$ and $\Omega = \bar{\omega}_r$, yields the equivalent viscous damping coefficient

$$c_{eqair} = \frac{16}{9\pi^2} C\rho d L_c X_r \bar{\omega}_r. \tag{E.23}$$

The corresponding modal damping ratio is then calculated as

$$\zeta_{eqair}^r = \frac{16}{9m\pi^2} C\rho d X_r. \tag{E.24}$$

The same results are produced when the in-plane motion is considered. The air damping equivalent modal damping ratios, calculated using the drag coefficient $C = 1$, the density of air $\rho = 1.29\ kg/m^3$ and the same modal amplitudes as for the internal damping ratios, are also presented in Table 4.

These calculations confirm Constancon's conclusion, namely that air damping is large compared with internal damping, and may play an important role in the catenary energy dissipation mechanism. Hence, the lateral modal damping ratios assumed in this analysis comply with the order of ζ^r_{eqair} values presented above.

Appendix F
MATLAB ODE function

```
function ydot=minode(t,y)
% NON-LINEAR MODEL OF A CATENARY-VERTICAL ROPE SYSTEM
global t1 t2 p v TT
global om_lat mrlat Clat Dlat cc om_lat beta zeta
global om_long c3d la3d mra zra c lom
global E A Ms Mc m Lc L0 kc d Rd alfa dmp2 l0
global T Fee wtot wdtot wddtot vtot vdtot vddtot
if t<=t1
l=l0+0.5*p*t^2;
ldot=p*t;
lddot=p;
elseif t<=t2
l=l0+0.5*p*t1^2+v*(t-t1);
ldot=v;
lddot=0;
else
l=l0+0.5*p*(t1^2-t2^2)+v*(t-t1)+p*(t2*t-0.5*t^2);
ldot=v-p*(t-t2);
lddot=-p;
end
L1=l+Lc;
omegalat=interp1(lom,om_lat,l);
omegalong=interp1(lom,om_long,l);
gamlong=omegalong/c;
mrlong=interp1(lom,mra,l);
Clong=interp1(lom,c3d,l);
```

```
Lalong=interp1(lom,la3d,l);
Zrlong=interp1(lom,zra,l);
wl=interp1(T,wtot,t);
wld=interp1(T,wdtot,t);
wldd=interp1(T,wddtot,t);
Fe=interp1(T,Fee,t);
if t<=TT
vl=0;
vld=0;
vldd=0;
elseif t<=t2
vl=0;
vld=interp1(T,vdtot,t);
vldd=interp1(T,vddtot,t);
else
vl=interp1(T,vtot,t);
vld=interp1(T,vdtot,t);
vldd=interp1(T,vddtot,t);
end
% construct [C}
% lateral motions v,w:
Cv=2/mrlat*ldot*Clat;
zz=2*zeta'.*omegalat;
for r=1:4
Cv(r,r)=Cv(r,r)+zz(r);
end
% longitudinal motion u:
La=zeros(4);
La=[Lalong(1) Lalong(2) Lalong(3) Lalong(4);...
```

```
Lalong(5) Lalong(6) Lalong(7) Lalong(8);...
Lalong(9) Lalong(10) Lalong(11) Lalong(12);...
Lalong(13) Lalong(14) Lalong(15) Lalong(16)];
Cl=zeros(4);
Cl=[Clong(1) Clong(2) Clong(3) Clong(4);...
Clong(5) Clong(6) Clong(7) Clong(8);...
Clong(9) Clong(10) Clong(11) Clong(12);...
Clong(13) Clong(14) Clong(15) Clong(16)];
Cu=-E*A*La+2*ldot*Cl;
gg=Ms*ldot*(1/Lc-Ms/m*gamlong.^2);
for r=1:4
Cu(:,r)=Cu(:,r)+gg(r);
end
for r=1:4
Cu(r,:)=Cu(r,:)/mrlong(r);
Cu(r,r)=Cu(r,r)+dmp2;
end
% total C:
C=[Cv zeros(4,8);zeros(4) Cv zeros(4);zeros(4,8) Cu];
% Construct [K]
% lateral motions v,w:
cc1=interp1(lom,cc,l);
FF=(1+(c/cc1)^2*Fe);
kk=FF*omegalat.^2;
Kv=(ldot^2*Dlat+lddot*Clat)/mrlat;
for r=1:4
Kv(r,r)=Kv(r,r)+kk(r);
end
% longitudinal motion u:
```

```
Ku=zeros(4);
omegalong2=omegalong.^2;
for r=1:4
Ku(r,r)=omegalong2(r);
end
% Total K:
K=[Kv zeros(4,8);zeros(4) Kv zeros(4);zeros(4,8) Ku];
% The main matrix:
AA=[zeros(12) eye(12); -K -C];
% Nonlinear terms:
Nv=-(c/cc1)^2*(sum(y(9:12))/Lc+sum(beta.^2'.*(y(1:4).^2+y(5:8).^2)))...
*omegalat.^2'.*y(1:4);
Nw=-(c/cc1)^2*(sum(y(9:12))/Lc+sum(beta.^2'.*(y(1:4).^2+y(5:8).^2)))...
*omegalat.^2'.*y(5:8);
Nu=-E*A*sum(beta.^2'.*(y(1:4).^2+y(5:8).^2))./mrlong';
N=[zeros(12,1);Nv;Nw;Nu];
% The excitation terms:
r=1:4;
P=-2*(vldd-(2*vld*ldot+vl*lddot)/Lc.*((-1).^r-1))/pi./r;
Q=-2*(wldd-(2*wld*ldot+wl*lddot)/Lc.*((-1).^r-1))/pi./r;
Z=-E*A*Fe./mrlong+lddot*Zrlong;
FT=[zeros(12,1);P';Q';Z'];
% The final system:
ydot=AA*y+N+FT;
```

Appendix G
Simulation Results

The numerical integration of non-linear equations leads to the determination of modal co-ordinates p_n, q_n and z_n. The simulation for various values of winding velocity have been conducted taking into consideration the Kloof Mine parameters. The Kloof results are plotted against the depth L_v in Figures 64-81. The dynamic behaviour of the Elandsrand winder system, with the nominal winding velocity, has also been simulated. The respective results obtained from this simulation are shown in Figures 82-84

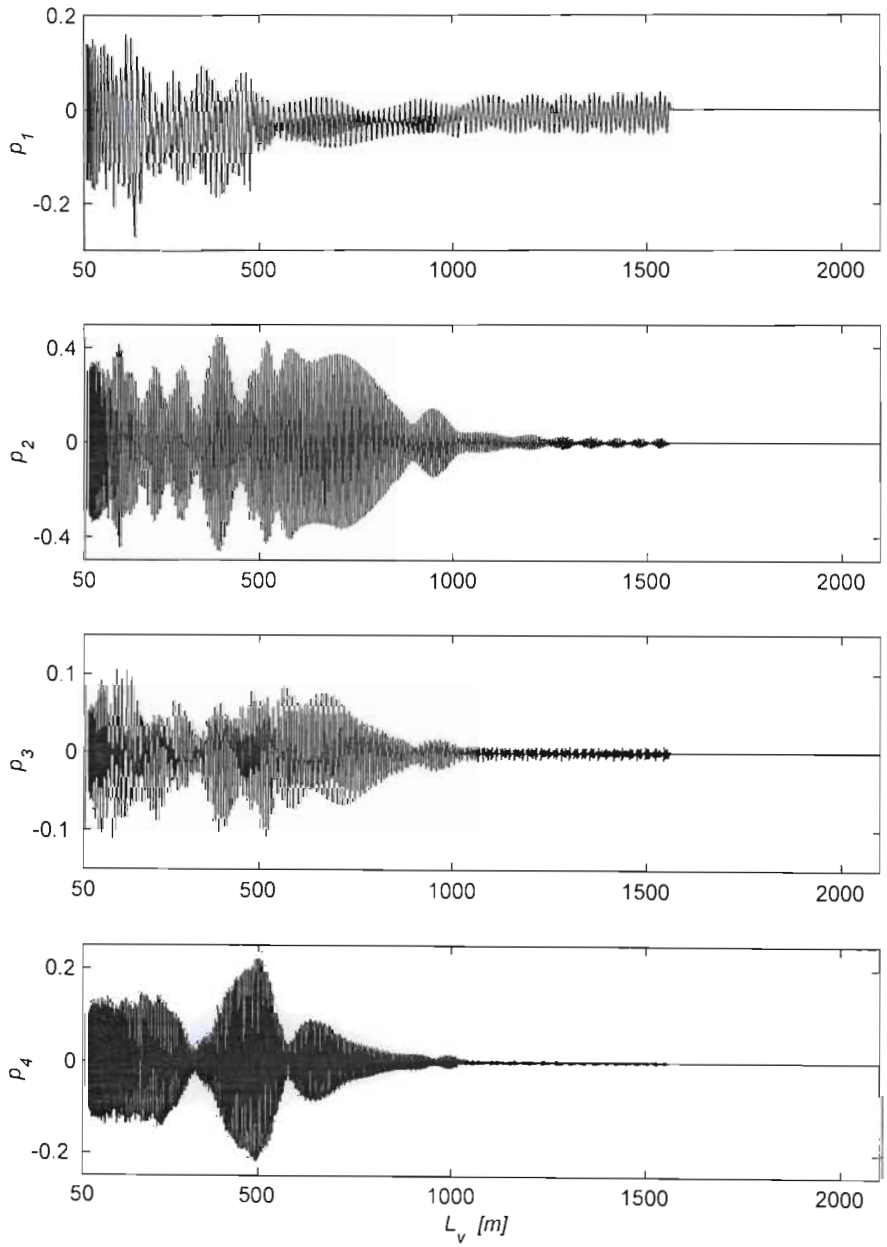

Figure 64. Lateral in-plane modal co-ordinates for Kloof simulation, $V_c = 15\ m/s$.

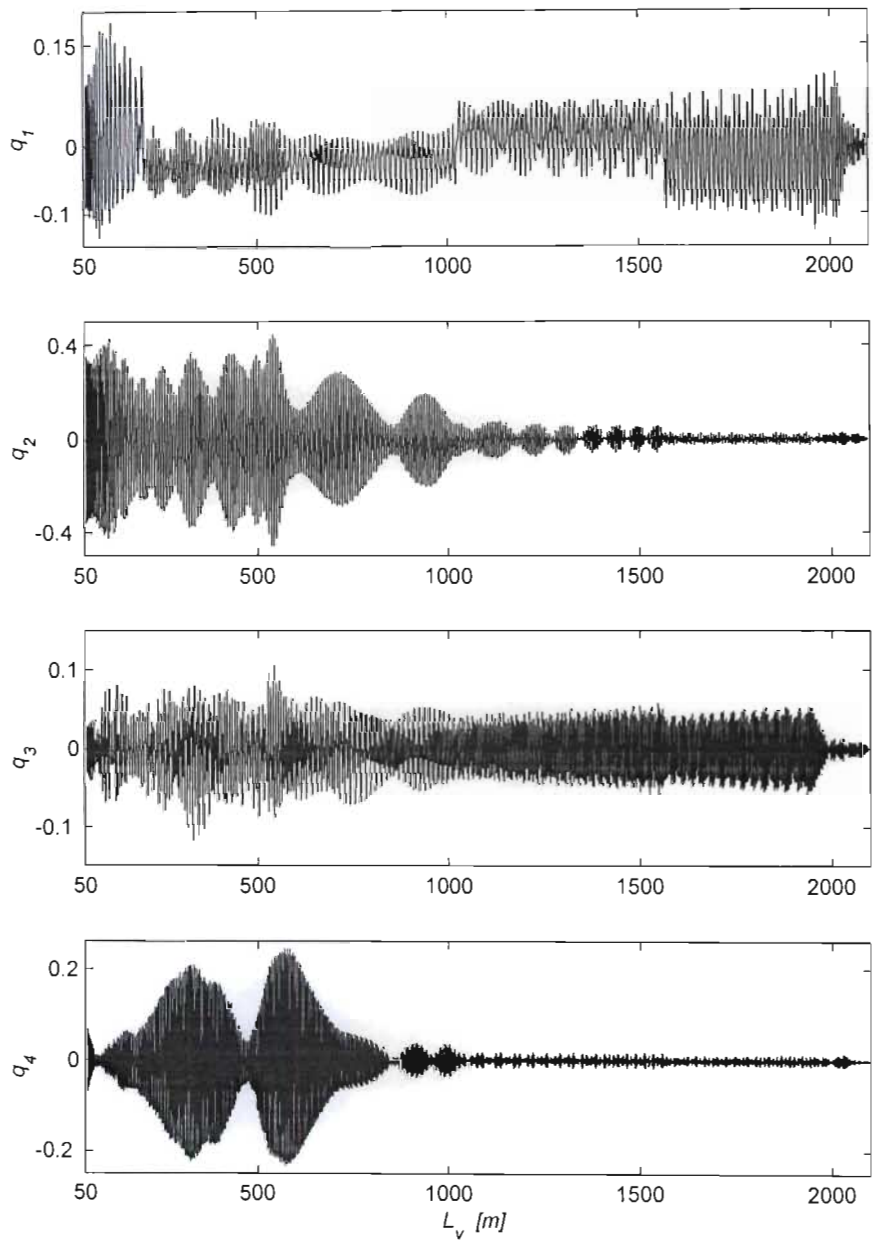

Figure 65. Lateral out-of-plane modal co-ordinates for Kloof simulation, $V_c = 15\ m/s$.

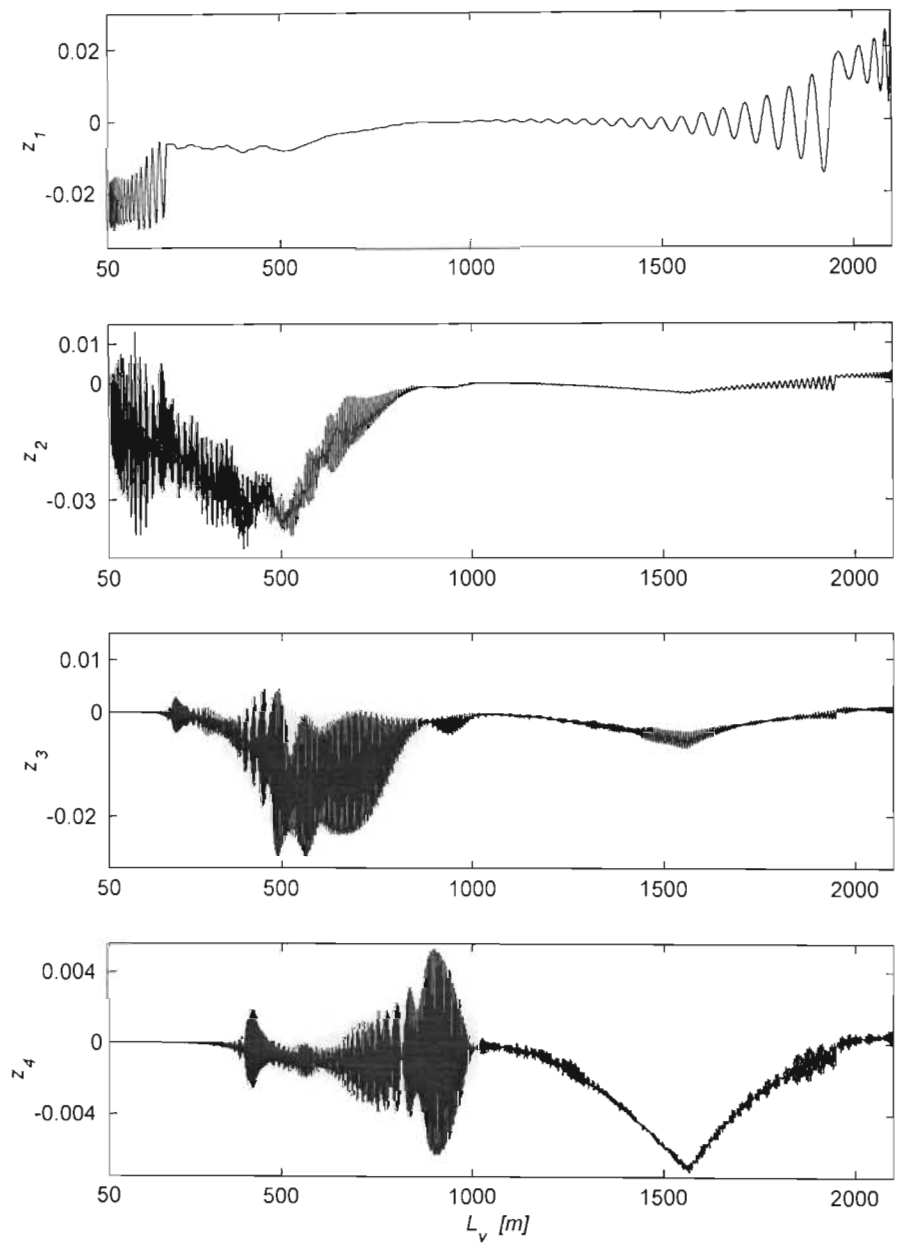

Figure 66. Longitudinal modal co-ordinates for Kloof simulation, $V_c = 15\ m/s$.

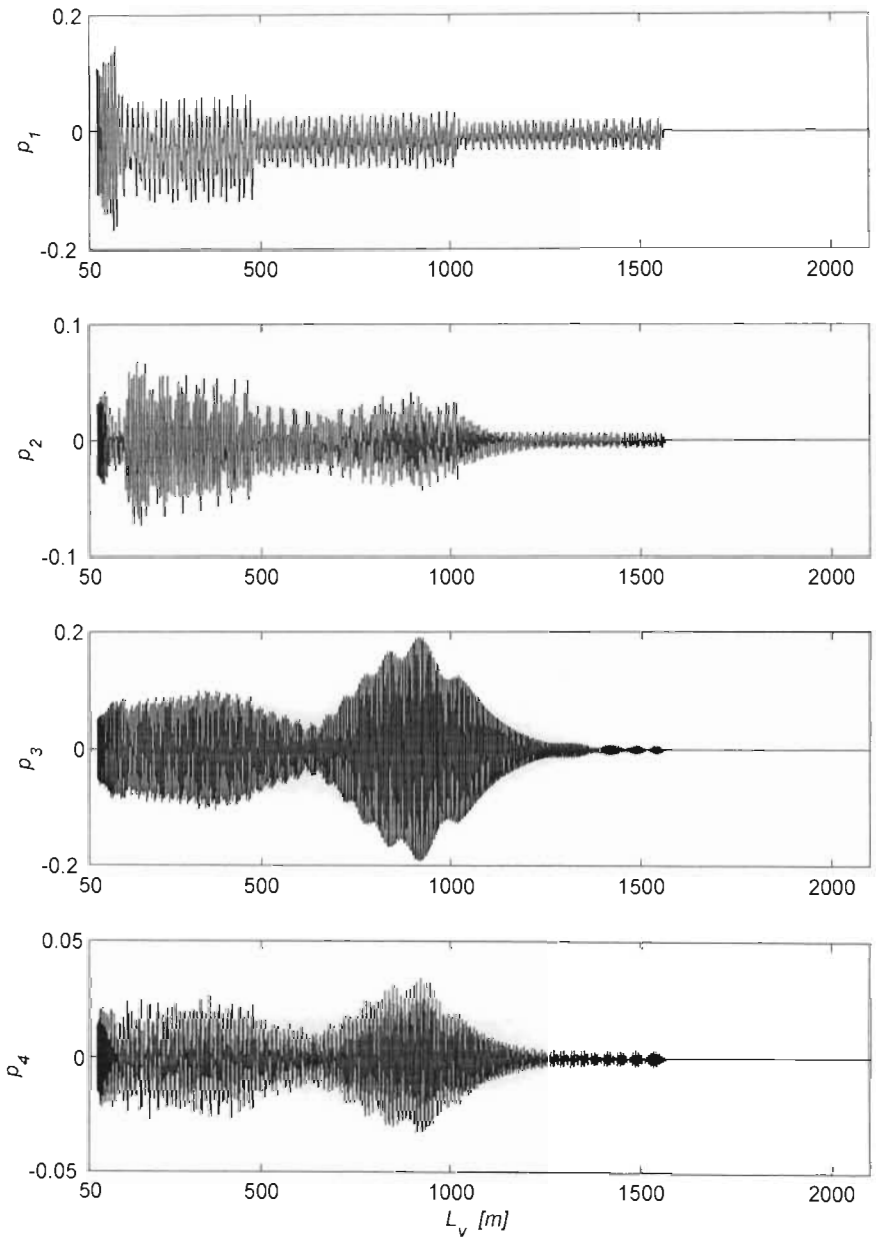

Figure 67. Lateral in-plane modal co-ordinates for Kloof simulation, $V_c = 12\ m/s$.

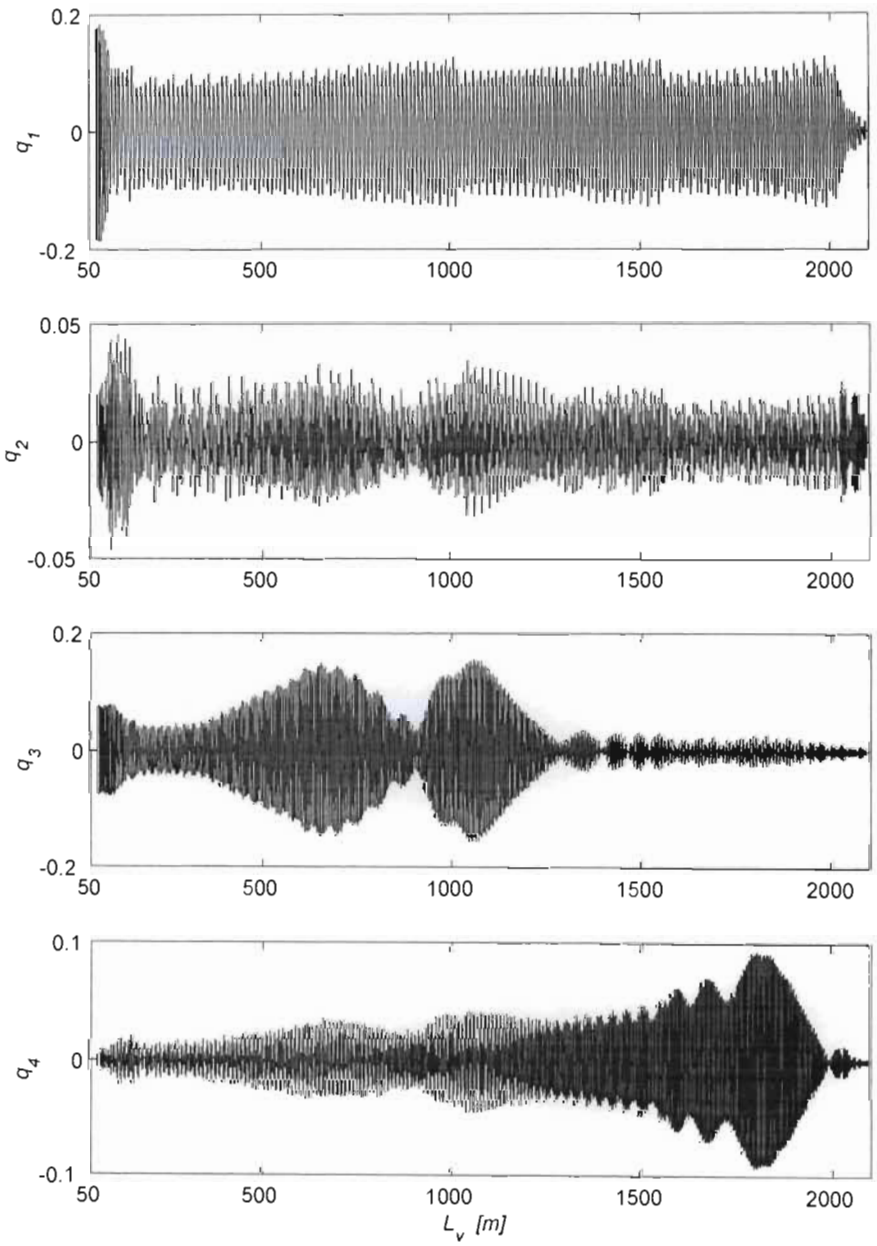

Figure 68. Lateral out-of-plane modal co-ordinates for Kloof simulation, $V_c = 12\ m/s$.

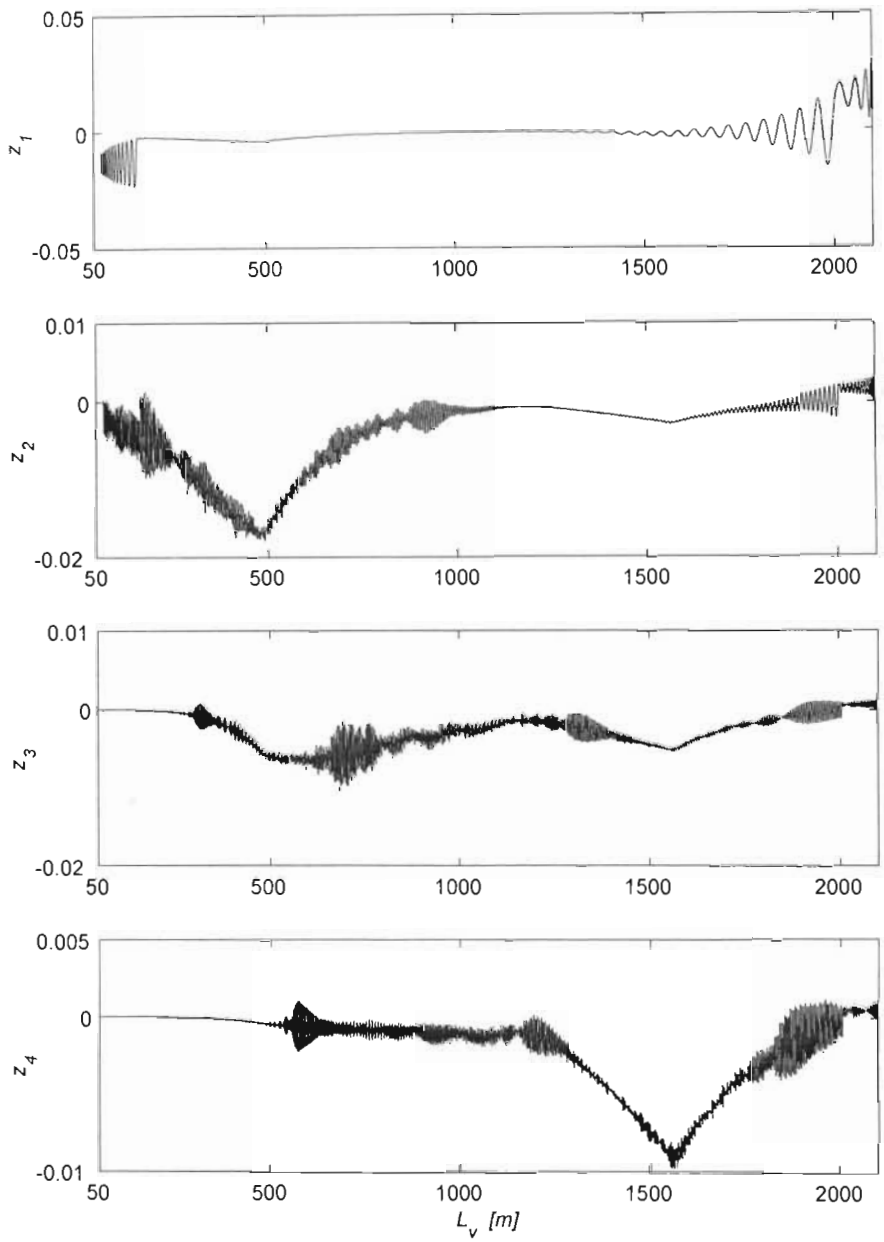

Figure 69. Longitudinal modal co-ordinates for Kloof simulation, $V_c = 12\ m/s$.

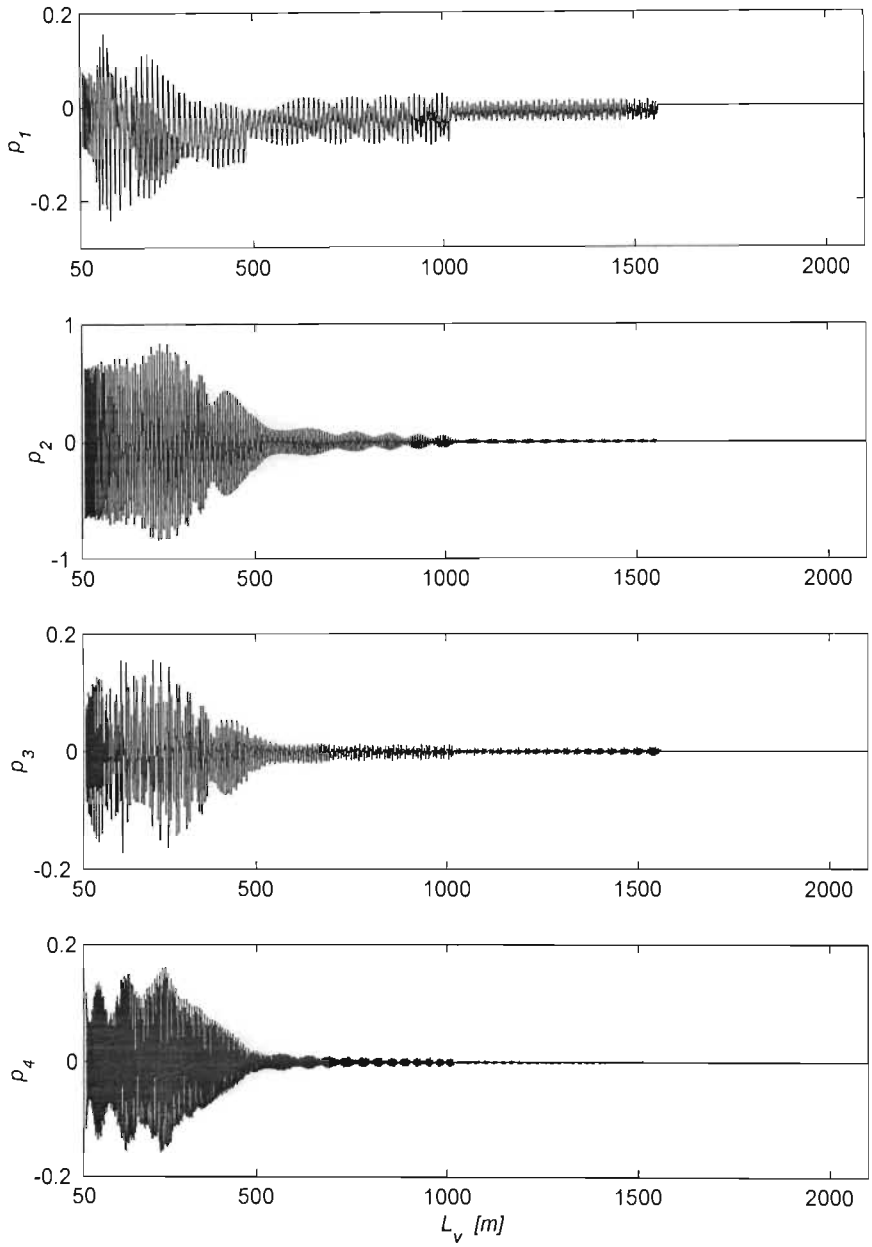

Figure 70. Lateral in-plane modal co-ordinates for Kloof simulation, $V_c = 14\ m/s$.

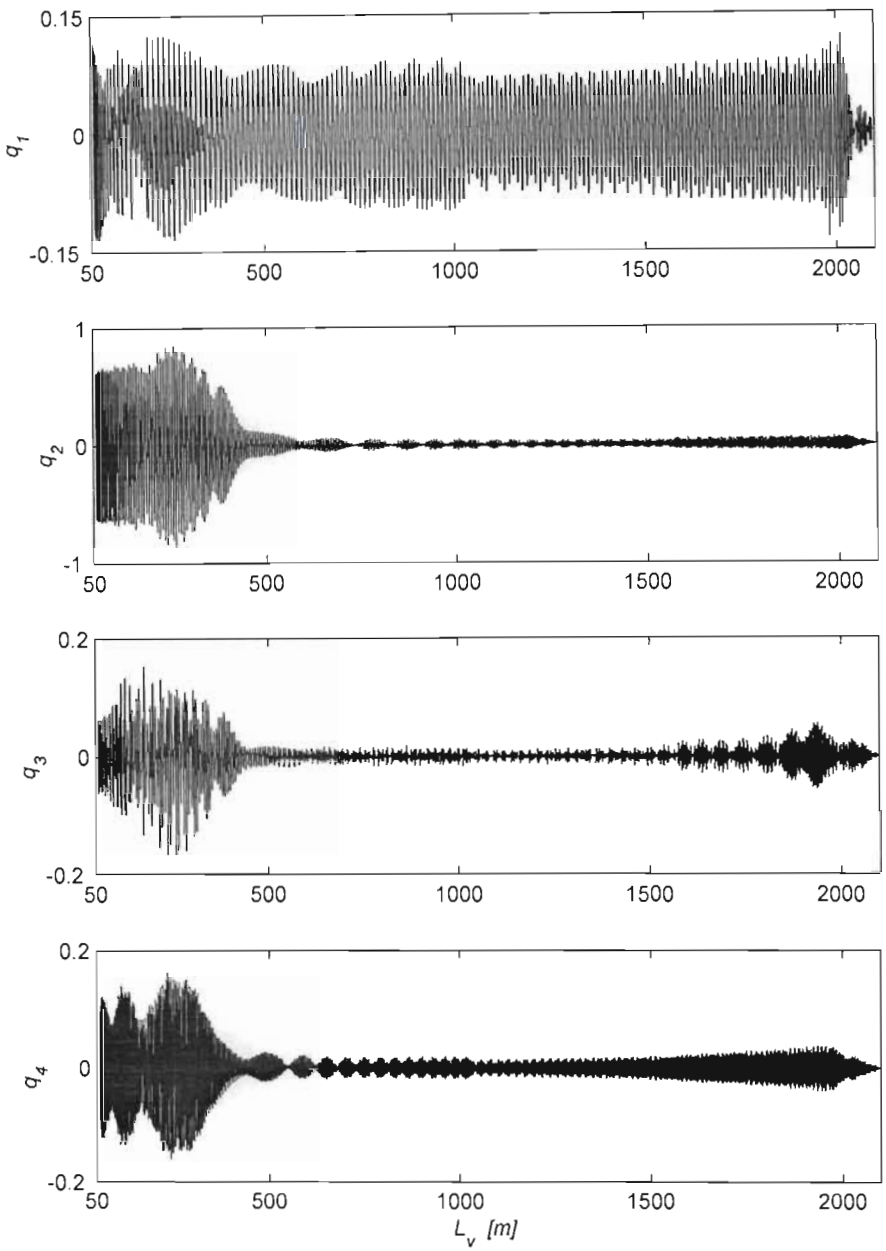

Figure 71. Lateral out-of-plane modal co-ordinates for Kloof simulation, $V_c = 14\ m/s$.

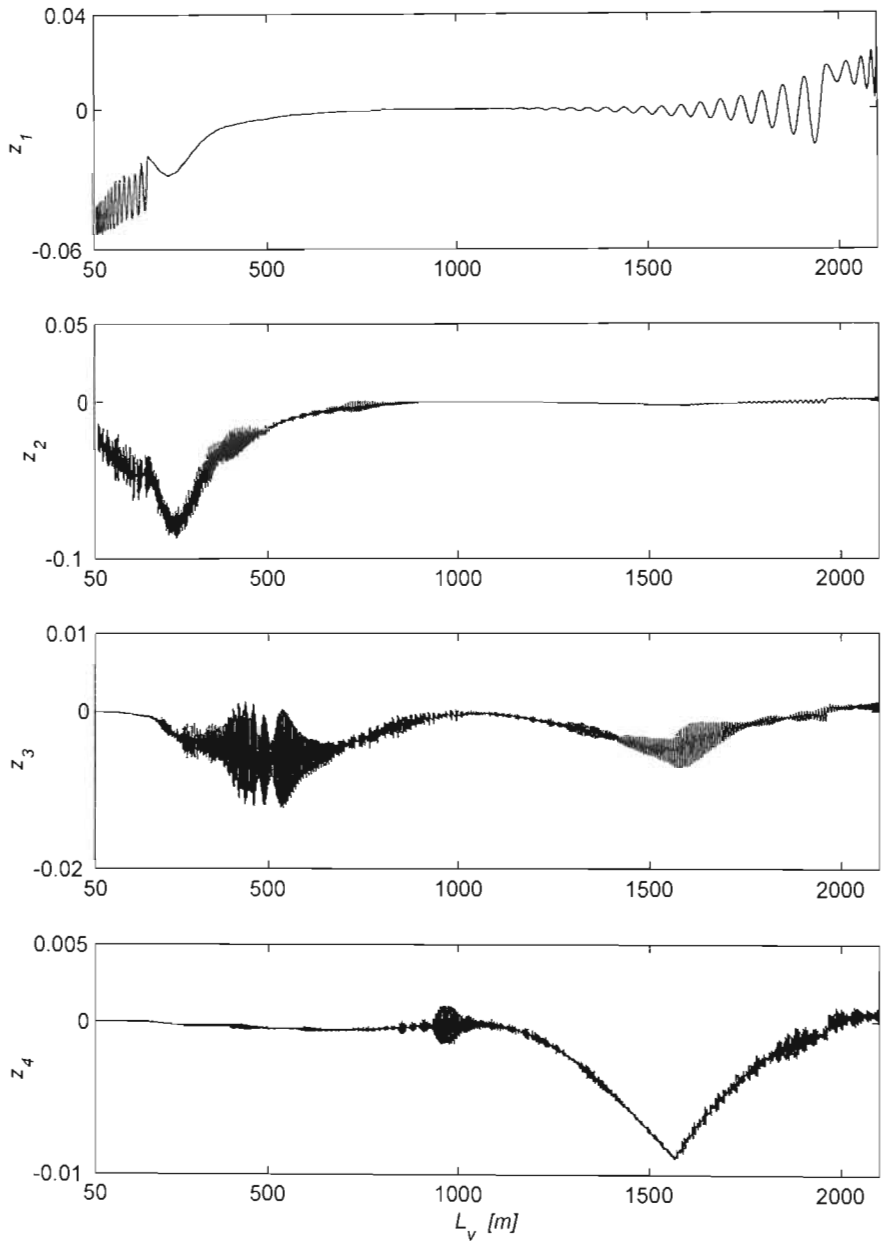

Figure 72. Longitudinal modal co-ordinates for Kloof simulation, $V_c = 14\ m/s$.

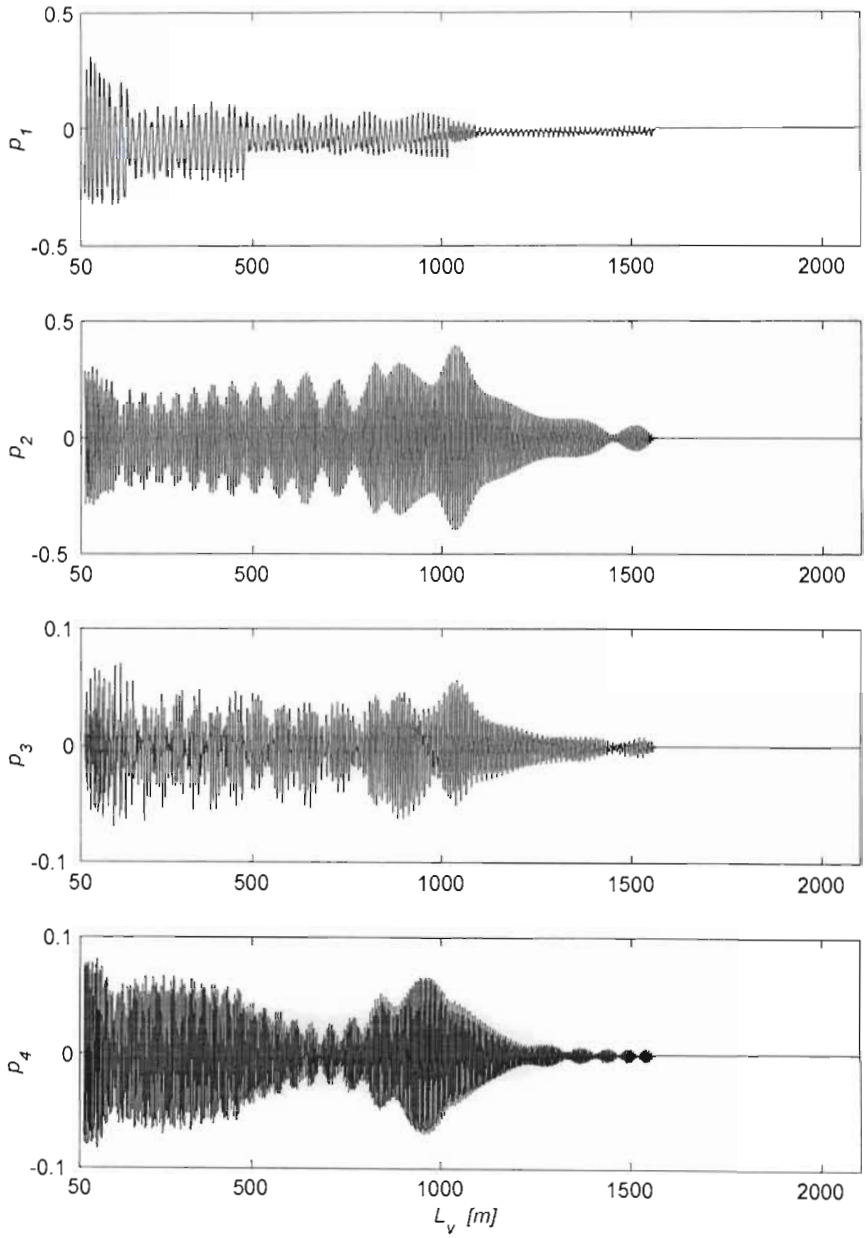

Figure 73. Lateral in-plane modal co-ordinates for Kloof simulation, $V_c = 16\ m/s$.

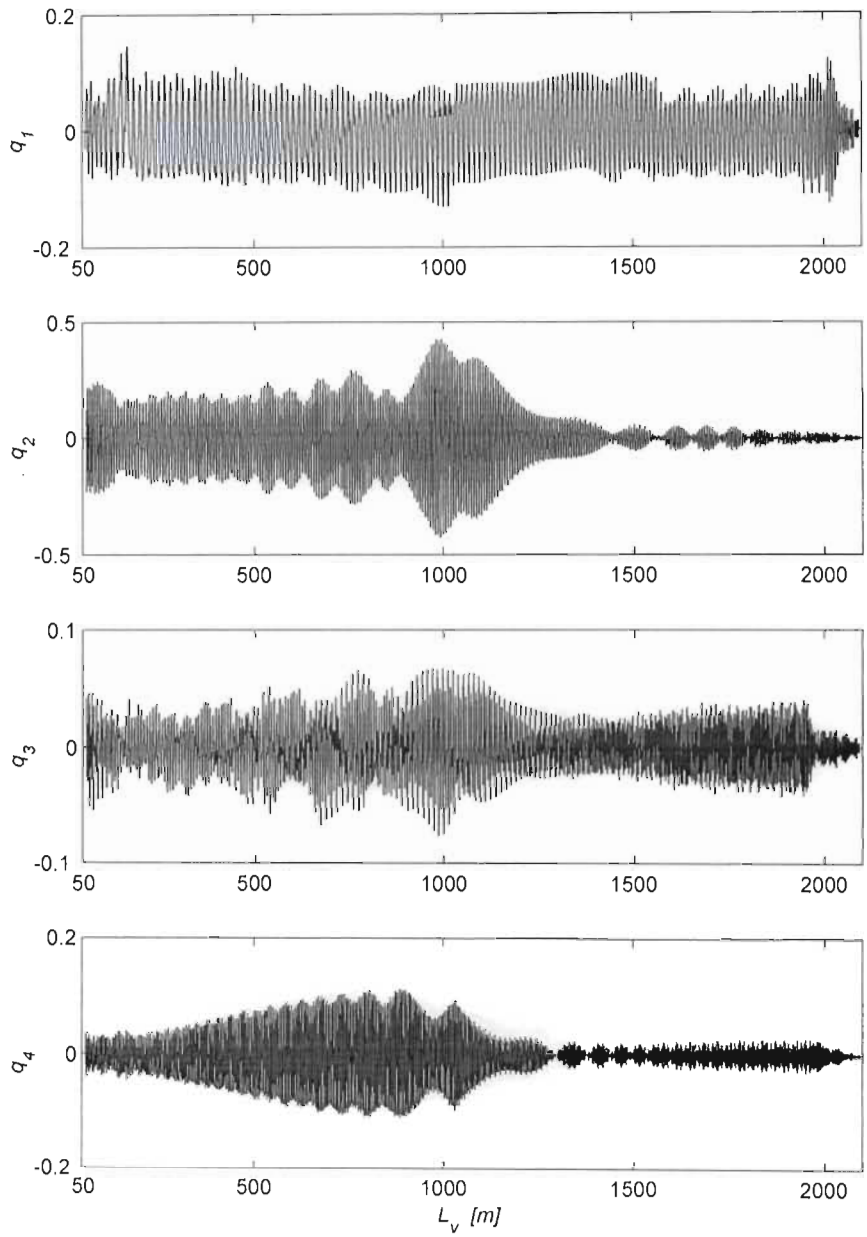

Figure 74. Lateral out-of-plane modal co-ordinates for Kloof simulation, $V_c = 16\ m/s$.

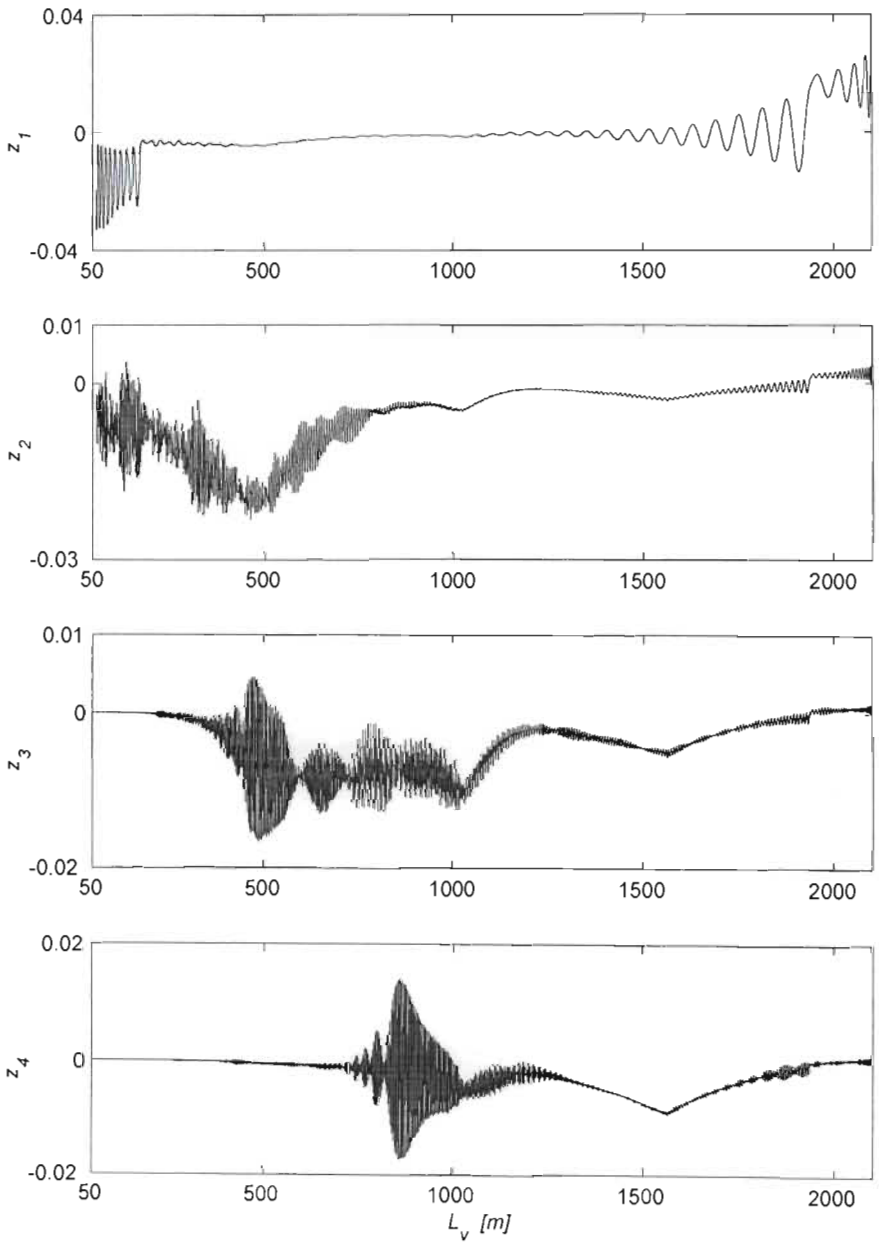

Figure 75. Longitudinal modal co-ordinates for Kloof simulation, $V_c = 16\ m/s$.

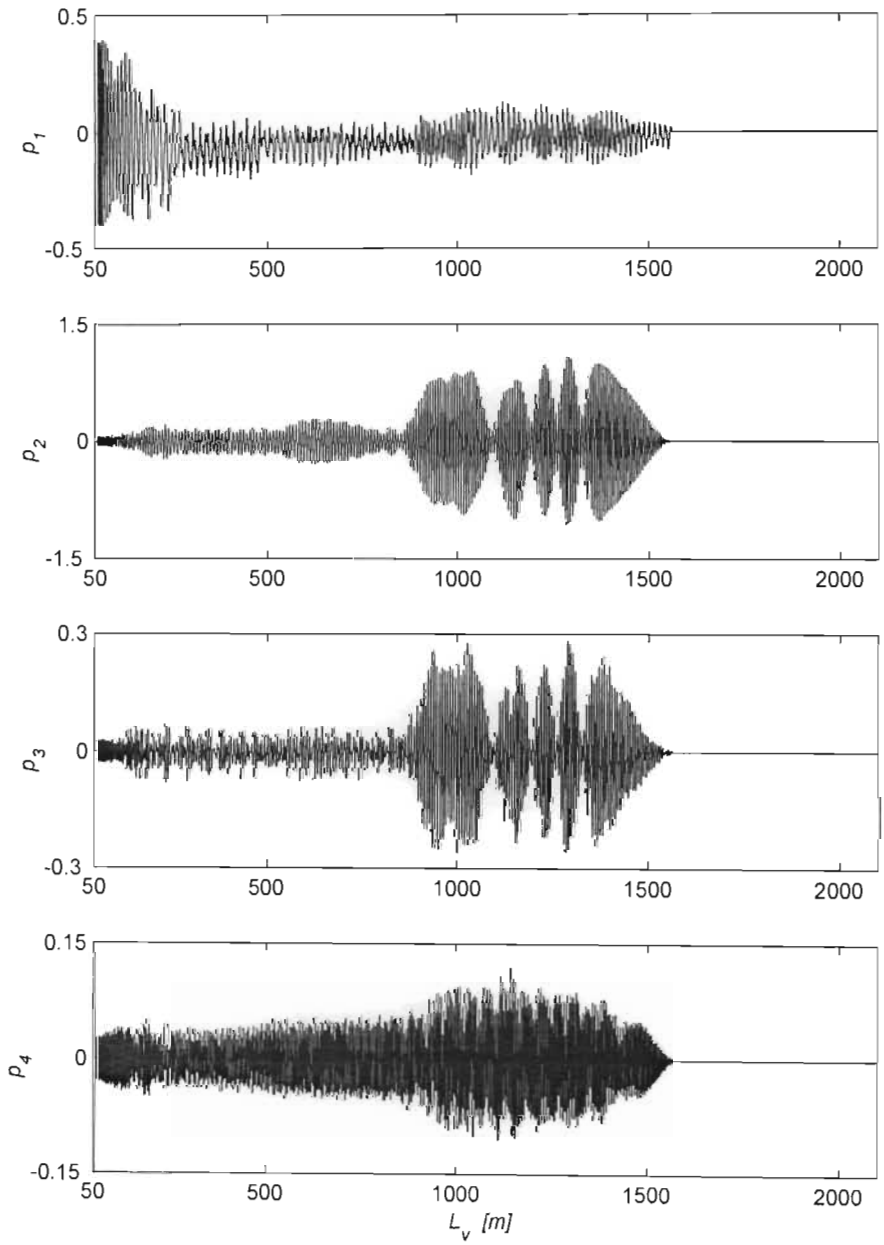

Figure 76. Lateral in-plane modal co-ordinates for Kloof simulation, $V_c = 18\ m/s$.

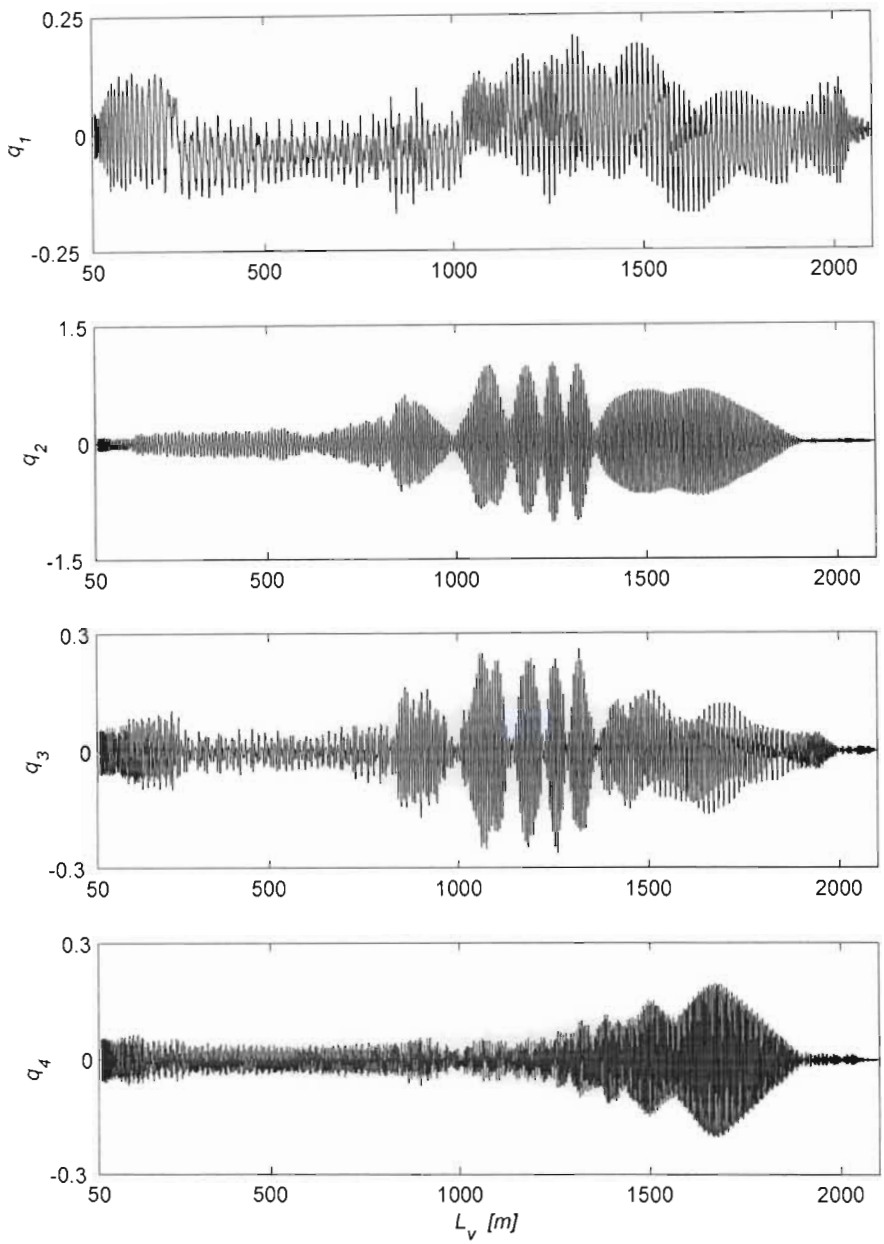

Figure 77. Lateral out-of-plane modal co-ordinates for Kloof simulation, $V_c = 18\ m/s$.

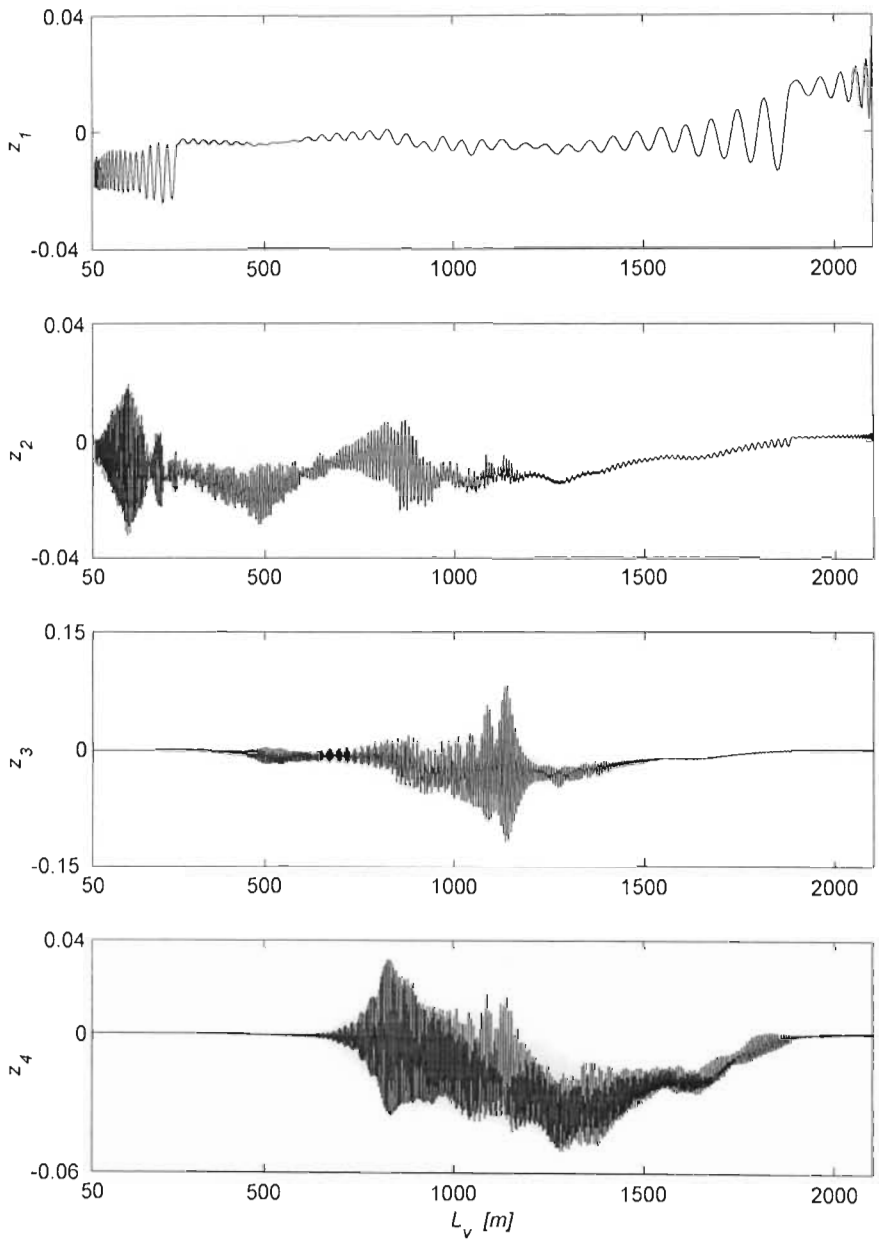

Figure 78. Longitudinal modal co-ordinates for Kloof simulation, $V_c = 18\ m/s$.

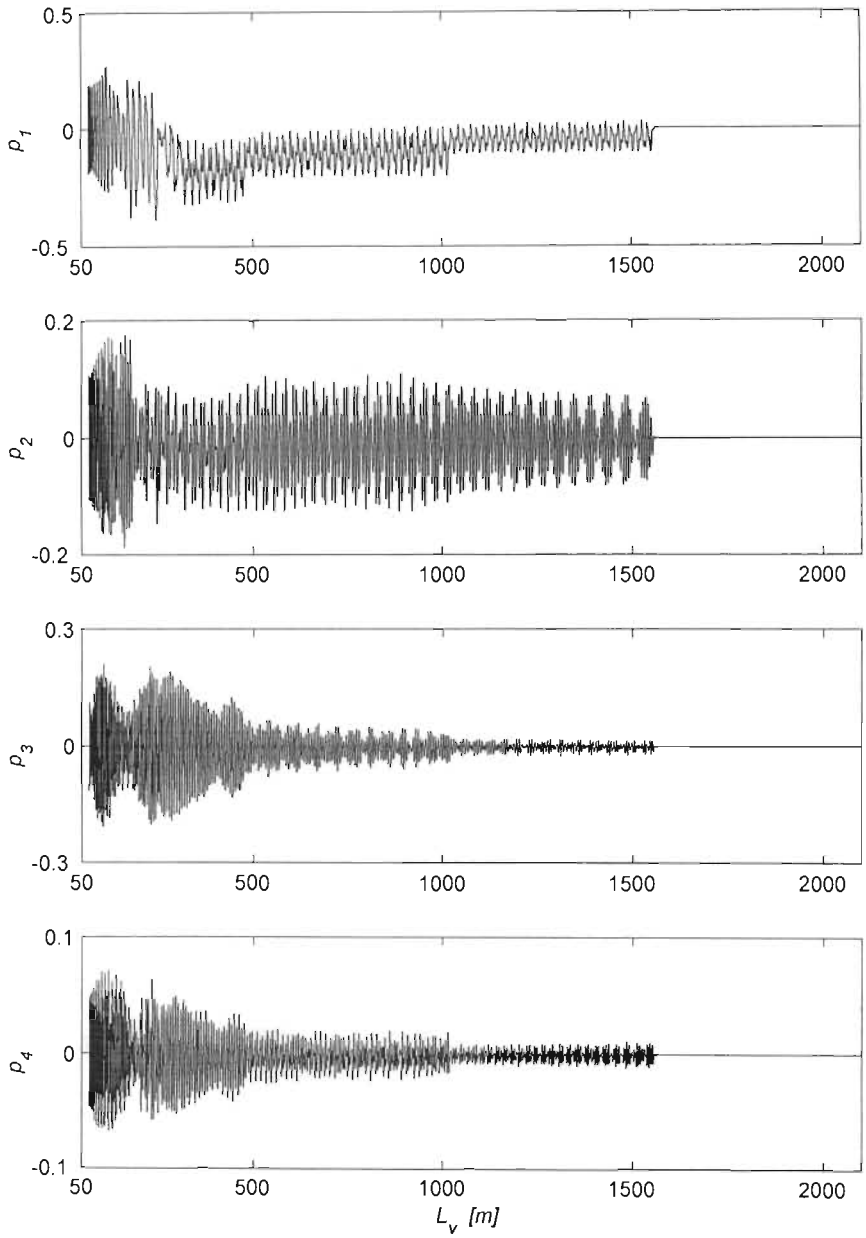

Figure 79. Lateral in-plane modal co-ordinates for Kloof simulation, $V_c = 19.5\ m/s$.

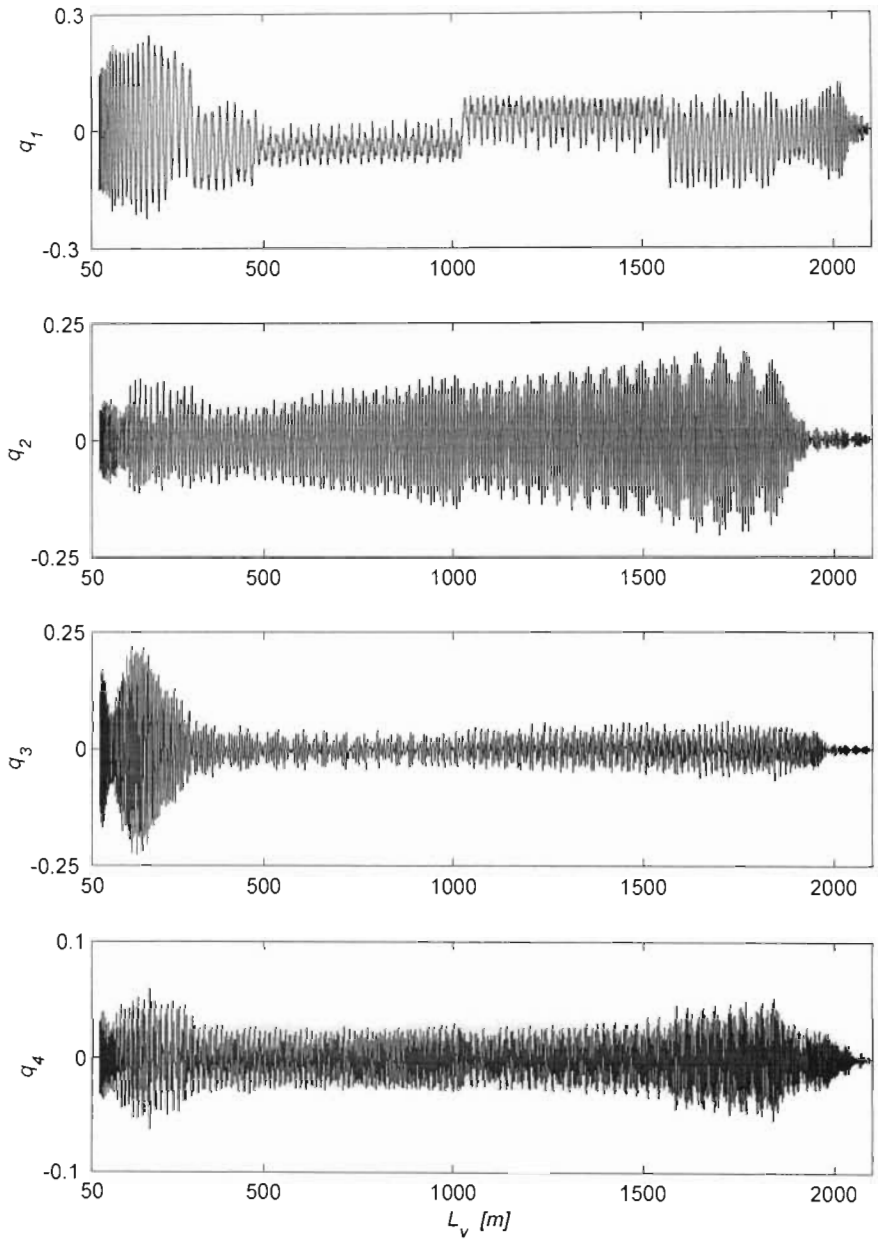

Figure 80. Lateral out-of-plane modal co-ordinates for Kloof simulation, $V_c = 19.5\ m/s$.

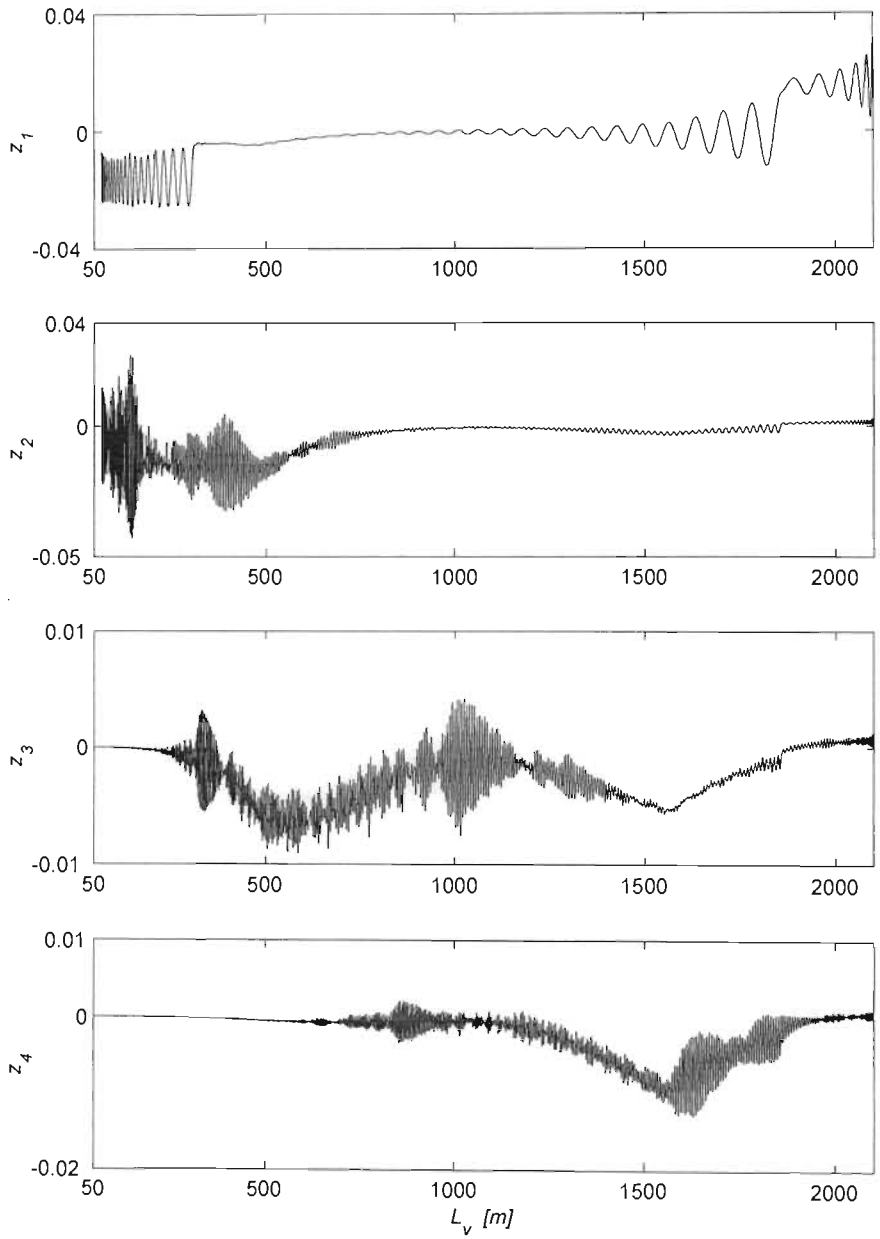

Figure 81. Longitudinal modal co-ordinates for Kloof simulation, $V_c = 19.5\ m/s$.

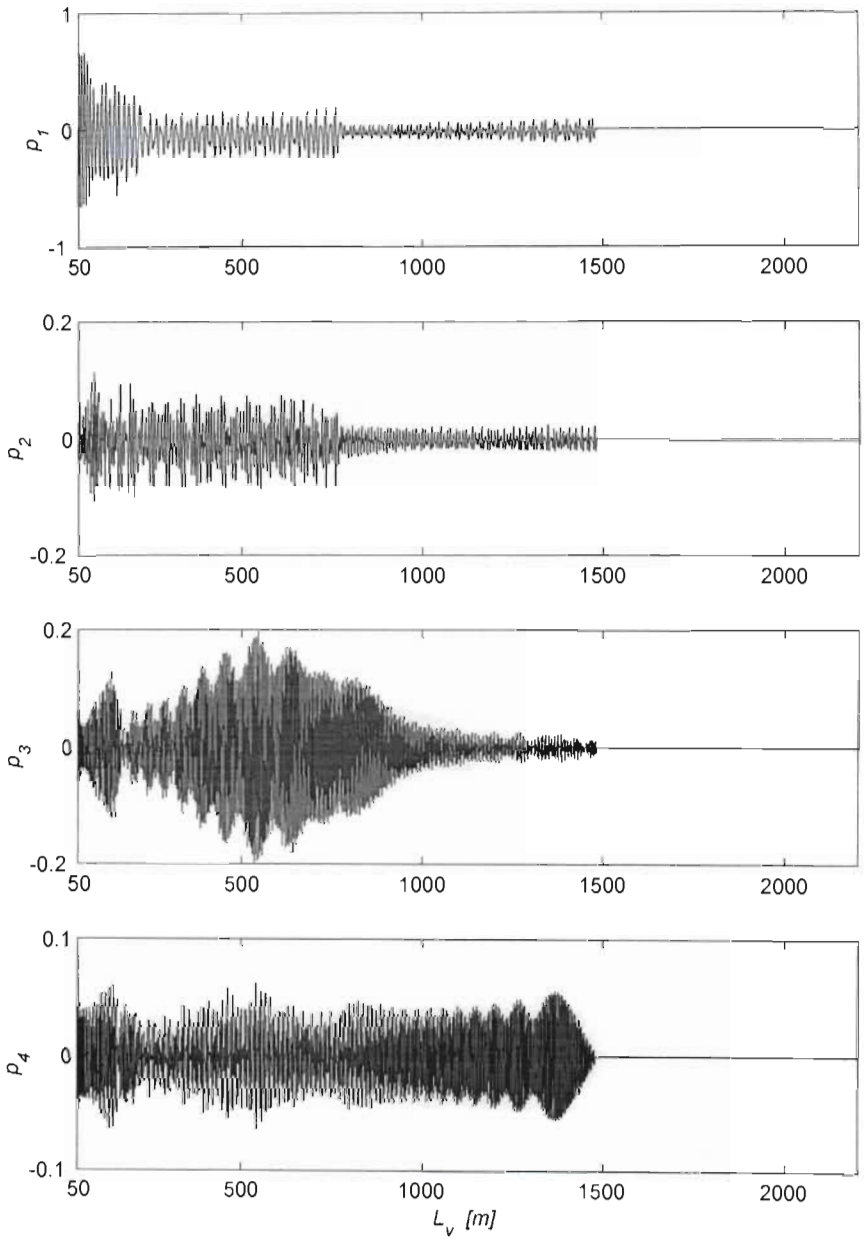

Figure 82. Lateral in-plane modal co-ordinates for Elandsrand simulation, $V_c = 16\ m/s$.

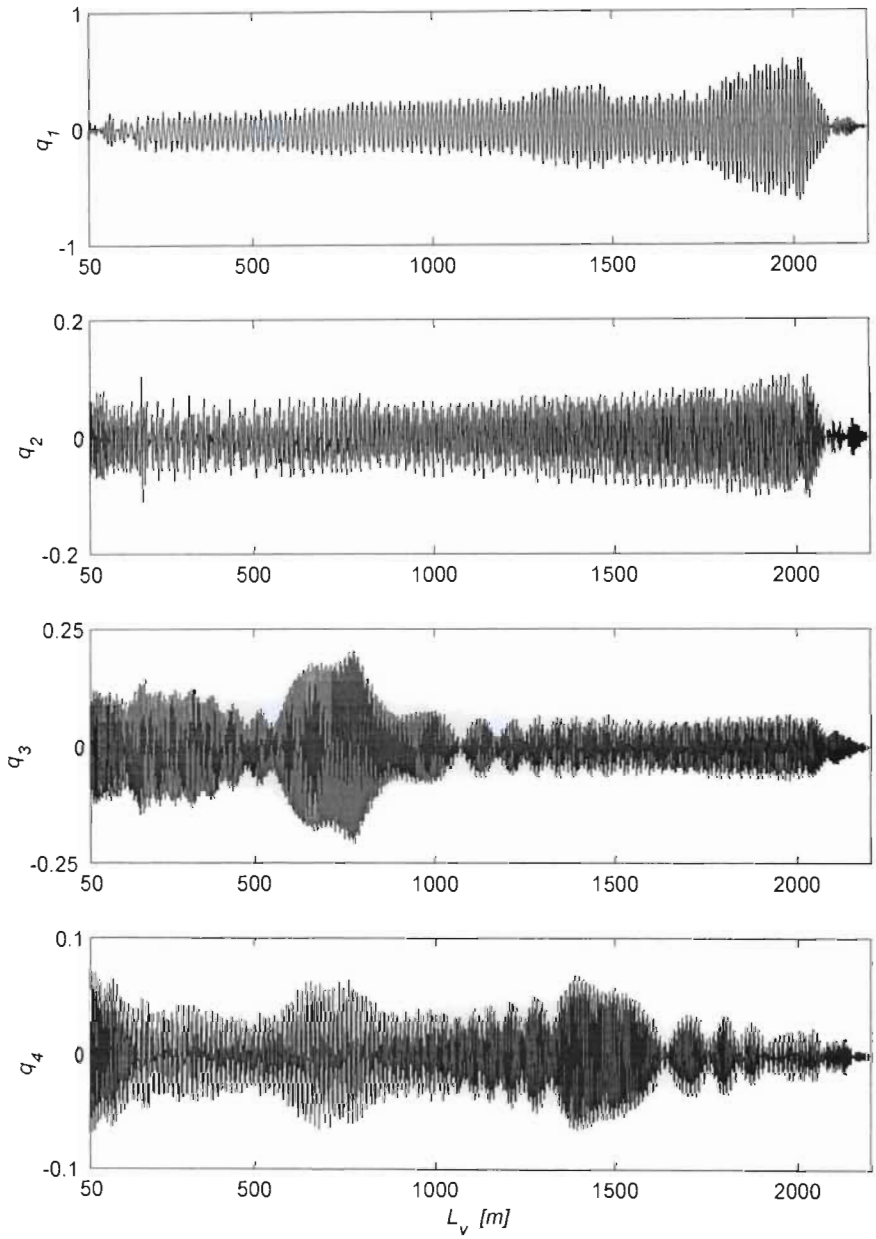

Figure 83. Lateral out-of-plane modal co-ordinates for Elandsrand simulation, $V_c = 16$ m/s.

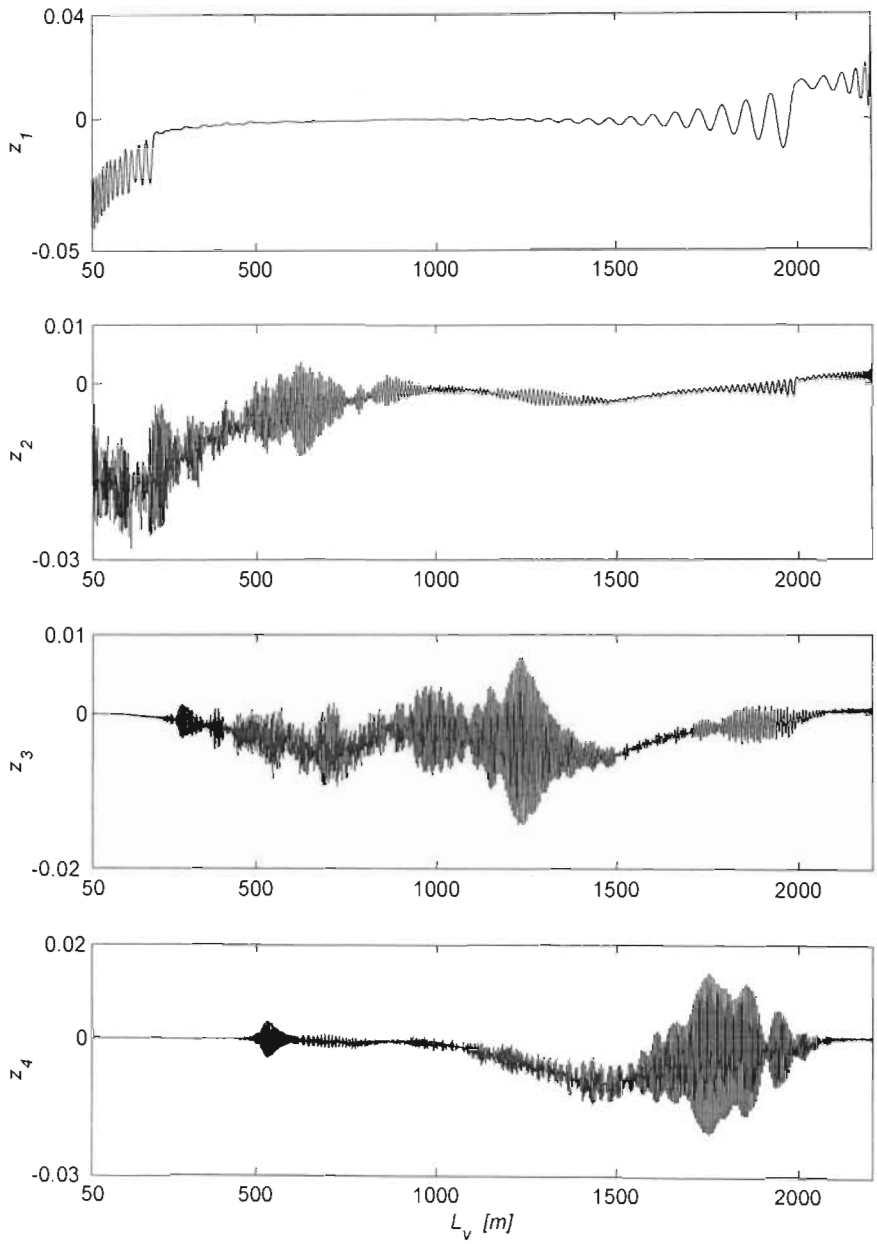

Figure 84. Longitudinal modal co-ordinates for Elandsrand simulation, $V_c = 16\ m/s$.